



The University of
Nottingham

UNITED KINGDOM • CHINA • MALAYSIA

**A STUDY OF POLYISOBUTYLENE AND ITS DERIVATIVES AT
HIGH TEMPERATURES**

SAM DENNIS BAILEY, MChem.

Thesis submitted to the University of Nottingham

for the degree of Engineering Doctorate

May 2016

Abstract

In recent years fuel injection equipment (FIE) has had to rapidly evolve to meet ever more stringent emission standards with developments such as higher fuel injection pressures and smaller injection orifices. The latest FIE technology, however, has been found to be more susceptible to deposit formation in injectors and filters which can be detrimental to the performance of the engine. The chemical resistivity, non-toxicity and high thermal stability of Polyisobutylenes (PIBs) makes these suitable precursors to polymeric dispersants which are engineered to help prevent deposit formation. The PIB molecules can be functionalised with succinimide/polyamine groups which facilitate adsorption of the polymers at the surface of carbonaceous materials which precipitate out of the fuel. Despite the fact the majority of processes involving these polymers occur at high temperatures almost all previous studies into the dispersancy behaviour of PIB and its derivatives are based at ambient or near ambient temperatures. Using high temperature analytical methods to investigate PIB type dispersions containing deposit surrogates will therefore allow insight into the dispersancy mechanism in the temperature range in which they normally operate.

High temperature rheometry and ^1H NMR have successfully been used in combination to study the fluidity of coal samples during coking and the pyrolysis of biomass polymers. This research presents for the first time a study of PIB type dispersions using these high temperature techniques. The aims of the project are (1) to establish a reproducible methodology for both the sample preparation and analysis of PIB type dispersions using high temperature rheometry and ^1H NMR, (2) to investigate the structure activity relationships of the polymers through the utilisation of various PIB derivatives, and (3) to investigate the effects of changing the deposit surrogate on the dispersion behaviour at high temperatures.

A reproducible methodology for both the sample preparation and the analysis has been established. Characterisation of PIB, and two functionalised derivatives, PIB

succinic anhydride (PIBSA) and PIB succinimide (PIBSI), demonstrates that the viscoelastic and hydrogen mobility measurements of dispersion can be an indication of the strength of the interaction between the polymer and carbon particles. The range of PIBSI type molecules has been expanded to investigate the structure activity relationships which include the effects of the number of amines in the head group and the length of the PIB hydrocarbon chains. The results indicate that the size of amine head groups have the most dominant effects on the viscoelastic and molecular mobility behaviour. The effect of changing the carbon type was investigated using ^1H NMR where a number of dispersions containing various types of commercially available carbons (that had previously been utilised as reference carbons in comparison with actual injector deposits) were analysed. The results show that changing the type of carbon used in a dispersion sample can significantly affect the measured mobility of the sample. It was indicated that the properties of the carbon material on the surface, such as the level of carbon and oxygen surface %, and the level of graphicity / amorphicity were the more dominant factors in effecting the mobility measurements as opposed to other factors such as particle size and surface area. This gives additional support that this method of high temperature measurement of dispersions can provide an indication of the strength of the interaction between the polymer and deposit surrogate particles rather than simply being controlled by the inherent physical properties of the polymers or carbons themselves.

Acknowledgements

Firstly, I would like to express my sincere gratitude to my supervisor Prof. Colin Snape whose immense knowledge and thoughtful insight have helped guide this project from inception to completion. Equal credit must also be given to my industrial supervisor at Innospec Ltd., Dr. Jim Barker. I would also like to thank my secondary supervisor Dr Miguel Castro Diaz for his valuable input. The financial contributions made by the EPSRC and Innospec Ltd. are also gratefully recognised. Many thanks go to Mr. Barry Cheeseman of Innospec Ltd. for the thermogravimetric analysis of the polymer samples.

I would like to especially thank Dr. Sylvia Nelima Kokonya for her assistance with rheometer and NMR instruments at the University of Nottingham, as well as her friendship throughout the project. Thanks also go to Dr. Malgorzata Wiatros Motyka for her support and advice, as well as being a friend in the lab.

Collaborations with other researchers within the Department of Chemical Engineering at the University of Nottingham have added greatly to the worth of this project. As such, thanks are due to Dr. Lee Stevens for assistance with the mastersizer, Mr. Nannan Sun for BET analysis and also Dr. Emily Smith for XPS analysis.

Thanks are due to all of those within the EFET EngD centre as well as the centre manager, Dr. Anup Patel.

For their constant encouragement and support I would like to thank my friends and family, with particular thanks to Lucy and Charlie. I must also express my heartfelt gratitude to Miss. Rachel Lewis for her infinite patience and reassurance. Finally, special thanks are due to my parents, Mr. Glyn and Mrs. Marie Bailey, for their unconditional support and encouragement both throughout this project and always.

Contents

Abstract.....	2
Acknowledgements	4
Table of Figures	10
Nomenclature	23
1 Introduction.....	25
1.1 Background.....	25
1.1.1 Engine emission standards	25
1.1.2 Fuel injection systems.....	25
1.1.3 Fuel injection equipment deposits.....	26
1.1.4 Introduction to fuel additives	28
1.1.5 Deposit control additives	28
1.1.6 Polyisobutylene and its derivatives	30
1.1.7 Background to polymeric dispersion theory.....	31
1.1.8 Polymer adsorption.....	33
1.2 Motivation for this study	34
1.3 Specific project aims and objectives	35
2 Literature Review	36
2.1 Engine deposit formation and structure	36
2.1.1 Introduction.....	36
2.1.2 Deposit formation mechanism.....	37
2.1.3 Morphology of carbonaceous type deposits	40
2.1.4 Morphology of polymeric type deposits.....	43
2.1.5 Ultra-Low Sulphur Diesel (ULSD) deposits	44
2.1.6 Metal carboxylates derived engine deposits	45
2.1.7 Biofuel derived engine deposits	46
2.2 Carbon black	48
2.3 Introduction to PIBs	49
2.3.1 Synthesis of polyisobutylene succinimide.....	49
2.4 PIBSI behaviour at ambient temperatures.....	51
2.4.1 Adsorption of PIBSI onto deposit surrogates	52
2.4.2 Effect of extending polyamine head group	53
2.4.3 Effect of extending PIB hydrocarbon tail length	57

2.4.4	Effect of PIB architecture.....	58
2.5	Thermal effects.....	60
2.5.1	Thermal degradation of PIBs.....	60
2.5.2	Stabilisation mechanism of PIB at high temperatures.....	61
2.6	Review of high temperature studies of non PIBs	66
2.6.1	High temperature NMR spectroscopy and rheometry.....	66
2.7	Chapter Summary.....	68
3	Experimental	71
3.1	NMR spectroscopy.....	71
3.1.1	Spin.....	71
3.1.2	Vector model	72
3.1.3	Pulsed magnetic field	73
3.1.4	Free induction decay (FID)	74
3.1.5	T ₁ relaxation (spin-lattice relaxation time)	74
3.1.6	T ₂ relaxation (spin-spin relaxation time).....	75
3.1.7	High temperature ¹ H NMR	75
3.2	¹³ C NMR.....	76
3.3	Rheology	76
3.3.1	Hooke's law of elasticity	77
3.3.2	Newton's Law of Viscosity.....	77
3.3.3	Dynamic oscillatory measurements of viscoelastic materials	78
3.4	Thermogravimetric analysis (TGA)	80
3.5	Temperature programmed oxidation (TPO)	81
3.6	Gel permeation chromatography (GPC).....	81
3.7	X-ray photoelectron spectroscopy (XPS)	81
3.8	Brunauer-Emmett-Teller (BET) analysis	82
3.9	Particle size analysis (via laser diffraction)	82
3.10	Materials.....	82
3.10.1	Summary of polymer samples.....	82
3.10.2	Summary of carbon samples.....	84
3.10.3	Solvent	86
3.11	Preparation of polymer carbon dispersion samples	86
3.12	Description of analytical techniques.....	87
3.12.1	High temperature ¹ H Nuclear Magnetic Resonance spectroscopy....	87

3.12.2	Solid state ¹³ C NMR spectroscopy	88
3.12.3	High temperature rheometry	88
3.12.4	Thermogravimetric analysis (TGA).....	90
3.12.5	Temperature programmed oxidation (TPO).....	90
3.12.6	Gel permeation chromatography (GPC).....	90
3.12.7	X-ray Photoelectron Spectroscopy (XPS)	91
3.12.8	Brunauer-Emmett-Teller (BET) Analysis	91
3.12.9	Particle size analysis (via laser diffraction).....	91
4	Optimisation of Sample Preparation and Main Analytical Methods	93
4.1	Experimental.....	93
4.1.1	Materials	93
4.1.2	Dispersion sample preparation	94
4.2	Optimisation conditions for characterisation of polymer/ carbon dispersions- rheometry	94
4.2.1	Auto tension adjustment on/off.....	95
4.2.2	Strain-sweep measurements.....	99
4.2.3	Sample reproducibility	100
4.2.4	TA AR-2000 rheometer instrument measurements	102
4.2.5	Effect of increasing carbon loading on viscoelastic behaviour	105
4.3	Optimisation conditions for characterisation of polymer Carbon dispersions- high temperature ¹ H NMR.....	106
4.3.1	Temperature range.....	106
4.3.2	¹ H NMR peak graph fitting	107
4.3.3	¹ H NMR repeatability.....	108
4.3.4	¹ H NMR reproducibility	110
4.3.5	Effect of removing sonication step	112
4.3.6	Error measurement of data processing.....	113
4.3.7	Effect of increasing solid loading on ¹ H NMR mobility measurements	115
4.3.8	Contribution from the carbon black to the ¹ H signal	117
4.4	Chapter summary	117
5	Characterisation of Polyisobutylene-Carbon Black Dispersions	119
5.1	Experimental.....	119
5.1.1	Materials	119

5.1.2	Sample preparation	120
5.1.3	Summary of analytical methods used.....	120
5.2	Results and discussion.....	120
5.2.1	Thermogravimetric analysis (TGA) of PIB, PIBSA, PIBSI-A, PIBSI-B 120	
5.2.2	High temperature rheological measurement of polyisobutylene ...	122
5.2.3	Rheological characterisation of PIB, PIBSA, PIBSI-A, PIBSI-B /MicroCB dispersions	124
5.2.4	High temperature ¹ H NMR measurement of PIB, PIBSA, PIBSI-A and PIBSI-B135	
5.2.5	High temperature ¹ H NMR peak half width ($\Delta H_{1/2}$) measurement of PIB, PIBSA, PIBSI-A, PIBSI-B – MicroCB dispersions.....	137
5.3	Chapter summary	142
6	Effect of Polymer Structure on Dispersion Behaviour.....	144
6.1	Experimental.....	144
6.1.1	Materials	144
6.1.2	Sample preparation	145
6.1.3	Summary of analytical methods	145
6.2	Results and discussion.....	146
6.2.1	Thermogravimetric analysis (TGA) results	146
6.2.2	Polar surface area calculations	147
6.2.3	Structure activity relationships at high polymer loadings	149
6.2.4	Structure activity relationships at low polymer loadings	166
6.2.5	Summary of structure activity relationships at low polymer loadings 179	
6.3	Chapter summary	187
7	Possible effects of deposit surrogate properties on dispersion behaviour at high temperatures.....	189
7.1	Experimental.....	189
7.1.1	Materials	189
7.1.2	Sample Preparation	190
7.1.3	Summary of Analytical Methods	190
7.2	Results and discussion.....	191
7.2.1	¹ H NMR spectroscopy results.....	191

7.2.2	Potential effect of carbon particle size on high temperature ^1H NMR $\Delta\text{H}_{1/2}$ measurements	193
7.2.3	Potential effect of carbon surface area on high temperature ^1H NMR $\Delta\text{H}_{1/2}$ measurements	194
7.2.4	Potential effect of carbon peak CO_2 emission temperature on high temperature ^1H NMR $\Delta\text{H}_{1/2}$ measurements	195
7.2.5	Potential effect of carbon elemental surface composition on high temperature ^1H NMR $\Delta\text{H}_{1/2}$ measurements	198
7.2.6	Polymer structure activity relationships with flake graphite (Micro850) 201	
7.3	Chapter summary	213
8	Conclusions and Recommendations for Future Work	216
8.1	Summary of conclusions and novelty of research	216
8.2	Recommendations for future Work	218
A	Polymer Structures	220
B	Strain-sweep measurements.....	223
C	Duplicate η^* measurements of PIB, PIBSA, PIBSI-A, PIBSI-B (65 %) MicroCB (35 %) dispersions.....	229
D	η^* measurements of various polymer MicroCB dispersions	231
E	Duplicate $\Delta\text{H}_{1/2}$ measurements of PIB, PIBSA, PIBSI-A (65 %) MicroCB (35 %) dispersions.....	235
F	$\Delta\text{H}_{1/2}$ measurements of various polymer MicroCB dispersions	237
G	$\Delta\text{H}_{1/2}$ measurements of PIBSI-H and PIBSI-F dispersions with various carbons 245	
H	$\Delta\text{H}_{1/2}$ measurements for various polymer Micro850 dispersions.....	248
I	Approximate calculation of PIBSI-A monolayer coverage of MicroCB	251
J	XPS analysis results of carbon samples	253
9	References	260

Table of Figures

Figure 1-1: (A) Clean injector needle, (B) fouled injector needle (Barker, Richards, Snape, & Meredith, 2011), (C) homogeneous fuel spray from clean injector, (D) inhomogeneous fuel spray from fouled injector (ATC, 2013).	27
Figure 1-2: Deposit control additive mechanism.....	29
Figure 1-3: Structures of PIB, PIBSA and PIBSI	31
Figure 1-4: Total Potential energy (V_t) diagram for two colloidal particles (Napper, 1970)	33
Figure 2-1: Mechanisms of Deposit formation (Lepperhoff & Houben, 1993)	38
Figure 2-2: Summary of generally-accepted scheme for jet fuel oxidation. R represents a generic alkyl group and Ar an aryl moiety (Cook & Richards, 2009).	39
Figure 2-3: SEM Image of solid deposit (Barker et al. 2009).	41
Figure 2-4: Schematic depth profile of injector deposit (Barker, Snape, & Scurr, 2012).	43
Figure 2-5: Polymerisation of PIB (Li, Cokoja, & Kuhn, 2011).	50
Figure 2-6: Synthesis of Polyisobutylene Succinimide (PIBSI) (Mortier & Orszulik, 1997).	50
Figure 2-7: Adsorption Isotherm of a PIBSI derivative from a xylene solution onto carbon black surface at 60 °C and the schemes of the adsorbed polymer layer in the mushroom and brush regimes (Chevalier, 2004).	52
Figure 3-1: Vector model of a collection of spin-1/2 nuclei at thermal equilibrium. (a) The magnetic moment of the individual spins. (b) The net magnetic moment (M_0) of a large number of spins (Hore, 1995).	73
Figure 3-2: Typical Fourier transformation of FID signal (Jacobsen, 2007).	74
Figure 3-3: Schematic representation of response to an oscillatory strain or stress for a viscoelastic system ($0^\circ < \delta < 90^\circ$) (Tadros, 2010).	79
Figure 3-4: (a) Image of Bruker MSL300 instrument and (b) Image of Doty 200 MHz NMR probe.....	88

Figure 3-5:(a) Image of RDA III high torque strain controlled rheometer (UoN), (b) Image of TA AR-2000 controlled-stress rheometer (Innospec Inc.)	89
Figure 4-1: Image of PIBSI 65% MicroCB 35% sample on rheometer plate prior to analysis.	95
Figure 4-2: Complex viscosity (η^*) as a function of temperature for PIB, PIBSA and PIBSI-A (65 %) MicroCB (35 %) dispersions using a heating rate of 3 °C min ⁻¹ ($\gamma=0.05$ %, $\omega=1$ Hz) (RDA-III instrument). Auto tension off.	96
Figure 4-3: Complex viscosity (η^*) as a function of temperature for PIB, PIBSA and PIBSI-A (75 %) MicroCB (25 %) dispersions using a heating rate of 3 °C min ⁻¹ ($\gamma=0.05$ %, $\omega=1$ Hz) (RDA-III instrument). Auto tension off.	97
Figure 4-4: η^* as a function of temperature for PIB, PIBSA, PIBSI-A and PIBSI-B (65 %) - MicroCB (35 %) dispersions using a heating rate of 3 °C min ⁻¹ in nitrogen ($\gamma = 0.05$, $\omega = 1$ Hz).(RDA-III instrument).	99
Figure 4-5: Storage (G') and loss (G'') moduli as a function of strain (γ) at 250 °C for PIBSI-A (65 %) MicroCB (35 %) dispersion.	100
Figure 4-6: Duplicate samples of PIBSI-A (65 %) and MicroCB (35 %) (1-4) using a heating rate of 3 °C min ⁻¹ in nitrogen ($\gamma = 0.05$, $\omega = 1$ Hz). (RDA-III instrument).....	101
Figure 4-7: Mean η^* as a function of temperature for 4 duplicate samples of PIBSI-A (65 %) and MicroCB (35 %) using a heating rate of 3 °C min ⁻¹ in nitrogen ($\gamma = 0.05$, $\omega = 1$ Hz). (RDA-III instrument). Error bars are to 1 standard deviation of the sample mean.	102
Figure 4-8: η^* , as a function of temperature for PIBSI-A (75 %) and MicroCB (25 %), using a heating rate of 3 °C min ⁻¹ in nitrogen ($\gamma = 0.05$, $\omega = 1$ Hz). (TA-2000 instrument).	103
Figure 4-9: η^* , as a function of temperature for PIBSA (75 %) and MicroCB (25 %), using a heating rate of 3 °C min ⁻¹ in nitrogen ($\gamma = 0.05$, $\omega = 1$ Hz). (TA-2000 instrument). .	104
Figure 4-10: Image showing residual PIBSA MicroCB dispersion material post heating. (TA AR-2000 rheometer).....	104

Figure 4-11: Complex viscosity (η^*) as a function of temperature for various PIBSI-A (75 – 45 %) and MicroCB (25 – 55 %) dispersions, using a heating rate of 3 °C min ⁻¹ in nitrogen ($\gamma = 0.05$, $\omega = 1$ Hz).....	105
Figure 4-12: ¹ H NMR spectra of PIBSI-A (85 %) MicroCB (15 %) dispersion at 250°C with Calculated and Experimental components.....	107
Figure 4-13: Evolution of the ¹ H NMR $\Delta H_{1/2}$ with temperature for a PIBSI-A (85 %) MicroCB (15 %) dispersion	108
Figure 4-14: Evolution of the ¹ H NMR $\Delta H_{1/2}$ with temperature for repeat analysis of a PIBSI-A (85 %) Micro CB (15 %) dispersion	109
Figure 4-15: Evolution of the mean ¹ H NMR $\Delta H_{1/2}$ with temperature for repeat analysis of a PIBSI-A (85 %) Micro CB (15 %) dispersion.....	110
Figure 4-16: Evolution of the ¹ H NMR $\Delta H_{1/2}$ with temperature for 3 duplicate PIBSI-A (85 %) Micro CB (15 %) dispersions (A, B, C) with sonication	111
Figure 4-17: Evolution of the mean ¹ H NMR $\Delta H_{1/2}$ with temperature for 3 duplicate PIBSI-A (85 %) Micro CB (15 %) dispersions (A, B, C). Error bars are to 1 standard deviation of the sample mean.	111
Figure 4-18: Evolution of the ¹ H NMR $\Delta H_{1/2}$ with temperature for 3 duplicate PIBSI-A (85 %) Micro CB (15 %) dispersions (D, E, F) without sonication.	112
Figure 4-19: Evolution of the mean ¹ H NMR $\Delta H_{1/2}$ with temperature for 6 duplicate PIBSI-A (85 %) Micro CB (15 %) dispersions with (A, B, C) and without (D, E, F) sonication step. Error bars are to 1 standard deviation of the sample mean.....	113
Figure 4-20: Evolution of the ¹ H NMR $\Delta H_{1/2}$ with temperature for a PIBSI-A (85 %) MicroCB (15 %) dispersion showing the FID transformed and processed 4 separate times.	114
Figure 4-21: Evolution of the mean ¹ H NMR $\Delta H_{1/2}$ with temperature for a PIBSI-A (85 %) MicroCB (15 %) dispersion transformed from the FID and processed 4 separate times. Error bars are to 1 standard deviation of the sample mean.....	114
Figure 4-22: Evolution of the ¹ H NMR $\Delta H_{1/2}$ with temperature for PIBSI-A (100 – 55 %) MicroCB (0 -45 %) dispersions.....	115

Figure 4-23: Evolution of the ^1H NMR $\Delta H_{1/2}$ with temperature for PIBSI-A (75 %) MicroCB (25 %) dispersion fitted with and without Gaussian components.	116
Figure 5-1: Weight percentage loss of PIB, PIBSA, PIBSI-A and PIBSI-B with temperature using a heating rate of $3\text{ }^\circ\text{C min}^{-1}$ in nitrogen.	122
Figure 5-2: η^* as a function of temperature for PIB using a heating rate of $3\text{ }^\circ\text{C min}^{-1}$ ($\gamma=0.05\%$, $\omega=1\text{ Hz}$) measured on Rheometrics RDA-III high torque controlled strain rheometer.	123
Figure 5-3: η^* as a function of temperature for PIB using a heating rate of $3\text{ }^\circ\text{C min}^{-1}$ ($\gamma=0.05\%$, $\omega=1\text{ Hz}$) measured on TA AR-2000 Controlled Stress rheometer.	123
Figure 5-4: η^* as a function of temperature for a PIB (65 %) MicroCB (35 %) dispersion, using a heating rate of $3\text{ }^\circ\text{C min}^{-1}$ in nitrogen ($\gamma = 0.05$, $\omega = 1\text{ Hz}$). (RDA-III instrument)	125
Figure 5-5: η^* as a function of temperature for PIB (65 %) and MicroCB (35 %) and PIBSI-A (65 %) and MicroCB (35 %) using a heating rate of $3\text{ }^\circ\text{C min}^{-1}$ in nitrogen ($\gamma = 0.05$, $\omega = 1\text{ Hz}$). (RDA-III instrument)	127
Figure 5-6. η^* as a function of temperature for PIB, PIBSA, PIBSI-A and PIBSI-B (65 %) - MicroCB (35 %) dispersions using a heating rate of $3\text{ }^\circ\text{C min}^{-1}$ in nitrogen ($\gamma = 0.05$, $\omega = 1\text{ Hz}$). (RDA-III instrument).....	128
Figure 5-7 η^* as a function of temperature for PIBSI-A (65 %) and MicroCB (35 %), PIBSI-B (65 %) and MicroCB (35 %) dispersions using a heating rate of $3\text{ }^\circ\text{C min}^{-1}$ in nitrogen ($\gamma = 0.05$, $\omega = 1\text{ Hz}$). (RDA-III instrument)	131
Figure 5-8: Mean η^* as a function of temperature for duplicate samples for PIB, PIBSA, PIBSI-A and PIBSI-B (65 %) and MicroCB (35 %) dispersions using a heating rate of $3\text{ }^\circ\text{C min}^{-1}$ in nitrogen ($\gamma = 0.05$, $\omega = 1\text{ Hz}$). (RDA-III instrument). Error bars are to 1 standard deviation of the sample mean.	132
Figure 5-9: η^* as a function of temperature for PIB, PIBSI-A and PIBSI-B (75 %) - MicroCB (25 %) dispersions using a heating rate of $3\text{ }^\circ\text{C min}^{-1}$ in nitrogen ($\gamma = 0.05$, $\omega = 1\text{ Hz}$). (TA AR-2000 Instrument)	134

Figure 5-10. η^* as a function of temperature for PIBSI-A and PIBSI-B (65-75 %) dispersions with MicroCB (35-25 %)-(RDA-III instrument), (25 %) (TA AR-2000 instrument)	135
Figure 5-11: Evolution of ^1H NMR $\Delta H_{1/2}$ with temperature for PIB, PIBSA, PIBSI-A and PIBSI-B using a heating rate of $3\text{ }^\circ\text{C min}^{-1}$ in nitrogen	137
Figure 5-12: Evolution of the ^1H NMR $\Delta H_{1/2}$ with temperature for PIB, PIBSA, PIBSI-A and PIBSI-B (65 %)-MicroCB (35 %) dispersions using a heating rate of $3\text{ }^\circ\text{C min}^{-1}$ in nitrogen. Error bars are to 1 standard deviation of the sample mean.....	139
Figure 5-13: Evolution of the ^1H NMR $\Delta H_{1/2}$ with temperature for PIB, PIBSA, PIBSI-A and PIBSI-B (75 %) MicroCB (25 %) dispersions using a heating rate of $3\text{ }^\circ\text{C min}^{-1}$ in nitrogen.	140
Figure 5-14: Evolution of the ^1H NMR $\Delta H_{1/2}$ with temperature for PIBSI-A and PIBSI-B MicroCB dispersions at various concentrations (polymer 100-65 %, MicroCB (0-35 %)).	141
Figure 6-1: Weight percentage loss as a function of temperature using a heating rate of $3\text{ }^\circ\text{C min}^{-1}$ for PIB, PIBSA (A-C), PIBSI (A-E) in nitrogen.	147
Figure 6-2: Weight percentage loss as a function of temperature using a heating rate of $3\text{ }^\circ\text{C min}^{-1}$ for PIBSI (F-K) in nitrogen.	147
Figure 6-3: η^* values at $250\text{ }^\circ\text{C}$ as a function of polymer % for various PIB and PIBSI-A MicroCB dispersions.....	150
Figure 6-4: ^1H NMR $\Delta H_{1/2}$ values at $250\text{ }^\circ\text{C}$ as a function of polymer % for various PIB and PIBSI-A MicroCB dispersions.....	151
Figure 6-5: η^* values at $250\text{ }^\circ\text{C}$ as a function of polymer % for various PIBSI-C and PIBSI-D MicroCB dispersions.....	152
Figure 6-6: ^1H NMR $\Delta H_{1/2}$ values at $250\text{ }^\circ\text{C}$ as a function of polymer % for various PIBSI-C and PIBSI-D MicroCB dispersions.	153
Figure 6-7: η^* values at $250\text{ }^\circ\text{C}$ as a function of polymer % for various PIBSI-C and PIBSI-E MicroCB dispersions.	155

Figure 6-8: ^1H NMR $\Delta H_{1/2}$ values at 250 °C as a function of polymer % for various PIBSI-C and PIBSI-E MicroCB dispersions.	156
Figure 6-9: η^* values at 250 °C as a function of polymer % for various PIBSI-G and PIBSI-H MicroCB dispersions.	157
Figure 6-10: ^1H NMR $\Delta H_{1/2}$ values at 250 °C as a function of polymer % for various PIBSI-G and PIBSI-H MicroCB dispersions.	158
Figure 6-11: η^* values at 250 °C as a function of polymer % for various PIBSI-D and PIBSI-F MicroCB dispersions.	159
Figure 6-12: η^* as a function of temperature for PIBSI-D and PIBSI-F (75%) MicroCB (25%) dispersions, using a heating rate of 3 °C min ⁻¹ in nitrogen ($\gamma = 0.05$, $\omega = 1$ Hz). (TA-2000 instrument).	160
Figure 6-13: η^* values at 200 °C as a function of polymer % for various PIBSI-D and PIBSI-F MicroCB dispersions.	161
Figure 6-14: ^1H NMR $\Delta H_{1/2}$ values at 250 °C as a function of polymer % for various PIBSI-D and PIBSI-F MicroCB dispersions.	162
Figure 6-15: ^1H NMR $\Delta H_{1/2}$ values at 200 °C as a function of polymer % for various PIBSI-D and PIBSI-F MicroCB dispersions.	163
Figure 6-16: η^* values at 250 °C as a function of polymer % for various polymer MicroCB dispersions.	164
Figure 6-17: ^1H NMR $\Delta H_{1/2}$ values at 250 °C as a function of polymer % for various polymer MicroCB dispersions.	164
Figure 6-18: η^* values at 250 °C as a function of polymer % for various polymer MicroCB dispersions.	165
Figure 6-19: ^1H NMR $\Delta H_{1/2}$ values at 250 °C as a function of polymer % for various polymer MicroCB dispersions.	166
Figure 6-20: ^1H NMR $\Delta H_{1/2}$ values at 250 °C as a function of polymer % for various PIB and PIBSI-A MicroCB dispersions.	168

Figure 6-21: ^{13}C NMR spectra of various PIBSI-A MicroCB dispersions (ambient temperature).....	169
Figure 6-22: Evolution of the ^1H NMR $\Delta\text{H}_{1/2}$ with temperature for 3 duplicate PIBSI-A (5 %) Micro CB (95 %) dispersions (A, B, C).	171
Figure 6-23: Evolution of the mean ^1H NMR $\Delta\text{H}_{1/2}$ with temperature for duplicate analysis of PIBSI-A (5 %) Micro CB (95 %) dispersions (A, B, C). Error bars are to 1 standard deviation of the sample mean.	171
Figure 6-24: ^1H NMR $\Delta\text{H}_{1/2}$ values at 250 °C as a function of polymer % for various PIBSI-C and PIBSI-D MicroCB dispersions.	172
Figure 6-25: ^1H NMR $\Delta\text{H}_{1/2}$ values at 250 °C as a function of polymer % for various polymer MicroCB dispersions.....	173
Figure 6-26: ^1H NMR $\Delta\text{H}_{1/2}$ values at 250 °C as a function of polymer % for various polymer (PIBSI-D, K) MicroCB dispersions.	174
Figure 6-27: ^1H NMR $\Delta\text{H}_{1/2}$ values at 250 °C as a function of polymer % for various polymer (PIBSI-G, I) MicroCB dispersions.	175
Figure 6-28: ^1H NMR $\Delta\text{H}_{1/2}$ values at 250 °C as a function of polymer % for various polymer (PIBSI-G, H) MicroCB dispersions.	176
Figure 6-29: ^1H NMR $\Delta\text{H}_{1/2}$ values at 250 °C as a function of polymer % for various polymer (PIBSI-D, F, J) MicroCB dispersions.	177
Figure 6-30: ^1H NMR $\Delta\text{H}_{1/2}$ values at 250 °C as a function of polymer % for various polymer (PIBSA-A, B, C,) MicroCB dispersions.....	178
Figure 6-31: ^1H NMR $\Delta\text{H}_{1/2}$ values at 250 °C as a function of polymer % for various polymer (PIBSI-I, K) MicroCB dispersions.	179
Figure 6-32: ^1H NMR $\Delta\text{H}_{1/2}$ values at 250 °C as a function of polymer % for various polymer MicroCB dispersions.....	181
Figure 6-33: ^1H NMR $\Delta\text{H}_{1/2}$ values at 250 °C as a function of the polar surface area of the polymer head groups for various polymer MicroCB dispersions.....	183

Figure 6-34: ^1H NMR $\Delta H_{1/2}$ values at 250 °C as a function of the molecular weight of the PIB backbone (PIB- M_n) for various polymer MicroCB dispersions.	184
Figure 6-35: ^1H NMR $\Delta H_{1/2}$ values at 250 °C as a function of the number average molecular weight (M_n) for various polymer MicroCB dispersions.	185
Figure 6-36: ^1H NMR $\Delta H_{1/2}$ values at 250 °C as a function of the weight average molecular weight (M_w) for various polymer MicroCB dispersions.	187
Figure 7-1: ^1H NMR $\Delta H_{1/2}$ values at 250 °C as a function of polymer % for various polymer (PIBSI-F, H) -Carbon dispersions.	192
Figure 7-2: ^1H NMR $\Delta H_{1/2}$ values at 250 °C as a function of the average particle size of the carbon for various polymer (PIBSI-F,H)- carbon dispersions.	194
Figure 7-3: ^1H NMR $\Delta H_{1/2}$ values at 250 °C as a function of the surface area of the carbon for various polymer (PIBSI-F, H) - carbon dispersions.....	195
Figure 7-4: ^1H NMR $\Delta H_{1/2}$ values at 250 °C as a function of the peak CO_2 emission temperature of the carbon for various polymer (PIBSI-F,H)- carbon dispersions.....	197
Figure 7-5: Peak CO_2 emission temperature (via TPO) against carbon surface composition (via XPS)	199
Figure 7-6: ^1H NMR $\Delta H_{1/2}$ values at 250 °C as a function of the carbon surface composition of the carbon for various polymer (PIBSI-F,H)- carbon dispersions.	200
Figure 7-7: ^1H NMR $\Delta H_{1/2}$ values at 250 °C as a function of the oxygen surface composition of the carbon for various polymer (PIBSI-F,H)- carbon dispersions.	201
Figure 7-8: ^1H NMR $\Delta H_{1/2}$ values at 250 °C as a function of polymer % for various polymer -Micro850 dispersions.	202
Figure 7-9: ^1H NMR $\Delta H_{1/2}$ values at 250 °C as a function of polymer % for various polymer (PIBSI-D, F) -Micro850 or MicroCB dispersions.....	203
Figure 7-10: ^1H NMR $\Delta H_{1/2}$ values at 250 °C as a function of polymer % for various polymer (PIBSI-D, K) -Micro850 or MicroCB dispersions.	204
Figure 7-11: ^1H NMR $\Delta H_{1/2}$ values at 250 °C as a function of polymer % for various polymer (PIBSI-G, H) -Micro850 or MicroCB dispersions.	205

Figure 7-12: ^1H NMR $\Delta H_{1/2}$ values at 250 °C as a function of polymer % for various polymer (PIBSI-I, K) -Micro850 or MicroCB dispersions.	206
Figure 7-13: ^1H NMR $\Delta H_{1/2}$ values at 250 °C as a function of polymer % for various polymer (PIBSI-G, I) -Micro850 or MicroCB dispersions.	207
Figure 7-14: ^1H NMR $\Delta H_{1/2}$ values at 250 °C as a function of polymer % for various polymer -Micro850 dispersions.	208
Figure 7-15: ^1H NMR $\Delta H_{1/2}$ values at 250 °C as a function of the polar surface area of the polymer head groups for various polymer MicroCB dispersions.	210
Figure 7-16: ^1H NMR $\Delta H_{1/2}$ values at 250 °C as a function of the molecular weight of the PIB backbone (PIB- M_n) for various polymer MicroCB dispersions.	211
Figure 7-17: ^1H NMR $\Delta H_{1/2}$ values at 250 °C as a function of the number average molecular weight (M_n) for various polymer MicroCB dispersions.	212
Figure 7-18: ^1H NMR $\Delta H_{1/2}$ values at 250 °C as a function of the weight average molecular weight (M_w) for various polymer MicroCB dispersions.	213
Figure B-1: Storage (G') and loss (G'') moduli as a function of strain (γ) at 100 °C for PIB 45% MicroCB 55% dispersion.	223
Figure B-2: Storage (G') and loss (G'') moduli as a function of strain (γ) at 250 °C for PIB 45% MicroCB 55% dispersion.	223
Figure B-3: Storage (G') and loss (G'') moduli as a function of strain (γ) at 350 °C for PIB 45% MicroCB 55% dispersion.	224
Figure B-4: Storage (G') and loss (G'') moduli as a function of strain (γ) at 100 °C for PIB 65% MicroCB 35% dispersion.	224
Figure B-5: Storage (G') and loss (G'') moduli as a function of strain (γ) at 250 °C for PIB 65% MicroCB 35% dispersion.	225
Figure B-6: Storage (G') and loss (G'') moduli as a function of strain (γ) at 350 °C for PIB 65% MicroCB 35% dispersion. (350°C)	225
Figure B-7 : Storage (G') and loss (G'') moduli as a function of strain (γ) at 100 °C for PIBSI-A 45% MicroCB 55% dispersion.	226

Figure B-8: Storage (G') and loss (G'') moduli as a function of strain (γ) at 250 °C for PIBSI-A 45% MicroCB 55% dispersion.	226
Figure B-9: Storage (G') and loss (G'') moduli as a function of strain (γ) at 350 °C for PIBSI-A 45% MicroCB 55% dispersion.	227
Figure B-10: Storage (G') and loss (G'') moduli as a function of strain (γ) at 100 °C for PIBSI-A 65% MicroCB 35% dispersion.	227
Figure B-11: Storage (G') and loss (G'') moduli as a function of strain (γ) at 250 °C for PIBSI-A 65% MicroCB 35% dispersion.	228
Figure B-12: Storage (G') and loss (G'') moduli as a function of strain (γ) at 350 °C for PIBSI-A 65% MicroCB 35% dispersion.	228
Figure C-1: Duplicate samples of PIB (65 %) and MicroCB (35 %) (A, B, C) using a heating rate of 3 °C min ⁻¹ in nitrogen ($\gamma = 0.05$, $\omega = 1$ Hz). (RDA-III instrument).....	229
Figure C-2: Duplicate samples of PIBSA-A (65 %) and MicroCB (35 %) (A, B, C, D) using a heating rate of 3 °C min ⁻¹ in nitrogen ($\gamma = 0.05$, $\omega = 1$ Hz). (RDA-III instrument). ..	229
Figure C-3: Duplicate samples of PIBSI-A (65 %) and MicroCB (35 %) (1-4) using a heating rate of 3 °C min ⁻¹ in nitrogen ($\gamma = 0.05$, $\omega = 1$ Hz). (RDA-III instrument).....	230
Figure C-4: Duplicate samples of PIBSA-B (65 %) and MicroCB (35 %) (A, B, C, D) using a heating rate of 3 °C min ⁻¹ in nitrogen ($\gamma = 0.05$, $\omega = 1$ Hz). (RDA-III instrument). ..	230
Figure D-1: η^* as a function of temperature for various PIB and MicroCB dispersions, using a heating rate of 3 °C min ⁻¹ in nitrogen ($\gamma = 0.05$, $\omega = 1$ Hz).	231
Figure D-2: Complex viscosity (η^*) as a function of temperature for various PIBSI-A and MicroCB dispersions, using a heating rate of 3 °C min ⁻¹ in nitrogen ($\gamma = 0.05$, $\omega = 1$ Hz).	231
Figure D-3: η^* as a function of temperature for various PIBSI-C MicroCB dispersions, using a heating rate of 3 °C min ⁻¹ in nitrogen ($\gamma = 0.05$, $\omega = 1$ Hz).....	232
Figure D-4: η^* as a function of temperature for various PIBSI-D MicroCB dispersions, using a heating rate of 3 °C min ⁻¹ in nitrogen ($\gamma = 0.05$, $\omega = 1$ Hz).....	232

Figure D-5: η^* as a function of temperature for various PIBSI-E MicroCB dispersions, using a heating rate of 3 °C min ⁻¹ in nitrogen ($\gamma = 0.05$, $\omega = 1$ Hz).....	233
Figure D-6: η^* as a function of temperature for various PIBSI-F MicroCB dispersions, using a heating rate of 3 °C min ⁻¹ in nitrogen ($\gamma = 0.05$, $\omega = 1$ Hz).....	233
Figure D-7: η^* as a function of temperature for various PIBSI-G MicroCB dispersions, using a heating rate of 3 °C min ⁻¹ in nitrogen ($\gamma = 0.05$, $\omega = 1$ Hz).....	234
Figure D-8: η^* as a function of temperature for various PIBSI-H MicroCB dispersions, using a heating rate of 3 °C min ⁻¹ in nitrogen ($\gamma = 0.05$, $\omega = 1$ Hz).....	234
Figure E-1: Evolution of the ¹ H NMR $\Delta H_{1/2}$ with temperature for 3 duplicate PIB (65 %) Micro CB (35 %) dispersions (A, B, C)	235
Figure E-2: Evolution of the ¹ H NMR $\Delta H_{1/2}$ with temperature for 3 duplicate PIBSA-A (65 %) Micro CB (35 %) dispersions (A, B, C)	235
Figure E-3 Evolution of the ¹ H NMR $\Delta H_{1/2}$ with temperature for 3 duplicate PIBSI-A (65 %) Micro CB (35 %) dispersions (A, B, C)	236
Figure F-1: Evolution of the ¹ H NMR $\Delta H_{1/2}$ with temperature for PIB (100 – 2.5 %) MicroCB (0 -97.5 %) dispersions	237
Figure F-2: Evolution of the ¹ H NMR $\Delta H_{1/2}$ with temperature for PIBSA-A (100 – 5 %) MicroCB (0 -95 %) dispersions.....	237
Figure F-3: Evolution of the ¹ H NMR $\Delta H_{1/2}$ with temperature for PIBSA-B (25 – 5 %) MicroCB (75 -95 %) dispersions.....	238
Figure F-4: Evolution of the ¹ H NMR $\Delta H_{1/2}$ with temperature for PIBSA-C (25 – 5 %) MicroCB (75 - 95 %) dispersions	238
Figure F-5: Evolution of the ¹ H NMR $\Delta H_{1/2}$ with temperature for PIBSI-A (100 – 5 %) MicroCB (0 - 95 %) dispersions.....	239
Figure F-6: Evolution of the ¹ H NMR $\Delta H_{1/2}$ with temperature for PIBSI-B (100 – 5 %) MicroCB (0 - 95 %) dispersions.....	239
Figure F-7: Evolution of the ¹ H NMR $\Delta H_{1/2}$ with temperature for PIBSI-C (75 – 5 %) MicroCB (25 - 95 %) dispersions	240

Figure F-8: Evolution of the ^1H NMR $\Delta H_{1/2}$ with temperature for PIBSI-D (75 – 5 %) MicroCB (25 - 95 %) dispersions	240
Figure F-9: Evolution of the ^1H NMR $\Delta H_{1/2}$ with temperature for PIBSI-E (75 – 5 %) MicroCB (25 - 95 %) dispersions	241
Figure F-10: Evolution of the ^1H NMR $\Delta H_{1/2}$ with temperature for PIBSI-F (75 – 5 %) MicroCB (25 - 95 %) dispersions	241
Figure F-11: Evolution of the ^1H NMR $\Delta H_{1/2}$ with temperature for PIBSI-G (75 – 5 %) MicroCB (25 - 95 %) dispersions	242
Figure F-12: Evolution of the ^1H NMR $\Delta H_{1/2}$ with temperature for PIBSI-H (75 – 5 %) MicroCB (25 - 95 %) dispersions	242
Figure F-13: Evolution of the ^1H NMR $\Delta H_{1/2}$ with temperature for PIBSI-I (25 – 5 %) MicroCB (75 - 95 %) dispersions	243
Figure F-14: Evolution of the ^1H NMR $\Delta H_{1/2}$ with temperature for PIBSI-J (25 – 5 %) MicroCB (75 - 95 %) dispersions	243
Figure F-15: Evolution of the ^1H NMR $\Delta H_{1/2}$ with temperature for PIBSI-K (25 – 5 %) MicroCB (75 - 95 %) dispersions	244
Figure G-1: Evolution of the ^1H NMR $\Delta H_{1/2}$ with temperature for various PIBSI-H (5 %) carbon (95 %) dispersions	245
Figure G-2: Evolution of the ^1H NMR $\Delta H_{1/2}$ with temperature for various PIBSI-H (15 %) carbon (85 %) dispersions	245
Figure G-3: Evolution of the ^1H NMR $\Delta H_{1/2}$ with temperature for various PIBSI-H (25 %) carbon (75 %) dispersions	246
Figure G-4: Evolution of the ^1H NMR $\Delta H_{1/2}$ with temperature for various PIBSI-F (5 %) carbon (95 %) dispersions	246
Figure G-5: Evolution of the ^1H NMR $\Delta H_{1/2}$ with temperature for various PIBSI-F (15 %) carbon (85 %) dispersions	247
Figure G-6: Evolution of the ^1H NMR $\Delta H_{1/2}$ with temperature for various PIBSI-F (25 %) carbon (75 %) dispersions	247

Figure H-1: Evolution of the ^1H NMR $\Delta H_{1/2}$ with temperature for PIBSI-C (25 - 5 %) Micro850 (75 - 95 %) dispersions	248
Figure H-2: Evolution of the ^1H NMR $\Delta H_{1/2}$ with temperature for PIBSI-D (25 - 5 %) Micro850 (75 - 95 %) dispersions	248
Figure H-3: Evolution of the ^1H NMR $\Delta H_{1/2}$ with temperature for PIBSI-G (25 - 5 %) Micro850 (75 - 95 %) dispersions	249
Figure H-4: Evolution of the ^1H NMR $\Delta H_{1/2}$ with temperature for PIBSI-I (25 - 5 %) Micro850 (75 - 95 %) dispersions	249
Figure H-5: Evolution of the ^1H NMR $\Delta H_{1/2}$ with temperature for PIBSI-K (25 - 5 %) Micro850 (75 - 95 %) dispersions	250

Nomenclature

AEP	Aminoethylpiperazine
BET	Brunauer-Emmet-Teller
BP	Boiling Point
Calcoke	Calcined Petroleum Coke
CB	Carbon Black
CMC	Critical Micelle Concentration
DCAs	Deposit Control Additives
DegCB	Degussa Carbon Black
DETA	Diethylene triamine
DMAPA	Dimethyleaminopropylamine
EDA	Ethylenediamine
EU	European Union
FAME	Fatty Acid Methyl Esters
FID	Free Induction Decay
FIE	Fuel Injection Equipment
FT-IR	Fourier Transform Infrared
GPC	Gel Permeation Chromatography
Hypermer B246	PEG 30-dipolyhydroxystearate
Hypermer LP1	Polyhydroxystearic acid
IB	Isobutene
IDIDs	Internal Diesel Injector Deposits
Kel-F	Chlorotrifluoroethene
LCST	Lower Critical Solution Temperature
MA	Maleic Anhydride
MAS	Magic Angle Spinning
Micro146	Flake Graphite ¹⁴⁶
Micro450	Synthetic Graphite ⁴⁵⁰

Micro850	Flake Graphite850
MicroCB	Mesoporous Carbon Black
MW	Molecular Weight
NMR	Nuclear Magnetic Resonance
PD	Polydispersity
PEHA	Pentaethylenhexamine
PIB	Polyisobutylene
PIB Func.	PIB Functionality
PIB-Mn	Number Average Molecular Weight of PIB backbone
PIBs	Polyisobutylenes
PIBSA	Polyisobutylene Succinic Anhydride
PIBSI	Polyisobutylene Succinimide
PSA	Polar Surface area
RF	Radio Frequency
SEC	Size Exclusion Chromatography
SEM	Scanning Electron Microscope
SPE	Single Pulse Excitation
TEPA	Tetraethylene pentamine
TETA	Triethylenetetramine
TGA	Thermogravimetric Analysis
THF	Tetrahydrofuran
TKS	Tetrakis(trimethylsilyl) silane
Tof-SIMS	Time-of-flight Secondary Ion Mass Spectrometry
TPO	Temperature Programmed Oxidation
TPSA	Topological Polar Surface Area
ULSD	Ultra-low Sulphur Diesel
UoN	University of Nottingham
XPS	X-ray Photoelectron Spectroscopy

1 Introduction

1.1 BACKGROUND

1.1.1 Engine emission standards

Stringent vehicle emission standards imposed by the European Union (EU) limit the amount of pollutants allowed to be released by petrol and diesel engines. These limits are known as the Euro standards and the latest legislation (Euro VI) approved for light passenger vehicles in January 2013 (European Parliament, 2007) limits emissions of CO to 500 mg/km and 1000 mg/km for diesel and petrol engines respectively. Nitrous oxides (NO_x) are limited to 80 mg/km for diesel engines and 60 mg/km for petrol engines and for both petrol and diesel engines with direct injection, particulate matter is limited to 5 mg/km. The emission of hydrocarbons is also limited by the EU standards. Given the increasingly stringent measures to cap emissions the technology used in diesel engines, with particular focus on the fuel injection equipment (FIE), has had to become increasingly more finely engineered in order to meet these regulations (environmental protection uk, 2015) (European Parliament, 2007).

1.1.2 Fuel injection systems

After over a century of development, FIE technology has come a long way since Rudolf Diesel first developed the original working prototype of the diesel engine as a means to improve the efficiency of the internal combustion engine. The concept was that by adding fuel at a controlled rate to compressed air the rate of heat released and the maximum cylinder temperature could both be more closely controlled. Over one hundred years later the same basic principles of the diesel engine remains despite obviously being far more sophisticated (Barker, Richards, Pinch, & Cheeseman, 2010).

To achieve the new emission standards engineers have had to develop engines that are increasingly more precise particularly within the FIE which has recently

had to rapidly evolve with developments such as higher fuel injection pressures and smaller injection orifices (Barker, Richards, Snape, & Meredith, 2009b). The most recent diesel engines use common rail fuel injection systems which are currently adopted by all automotive companies that produce passenger cars (Petruzzelli, 2013). The term "common rail" is used because multiple fuel injectors are supplied with high pressure fuel by the same rail (or accumulator). The injectors are electronically controlled and once activated fuel is sprayed at the desired pressure into the combustion chamber (Petruzzelli, 2013). These systems operate at increasingly higher temperatures and pressures with diesel common rail systems up to 3,000 bar currently in development (Denso, 2013). As a consequence of the harsher operating conditions the latest FIE technology has been found to be less tolerant to deposit formation than its less finely engineered predecessors, with an increase in the number of reports of deposits being found in injector needles and tips as well as filters, which can be detrimental to the performance of the engine (Barker, Langley, & Richards, 2010).

1.1.3 Fuel injection equipment deposits

Fuel filtrations systems are used to prevent the passage of solid contaminants within the fuel from reaching the injectors which can affect their performance. However due to the high temperatures and pressures that direct injection systems are exposed to the fuel can undergo chemical change within the fuel injectors leading to more solid like deposits (Barker, Richards, Pinch, & Cheeseman, 2010). Build-up of carbonaceous deposits on the parts of the injector exposed to hot combustion gases which can affect both the fuel flow and atomisation resulting in decreased engine performance (Owen, 1989). The other main type of deposit concerns the build-up of gum or resinous degradation products in the injection system leading to valve sticking on the pump plunges and the injector pintles or needles (Owen, 1989). In the US the issue is predominantly the build-up of carbonaceous deposits whereas in Europe the concern is more about internal

lacquer formation (Barker & Cook, 2013). Variation between the refinery and fuel distribution technologies in the US and Europe as well as differences in the diesel vehicle fleet could exaggerate the apparent differences in the type of deposit (Barker & Cook, 2013). In addition to the harsher conditions that the fuels are exposed to, recent increase of the use of ultra-low sulphur diesel (ULSD) and biofuels which themselves are being introduced to cut emissions and maximise resources have coincided with the reports regarding FIE deposits making the situation even more complex (Barker, Langley, & Richards, 2010). Scanning electron microscope (SEM) images of a clean and fouled injector needle are shown in Figure 1-1 (A) and (B) respectively (Barker, Richards, Snape, & Meredith, 2011) and images showing the potential effects on fuel atomisation are shown in Figure 1-1 (C) and (D) (ATC, 2013).

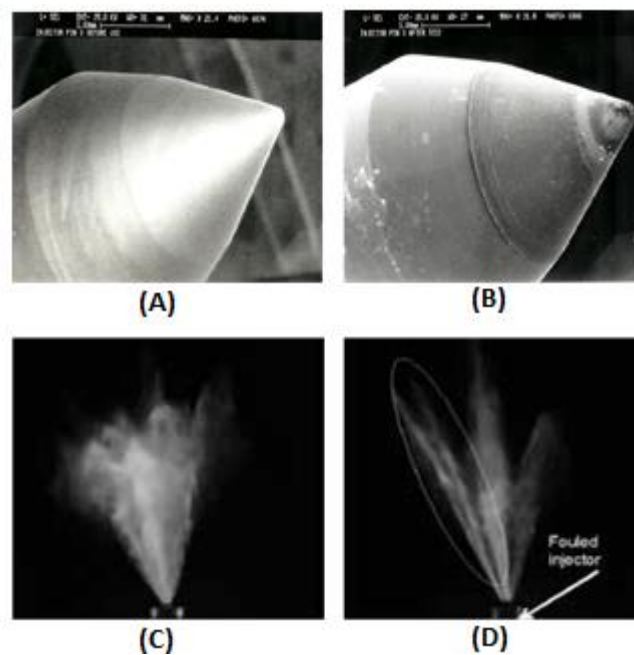


Figure 1-1: (A) Clean injector needle, (B) fouled injector needle (Barker, Richards, Snape, & Meredith, 2011), (C) homogeneous fuel spray from clean injector, (D) inhomogeneous fuel spray from fouled injector (ATC, 2013).

1.1.4 Introduction to fuel additives

The increased pressure on vehicle manufactures to improve engine efficiencies and lower emissions has seen the fuel additives industry become ever more competitive. The EU27 market for fuel additives is over 200,000 tons per annum with a value of over €500 million (ATC, 2013). It is estimated that over 95% of road retail fuel (both gasoline and diesel) is treated with performance additives with a wide range of fuel additive products available with different functions in different areas of fuel use. These include problems encountered at a refinery, distribution systems, storage tanks or various transport applications. They can be used as a single stand-alone product with a specific task or maybe combined with other products to form a multi-functional package for use in finished fuels for the automotive industry (ATC, 2013). Automotive performance enhancement products include deposit control additives, cetane improvers, lubricity additives, friction modifiers, antifoam additives, corrosion inhibitors, demulsifiers and dehazers, anti-valve seat recession additives and fuel borne catalysts for particulates filters. Fuel additive treatment levels are low with some used at single figure mg/kg (ppm) levels (ATC, 2013).

1.1.5 Deposit control additives

Deposit control additives (DCAs) are designed to maintain the cleanliness of the fuel systems. DCAs for both diesel and gasoline systems are very similar usually consisting of a polar head group with an affinity for carbonaceous deposits and metal surfaces and hydrocarbon tail which protrudes into the fuel enabling the additive to be fully soluble (ATC, 2013).

Typical diesel DCAs contain molecules such as amines, imidazolines, amides, fatty acid succinimides, polyalkylenes succinimides, polyalkylene amines and polyether amines (Owen, 1989) whereas gasoline DCAs contain molecules such as amides, amines, polybutene succinimides, polyether amines, poly olefin amines and

Mannich amines (ATC, 2013). Gasoline DCAs generally maintain the cleanness of the entire fuel systems particular the intake valves and fuel injectors. Within diesel engines the intake valves do not come into contact with liquid fuel therefore with diesel DCAs, the most significant focus lies in the fuel injector which atomises the liquid fuel being delivered into the combustion chamber just before the combustion of the fuel during each power stroke (ATC, 2013). DCAs of both types have three main functions: a surfactant or protection action which provides a film barrier to critical surfaces, dispersancy action which helps to prevent agglomeration of particles and detergency action which enables additives to dissolve pre-formed deposits by altering the equilibrium between the deposit accumulation and removal mechanisms (Owen, 1989). DCAs are intended to be used on a continual basis and typical treatment levels are 10 – 200 mg/kg although this can higher if intended for existing deposit clean up. The various DCA mechanisms are shown in Figure 1-2.

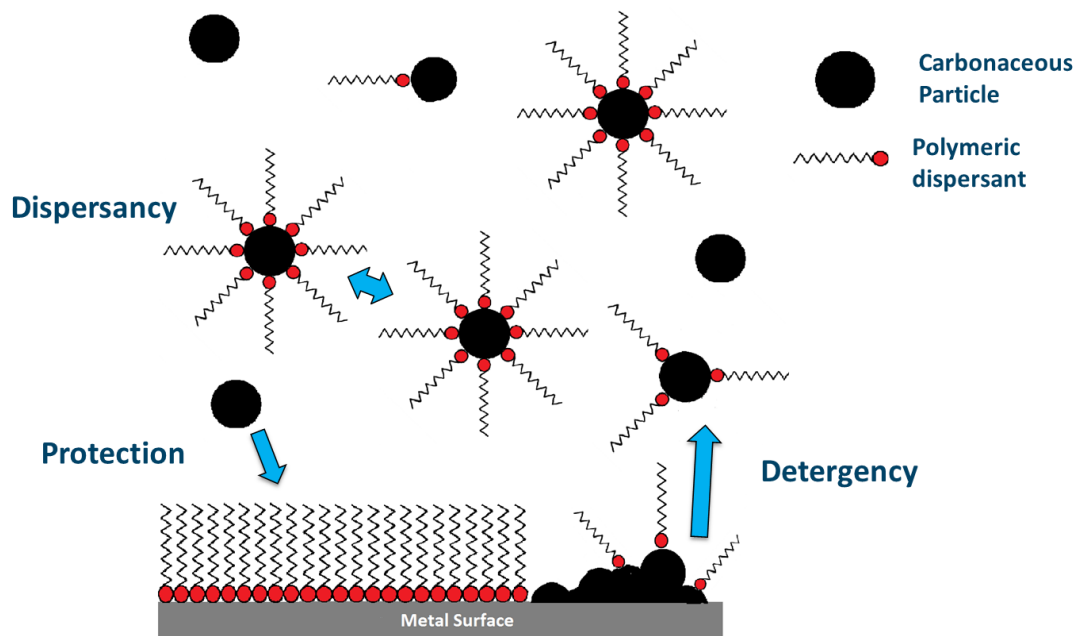


Figure 1-2: Deposit control additive mechanism

1.1.6 Polyisobutylene and its derivatives

If a molecule is to be utilised as a DCA it must meet certain criteria. Firstly, it must be able to perform effectively under the high temperature operating conditions of the engine. The additive must also undergo complete combustion along with the fuel so as to not add to the deposits it is trying to prevent (these are referred to as ash-less dispersants). The additive must be non-toxic to satisfy environmental and health legislation and have high chemical resistivity to prevent any unwanted by-products. Finally, the fuel additive must be economical enough to be used on a commercial scale. Polyisobutylenes (PIBs) chemical resistivity, non-toxicity and high thermal stability makes them suitable as precursors to polymeric surfactants for use in fuel and oil additives (Li, Cokoja, & Kuhn, 2011). Two derivatives of PIBs that are commonly used as precursors to commercial dispersants are polyisobutylene succinic anhydride (PIBSA) and polyisobutylene succinimide (PIBSI) which can be modified with various sizes of amine groups that can provide the functionality to anchor to the carbon particles. The term PIBSI can cover a multitude of different chemical structures which can sometimes lead to confusion. PIBSI includes any species which has been synthesised from polyisobutylene (PIB) of any molecular weight distribution and has been reacted with maleic anhydride to form polyisobutylene succinic anhydride (PIBSA) which is then reacted with an amine to form the PIBSI. The amine may be any amine that contains at least one primary nitrogen atom group capable of reacting with the anhydride (Reid & Barker, 2013). The functionalisation of the PIBSI molecules facilitates the adsorption of the polymers at the surface of solid carbonaceous particles and acidic materials, such as oxidised aromatics that precipitate out of the fuel, as well as to the surface of the metal wall of engines (Chevalier, 2004). The structures of PIB, PIBSA and PIBSI are shown in Figure 1-3.

$$V_A(h) = -\frac{a H_{121}}{12 h} \quad (1-1)$$

where H_{121} is the Hamaker coefficient.

Colloidal stability of suspensions of the particles may therefore be achieved by the interposition of repulsive forces of significant magnitude to overcome these forces (Barrett, 1985). This can be achieved electrostatically or sterically or a combination of both. Figure 1-4 shows the total potential energy (V_t) diagram for two colloidal particles. The total potential energy curve is characterised by a potential energy maximum (V_m) which functions as an activation energy. The potential energy minimum arises from short range overlap repulsive forces. The secondary minimum is due to the fall-off in repulsive potential energy being more rapid than that of the attractive potential energy.

If particles have a surface charge then an atmosphere of counter-ions and co-ions form around each particle forming an electrical double layer. The stability of the dispersion is dependent on the properties of this double layer. When the electrical double layers for like-charged particles overlap, a repulsive inter-particle potential arises. This acts to stabilise the dispersion, and is known as electrostatic stabilisation. When the attractive (London dispersion force) potential energy and the repulsive (electrostatic) force are combined a quantitative theory of stability known as DLVO theory can be formulated. The total potential energy (V_T) in DLVO theory is calculated by adding together the attractive potential energy (V_A) and the repulsive potential energy (V_R) as shown in Equation (1-2) (Napper, 1970).

$$V_T = V_R + V_A \quad (1-2)$$

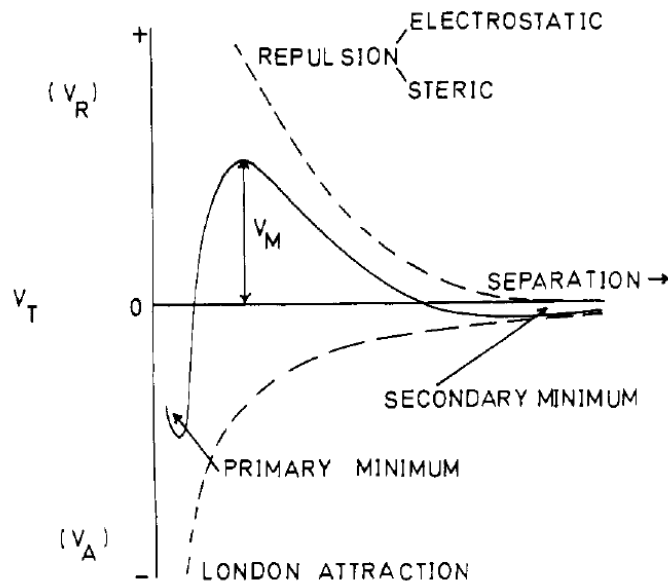


Figure 1-4: Total Potential energy (V_t) diagram for two colloidal particles (Napper, 1970)

Steric stabilisation can be achieved when polymers adsorb onto the surface of the particles and extend far enough into the medium that when particles agglomerate they are kept far enough apart by the chains that the London dispersion force attractions do not become strong enough to hold the particles together (Pugh, Matsunaga, & Fowkes, 1983). This can be achieved using polymer dispersants such as PIBSI which consist of an attractive head group that anchors to the particle, and a hydrocarbon chain that protrudes into the fuel. The polymer dispersants thus surround the particles and the polymer layer prevents particles coming into contact with each other. This also ensures that at the distance of closest approach, the attraction between them is small enough that thermal energy renders contact reversible (Barrett, 1985). The repulsive force that brings about the stabilisation of the particles is considered to be mostly achieved through steric hindrance although some studies suggest electrostatic forces may play a role (Kornbrekke, Morrison & Oja et al., 1992).

1.1.8 Polymer adsorption

Polymer adsorption on particles can be used to influence the interparticle forces.

The adsorption energy depends on the nature of the substrate and the solvent and may be driven by covalent or ionic bonds, polar or van der Waals forces.

The forces are short range (in the order of Angströms) and only effect segments that are very close to the surface. Randomly attached polymers can be described in terms of three types of subchains: *trains* which have all their units in contact with the interface, *loops* which connect two trains and have no contact with the surface and *tails* which are non-adsorbing chain ends (Fleer et al., (1993). With terminally or end attached polymers the attachment may be through a single group (ionic or chemically selective) or a block of segments (such as with a block copolymer). The amount of surface coverage (adsorbed amount) will affect the behaviour of the conformation of the polymer chains. At very low surface coverage the chains have a tendency to flatten so that the conformation of the adsorbed chains is unperturbed; the gyration radius of the adsorbed polymer coils is the same as in dilute solution which is known as the mushroom regime. At the other extreme, at high surface coverage, lateral interactions of adjacent polymer chains will force the chains to stretch perpendicular to the surface (known as the brush regime) (Chevalier et al., (2004). In both cases, conformation of the polymer chains are affected by the interaction with the surface, the solvent and each other.

1.2 MOTIVATION FOR THIS STUDY

The theories describing the mechanisms of PIB based carbon dispersancy are almost all based on studies conducted at ambient temperatures usually based around adsorption. Studies of the polymers using high temperature analytical methods will therefore allow insight into the dispersancy mechanism in the temperature range that is within the polymers normal sphere of operation. A long term goal is to develop reliable and inexpensive laboratory techniques that are able to accurately predict the behaviour of these dispersants without having to rely upon expensive full scale engine tests. Also, a thorough understanding of these polymers will aid in the development of the next generation of fossil fuel

engine additives which can help in maintaining engine efficiencies and the lowering of harmful emissions.

1.3 SPECIFIC PROJECT AIMS AND OBJECTIVES

High temperature rheometry and ^1H NMR have previously been used in combination to study the fluidity of coal samples during coking and the pyrolysis of biomass polymers. This research presents for the first time a study of PIB type dispersions using both these high temperature techniques. The first aim of this project is therefore to optimise the conditions for sample preparation and analytical methodologies in order to produce reproducible analysis with the high temperature rheometry and ^1H NMR. This will be investigated using dispersions of polyisobutylene succinimide (PIBSI) and carbon black which has been known to mimic the properties of engine deposits (Clague & Donnet, 1999).

Once conditions for sample preparation and analysis have been established the next aim is to characterise dispersions of a carbon black with PIB, PIBSA and PIBSI in an attempt to investigate whether the different dispersions can be distinguished using the techniques. The range of polymers will then be expanded to include the effects of the size of the polar head groups and the length of the PIB hydrocarbon chains as well as the dispersion behaviour at various polymer/carbon concentrations. The final aim of this work is to investigate the effects of the carbon properties on the dispersion behaviour by analysing dispersions containing different deposit surrogates and attempting to relate the properties to the analysis results.

2 Literature Review

The aim of this literature review is to examine the research that has been carried out on engine deposit formation and the PIB derivatives that are manufactured to prevent their formation through dispersion. Special attention will be made to thermally induced effects as to suit the conditions that are within the polymers normal sphere of operation.

2.1 ENGINE DEPOSIT FORMATION AND STRUCTURE

2.1.1 Introduction

Fuel injection equipment (FIE) has had to rapidly evolve to meet emission standards with developments such as higher fuel injection pressures and smaller injection orifices (Barker et al., 2009). However, as a consequence of these developments the latest FIE technology has been found to be less tolerant to deposit formation than the less finely engineered predecessors, with deposits found in injector needles and tips as well as in the filters which can be detrimental to the performance of the engine. In addition, a recent increase in the use of ULSD and biofuels has coincided with increased reports regarding engine deposits within injectors and filters (Barker, Langley, & Richards, 2010). These contributing factors have meant that fuels and fuel additives have also had to evolve so as to maintain engine efficiencies.

Deposits in the injector nozzle hole can cause a reduction in their hydraulic efficiency, decreasing engine power. This is not only due to the reduction in the nozzle cross sectional area but also to the irregular deposit topography which will increase frictional flow loss. As the injected fuel quantity is measured via time and not volume basis, reduced nozzle flow will lead to a reduction in the amount of fuel to combust and also effect the spray formation and atomisation resulting in reduced combustion efficiency, increased fuel consumption and increased

emissions (Smith & Williams, 2015). The effects of internal diesel injector deposits (IDIDs) as summarised by Barker, Snape, & Scurr, (2014) are shown below:

- Reduced fuel economy
- Higher emissions
- Misfiring
- Stalling
- Rough idling
- Lack of power
- Increase in smoke
- No cold start performance

2.1.2 Deposit formation mechanism

A basic mechanism summarised by Lepperhoff & Houben (1993) and describing deposit formation is shown in figure 2-1. The mechanism is independent of the location of the deposit and of any combustion process (diesel/gasoline) (Lepperhoff & Houben, 1993). The first phase (the induction phase) involves condensation of gaseous components onto the relatively cooler engine wall and the deposition of particles via sticking (which is caused by adhesive forces between the wall and the particles), incorporation (which is the attachment of the particles in a liquid surface layer) and impaction (which takes place via thermophoresis). The second phase, described as the deposit growth stage, involves adsorption of gaseous components and reaction with hydrocarbons further building up a highly sticky layer in which more particles become incorporated. As the deposit temperature increases the density increases as the more gaseous components diffuse through the porous layer. Once the deposits are attached to the wall the additional chemical reactions such as pyrolysis, dehydration and polymerisation can take place.

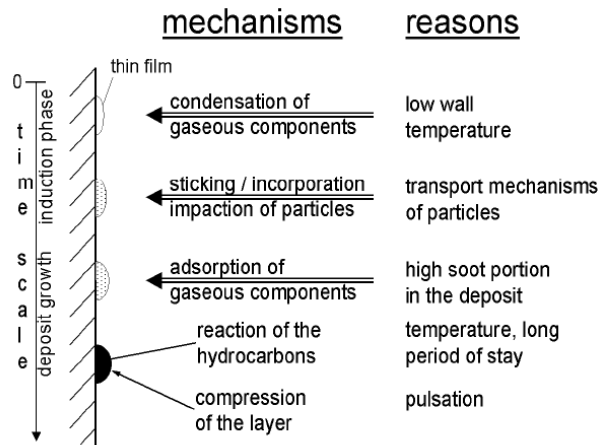


Figure 2-1: Mechanisms of Deposit formation (Lepperhoff & Houben, 1993)

The main causes for the recent increase in reports of deposit formation in the FIE are more specifically summarised in a review paper by Cook & Richards (2009):

- Increased injection pressure to meet tighter emission requirements
- Shear and / or resulting temperature generated within injectors
- Increasingly severe hydro treatment of harder to refine fuel sources
- Incorporation of bio-derived components.
- Presence of acid in the fuel (Barker, Snape, & Scurr, 2014).

The concomitant change in injector technology associated with the introduction of common rail fuel injection systems has seen the development of fuel injection systems capable of pressures up to 300 MPa. The reduction in the nozzle hole diameter has seen an associated significant increase in operating temperatures. Nozzles of 100 μm have been developed to create better fuel spray atomisation and improve emissions (Barker, Snape, & Scurr, 2012).

The increased pressure provides plausible mechanisms which produce species of increased molecular weight and reduced solubility, and are known for accelerating a number of reactions occurring such as Dies-Alder, ene and carbonyl-ene where reactants are known to form from free radical oxidation of various fuels at moderately elevated temperatures. In a review paper by Cook & Richards (2009)

the interlinked processes of fuel oxidation and deposit generation are discussed in order to establish which components of fuels are most likely to be associated with the recent increases in injector fouling and filter blocking. The deposits formed from diesel fuel in injectors at high pressures at unknown temperatures are said to be very similar to the deposits formed from the oxidation of jet fuels at 260 °C and in excess of 300 °C and the mechanism is shown in Figure 2-2. This involves molecular oxygen reacting rapidly with carbon centred radicals which can then undergo hydrogen abstraction to form a new carbon centred radical. The initiation step of this reaction is still not well understood although possible explanations are oxidation of highly vulnerable components such as diallylic methylene groups, homolysis of existing hydroperoxide or the step may be even metal catalysed.

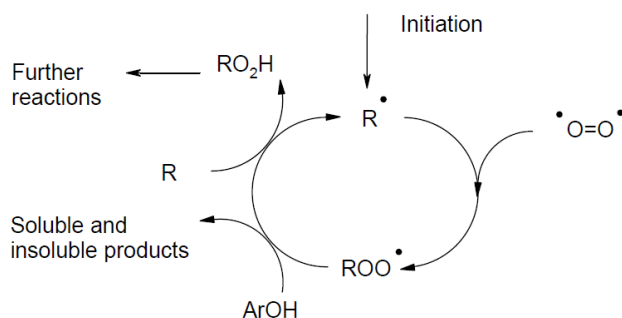


Figure 2-2: Summary of generally-accepted scheme for jet fuel oxidation. R represents a generic alkyl group and Ar an aryl moiety (Cook & Richards, 2009).

Another process believed to be comparable to fuel oxidation is the oxidation of hexadecane which is reported to occur at temperatures between 120 and 190 °C and shows intramolecular reactions leading to keto- hydroperoxides, fragmentation to yield aldehydes, olefins, and carboxylic acids, and cyclic ether products (Cook & Richards, 2009). Other reactions where oxygen is limited are also possible where hydroperoxides and free radicals once formed in plentiful

supply of oxygen can then go on to form benzylic radicals from alkylated aromatics leading to coupling of aromatic structures in a limited oxygen environment.

From the review of the literature the general mechanism for deposit formation from fuel oxidation is summarised by Cook & Richards (2009) as follows:

- The variation between different types of fuel deposits is dependent on the intensity and duration of the thermal, oxidative and mechanical stresses undergone.
- The initial stages are most likely the formation of hydroperoxides from n-alkanes or n-alkane like fragments of other molecules. These initial stages maybe metal catalysed or due to exceptionally reactive components.
- According to the levels of the components in a sample the oxygen and /or nitrogen containing species act as radical traps, become oxidised and undergo coupling and/or acid/base reactions.
- As the molecular weight and the polarity of oxidised products increases and /or the fuel cools down the solubility limit is reached and phase separation occurs.

2.1.3 Morphology of carbonaceous type deposits

The morphology of IDIDs has been investigated in numerous studies. Barker et al., (2009a) attempted to study the resultant deposits formed on fuel injectors and filters in the field in an attempt to identify possible deposit precursors. Energy dispersive X-ray analysis confirmed the deposits were mainly organic. The (polymeric) residue from the filter deposits were washed and a black solid was isolated (for example see SEM images in Figure 2-3) which showed the deposits to be granular in nature. Diffuse Reflectance Infrared Fourier Transform Spectroscopy indicated there to be a high carbon content with some functionality present namely C=O, C-O and evidence of aromatics. Elemental analysis indicated carbon species to be present as a mixture of graphitic and organic species with

oxygenated organics and aromatics being part of the matrix. GC/MS analysis was also carried out on a set of fuels known to cause deposits within injector and /or fuel filters to investigate the impact of ULSD and biofuels have on the level of deposit formation. It was found that the formation of the deposits was independent of whether a biodiesel blend or straight run ULSD was used. The high thermal and pressure loads that the fuel is subjected to were therefore proposed as a possible reason for deposition.

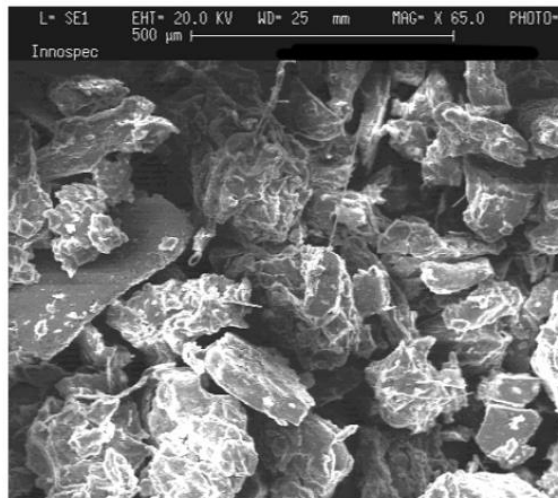


Figure 2-3: SEM Image of solid deposit (Barker et al. 2009).

Barker et al. (2009b) (different study) also determined that the deposits found in fuel filters of diesel engines (employing high pressure fuel injection equipment) contained the presence of n-C₁₆ and C₁₈ carbon backbones that are said to have originated from carboxylic acid residue. This study, together with the study by Barker et al. (2009a), concluded that the filter deposits analysed were shown to be a complex mixture of graphite carbon, polyaromatics, cycloalkanes, aromatics, straight chain and substituted alkanes, acids and inorganics.

The morphology of the FIE deposits was also reviewed by Cook & Richards (2009). As stated above the deposits formed from diesel fuel in injectors at high pressures at unknown temperatures were found to be very similar to the deposits formed from the oxidation of hexadecane at 160 °C as well as from jet fuels at 260 °C

and in excess of 300 °C. The deposits' appearance is consistent with their formation as small (<100 nm) liquid spheres before impaction on the surface before or after agglomeration or aggregation. It is concluded from studies reviewed that deposits comprise of chemically non-reactive heterocyclic and polycyclic aromatic hydrocarbons physically adsorbed onto a core of polar, possibly polymeric material containing a large amount of phenolic hydroxyl groups. This is significant as the aromatic species and polyaromatics are known to be precursors in the thermodynamic process to graphitic carbon. Also, the presence of acids is said to be significant as oxygen species are deposit precursors and occurrence was explained by the ability of carbon to absorb acids.

Further studies by the Barker research group utilised novel techniques such as Barker et al. (2011) where hydrolysis is used to show IDIDs to contain small archipelago structures of small ring size heavily alkyl substituted aromatics and Barker et al. (2010) which utilised Temperature Programmed Oxidation (TPO) to show IDIDs to have a greater degree of crystallinity in the carbon than in external deposit thought to be a consequence of the rapid degradation of the fuel by the high temperatures and pressures of the fuel system. More recently Barker, Snape, & Scurr (2012) used Time-of-Flight Secondary Ion Mass Spectrometry (ToF-SIMS) to analyse the IDIDs which showed deposits on the injector needle to be more complex than categorised by the industry, with common links between filter and injector deposits. A summary of the findings is shown in Figure 2-4. These studies confirmed that there are highly structured aromatic ring structures in diesel injector and filter systems.

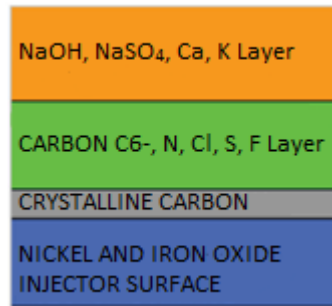


Figure 2-4: Schematic depth profile of injector deposit (Barker, Snape, & Scurr, 2012).

2.1.4 Morphology of polymeric type deposits

There is some evidence that fuel additives themselves can be indirectly involved in deposit formation. For instance Ullmann et al., (2008) observed injector deposits containing an ash-less organic polymeric material which was found on the upper part of the body on common rail injectors. Although no actual evidence of the additive in question, polyisobutylene succinimide (PIBSI) was observed (PIBSI films are said to be beyond the detection limit) evidence of isobutylene, amino groups and amide bonds was found. Due to the insolubility of the deposits in organic solvents the chemical structure of the polymeric material could not be fully characterised therefore it was attempted to reproduce deposit formation by mixing PIBSI with other fuel additives consisting of dimer acids and acid and ester based lubricity additives. It was observed that in isolation none of the additives formed any degradation products however in combination it was found that the deposits formed, most critically, when PIBSI was mixed with the di-fatty acids. It was finally concluded that the presence of formic acid added to deposit formation. More recently the propensity of PIBSI to cause injector sticking /internal injector deposits (IDIDs) was investigated in two recent publications. In the first paper by Reid & Barker (2013) a non-commercial low molecular weight PIBSI was synthesised, and used in a Dw10B engine test and compared to a commercial deposit control additive (DCA). While the commercial PIBSI caused no injector

sticking, the low molecular weight PIBSI test produced IDIDs which did lead to injector needle sticking. The analysis of the same deposits was presented by Barker et al., (2014). Using mainly ToF-SIMS in combination various other spectroscopic analysis techniques it was shown that the outer layer of the deposits to be amide in nature although there was plenty of evidence to suggest that the deposits were more complicated with both aromatics, high molecular weight alkanes and the low molecular weight PIBSI which was found to be in one of the inner layers. At the beginning of the test, low Mw PIBSI was in the imide form so it is hypothesised that a polar species within the fuel formed the amide under the influence of the high temperature and pressure. This conclusion was reinforced by the fact that in the former study, engine testing of the low molecular weight PIBSI with fuel that had been clay filtered to remove an additive species (which also would remove any other polar species contained naturally within the fuel) yielded no deposits. An explanation as to why the low molecular weight PIBSI was more susceptible to deposit formation compared with high molecular weight commercial deposit control additives is attributed to the low solubility in the fuel due to the short tails and polar head groups which increase the propensity to drop out of solution- the high molecular weight commercial additives have long chains which help solubilise the molecules hence they do not drop out of solution or form deposits.

2.1.5 Ultra-Low Sulphur Diesel (ULSD) deposits

ULSD, which was introduced to mitigate the effects of sulphur on the environment (such as acid rain), is becoming increasingly more common in order to meet the ever more stringent emission standards. As such, the sulphur content in fuel is now limited to 15 mg/kg in the US (Barker et al., 2010). However this recent switch to ULSD has coincided with the recent outbreak of reports concerning engine deposits which has coincided with the introduction of biofuels and increased injector pressures (Cook & Richards, 2009). Increasingly severe

hydrotreatment of harder to refine fuel sources has been cited as a possible for the recent increase in deposit formation and is almost always used in the production of ULSD. Although reducing the concentrations of polar species (namely O and N containing species) during hydrotreatment will reduce deposit forming tendencies, the reduction in polar species will mean a reduction in solubility for the oligomers that are formed from any remaining O and N containing species. The two consequences of hydrotreatment have therefore been reported to have the opposite effects on tendency to form deposits (Cook & Richards, 2009).

2.1.6 Metal carboxylates derived engine deposits

The increase in the use of ULSD has increased the need for corrosion inhibitors which although have been cost effective have been shown to be unstable, and in combination with poor storage conditions (with problems such as water contamination) can aggravate the formation of organic based deposit precursor, soap or metal carboxylates (although dry, contaminate free ULSD has not been found to directly form IDIDs (Trobaugh et al., 2013). Water contaminants can form clusters of water molecules in diesel fuel. Polar metal carboxylates can gravitate towards the water clusters which can lead to the formation of reverse micelles which can solubilise the components. This allows the metal carboxylate to travel through the injection system until the harsher conditions (higher pressures, temperatures and shear forces) destabilise the micelle structure and lead to deposition of the metal carboxylate (Trobaugh et al., 2013). It has been generally found that the combination of the presence of any acidic species in fuel and direct contact with a source of sodium base runs the risk of causing internal injector deposit issues (Reid, Cook, & Barker, 2014). Controlling the quantity of carboxylates and sodium and reducing fuel temperature can control carboxylate salt deposition (Tanaka et al., 2013).

Barker, Langley, & Richards (2010), however, showed that there was no correlation between the presence of the metals such as zinc and sodium and the propensity of the fuel to form deposits nor was there any correlation between other metals and deposit formation. Mass spectroscopy of various fuels with and without the propensity to cause deposition indicated there was an ion associated with a C₁₉ carboxylic acid salt which was more abundant in fuels with the deposit forming tendency although both deposit and non-deposit forming fuels were both found to contain a high molecular weight carboxylic acid salt indicating overall carboxylic acid does not necessarily cause deposit formation. Later, Barker & Cook (2013) showed, by using a diesel engine nozzle coking test, that a sodium hydroxide and mono-acid lubricity improver could lead to filter blocking and the same mono-acid lubricity improver with a "fuel soluble" sodium salt (sodium 2-ethylhexanoate) resulted in injector sticking while an ester based lubricity improver was found to cause neither issue.

2.1.7 Biofuel derived engine deposits

The use of biodiesel as an alternative to traditional fossil diesel fuels is widely recognised as significantly reducing the emissions of CO₂ as well as having other environmental benefits (Richards et al., 2007). The result of this has therefore led to the inclusion of biodiesel or fatty acid methyl esters (FAME) as a blending component for finished diesel fuel (Barker et al. 2009b). However this has recently been cited as a possible cause for the rise of deposit formation in the FIE, as FAME has been shown to be more susceptible to oxidation than petroleum diesel and degraded biodiesel is known to produce gums and lacquers (Richards et al., 2007). The contribution of increased levels of FAME to diesel has therefore recently been under enhanced scrutiny (Barker, Langley, & Richards, (2010).

Omori, Tanaka, & Bunne (2011) used FTIR to investigate the morphology of deposits derived from deteriorated biodiesel fuel. The results showed the main component of the deposit to be FAME polymer with the presence of lower

carboxylic acid salt layer between the base metal and the polymer layer. FAME contained in biodiesel fuel is subject to oxidative degradation which is then promoted via increased heat and O₂ generating the lower acid via polymerisation and decomposition. The acid causes local corrosion on the surface of the material (iron) to form a film of lower carboxylate iron salt which is able to trap FAME polymers by physical adsorption and the polymers that are generated by oxidation deterioration adhere to the surface. Sliding of the injector needle causes frictional heat which promotes FAME polymerisation, increasing deposit quantity and increases sliding resistance leading to changes in the fuel injection.

One review study by Richards et al., (2007) highlighted the compatibility of fuel injection equipment with new FAME blends where the use of FAME was found to lead to a number of issues. These include incomplete filtering of FAME leading to inorganic components that can cause increased wear in the fuel pump and injector nozzles, and effects such as hydrolysis of FAME caused by presence of free water leading to fatty acids and methanol. It was concluded that although it is possible that the increased use of biofuels could potentially be responsible for the recent increase in deposit formation, problems have been encountered in fuels with no biofuels content therefore this cannot be the only contributing factor.

Despite the substantial complexity in the formation and morphology of IDIDs, they have been categorised by the industry (Barker et al., 2014) into the following types:

- Metal carboxylates: carboxylic acid salts of metals such as sodium or calcium
- Carbonaceous: carbon based deposits from fuel stressing and subsequent degradation
- Amide based polymeric amide
- Lacquer: films, polymeric
- "Sticky" deposits: from aged fuels

2.2 CARBON BLACK

When investigating the properties of dispersant additives carbon black (CB) may be used as a model for soot or IDIDs. Carbon black is an amorphous carbon solid that is manufactured by the decomposition of solid particulates formed in the gas phase (Barker, et al., 2010). In general it is manufactured by thermal cracking or combustion of a hydrocarbon fuel under reducing conditions which gives its inherent low particle size (Barker, et al., 2010) although most of the properties of the CB are a function of the fuel and type of combustion process applied. For instance, the porosity, particle size, degree of oxidation and even the oxidised group functionality (acidic or basic in nature) may be adjusted during the combustion process or by post-manufacture chemical treatments (Kozak, Moreton, & Vincent, 2009). Clague & Donnet (1999) attempted to account for the observations of the similarities and differences of CB and diesel engine/exhaust soots to validate CB as a soot surrogate to mimic soot behaviour for the purpose of lab bench tests. Although elemental analysis showed the oxygen content of the engine soot was higher than that of CBs both overall and on the surface which demonstrated that the surface of the soot was more polar, microscopy studies revealed similarities between the internal structure and morphology of CB and soot on a primary particle where both showed evidence of perturbed graphite layers (or turbostratic structure). There were also no obvious differences on the atomic scale. It was concluded that CBs with intermediate primary particle size and porosities, with a surface area of approximately $300 \text{ m}^2\text{g}^{-1}$ and some degree of surface polarity, should be capable of mimicking the behaviour patterns of soots in oils. Studies where carbon black has been used as a soot surrogate in PIB type dispersions include Pugh & Fowkes (1984), Kornbrekke, Morrison & Oja et al. (1992), Cox et al. (2001), Dubois-Clochard et al. (2001), Jakab & Omastova (2005), Won et al., (2005) Shen & Duhamel (2008), Kozak, Moreton, & Vincent (2009) and Yasin et al., (2013).

2.3 INTRODUCTION TO PIBS

Polyisobutylenes (PIBs) have a wide range of applications and may be classified by their molecular weight (MW). High MW PIBs (>300 000 g/mol) are utilised in sealants and roofing, medium MW PIBs (4000-120000 g/mol) may be found in adhesives, extenders and in chewing gum bases and low MW (500-5000 g/mol) PIBs are used in glues, lubricants and modifiers and oil additives (Li, Cokoja, & Kuhn, 2011). PIBs chemical resistivity, non-toxicity and high thermal stability makes them suitable as precursors to polymeric surfactants and as such the low MW PIBs used in lubricating oils, additives for lubricants gasoline and diesel fuels represent 75-80 % of the PIB market (Li, Cokoja, & Kuhn, 2011).

2.3.1 Synthesis of polyisobutylene succinimide

The general scheme for the synthesis of PIBs is described by Li, Cokoja, & Kuhn, (2011) and is dominated by use of Lewis acids as co-initiators and traces of water or alcohol as initiators e.g. $\text{H}_2\text{O}/\text{BF}_3$. Isobutene (IB) undergoes cationic polymerisation, whereby the proton adds to the monomer to produce a carbenium ion which undergoes electrophilic attack of another monomer. Proton abstraction to monomer or solvent can then produce either exo or endo terminal double bond end groups (Figure 2-5). Exo end groups are highly reactive, whereas endo are more thermodynamically favourable and more stable.

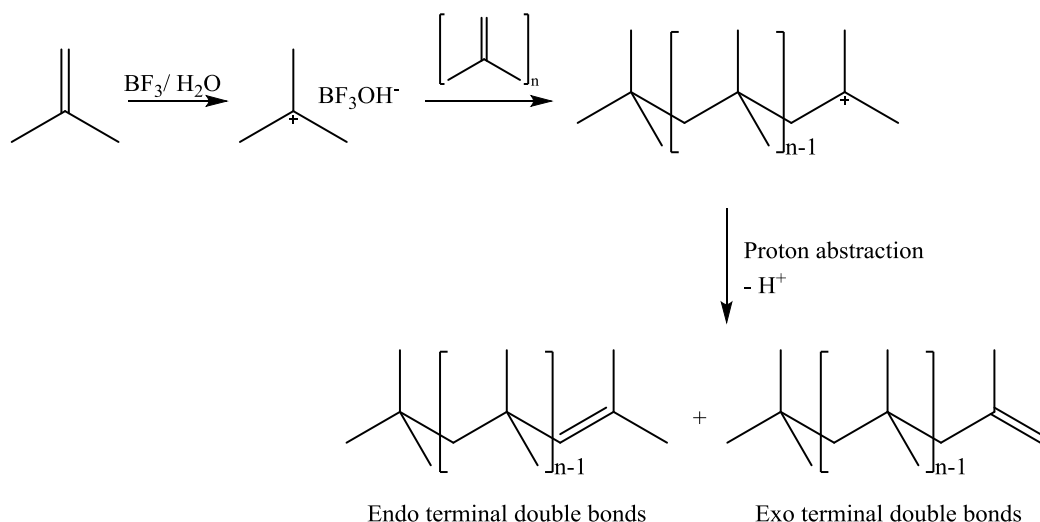


Figure 2-5: Polymerisation of PIB (Li, Cokoja, & Kuhn, 2011).

Polyisobutylene succinic anhydride (PIBSA) is a common succinimide precursor derived from PIB and may be synthesised as described by Mortier & Orszulik (1997) using an ene process whereby excess maleic anhydride (MA) is added and the materials are heated at high temperature (usually between 220 and 240 °C). Polyisobutylene succinimide (PIBSI), a common fuel and lubricant additive, can then be made by reacting PIBSA with equimolar amount of suitable polyamine. The structures of PIB, PIBSA and PIBSI are shown in Figure 2-6.

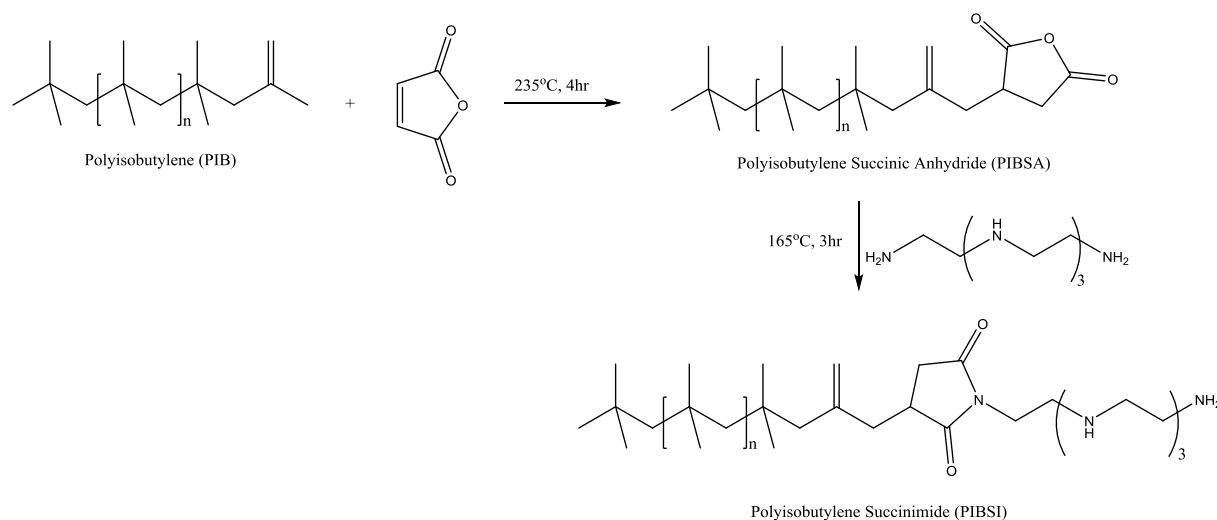


Figure 2-6: Synthesis of Polyisobutylene Succinimide (PIBSI) (Mortier & Orszulik, 1997).

An alternative, older, synthetic route to form PIBSA uses a Diels-Alder type reaction. Cationic polymerisation of PIBs is typically carried out at costly cryogenic temperatures (-100 to -20 °C). Use of chlorinated solvents minimises chain transfer reactions. The PIB is prepared in the presence of an aluminium chloride (AlCl₃) catalyst. Although the PIB used does contain unsaturated groups a lower proportion of these are vinylidene which makes the material less reactive towards MA (Lehrle, et al., 2002). This synthetic route occurs at lower temperatures (180 to 190 °C) and chlorine is used to help to produce the PIBSA. Although this method is generally less expensive than the thermal route the resulting additives are thought to give a lower level of engine performance and this older technology is becoming less and less common throughout the additive industry (Rivera-Tirado, Aaserud, & Wesdemiotis, 2012).

2.4 PIBSI BEHAVIOUR AT AMBIENT TEMPERATURES

The knowledge base surrounding PIB and its derivatives at ambient temperatures is significant, the majority of which are based around adsorption. Other methods of analysis include atomic force microscopy (Sharma, Moreton, & Vincent, 2003) (Puskas, et al., 2003), (Yasin et al., 2014), fluorescence spectroscopy (Pucci, Rausa, & Ciardelli, 2008), small angle neutron scattering (Reynolds, Henderson, & White, 2004), dynamic light scattering (Parent et al., 2011), small angle X-ray scattering, conductivity measurements (Yasin et al., 2013), surface calorimetry (Pugh & Fowkes, 1984), FT-IR (Nsib, Ayed, & Chevalier, 2006), and NMR (McGrath, Ngai, & Roland, 1992) amongst others. Some of these studies have investigated the various structure activity relationships focusing on parameters such as the effects of the length of the polyamine head group, the nature of the amino groups in the head group, the architecture of the block copolymers (brush/comb like) or number and length of the PIB chains (Chevalier, 2004). In some cases, as well as a dispersion model approach, the structure activity relationships have been investigated using actual engine tests which use polymers

of different types and directly measure the amount of deposits that formed in order to directly evaluate their dispersion efficiency. The following discussion on the structure activity relationships will include both methodologies, focussing on the effects of the polymer structure itself.

2.4.1 Adsorption of PIBSI onto deposit surrogates

The various structural properties of the PIB derivatives and similar molecules have been shown to greatly affect their activity in the model experiments which simulate the in situ engine conditions. These studies mostly involve adsorption studies of dispersions containing PIBSI type molecules and deposit surrogates. The greatest relationships between adsorption and actual performance have been found in lubricant dispersant applications where the dispersant is used to prevent aggregation of the soot particles in the oils (Dubois-Clochard, et al., 2001). Two regimes have been identified concerning coverage of particles with end attached polymers with a low coverage (mushroom regime) and high coverage (brush regime) (Chevalier, 2004). Figure 2-7 shows a typical experimental adsorption isotherm for a PIBSI derivative adsorbed onto carbon black which demonstrates the two regimes.

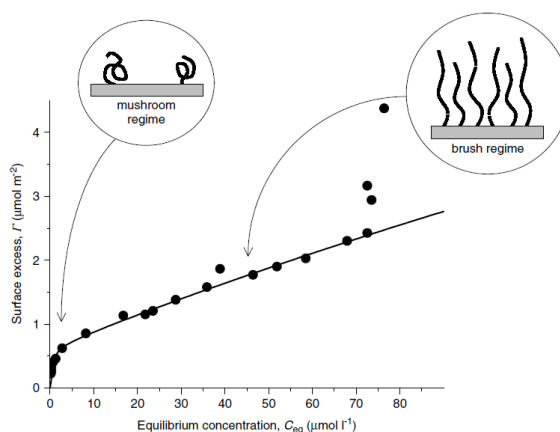


Figure 2-7: Adsorption Isotherm of a PIBSI derivative from a xylene solution onto carbon black surface at 60 °C and the schemes of the adsorbed polymer layer in the mushroom and brush regimes (Chevalier, 2004).

2.4.2 Effect of extending polyamine head group

It has generally been found that polarity of the head groups of the PIBSI type dispersants has been shown to affect the adsorption amounts and subsequently the efficiency of the dispersants in reducing the amount of carbon deposits. The dispersant head group polarity is usually enhanced by increasing the number of nitrogen atoms. For instance Forbes & Neustadter (1972) studied the effect of two head groups on PIBSI diethylene triamine (DETA) and tetraethylene pentamine (TEPA) using powder bed detergency tests. It was found that the dispersant containing the DETA head group was unable to stabilise one of the carbons used in the tests however for the dispersant containing the longer TEPA head group the stabilisation increased. While one study by Aleman-Vasquez & Villagomez-Ibarra (2001) found that there was no relation between the structure of the amine moiety and the detergent-dispersant effect, other studies have observed improvements. For instance Mekewi (2002) studied the oxidative stability of lubricant oil samples with four PIBSA additives with varying numbers of amine groups. The dispersivity values showed that as the number of nitrogen atoms and therefore basic character of the additive increased, so did the neutralisation efficiency. The results showed that as the nitrogen content of the additive was increased the efficiency of dispersion increased due to the increase of the basic character.

Dubois-Clochard, et al. (2001) also provides good evidence to suggest that there is a relationship between the number of amine groups in the hydrophilic polyamine part and the dispersant effectiveness. In the study the adsorption of PIBSI derivatives at a solid hydrocarbon interface were investigated. The specific derivatives studied were TEPA, triethylenetetramine (TETA), DETA, and aminoethylpiperazine (AEP).

The mechanism by which adsorption occurred was modelled by two steps: a low coverage regime where molecules were adsorbed onto strong acidic sites and a

higher coverage regime where weaker acidic sites could be reached and the steric hindrance of the macromolecular tails contributed to the thermodynamics of the adsorption. The higher the number of amine groups in the hydrophilic polyamine part the higher the affinity of the PIBSI for the solid surface became as both the adsorption enthalpy and Gibbs free energy were enhanced. It was found that some derivatives such as PIBSI-AEP bound weakly to the CB but this was attributed to the large steric hindrance of the piperzine ring.

The effect of the amine head group length was also investigated by Shen & Duhamel (2008) who investigated the efficiency of dispersants at stabilizing carbon particles in oil. A series of PIBSI type dispersants with varying numbers of amines in the head groups were compared based on their respective critical micelle concentrations (CMC) determined by steady state fluorescence. The study found that increasing the number of secondary amines in the polyamine core can lead to an increase of association strength of the dispersant as the CMC took place at a smaller dispersant concentration. This is said to enable a stronger anchoring of the dispersant onto the CB surface leading to greater dispersant efficiency.

A more recent study by Kozak, Moreton, & Vincent (2009) investigated the adsorption of amine containing PIB based surfactants onto CB particles. The study was carried out by examining the adsorption of various surfactants containing PIB tails of varying head groups and lengths onto CB. The stability of the CB dispersions was also assessed by measuring the light transmission. The results showed that there was strong and seemingly irreversible adsorption onto the CB particles although differences were observed in the maximum adsorbed amounts (Γ_{max}) for the various surfactants. It was found that Γ_{max} increased with increasing number of tertiary amine groups from zero to four. The molar enthalpies of adsorption (ΔH_{ads}^m) for the surfactant containing no amine groups had a value of -12 kJ mol⁻¹ whereas the surfactants with the amine groups present were all similar ($\Delta H_{ads}^m \sim 30-35$ kJ mol⁻¹). The explanation given to describe this behaviour is a

mechanism whereby the more polar (or larger) the head group the more it is rejected from the solvent. Further evidence to support this mechanism came from keeping the total number of amine groups the same but increasing the polarity of the head group by replacing some of the tertiary amines for primary or secondary amines. The Γ_{max} values increased with the polarity of the head group. PIBSI derivatives ethylenediamine (EDA) and dimethyleaminopropylamine (DMAPA) (both with 1000 Mw PIB- M_n) were found to improve the stability of the CB dispersions. These derivatives contained primary and secondary amine groups rather than just tertiary and it is postulated these gave rise to the electrostatic repulsion involving proton exchange between the head groups and the acid sites on the surface giving rise to surface charge. It was therefore concluded that in addition to the steric repulsion a longer range, electrostatic repulsive force was present between the particles. This hypothesis was further backed up by the observation that EDA which contains three N-H moieties had greater stabilisation than DMAPA which has only one N-H moiety.

A recent study by Yasin et al. (2013) used adsorption, rheology and conductivity measurements to investigate the dispersibility of graphitic carbon black dispersions as a model for carbon nanotubes. The dispersants investigated were a polyhydroxystearic acid (Hypermer LP1), PEG 30-dipolyhydroxystearate (Hypermer B246) and a PIBSI. Hypermer B246 and PIBSI were found to be effective stabilisers as they produced dispersions of lower viscosity while Hypermer LP1 was not an effective stabiliser as it produced higher viscosity suspensions with the same carbon volume fraction. The poor stability was attributed to the flatter conformation due to the higher adsorption affinity of the whole polymer on the surface thus reducing the length of the stabilising layer. The adsorption results showed that the PIBSI gave higher molar amounts of adsorbed polymer on the carbon surface than the other two polymers, which was attributed to the presence of the amine groups in the anchoring group.

A very recent study by Kim et al. (2015) investigated the effectiveness of PIBSI type dispersants in reducing the carbon deposits formed by thermal oxidative decomposition of jet fuel (Jet A-1) in a stainless steel batch reactor which was pressurised to 1 atm and heated to 200 °C for five minutes. A number of PIBSI alkyleneamine head groups were studied such as DETA, TETA TEPA and pentaethylenhexamine (PEHA). In addition to this a number of amino ether head groups were also studied. It was found in this study that as the polarity of the head group increased, which is dependent on the polar surface area and orbital electronegativity, the efficiency of the dispersants in reducing the amount of carbon deposits also increased. For instance the carbon deposit amounts were 4.9 mg, 4.5 mg, 3.7 mg and 3.4 mg for PIBSI-DETA, PIBSI-TETA, PIBSI-TEPA and PIBSI-PEHA respectively. The polar surface area was calculated as a summation of the polar fragment distributions in each molecule (as developed by Ertl, Rohde, & Selzer, (2000)). It was therefore hypothesised that the efficiency of the dispersants in reducing the amount of carbon deposits increased with an increase in the number of amino groups (in a similar manner as Kozak, Moreton, & Vincent, (2009) demonstrated through PIBSI carbon black adsorption studies). It was also found that compared with the linear alkyleneamine head groups that the amino ether dispersants gave lesser amounts of deposits. It was therefore hypothesised that the polar heads containing an amino ether group adsorbed onto the carbon deposit precursors more strongly and irreversibly than the polar head containing alkyleneamine groups. A number of nonlinear structures/ head groups were also studied which were found to be more affected by steric hindrance. For instance AEP with a sterically hindered structure gave more carbon deposit than the PIBSIs containing more linear head groups. It was postulated that although the secondary amine was able to absorb onto the carbon deposits the tertiary amine was unable to do so due to the large steric hindrance. This was also observed by Dubois-Clochard, et al. (2001) for a PIBSI-AEP surfactant.

2.4.3 Effect of extending PIB hydrocarbon tail length

The function of the hydrocarbon (PIB) chain that protrudes into the fuel (or oil) is to provide the steric / electrostatic barrier preventing further deposit build up while also maintaining the solubility of the dispersant in the fuel. As well as the effect of the amine groups, the effect of the polymer architecture on the dispersion efficiency has been investigated in numerous studies. Forbes & Neustadter (1972) carried out some adsorption studies on PIBSI dispersants used in oil additives investigating the molecular weight of the PIB in the range 650-2800. It was found that PIBs with the molecular weight range of 900-1000 gave the best performance in terms of stabilisation and that the sludge suspension was stabilised by a steric mechanism and not by either electrostatic repulsion or micellar solubilisation. It was demonstrated that the greater the suspended particle diameter the longer the polymer chain must be to afford adequate protection against flocculation (Forbes & Neustadter, 1972). Tomlinson et al. (2000) also investigated how the hydrocarbon chain length can have an effect on the dispersancy efficiency. Comparisons were made between low molecular weight model dispersants and high molecular weight commercial dispersants. Adsorption isotherms for the model dispersants showed evidence of multilayer formation at high concentrations with an increase in the amount of absorption beyond monolayer coverage. Also the adsorption of the model dispersants was found to have occurred on a large proportion of the porous network inside the carbon substrate. The model dispersants were found to absorb 3-10 times more than the commercial dispersants did due to the longer hydrocarbon back-bone and branching of the commercial dispersants which led to a lower chain flexibility preventing adsorption on the inner surface of the carbon substrate. Also, the more inflexible backbone of the commercial dispersants may have occupied a greater area of the carbon surface than the model dispersant. It was concluded that a long and rigid

hydrocarbon chain backbone gives greatest dispersion although the chain length cannot be too long as to be detrimental to the performance of the engine oil. The PIB length was also investigated by Kozak, Moreton, & Vincent (2009) whereby the adsorption isotherms and Γ_{max} were measured for three surfactants containing 318, 550 and 1000 MW tails. The Γ_{max} values increased steadily with decreasing tail size. The surfactant rejection from the solvent described above was strongest for the surfactant with the shortest tail.

2.4.4 Effect of PIB architecture

As well as the length of the hydrocarbon PIB chain the number of PIB chains (sometimes referred to as functionality) have also been found to effect the stabilisation efficiency. Cox et al. (2001) studied the effect of the polymer chain architecture on the adsorption properties of PIB derivatives at the carbon / hydrocarbon medium interface using nine PIB derivatives of *mono*, *bis*, and *tris* functionalities. The *bis* PIB derivatives were found to be more efficient than the *mono* or *tri* derivatives in the stabilisation of CB. The reason for greater stabilisation than the *mono* derivative was the presence of two anchoring groups which increased the affinity and provided greater solubility. The *tri* PIB derivative was found to have adsorbed greater amounts than the *mono* derivative but less than the *bis* derivative despite having the most anchoring groups. This was attributed to the *tri* being more bulky and less flexible and therefore could not adsorb as efficiently at the surface of the CB. In contrast Tomlinson et al. (2000) found that mono functionalised surfactants did not appear to show greater affinity than more highly substituted *bis* and *tri* compounds although these compounds contained the same number of anchor head groups.

The amount of adsorption of PIBSI type molecules has been shown to be enhanced by changing the polymers from linear to comb-like architectures. Dubois-Clochard et al. (2001) investigated two families of polymers: linear PIBSI derivatives and a comb-like poly(PIBSI) derivatives both functionalised with AEP and DETA. From

the corresponding adsorption isotherms it was found that when changing from a linear to a comb like structure the amount of adsorption was enhanced. The adsorption enthalpy was found to be strongly exothermic at low coverage (mushroom regime) but became reduced at higher coverage (brush regime). The adsorption was found to be limited at high coverage for the linear PIBSI when the brush regime was entered because of the lateral interactions of PIB chains. However comb-like polyPIBSI allowed this to be overcome because the PIB chains were already close to each other in the macromolecule therefore the adsorption reached higher saturation values. This was attributed to the hydrophilic parts becoming closer together as their number increased and so the stretching of the hydrophilic parts during adsorption decreased giving a denser and entropically more stable monolayer. The thickness of the monolayer was measured as 30 Å which is said to be close to the length of a fully stretched PIB chain (Dubois-Clochard et al., 2001). However at higher concentrations there was a large increase in the amount of adsorbed polymer that exceeded the monolayer coverage. This process was found to be reversible but the binding of the underlying monolayer was irreversible which showed that the polymer-polymer interactions were weaker than the acid-basic interactions between the polymer and the CB surface.

2.5 THERMAL EFFECTS

2.5.1 Thermal degradation of PIBs

Although the knowledge base surrounding the stabilisation mechanisms of PIBs is significant, most of these studies involve ambient temperature conditions. As the polymer dispersants operate at temperatures exceeding 300 °C (Mortier & Orszulik, 1997) it is important therefore to pay special attention to studies investigating thermal effects. Thermal degradation of PIBs and PIBSAs has been investigated by Lehrle et al. (2002) via mass spectrometric methods. Evaporation was found to occur up to 250 °C although the sample with the lowest MW distribution was the most volatile. Two separate stages of degradation were observed: the first stage occurring at 300 – ca. 480 °C, the second stage occurring above ca. 460 °C. This two stage degradation mechanism was ascribed to correspond to a proposed mechanism via monomer formation by unzipped chains that are initiated via double bonds at the end of the molecule and secondly via main chain scissions. The temperature at which the onset of degradation occurred was similar for both PIB and PIBSA samples although for PIBSA this was slightly lower and it is postulated that this was due to greater substitution of the double bonds on the PIBSA which meant that allylic hydrogen abstraction was more favourable. It was therefore suggested that the thermal stability of liquid PIB polymers could be increased by hindering or saturating the double bonds by the addition of the succinic anhydride head groups.

The two competing models by Lehrle and Sawaguchi of the pyrolysis of PIB are reviewed by Poutsma (2005) to rationalise the formation of volatile oligomers from PIB between 300 – 400 °C. Briefly, the Lehrle model is statistical and ascribes formation of oligomers to predominantly random scission pathways specifically via consecutive hydrogen transfer- β -scission events with a minor contribution from back biting, whereas the Sawaguchi model was mechanistic and assigns all oligomer formation to back biting specifically via intramolecular

hydrogen shifts to form oligomers and to a lesser extent monomer through unzipping. It is concluded that the Sawaguchi model is the more accurate since it does not over predict the formation of dienes (unlike the Lehrle model) and accounts for a number of observations that Lehrle model does not, such as the formation of iso-propyl terminated monomers.

Jakab & Omastova (2005) investigated the thermal decomposition of various CB composites including PIB. The study found the thermal decomposition of the polymers was dependent on the type of carbon and on its amount in composites. The CBs with a low volatile content were shown to enhance the thermal stability of the polymers. It was found that CB with a high volatile content caused changes in the pyrogram of PIB. The oligomeric products intensity strongly decreased while the formation of monomer was promoted. The decomposition of PIB composites containing high volatile content CB shifts to lower temperature when compared to CB free PIB sample. This is attributed to the degrading CB initiating depolymerisation at the chain ends of PIB.

2.5.2 Stabilisation mechanism of PIB at high temperatures

Three mechanisms have been proposed for thermally induced effects for PIBSI type molecules. These include a temperature dependence of the adsorption and desorption of the dispersant on the surface of the soot, dispersant mediated coulombic charging of the soot and a temperature dependence of the solvency of the dispersant molecules in the oil phase (Won et al., 2005).

Concerning the first proposed mechanism there are contrasting reports as to whether there is an increase or decrease in adsorption with increasing temperature. Pugh & Fowkes (1984) argued there was an increase. Adsorption isotherms for PIBSI derivatives absorbed onto CB were characterised by two distinct regions, strong adsorption at low dispersant concentration followed by a low affinity at higher dispersant levels. The high affinity step was independent of dispersant concentration. The low affinity adsorption step was dependent on the

dispersant concentration and increased with temperature. This was attributed to the diffusion of the dispersant into the pores of the CB made plausible by an observed increase in diffusion coefficient with temperature. Dubois-Clochard et al. (2001) also observed an increase in adsorption with temperature although the sample of CB used in this study was analysed by BET and no evidence of microporosity was found, therefore the increase was attributed to a large variation in the adsorption enthalpy or entropy as a function of temperature. In contrast, Cox et al. (2001) noticed an adsorption decrease with an increase in temperature. Increasing the temperature from 25 - 50 °C lead to a decrease in the amount of derivatised PIB adsorbed and was attributed to an increase in polymer chain solubility in n-heptane with temperature.

Concerning the role of charge in the stabilization of the soot there have been contrasting reports on whether the electrostatic forces are strong enough at high temperatures to play a role. Most studies argue that steric factors alone are insufficient and so there must be other factors present. Forbes & Neustadter (1972) however claimed additives stabilise sludge suspensions via steric mechanism only. The high affinity step at low dispersant concentration observed by Pugh & Fowkes (1984) was independent of the dispersant concentration of the solution and was said to be attributed to the dispersant mediated coulombic charging of the soot. This was also observed in earlier work by Pugh, Matsunaga, & Fowkes (1983) where conductivity measurements on similar samples showed a negative surface potential of CB dispersed in low dielectric media in the presence of the basic dispersants. As CB is highly conductive while hydrocarbons have low conductivity the overall conductivity of a dispersion solution gives a measure of the degree of aggregation. The effect of the dispersant is explained by a charge separation mechanism where protons are transferred from acidic surface sites to the dispersants basic sites. The final stage in the mechanism was said to involve desorption of the proton carrying dispersant back into the hydrocarbon media

leaving behind a negative charge on the CB particle. When the dispersant was not present the CB particles were in contact and so electrons could flow between particles giving rise to relatively high conductivity. At low concentrations of dispersant adsorption of the dispersant produced a steric barrier around the particles, reducing interparticle contact thus reducing the conductivity of the dispersion. At higher concentrations the particles had a sufficient zeta potential to repel one another. The development of a high surface potential and the presence of conducting ions in the solution therefore led to an increase in the conductivity of the system. In contrast a study by Georges, Georges & Hollinger (1997) suggested the electrostatic forces are too weak to contribute and stability is due to steric factors alone. The study involved using surface force apparatus to study the adhesive force between two smooth amorphous carbon surfaces in air and the repulsive force due to the contact of two dense brush PIB layers adsorbed on carbon surfaces. The measured pressure distance profile was much lower than that which would be observed if electrostatic force played a role in stabilisation. Kornbrekke, Morrison & Oja et al., (1992) provided further evidence that electrostatics play a role in the dispersancy mechanism. Electrophoresis was utilised to measure the mobility of suspensions of CB and investigate the effect of PIBSI on the charging of the CB particles. It was found that the addition of the commercial PIBSI caused the CB to become negatively charged which increased with dispersant concentration thus providing further evidence that electrostatics play a role in the dispersancy mechanism.

The third proposed mechanism is a temperature dependency of the solvency of the dispersant molecules in the oil. This can be complex to analyse as an increase in temperature may affect the solvency of PIB in hydrocarbon medium causing the polymer chain to collapse. Luna-Barcenas et al. (1997) investigated polymer chain collapse near the lower critical solution temperature (LCST) through use of computer simulations. The LCST is where phase separation is induced by raising

the temperature and is entropically driven. This phase separation occurs in “poor” non-dilute solutions when the polymers split into a phase rich in polymer and another depleted in polymer as opposed to the chains adopting expanded coil like conformations that overlap. It was found that the polymer chain collapse did indeed occur near a LCST phase boundary. The polymer chains were expanded coil like conformations below the LCST. Above the LCST in the two phase region the chains in the polymer rich phase were still expanded but in the dilute polymer phase the chains were partially collapsed. Increasing the temperature further to well above the LCST the chains began to expand again suggesting a one phase region above the LCST was plausible.

In order to clarify the origin of the viscosity increase with temperature of soot in oil in the presence of PIBSI, Won et al. (2005) used dynamic (oscillatory) and steady-shear rheology as well as FTIR to investigate the structure and interactions in CB suspensions as a function of temperature. The effects of temperature on the repulsive portion of the interparticle interaction potential due to the steric stabilisation of the dispersant as well as the attractive interaction resulting from the van der Waals forces was also studied. The results of this study showed the structure of the CB aggregates and the resultant suspension rheology changed as the temperature was increased. At low temperatures, fluid-like well separated primary aggregates were observed whereas at high temperatures primary aggregates agglomerated resulting in a solid-like rheology as a result of an increase in the interparticle interactions. The adsorption isotherms of dispersant on CB made by FTIR indicated the adsorption of the dispersant did not vary with temperature therefore a temperature dependence of adsorption was concluded not to be the reason for the flocculation observed at high temperatures. The rheological measurements also showed no temperature dependence on the viscosity of a CB sample with no added dispersant therefore it was concluded that it was unlikely increasing temperature increased the attractive van der Waal

interactions between the CB particles. The rheological measurements did show that it was the viscosity that was intrinsically dependent on temperature and it was therefore postulated that increasing the temperature caused conformational changes in the hydrocarbon chain of the dispersant causing it to collapse, decreasing the efficiency to inhibit agglomeration. The results therefore suggested steric repulsion due to adsorbed dispersant is the dominant mechanism stabilizing the CB in the oil. The temperature dependence of the PIB hydrocarbon tail conformation of the adsorbed dispersant was therefore found to be the origin of the anomalous temperature dependence of the stability of the CB.

Work by Yang et al., (2007) supported the findings of Won et al., (2005). In this study the rheological behaviours of carbon nanotube dispersions in oil which were stabilised by PIBSI were studied at different temperatures. A PIBSI dispersant of molecular weight 1000 (PIBSI 1000) was found to disperse carbon nanotubes in oil efficiently at room temperature but failed to disperse them at temperatures higher than 60 °C shown by sudden increase in the storage and loss moduli. The moduli were then constant for a brief period where a network structure was believed to have been formed by the nanotubes with the long chain dispersant molecules. This subsequently collapsed on further heating at around 80 °C characterised by a loss in the storage moduli. It was found that compared with a shorter molecular weight PIBSI (PIBSI 550) the dispersion with the longer chain had higher moduli than the dispersion containing the shorter chain. It was suggested that the long chain polymer contributed more to the agglomeration of the dispersing system at high temperatures. As conformational changes occurred as the temperature was increased the entanglement of the polymer chains that had adsorbed onto the surface of the nanotubes helped to cause the network structure. Previously it has been found that the viscoelastic response can serve as an indirect qualitative measure of the dispersion state of nanotubes in polymer

composites, where a higher G' can be an indication of a better dispersion (Moniruzzaman & Winey, 2006).

2.6 REVIEW OF HIGH TEMPERATURE STUDIES OF NON PIBS

2.6.1 High temperature NMR spectroscopy and rheometry

While there has been a limited number high temperature studies of PIBs many of which are mentioned above there are even fewer that have utilised nuclear magnetic resonance spectroscopy (NMR) at high temperatures. McGrath, Ngai, & Roland (1992) for instance studied the temperature dependence of segmental motion in PIB and poly(vinylethylene) using ^{13}C NMR up to 370 K. Karatasos et al. (2002) also used ^{13}C NMR in combination with simulations to study methyl motion of PIB to similar temperatures. There are virtually no previous studies that have utilised NMR to investigate PIB type dispersions at high temperatures. There are, of course, high temperature studies of other substances. High temperature ^1H NMR is one such technique that has been successfully utilised to study coal biomass fluidity. Miyazawa, Yokono, & Sanada (1979) was one of the first to use high temperature ^1H NMR to study coal carbonisation. More recently a number of studies by the Snape research group have developed the technique further to study coal and biomass fluidity usually in conjunction with rheometry.

Martin, Liggat, & Snape (2001) used the technique to examine samples of polyacrylonitrile at elevated temperatures allowing hydrogen distribution and changes in mobility of the polymer to be assessed and related to known structural variations. Gao et al. (2014) studied the segmental dynamics in polybutadiene organo-clay nanocomposite systems using ^1H NMR. Steel et al. (2004) combined the use of rheometry and ^1H NMR spectroscopy for understanding the mechanisms behind the generation of excessive wall pressures during coking. Steel et al. (2006) used ^1H NMR and rheometry to study coal and biomass fluidity development at high temperatures. More recently, Dufour et al. (2012a) and

Dufour et al. (2012b) used high temperature ^1H NMR in conjunction with rheology to analyse the pyrolysis of biomass polymers in situ.

Recently Goldansaz et al., (2015) used a combination of ^1H NMR relaxometry and rheology to study the network formation of melt dynamics of poly(ethylene oxide)-nickel chloride systems up to 150 °C. The presence of a high temperature plateau in the spin-spin relaxation time (T_2) vs. reciprocal temperature at medium and high concentrations illustrated network formation.

Spěváček et al. (2001) investigated the effect of temperature on poly(diethylacrylamide) gels in order to further understand the volume phase transition. It was found using ^1H NMR that the phase transitions in the polymer coils from linear to compact globular conformations caused a reduction in mobility and also a reduction in signal intensity. Phase transitions of polymers were also studied by Larsson et al. (2001) where ^1H NMR was used to qualitatively monitor the mobility of polymer segments and thus the coil-to-globule transition at the lower critical solution temperature (LCST). Above the phase transition temperature there was a loss of the signal reflecting the decrease of the relaxation time T_2 with the formation of solid structures. Again it was confirmed using ^1H NMR that the coil-globule-transition had caused reduction mobility as well as the reduction in signal intensity. A more recent study by Lee et al. (2007) used high resolution solid state ^1H NMR to study Poly (vinyl phosphonic acid) at temperatures between 250 and 430 K to monitor the mobility of the P-OH protons and the backbone protons. As the temperature was increased the line width of the P-OH protons decreased. The narrowing of the P-OH resonance with increasing temperature agreed with the rapid exchange motions in the temperature range investigated. It was found using high temperature ^1H NMR that the P-OH protons were mobile at high temperatures and therefore able to contribute to the proton conductivity. Li et al. (2010) used wide line ^1H NMR to investigate the phase structure and molecular mobility of novel exfoliated polyethylene and palygorskite

nanocomposites at high temperatures. The line widths reflected the relative chain mobility in different phases. The line widths of a crystalline phase and an amorphous phase versus temperature were studied. The line widths of the crystalline phase were broad as would be expected due to lower mobility of the chains. The line width of the crystalline phase increased with increasing palygorskite load in the nanocomposite which indicated a reduction in mobility of the chains. This was because of more rigid molecular chains being generated by adsorption or bonding to the palygorskite clay. Increasing the temperature to 400 K lead to a decrease in line width, indicating an increase in mobility and a reduction in interaction. For the amorphous chains it was found that introduction of palygorskite lead to a decrease in mobility due to the stronger adsorption interaction between the palygorskite and the chains. However it was found that increasing the palygorskite load further could also result in an increase in mobility particularly at high temperatures which suggested that the adsorption interaction between the palygorskite and the amorphous chains is reduced in the lower amorphous phase.

2.7 CHAPTER SUMMARY

This review has looked at the literature on engine deposit formation and the PIB derivatives that are manufactured to prevent their formation through dispersion. Special attention was paid to the thermally induced effects as to suit the conditions that are within the polymers normal sphere of operation. The following are the main findings from the literature review:

- Recent tightening of legislation to cut emissions has led to more precisely engineered engines and as a consequence, together with the introduction of ULSD and biofuels, has led to an increase in the number of reports regarding deposits being found in fuel injection equipment.
- IDIDs can lead to reduced fuel economy, higher emissions and loss of power. IDIDs mostly comprise of carbonaceous deposits and lacquer type

films: A complex mixture of graphite carbon, polyaromatics, cycloalkanes, aromatics, straight chain and substituted alkanes, acids and inorganics.

- PIBs chemical resistivity, non-toxicity and high thermal stability make them suitable as precursors to polymeric surfactants.
- PIBs can be functionalised with succinimide/ polyamine groups which facilitate the adsorption of the polymers at the surface of the metal walls of engines as well as the surface of the carbonaceous materials which precipitate out of the fuel.
- Two regimes have been identified concerning the coverage of particles with surfactant type dispersants known as the mushroom regime (low coverage) and brush regime (high coverage).
- Extending the length of the polyamine chain can lead to increased stabilisation of CB particles, increased adsorption amounts, enhanced adsorption enthalpy and Gibbs free energy. Additional primary and secondary amines were found to improve the adsorption the most where as additional tertiary amines had little impact due to steric effects.
- A long and rigid hydrocarbon PIB backbone gives greatest dispersion although the chain length cannot be too long to be detrimental to the performance. Generally MW 900-1000 yields the best performance. A shorter polymer chain could lead to flocculation. *Bis* functional PIB derivatives were found to be more efficient than *mono* or *tri* derivatives in the stabilisation of CB in one case.
- The effect of temperature on the rheological behaviour on PIBSI type dispersions has shown there to be an increase in viscosity at around 60 °C brought about by the conformational changes affecting the dispersancy efficiency leading to agglomeration of the carbon particles. In some instances where there was high particle concentration and long polymer chains a network structure formed, characterised by constant storage and

loss moduli. The amount of adsorbed dispersant on a solid surface (carbon nanotubes) was not sensitive to temperature change. Although a slight increase and decrease of the adsorption have both been reported at high temperatures this was not the main cause for the flocculation of particles.

- High temperature rheometry and ^1H NMR has been used previously to study the fluidity of coal samples during coking (and coal pyrolysis) and the pyrolysis of biomass polymers. The two techniques have never been used in combination to study PIB type dispersions.

3 Experimental

The first part of this chapter provides an overview of the background to the experimental techniques that were used in this work to study the various polymers, carbon blacks and polymer-carbon black dispersions. Special attention is made to nuclear magnetic resonance and rheometry. The second part provides an overview of the experimental methodologies that were used to prepare and analyse the various polymers, carbon blacks and polymer-carbon black dispersions as well as a summary of the materials used.

3.1 NMR SPECTROSCOPY

Nuclear Magnetic Resonance (NMR) is a spectroscopic technique that utilises the magnetic properties of atomic nuclei. When immersed in a static magnetic field and exposed to a secondary oscillating magnetic field certain nuclei resonate at a characteristic specific frequency that is dependent on the strength of the magnetic field and the magnetic properties of the atomic nucleus. Whether a nucleus is susceptible to this phenomenon or not depends on a property known as spin (Hore, 1995).

3.1.1 Spin

Magnetic nuclei possess fundamental property known as spin which determines the number of quantum states available for a given nucleus (Jacobsen, 2007). The atomic nucleus may be conceptualised as a positively charged sphere that is spinning on its axis. As the charge is spinning it creates a small magnetic field that is aligned with the axis of the spin. When a spin- $\frac{1}{2}$ nucleus (such as ^1H) is placed in an external magnetic field the nucleus attempts to align itself with that field. As the nucleus is already spinning (and therefore has angular momentum) the effect is that the nucleus will precess around the magnetic field direction at a rate that is known as the resonant frequency (Hore, 1995). A spin $\frac{1}{2}$ nucleus can be viewed as having two quantum states $+\frac{1}{2}$ or $-\frac{1}{2}$ with a spin axis at a 45°

angle with the external magnetic field and one with the spin axis at a 135° angle against the external magnetic field. The nucleus precesses about the z axis at a 45° (or 135°) angle at a rate that is equal to the Larmor frequency ν_o (which is in the radio frequency range of the electromagnetic spectrum) which is calculated using Equation (3-1):

$$\nu_o = \gamma B_o / 2\pi \quad (3-1)$$

where γ is a measure of the magnetic field strength of the nucleus (also known as gyromagnetic ratio) and B_o is the magnetic field strength in which the nucleus is placed.

Nuclei that are aligned with the external magnetic field are lower in energy than nuclei that are aligned against the magnetic field. The energy difference ΔE between the two states is proportional to B_o and γ and is given by Equation (3-2):

$$\Delta E = h\nu_o = h\gamma B_o / 2\pi \quad (3-2)$$

where h is Planck's constant. At thermal equilibrium just over half of the population of spins will be in the lower energy state and just less than half will be in the upper energy state. At this point, although the nuclei are all spinning (or precessing) at the same rate (or frequency), the spins are out of sync from each other i.e. there is no phase coherence (Jacobsen, 2007).

3.1.2 Vector model

The net magnetisation is the vector sum of all the nuclear magnets in a sample. If the origin of the vector is moved to the centre of an x, y, and z coordinate system, at equilibrium, the x and y components of the net magnetisation will be zero. In the vector model, the lower energy state spins cancel out the spins in the higher energy spins but since there are slightly more spin packets in the up state the result is a small net magnetisation along the z axis (Jacobsen, 2007). At

equilibrium therefore the total magnetisation of a very large number of spins has a magnitude of M_0 and is aligned along the positive z axis as shown in Figure 3-1 (Hore, 1995).

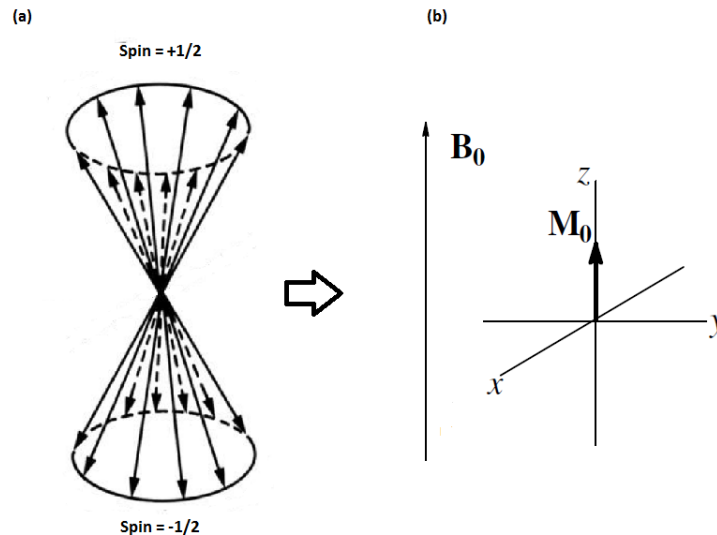


Figure 3-1: Vector model of a collection of spin-1/2 nuclei at thermal equilibrium. (a) The magnetic moment of the individual spins. (b) The net magnetic moment (M_0) of a large number of spins (Hore, 1995).

3.1.3 Pulsed magnetic field

In a typical NMR experiment a brief pulse of high-power radio frequency (RF) energy is used to excite the nuclei of a given type (such as ^1H). Immediately after the pulse the nuclei become organised so that their magnets sum together to form a net magnetisation which rotates at the Larmor frequency. The spins all point in the same direction in the x-y plane meaning there is a net magnetisation vector that rotates in the transverse plane at the Larmor frequency. The net magnetisation along the z axis at this point is now zero. The magnetic fields of the nuclei add together to give a measurable rotating magnetic field that induces an electrical voltage in a coil placed next to the sample. The coil that was used to transmit the RF is then used as a receiver and the signal is observed at the precise Larmor frequency (Jacobsen, 2007).

3.1.4 Free induction decay (FID)

After the initial RF pulse the individual nuclei become out of sync and the macroscopic signal dies down. The phase coherence decays with time due to the inhomogeneity of the magnetic field and small differences in the local magnetic field experienced by each of the spins (Jacobsen, 2007).

This echo of the pulse observed in the coil is called the free induction decay (FID) and contains all the resonant frequencies of the sample nuclei and is digitised by a computer where a software program can apply a Fourier transformation, converting the FID signal as a function of time (time domain) to a plot of intensity as a function of frequency (frequency domain). The experiment can be repeated many times by increasing the number of scans and summing the resulting data to increase sensitivity and get a stronger signal (Jacobsen, 2007).

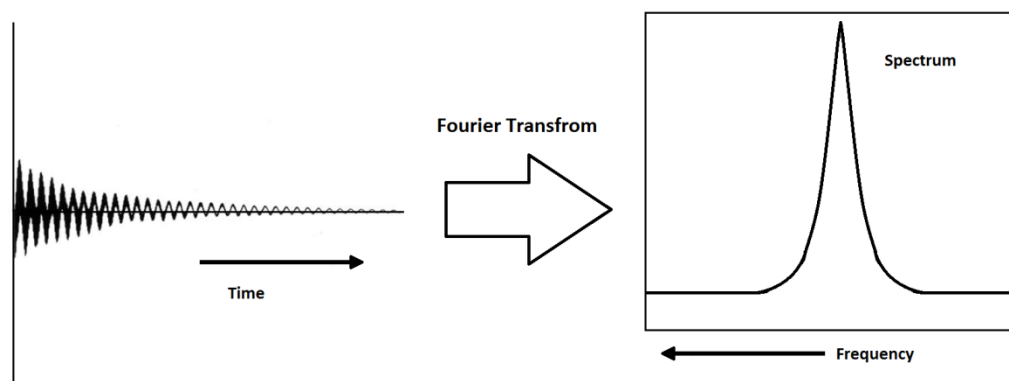


Figure 3-2: Typical Fourier transformation of FID signal (Jacobsen, 2007).

3.1.5 T_1 relaxation (spin-lattice relaxation time)

The z component of the net magnetisation vector represents the difference in the population between the two spins states. The spin-lattice relaxation time (T_1) is the length of time required for the excited spin packets to return to 63% of the way towards equilibrium (Jacobsen, 2007). It characterises the rate at which the z component of the magnetisation vector recovers (or decays) to thermal equilibrium after being flipped by a 90° RF pulse into the magnetic transverse

plane (Jacobsen, 2007). The equation controlling this behaviour as a function of the time t after its displacement is given by Equation (3-3):

$$M_z = M_0(1 - e^{-\frac{t}{T_1}}) \quad (3-3)$$

3.1.6 T_2 relaxation (spin-spin relaxation time)

The spin-spin relaxation time (T_2) is the time to reduce the transverse magnetization by a factor of e . The exponential decay of the x-y components of the net magnetisation after a 90° pulse can be represented by the following Equations (3-4) and (3-5):

$$M_y = -M_0 \cos(2\pi\nu_0 t) e^{-t/T_2} \quad (3-4)$$

$$M_x = -M_0 \sin(2\pi\nu_0 t) e^{-t/T_2} \quad (3-5)$$

Both types of relaxation (T_1 and T_2) occur simultaneously where $T_2 < T_1$. (Jacobsen, 2007).

3.1.7 High temperature ^1H NMR

High temperature ^1H NMR spectroscopy is a technique that determines changes in the dynamics of polymer molecules with temperature. The spectra obtained are normally deconvoluted into a Lorentzian distribution function which originates from protons associated with the mobile phase in the sample, and a Gaussian distribution function which originates from the protons associated with the rigid phase (Steel, Diaz, Patrick, & Snape, 2004). The spin-spin relaxation time T_2 is inversely proportional to the peak width at half-height ($\Delta H_{1/2}$) (as shown by Equation (3-6)) and is fulfilled for Lorentzian distribution functions only (Steel, Diaz, Patrick, & Snape, 2004).

$$T_2 = \frac{1}{\pi\Delta H_{1/2}} \quad (3-6)$$

As $\Delta H_{1/2}$ decreases, T_2 increases, indicating that mobility of the fluid phase is increasing.

3.2 ^{13}C NMR

^{13}C NMR spectroscopy is the application of NMR spectroscopy to carbon nuclei. ^{13}C NMR spectroscopy is much less sensitive to carbon than ^1H NMR is to hydrogen, as the major isotope of carbon, ^{12}C , has a spin quantum number of zero meaning it is not magnetically active and therefore not detectable by NMR. The less abundant ^{13}C isotope (natural abundance 1.1 %) has a spin quantum number of $\frac{1}{2}$ so is therefore detectable by NMR. The most basic pulse sequence used in ^{13}C NMR is the single pulse excitation (SPE), where there is only one pulse followed by detection of the signal.

Magic angle spinning (MAS) is often used in solid-state NMR experiments to combat line broadening caused by dipolar, chemical shift anisotropy and quadrupolar interactions experienced by the nuclear spin. In solid samples these three types of interaction are orientation-dependent and can be averaged by using MAS. By spinning the sample at the magic angle, $\theta = 54^\circ 74'$ (where $3\cos^2\theta - 1 = 0$), with respect to the direction of the magnetic field, the dipole interactions disappear and the broad lines become narrower thereby increasing the resolution of the spectrum allowing for better analysis (Akitt & Mann, 2000).

3.3 RHEOLOGY

Rheology is the study of the deformation and flow of matter. Making measurements of rheological material functions is called rheometry. Types of rheological behaviour of different materials can depend on how the material responds when a shear stress is applied and then removed by examining the effect on the response of the material i.e. the resulting strain (Tadros, 2010). If no strain

recovery occurs after deformation the material may be classified as ideally viscous whereas an ideally elastic material would recover instantaneously. If partial recovery occurs the material may be classified as an elastic liquid and includes materials such adhesives. A material that exhibits slow recovery behaviour is said to be viscoelastic. Viscoelastic materials can include polymer solutions, suspensions and emulsions (Tadros, 2010).

3.3.1 Hooke's law of elasticity

Hooke's law describes the behaviour of a perfect elastic solid and can be described using Equation (3-7):

$$\sigma = G\gamma \quad (3-7)$$

where σ is the applied stress (force per unit surface), γ is the strain and G is the elastic modulus (Menard, 1999). Hooke's law therefore states that the stress (force per unit area) is proportional to the strain (relative deformation). A material which obeys Hooke's law is known as a Hookean solid (Tadros, 2010).

3.3.2 Newton's Law of Viscosity

Constitutive law applies to viscous fluids and may be described by Equation (3-8):

$$\sigma = \eta\dot{\gamma} \quad (3-8)$$

where σ is the applied stress, η is the dynamic shear viscosity and $\dot{\gamma}$ is the velocity gradient (or shear rate). Viscous fluids that obey this law are known as Newtonian. $\dot{\gamma}$ is measured in s^{-1} therefore the viscosity is measured on Pascal seconds, Pa.s also known as poiseuille (SI units) or in poise (P) in CGS system ($1 \text{ Pa.s} = 10 \text{ P}$) (Oswald, 2009). The resistance that arises from the lack of slipperiness of parts of a liquid (all other things being equal) is proportional to the velocity with which

the parts of the liquid are separated from one another. The strain rate $\dot{\gamma}$ is a single values function of stress as displayed in Equation (3-9) (Tadros, 2010).

$$\dot{\gamma} = f(\sigma) \quad (3-9)$$

The stress (σ) versus shear rate ($\dot{\gamma}$) is linear and the slope is equal to the viscosity (η). The viscosity (η) is given by the ratio of shear stress over shear rate as shown in Equation (3-10):

$$\eta = \frac{\sigma}{\dot{\gamma}} = \frac{Nm^{-2}}{s^{-1}} = Nm^{-2}s = Pa.s \quad (3-10)$$

3.3.3 Dynamic oscillatory measurements of viscoelastic materials

A viscoelastic substance has both an elastic component and a viscous component. Dynamic oscillatory measurements refer to experiments in which both stress and strain vary harmonically (Tadros, 2010). The viscoelastic behaviour of a sample can be obtained by measuring the phase angle (δ) of a sample. If a particular sample measured behaves as an ideal elastic material, the strain and stress curves over time are identical and $\delta = 0^\circ$. If a sample behaves as an ideal viscous material the strain and stress curves over time would be out of phase by 90° . As Figure 3-3 shows there is a loss in amplitude between the input strain and the response stress due to viscous energy dissipation (Tadros, 2010).

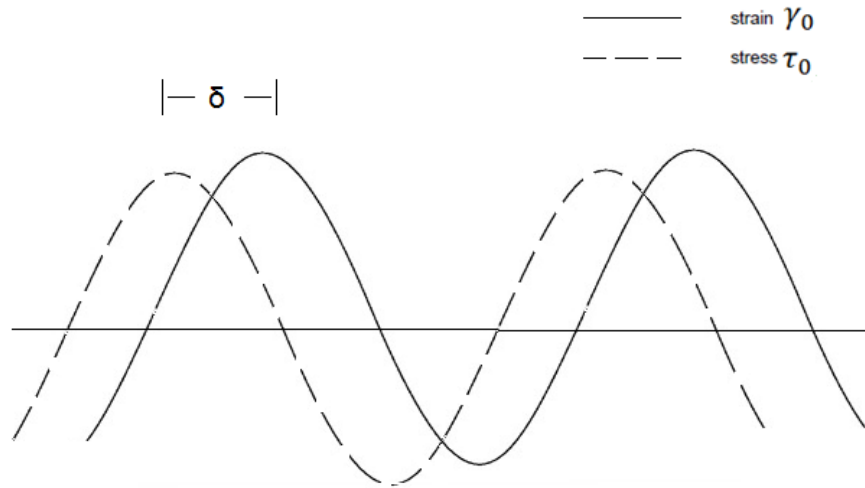


Figure 3-3: Schematic representation of response to an oscillatory strain or stress for a viscoelastic system ($0^\circ < \delta < 90^\circ$) (Tadros, 2010).

Viscoelastic materials have a phase angle value between 0 and 90°. The storage modulus (G') is proportional to the elastic energy that is stored and recovered (elastic component) and the loss modulus (G'') proportional to the energy dissipated in flow (viscous component). G' and G'' are given by Equations (3-11) and (3-12) respectively:

$$G' = \frac{\tau_0}{\gamma_0} \cos \delta \quad (3-11)$$

$$G'' = \frac{\tau_0}{\gamma_0} \sin \delta \quad (3-12)$$

where τ_0 is the maximum stress response measured in the sinusoidal motion and γ_0 is the maximum applied strain in the sinusoidal motion.

The ratio of the maximum stress τ_0 to the maximum strain γ_0 gives the complex modulus G^* (Tadros, 2010).

$$G^* = \frac{\tau_0}{\gamma_0} \quad (3-13)$$

G^* may be resolved into G' which is the real component of the complex modulus and G'' which is the imaginary component of the complex modulus as shown by Equation (3-14):

$$G^* = G' + iG'' \quad (3-14)$$

where i is the imaginary number that is equal to $\sqrt{-1}$ (Tadros, 2010).

The complex viscosity η^* is given by the Equation (3-15) where ω is the frequency (Steel, Diaz, Patrick, & Snape, 2004).

$$|\eta^*| = \frac{\sqrt{(G')^2 + (G'')^2}}{\omega} \quad (3-15)$$

It is important when measuring η^* that tests are conducted in the linear viscoelastic region i.e. where the stress of the sample is proportional to strain. To test whether the rheometer is operating in the linear viscoelastic region a strain sweep test is usually performed where the strain is varied and G' and G'' are measured. If G' and G'' are constant with the strain rate then the sample is said to be within the linear viscoelastic region. If measurements are outside of the linear viscoelastic region then the results are more dependent on experimental details and it is harder to relate to the unique properties of the material (Steel, Diaz, Patrick, & Snape, 2004).

3.4 THERMOGRAVIMETRIC ANALYSIS (TGA)

Thermogravimetric analysis (TGA) is a technique to measure the amount and rate of change in the weight of a material as a function of temperature or time as the sample specimen is subjected to a controlled temperature program in a controlled atmosphere. TGA is used to determine a materials thermal stability and its fraction of volatile components. In TGA, a sample pan is supported on a precision balance which is housed in a furnace that is heated or cooled according to the temperature program for the experiment. The sample mass is monitored throughout the

experiment. The sample environment is controlled by a purge gas which may either be an inert gas or a reactive gas which flows over the sample and exits through an exhaust (Perkin Elmer, 2010).

3.5 TEMPERATURE PROGRAMMED OXIDATION (TPO)

In TPO a sample is heated in an oxygen atmosphere and the evolution of carbon dioxide is recorded. More amorphous carbon is more reactive than more structured graphitic carbon and therefore oxidises at a lower temperature. The sample is heated in a temperature controlled furnace. The CO₂ resulting from the oxidation of the carbon is detected by IR detectors (Barker et al., 2010).

3.6 GEL PERMEATION CHROMATOGRAPHY (GPC)

Gel permeation chromatography (GPC) is a powerful and versatile analytical technique used to understand and predict polymer performance. GPC can determine several important parameters including number average molecular weight, weight average molecular weight and the molecular weight distribution of the polymer. GPC separates molecules in a solution by size and as such, is a size exclusion chromatography (SEC) technique (Waters, 2015) .

3.7 X-RAY PHOTOELECTRON SPECTROSCOPY (XPS)

X-ray photoelectron spectroscopy (XPS) is a surface analysis technique which is used to measure the elemental composition of a material. The material is bombarded with X-rays and photons are adsorbed by elements on the surface of the sample. This leads to ionisation and the emission of core electrons. Measuring the kinetic energy distribution of the photoelectrons which are emitted allows determination of the electron binding energies. Each element has a characteristic binding energy associated with the core atomic orbital and therefore any given element has its own characteristic peak in the photoelectron spectrum. The intensities of the peaks can be related to the concentration of the given element in the sampled region, allowing XPS to provide quantitative analysis of the surface

composition. Small changes in peak positions, known as chemical shifts, arise from small changes in binding energy due to changes in oxidation state or chemical environment. XPS is not sensitive to hydrogen or helium but can detect all other elements (University of Nottingham, 2015).

3.8 BRUNAUER-EMMETT-TELLER (BET) ANALYSIS

Brunauer-Emmett-Teller (BET) analysis is a precise, specific surface area measurement technique. The surface area of a powder is determined by physically adsorbing a gas onto the surface of the solid and calculating the amount of adsorbed gas which corresponds to a monomolecular layer on the solid surface. The physical adsorption is a result of van der Waals forces between the adsorbate gas molecules and the adsorbent surface of the test sample (Particle Analytical, 2015).

3.9 PARTICLE SIZE ANALYSIS (VIA LASER DIFFRACTION)

In laser diffraction, the sample material is passed through a laser beam which results in the laser light scattering at a wide range of angles. Detectors at fixed angles measure the intensity of the scattered light and particle size distribution is calculated by a mathematical model. The final result is reported as equivalent spherical volume. Laser diffraction can generate the $D[4,3]$ or equivalent volume mean, which is identical to the weight equivalent mean if density is constant (Malvern, 1994).

3.10 MATERIALS

3.10.1 Summary of polymer samples

The commercial polymers used in this study were supplied by Innospec Inc. A summary of the properties of the polymers used are shown in Table 3-1. The number average molecular weight of the PIB backbone (PIB- M_n) from which the polymers are derived is also presented as is the PIB functionality (PIB Func.) which

corresponds to the number of PIB hydrocarbon tails that is chemically bonded to the head group. All polymers with (the exception of PIBSI-B) were synthesised via thermal synthetic route (ENE type reaction). PIBSI-B was synthesised via chlorine synthetic route (Dien Alder type reaction). The chemical structures of the head groups can be found in Appendix A.

Table 3-1: Polymer Properties

Polymer Reference	PIB-M_n (g/mol)	PIB Funct.	Head group
PIB	750	N/A	N/A
PIBSA(-A)	750	<i>mono</i>	Succinic Anhydride
PIBSA-B	260	<i>mono</i>	Succinic Anhydride
PIBSA-C	1000	<i>mono</i>	Succinic Anhydride
PIBSI-A	750	<i>mono</i>	Succinimide with tetraethylenepentamine (TEPA)
PIBSI-B	1000	<i>mono</i>	Succinimide with tetraethylenepentamine (TEPA)
PIBSI-C	750	<i>mono</i>	Succinimide with Aminoethylethanolamine (AEEA)
PIBSI-D	750	<i>mono</i>	Succinimide with Ethanolamine
PIBSI-E	750	<i>mono</i>	Succinimide with Aminoethylethanolamine (AEEA)
PIBSI-F	260	<i>mono</i>	Succinimide with Ethanolamine
PIBSI-G	1000	<i>bis</i>	Succinimide with tetraethylenepentamine (TEPA)
PIBSI-H	1000	<i>bis</i>	Succinimide with tetraethylenepentamine (TEPA)
PIBSI-I	750	<i>bis</i>	Succinimide with ethylenediamine (EDA)
PIBSI-J	1000	<i>mono</i>	Succinimide with Ethanolamine
PIBSI-K	750	<i>mono</i>	Succinimide with ethylenediamine (EDA)

The number average molecular weight (M_n), weight average molecular weight (M_w) and polydispersity values (PD) of the final polymer products obtained from GPC analysis are displayed in Table 3-2.

Table 3-2: Average molecular weights and polydispersity of polymer samples.

Polymer	M_n (g/mol)	M_w (g/mol)	PD
PIB	771	1075	1.4
PIBSA-A	904	1170	1.3
PIBSA-B	347	363	1.0
PIBSA-C	1046	1342	1.3
PIBSI-A	1253	2049	1.6
PIBSI-B	1740	2648	1.5
PIBSI-C	748	1794	2.4
PIBSI-D	1005	1352	1.3
PIBSI-E	1277	2037	1.6
PIBSI-F	382	442	1.2
PIBSI-G	1921	3473	1.8
PIBSI-H	1858	2793	1.5
PIBSI-I	1490	2055	1.4
PIBSI-J	1118	1469	1.3
PIBSI-K	1653	2717	1.6

3.10.2 Summary of carbon samples

The primary carbon used in this study was small particle mesoporous carbon black adsorbent (MicroCB) and was obtained from Sigma Aldrich. The remaining commercial carbon samples were supplied from Innospec Inc. and were originally sourced from Ashbury Carbons or Degussa. A brief description of the carbons is below. A more detailed description of each may be found at Barker et al., (2010) (excluding MicroCB).

Mesoporous carbon black (MicroCB) - Sigma Aldrich

Mesoporous carbon black (MicroCB) is a graphitised carbon black adsorbent with a 100 Å average pore diameter and particle size of 45 µm ± 5. The pore structure allows for efficient, selective adsorption of polar molecules (Sigma Aldrich, 2015).

Degussa Carbon Black (DegCB) - Degussa

Degussa carbon black (DegCB) is an amorphous solid that is manufactured by the deposition of solid carbon particulates in the gas phase. It is manufactured by combustion or thermal cracking of hydrocarbon fuel under reducing conditions.

Green Coke (GreenCoke) - Ashbury carbons

Green coke is a manufactured carbon product resulting from the thermal processing of residual oil. The coke contains around 15-20 % residual hydrocarbon materials.

Calcined Petroleum Coke (Calcoke)-Ashbury Carbons

Calcined petroleum coke is manufactured by heating green coke in a rotary kiln to approx. 1300 °C to remove residual hydrocarbons.

Synthetic graphite450 (Micro450) – Ashbury carbons

Synthetic graphite is made by high-temperature treatment of certain amorphous carbon materials. Ultra-high processing ensures a purity higher than 98 % carbon.

Flake graphite850 (Micro850)

Flake graphite is a naturally occurring form of graphite that has been treated to reduce the level of naturally occurring ash constituents to < 1 %. This form of graphite has a high degree of crystallinity, and high thermal and electrical conductivity.

Flake graphite146 (Micro146)

Micro164 is milled, natural flake graphite which has been processed directly from graphite flakes that have not undergone any post-floatation purification process.

The carbon properties are summarised in Table 3-3. Unless otherwise stated the properties were obtained from relevant product data sheets and are nominal values.

Table 3-3: Carbon Properties

Carbon Black	Average Particle size (μm)	Surface Area (m^2/g)
Mesoporous Carbon Black Adsorbent (MicroCB)	45	205
Degussa Carbon Black (DegCB)	43 D[4,3] (From particle size analysis)	417 (From BET analysis)
Flake graphite146 (Micro146)	21	6
Flake graphite850 (Micro850)	5	13
Synthetic graphite450 (Micro450)	5	17
Green Coke (GreenCoke)	2	10
Calcined Coke (CalCoke)	6	20

3.10.3 Solvent

Hexane (Aldrich, > 95 %) (BP. 69°C) was used as a solvent in the preparation of all the dispersions in this study.

3.11 PREPARATION OF POLYMER CARBON DISPERSION SAMPLES

The following sample preparation was developed in collaboration with Dr. Miguel Castro Díaz through examination of the relevant literature. The dispersions were prepared by adding approximately 10 ml of hexane (Aldrich, > 95 %) to the polymer and mixing the solution vigorously with a magnetic stirrer until the polymer was completely dissolved in the hexane. Afterwards, the carbon black particles were added to the solution whilst continuously stirring the mixture. The dispersion was then ultrasonicated for 5 minutes and stirred for 24 hours after which the dispersed particles were left to settle down and the hexane allowed to almost evaporate. The dispersions were prepared using a total mass of carbon black and polymer of 1.6 g.

3.12 DESCRIPTION OF ANALYTICAL TECHNIQUES

3.12.1 High temperature ^1H Nuclear Magnetic Resonance spectroscopy

A high-temperature Doty 200 MHz NMR probe was used in conjunction with a Bruker MSL300 instrument to study the thermal behaviour of the dispersants and carbon black. A flow of $18 \text{ dm}^3 \text{ min}^{-1}$ dry nitrogen was used to transfer heat to the samples and to remove the volatiles that escaped from the container. Below the sample region, a flow of $65 - 75 \text{ dm}^3 \text{ min}^{-1}$ of dry air prevented the temperature rising above $50 \text{ }^\circ\text{C}$ to protect the electrical components. Air was blown at $20 \text{ dm}^3 \text{ min}^{-1}$ into the region between the top bell Dewar enclosing the sample region and the outer side of the probe to prevent the temperature from exceeding $110 \text{ }^\circ\text{C}$. The sample temperature was monitored using a thermocouple in direct contact with the sample container. A standard solid echo pulse sequence ($90^\circ - \tau - 90^\circ$) which has previously been used by Steel et al., (2004) to measure ^1H mobility in coals was used to acquire the data. A pulse length of $3.50 \mu\text{s}$ was maintained throughout the test. Approximately 100 mg of sample was placed in a ceramic capsule, and 100 scans were accumulated using a recycle delay of 0.3 s. The samples were heated from room temperature with a heating rate of approximately $3 \text{ }^\circ\text{C min}^{-1}$. This heating rate was chosen as it allowed sufficient time for the temperature to increase between each acquisition of the spectra. Almost no Gaussian distribution functions were observed in the spectra, and the NMR signal was composed in most cases of a Lorentzian distribution function only. As T_2 is inversely proportional to $\Delta H_{1/2}$, this measurement could be used to obtain information about the mobility of the fluid ^1H of the polymer dispersant adsorbed onto the carbon black as a function of temperature. The tip of the NMR probe was cleaned between runs by ultrasonicing in tetrahydrofuran (THF) GPC grade (Aldrich) for 10 minutes.

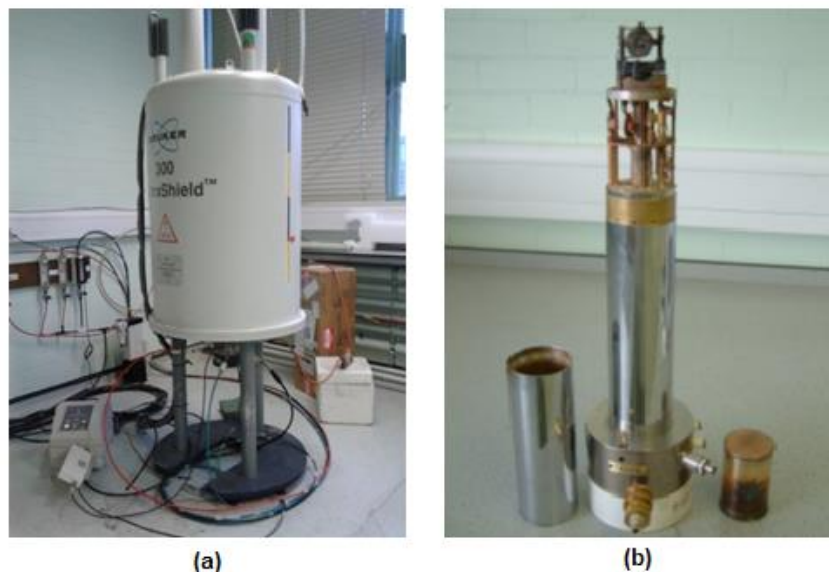


Figure 3-4: (a) Image of Bruker MSL300 instrument and (b) Image of Doty 200 MHz NMR probe

3.12.2 Solid state ^{13}C NMR spectroscopy

High-resolution solid state 50 MHz ^{13}C NMR analyses was carried out in a Bruker MSL300 instrument using a standard single pulse excitation (SPE) pulse sequence in conjunction with magic angle spinning (MAS) at ambient temperature. The acquisition time was 0.03 s, the relaxation delay was 30 s. The spectra were obtained with 7500 scans. The samples were packed tight into a cylindrical (7 mm) zirconia rotor with a cap made of a homopolymer of chlorotrifluoroethene (Kel-F) and spun at the magic angle ($54^{\circ}74'$) with a spinning rate of approximately 3 kHz. Tetrakis(trimethylsilyl) silane (TKS) was added to the samples as an internal standard.

3.12.3 High temperature rheometry

The majority of the rheological measurements were carried out at the University of Nottingham (UoN) on a RDA III high torque strain controlled rheometer. A limited number of analyses were also carried out at Innospec Inc. on a TA AR-2000 controlled-stress rheometer. The general test conditions unless stated otherwise were the same for both instruments. The rheometer tests involved

placing the carbon black/polymer dispersions between two 25 mm parallel plates. The amount of sample for each test was chosen to fill a 1 mm gap between the plates. The sample was heated from 30-50 °C up to 300-400 °C at a heating rate of 3 °C min⁻¹ to mimic ¹H NMR conditions. The furnace surrounding the sample was purged with a constant flow of nitrogen to transfer heat to the sample and remove any volatiles. The sample temperature was monitored using a thermocouple in direct contact with the bottom plate. The viscoelasticity of the dispersions was measured at a frequency of 1 Hz to obtain the complex viscosity (η^*) as a function of temperature. The majority of the analysis (RDA III instrument only) was carried out with auto tension adjustment with a constant normal force of 20 g. This allowed the plate gap to change with the expansion and contraction of the sample. Strain-sweep tests were performed on the RDA III instrument to ensure that measurements were within the linear viscoelastic region. The strain-sweeps were performed at 100, 250 and 350 °C in the strain region $\gamma = 0.01\% - 10\%$. The minimum η^* that the Rheometrics RDA-III rheometer instrument can measure is approx. 10^3 Pa.s while the minimum η^* that the TA AR-2000 rheometer instrument can measure is approx. 10^1 Pa.s.

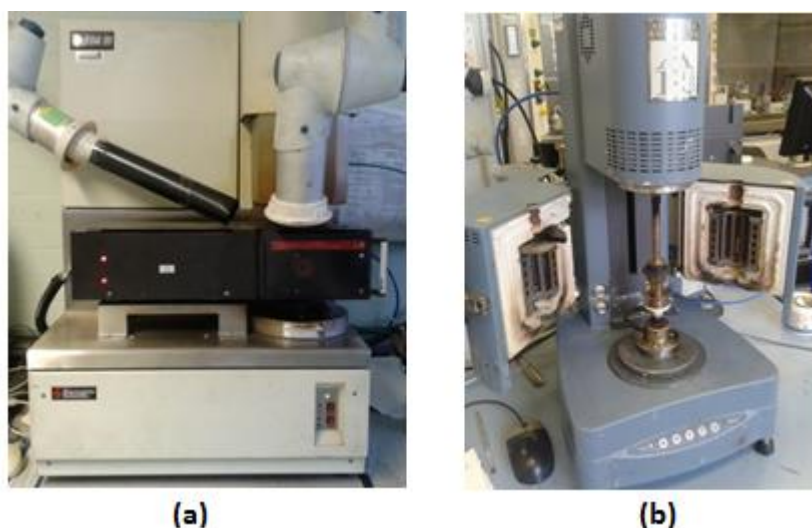


Figure 3-5:(a) Image of RDA III high torque strain controlled rheometer (UoN), (b) Image of TA AR-2000 controlled-stress rheometer (Innospec Inc.)

3.12.4 Thermogravimetric analysis (TGA)

TGA measurements of the polymers and dispersions were carried out on a TA Q500 thermogravimetric analyser. Approximately 10 mg of sample was placed in the pan. An isothermal test at 30 °C was initially carried out to purge the air in the system. Then, the samples were pyrolysed at a constant heating rate of 3 °C min⁻¹ to 500 °C in a nitrogen atmosphere to mimic ¹H NMR and rheometry conditions. A nitrogen flow rate of 100 cm³ min⁻¹ was used to sweep out the volatile products. The majority of the measurements were carried out at Innospec Inc. by Mr Barry Cheeseman.

3.12.5 Temperature programmed oxidation (TPO)

TPO experiments were performed using a Leco[®] RC612 Carbon/Hydrogen/Moisture determinator. In TPO a sample is heated in an oxygen atmosphere and the evolution of carbon dioxide is recorded. More amorphous carbon is more reactive than more structured graphitic carbon and therefore oxidises at a lower temperature. The sample is heated in a temperature controlled furnace. The CO₂ resulting from the oxidation of the carbon is detected by IR detectors (Barker et al., 2010). The TPO analysis for this work was carried at Innospec Inc. by Mr David Pinch.

3.12.6 Gel permeation chromatography (GPC).

Molecular weights (M_n and M_w) and polydispersity (M_w/M_n) were determined with respect to polyisobutylene standards by gel permeation chromatography (GPC). The Waters Alliance 2695 system that was used was equipped with a Waters refractive index Detector 2414. Four Waters Syragel[®] gel columns (HR 4, 2, 1, 0.5 ((7.8 x 300 mm)) were used. Tetrahydrofuran (THF) GPC grade (Fischer) was used as an eluent and was delivered at a flow rate of 1.0 mL min⁻¹. Approx. 0.1-0.2 g sample was weighed into a 25 ml grade A volumetric flask. The flask was then made up to the mark with THF. The injection volume was 100 µL. All samples

were analysed at 39 °C. The samples were then run against a calibration graph generated by a relevant set of standards and the Mw/Mn calculated using Empower Pro software. The majority of the GPC analysis was carried out at Innospec Inc. by Dr. Jim Barker.

3.12.7 X-ray Photoelectron Spectroscopy (XPS)

X-ray photoelectron spectrum (XPS) measurements were carried out to determine the surface elemental composition of the carbon samples on a PHI5300 X-ray photoelectron spectrometer. A monochromatic Al K α source (1486.6 eV) was used at power 210 W. The instrument was used in fixed analyser transmission mode, with pass energy of 80 eV for wide scans and 20 eV for high resolution scans. Elements of interest included carbon, nitrogen, oxygen, iron, nickel, and cobalt. All XPS analysis was carried out at the University of Nottingham by Dr. Emily Smith.

3.12.8 Brunauer-Emmett-Teller (BET) Analysis

The surface of one of the carbons was investigated by N₂ adsorption/desorption at -196 °C using an ASAP 2020 micrometrics instrument. Approx. 0.1 g sample was degassed at 80 °C in a vacuum for 16 h prior to analysis. Experimental adsorption data at a relative pressure (P/P_0) from 0.01 to 0.99 were used to calculate the surface area using micrometrics software programme. BET analysis for this work was carried out at the University of Nottingham by Mr. Nannan Sun.

3.12.9 Particle size analysis (via laser diffraction)

The particle size was measured on a Malvern Mastersizer type S instrument. After measuring the background, the approx. 10 mg sample is added to the ultra-pure water within the instrument Mastersizer so that the obscuration monitor is between 10 and 40 %. The sample is measured for 10-30 s to ensure that all particles are represented in the measurement and to average out fluctuations

caused by the dispersing medium. The analysis was carried out with the assistance of Dr. Lee Stevens.

4 Optimisation of Sample Preparation and Main Analytical Methods

This chapter includes initial experimental attempts to characterise dispersions of polyisobutylene succinimide (PIBSI) and a carbon black (MicroCB) using rheometry and ^1H NMR at high temperatures in order to optimise the conditions for sample preparation and analytical methodologies. In some cases corresponding PIB and PIBSA dispersions are also included to highlight the level of distinguishability between the viscosity and mobility trends of the polymers. The actual rheological and ^1H NMR mobility behaviour of the polymer dispersions will be described and discussed in chapter 5.

4.1 EXPERIMENTAL

4.1.1 Materials

The commercial polymers used in this chapter were supplied by Innospec Inc. A summary of the structures are shown in Table 4-1. The number and weight average molecular weight and polydispersity values are also presented in Table 4-1.

A particular PIBSI (PIBSI-A) was chosen for the majority of the optimisation tests as a PIBSI with a large tetraethylenepentamine (TEPA) head group with multiple amines should exhibit a strong interaction with the carbon black therefore provide an indication of how a “good” dispersant would behave, setting a precedent for future tests.

Table 4-1: Head groups, average molecular weights, polydispersity and functionality of polymer samples.

Polymer reference	Polymer Head group*	PIB-M_n (g/mol)	M_n (g/mol)	M_w (g/mol)	PD	PIB Funct.
PIB	N/A	750	771	1075	1.4	N/A
PIBSA(-A)	Succinic Anhydride	750	904	1170	1.3	<i>mono</i>
PIBSI-A	TEPA	750	1253	2049	1.6	<i>mono</i>

*Refer to section 3.10.1 for head group abbreviations

A commercial carbon black (MicroCB) with an average particle size of 45 μm and surface area of 205 m^2g^{-1} is used in this chapter. A description of this carbon can be found in section 3.10.2. Hexane (Aldrich 95 % was used) was used as a solvent.

4.1.2 Dispersion sample preparation

The PIBSI MicroCB (and PIB and PIBSA) dispersions were prepared as described in the experimental section 3.11. Any variations to the sample preparation to optimise the conditions for analysis are included in this chapter.

4.2 OPTIMISATION CONDITIONS FOR CHARACTERISATION OF POLYMER/ CARBON

DISPERSIONS- RHEOMETRY

Initial rheological measurements were performed on a Rheometrics RDA-III high torque controlled strain rheometer. The rheometer tests were carried out as described in section 3.12.3. Variations to the analysis conditions are included herein. This rheometer instrument was designed for more solid like samples such as coal and biomass samples therefore dispersions containing 25 % and 35 % MicroCB loadings were initially prepared as it was believed this would yield samples sufficiently viscous enough to yield η^* values that were within the limit of the instrument (minimum $\eta^* \sim 10^3$ Pa.s.). The samples were prepared as described in section 3.11 and then transferred to the rheometer plate using a spatula. It was found after a few attempts that the easiest way to transfer the

dispersion sample was to retain some hexane in the sample so that it remained fluid for easier transfer to the rheometer lower plate. If this was not done, the sample would stick to the spatula (or to the inside of the jar) and would have to be “pasted” onto the plate rather than gently dropped. A photograph of the sample on the lower plate prior to being analysed is shown in Figure 4-1. Once the sample had been transferred the top plate was lowered to give a 1 mm gap and any excess sample was carefully wiped away (this ensured the same amount of sample could be replicated for each test).



Figure 4-1: Image of PIBSI 65% MicroCB 35% sample on rheometer plate prior to analysis.

4.2.1 Auto tension adjustment on/off

Figure 4-2 presents the complex viscosity (η^*) of the dispersions of PIB, PIBSA and PIBSI-A (65 %) with MicroCB (35 %) as a function of temperature under a nitrogen atmosphere and using a heating rate of $3\text{ }^\circ\text{C min}^{-1}$, a strain of 0.05 % and a frequency of 1 Hz (6.283 rad s^{-1}). The plate gap was fixed at 1 mm throughout the duration of the tests (also referred to as “Auto tension off”). The graph shows that the viscosity of the dispersions with different polymers with the same MicroCB loading increased largely linearly with temperature and overall the three polymer dispersions show similar trends (although the PIBSI-A does exhibit

high η^* values throughout the test). It was found that when doing these tests the force exerted on the top plate was considerable (almost 2000 g) due to the fixed plate gap (auto tension off). While not only having the potential to damage the instrument this also amplified the η^* data and so the η^* trend resulted in very high η^* values (up to 2.6×10^7 Pa.s), particularly at high temperatures.

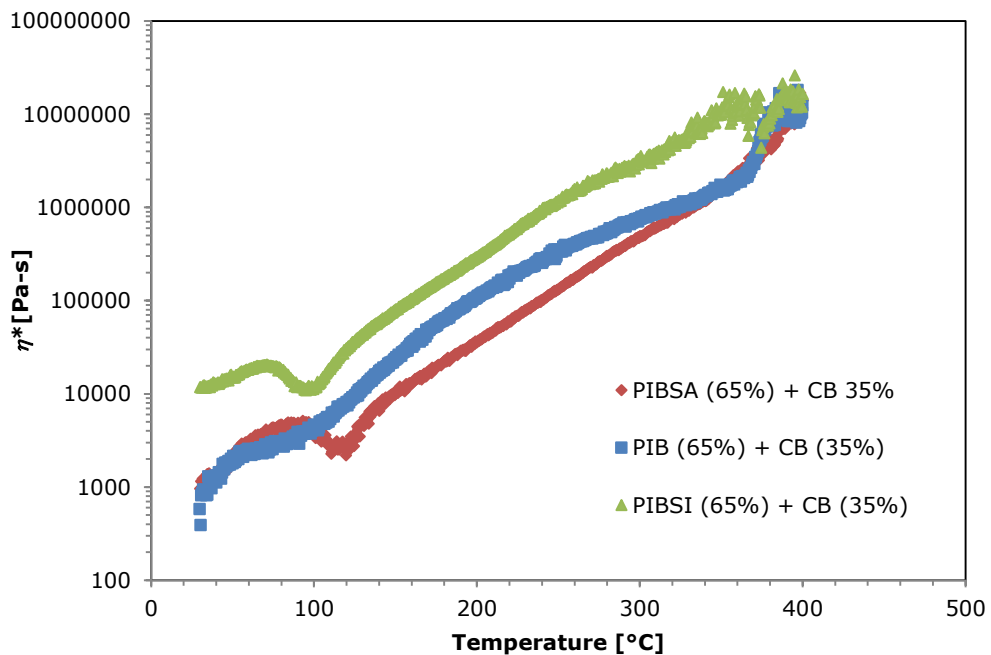


Figure 4-2: Complex viscosity (η^*) as a function of temperature for PIB, PIBSA and PIBSI-A (65 %) MicroCB (35 %) dispersions using a heating rate of $3 \text{ }^\circ\text{C min}^{-1}$ ($\gamma=0.05 \%$, $\omega=1 \text{ Hz}$) (RDA-III instrument). Auto tension off.

A number of tests were carried out at lower solid loading to attempt to investigate whether the η^* trends could be more easily distinguished as well as to limit the force exerted on the top plate of the rheometer. Figure 4-3 shows the η^* trend for PIB, PIBSA and PIBSI-A (75 %) MicroCB (25 %) dispersions. The graph shows that decreasing the solid loading to 25 % once again gave largely linear η^* trends albeit at lower η^* values. While the PIBSI-A dispersion exhibits higher η^* values throughout heating the PIB and the PIBSA dispersion trends are largely indistinguishable. Also, at high temperatures ($> 300 \text{ }^\circ\text{C}$) the force exerted on the

top rheometer plate was still very high which again risked damaging the instrument as well as amplifying the η^* values.

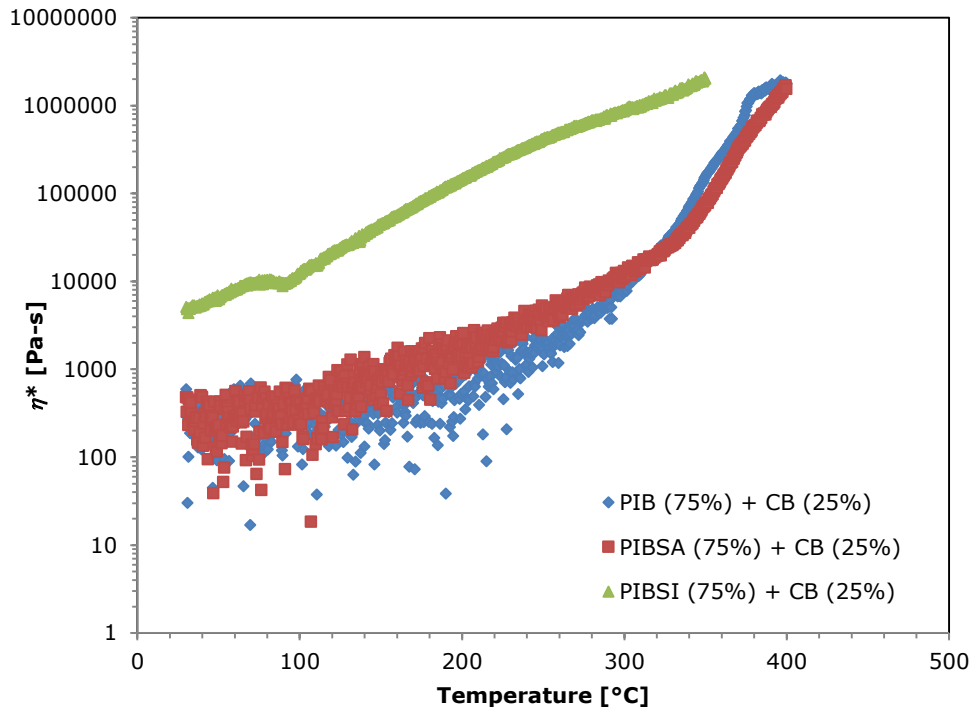


Figure 4-3: Complex viscosity (η^*) as a function of temperature for PIB, PIBSA and PIBSI-A (75 %) MicroCB (25 %) dispersions using a heating rate of 3 °C min^{-1} ($\gamma=0.05$ %, $\omega=1$ Hz) (RDA-III instrument). Auto tension off.

To rectify this, the tests were repeated with the dispersions with the auto tension adjustment switched on. This meant that instead of a fixed plate gap the top plate gap would automatically change in order to maintain a constant force on the sample. This method has been used previously when analysing the expansion and contraction of biomass samples (Dufour, et al., 2012).

A number of samples were again made and analysed with the auto tension adjustment setting turned on. A constant force of 20 g was maintained throughout the test. Initially, a number of PIBSI (75 %) MicroCB (25 %) samples were made and the analysis attempted. However these were all unsuccessful due to the top

plate squashing the sample so much that the dispersion overflowed over the edge of the bottom plate. The force was adjusted to 10 g but the same result occurred. The force was then adjusted to 5 g which was successful in that the sample was not squashed so much that it was lost from the plate however after a few minutes the plate gap rose suddenly so that it was no longer in contact with the sample. This meant that the sensitivity was too high and the test had to be aborted. Consequently, a PIBSI-A (65 %) MicroCB (35 %) sample was made and it was found that it was sufficiently viscous enough that the sample remained between the plates with a constant force of 20 g.

Figure 4-4 shows the η^* values of a dispersion of PIBSI-A (65%) and MicroCB (35%) as a function of temperature. Corresponding PIB and PIBSA dispersions are also shown. With the top plate free to move up and down with the expansion/contraction of the sample it was ensured that the force exerted onto the top plate did not affect the η^* trend. The graph shows that the viscoelastic trends of the three polymers are much more distinguishable with the auto tension adjustment. A description of the η^* trends and explanations for the differences in the viscoelastic behaviour of the PIB, PIBSA and PIBSI-A MicroCB dispersions is presented in chapter 5.

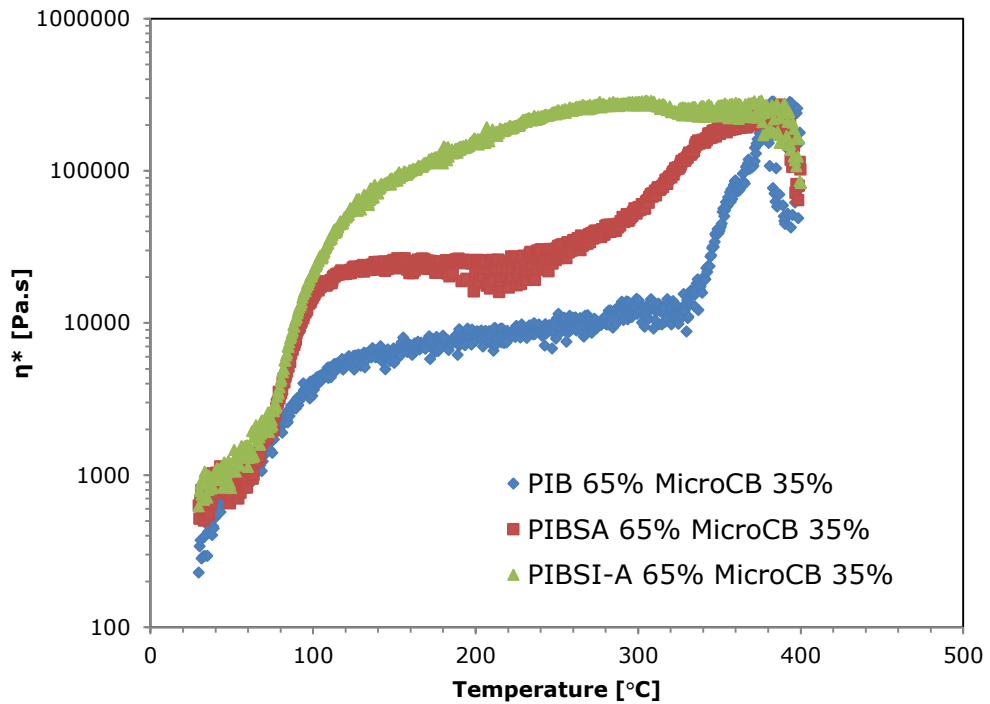


Figure 4-4: η^* as a function of temperature for PIB, PIBSA, PIBSI-A and PIBSI-B (65 %) - MicroCB (35 %) dispersions using a heating rate of $3 \text{ }^\circ\text{C min}^{-1}$ in nitrogen ($\gamma = 0.05$, $\omega = 1 \text{ Hz}$). (RDA-III instrument).

4.2.2 Strain-sweep measurements

In order to verify that the dispersion measurement was within the linear viscoelastic region at this carbon loading a number of strain-sweep tests were carried out using PIBSI dispersions (65 % polymer 35 % MicroCB). The strain-sweeps were performed at 100, 250 and 350 °C in the strain region $\gamma = 0.01 \text{ \%} - 10 \text{ \%}$. It was found that the storage modulus (G') and loss modulus (G'') for the dispersions remain fairly constant at strains $< 0.1 \text{ \%}$. This therefore showed that the viscoelastic properties of the dispersions are not affected by strains of 0.05 %. An example of one of the strain sweep test carried out at 100 °C is shown in Figure 4-5. Other strain sweep tests at different temperatures for PIBSI-A (as well as PIB) dispersions may be found in Appendix B.

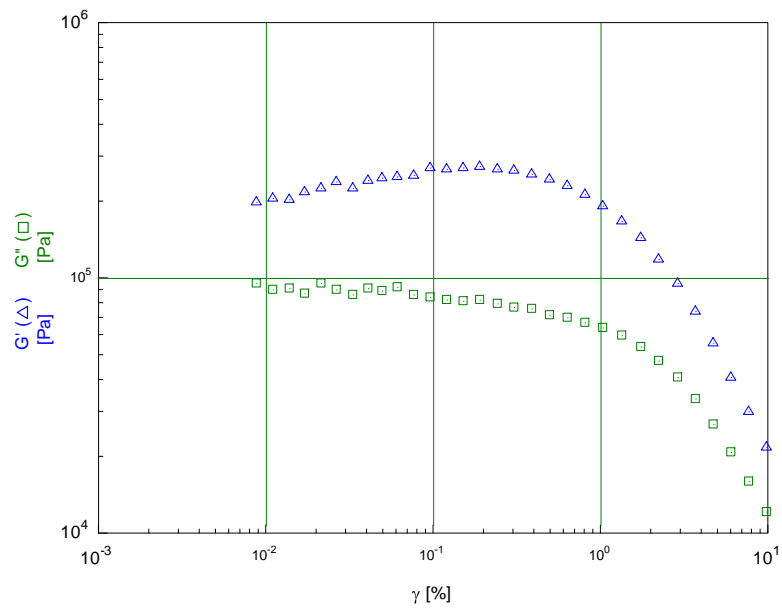


Figure 4-5: Storage (G') and loss (G'') moduli as a function of strain (γ) at 250 °C for PIBSI-A (65 %) MicroCB (35 %) dispersion.

4.2.3 Sample reproducibility

Duplicate tests of the PIBSI-A (65 %) MicroCB (35 %) sample using the same methodology were carried out to ensure reproducibility. Figure 4-6 shows the data for each individual run replicated three additional times. Figure 4-7 shows the mean η^* as a function of temperature for these tests. A filter has been applied to the data so that the error bars which are to 1 standard deviation of the sample mean can be presented. The graph provides evidence that samples prepared using the methodology described gave reproducible trends. The error measurement increases as the increasing temperature caused an increase in the η^* of the sample. For instance the standard error of the sample mean at 100 °C is ± 9177 Pa.s whereas the error at 250 °C was ± 75051 Pa.s. Whether this is a good or bad experimental error depends on whether different polymer dispersions are

distinguishable within this error and this is demonstrated in chapter 4 when characterising PIB, PIBSA, and PIBSI-dispersions.

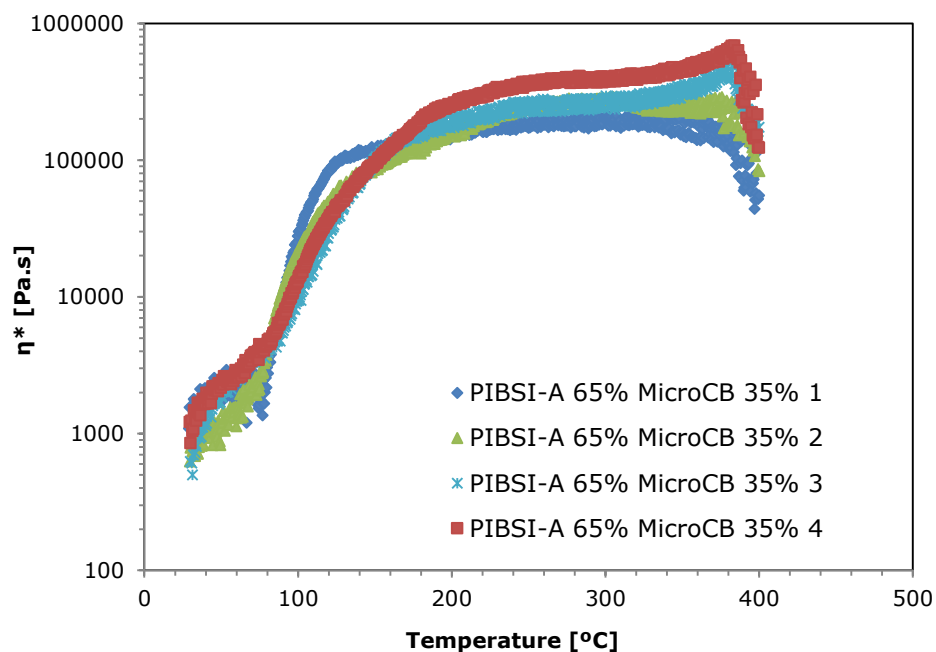


Figure 4-6: Duplicate samples of PIBSI-A (65 %) and MicroCB (35 %) (1-4) using a heating rate of $3 \text{ }^\circ\text{C min}^{-1}$ in nitrogen ($\gamma = 0.05$, $\omega = 1 \text{ Hz}$). (RDA-III instrument).

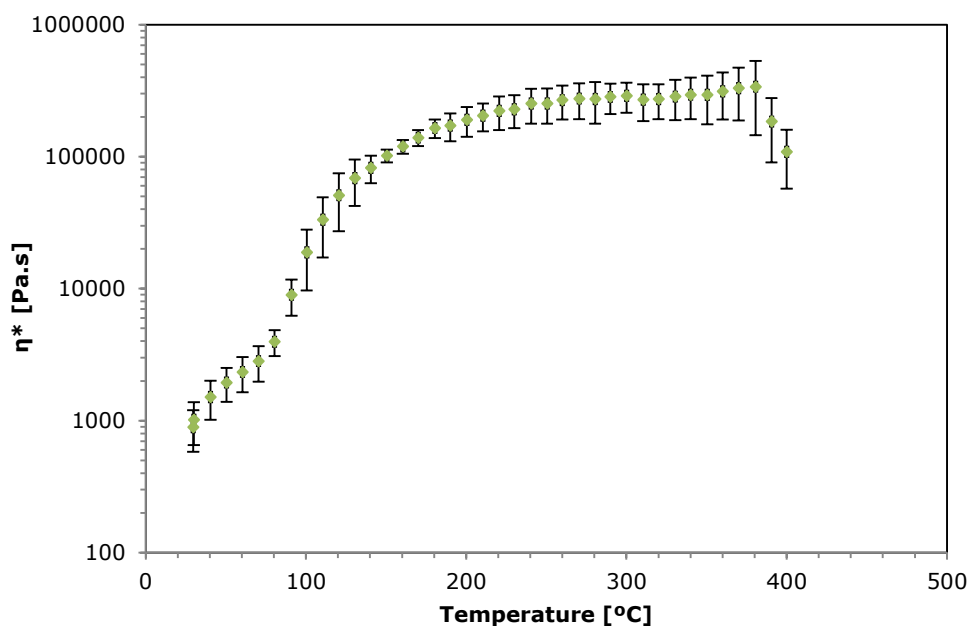


Figure 4-7: Mean η^* as a function of temperature for 4 duplicate samples of PIBSI-A (65 %) and MicroCB (35 %) using a heating rate of $3\text{ }^\circ\text{C min}^{-1}$ in nitrogen ($\gamma = 0.05$, $\omega = 1\text{ Hz}$). (RDA-III instrument). Error bars are to 1 standard deviation of the sample mean.

4.2.4 TA AR-2000 rheometer instrument measurements

As mentioned previously, decreasing the solid loading $< 35\%$ was not successful on the RDA-III instrument using the auto tension adjustment setting due to the plate squashing the samples. To characterise samples of lower viscosity, polymer (75 %) MicroCB (25 %) samples were analysed on the TA AR-2000 instrument which is more sensitive (minimum $\eta^* \sim 10^1\text{ Pa.s}$). Figure 4-8 shows an example of the viscoelastic analysis of a dispersion of PIBSI-A (75 %) and MicroCB (25 %) as a function of temperature measured on the TA AR-2000 instrument. A description of the η^* trends and explanations for the viscoelastic behaviour is presented in chapter 5.

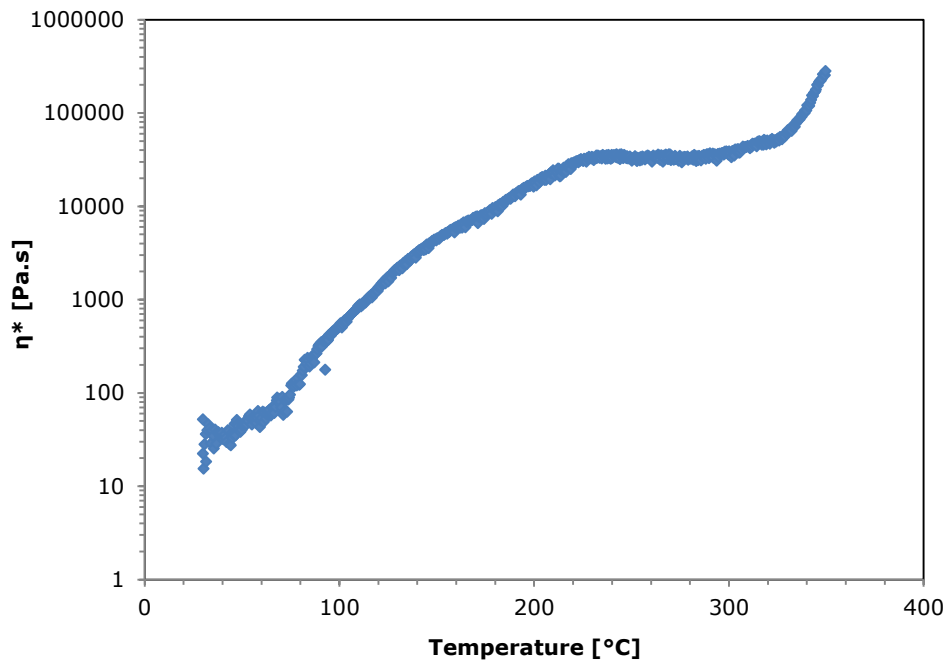


Figure 4-8: η^* , as a function of temperature for PIBSI-A (75 %) and MicroCB (25 %), using a heating rate of $3 \text{ }^\circ\text{C min}^{-1}$ in nitrogen ($\gamma = 0.05$, $\omega = 1 \text{ Hz}$). (TA-2000 instrument).

There was a significant issue that must be mentioned with regards a number of analyses carried out on this instrument. A number of tests failed due to the loss of sample from between the plates on initial heating most likely caused by the high fluidity of the samples. This meant that the polymer flowed off the plate which substantially affected the results. Figure 4-10 shows an image of such a dispersion (taken after the rheometer had cooled). Figure 4-9 shows the viscoelastic trend of this failed analysis. Because of this, and because time was limited on this instrument a number of tests (despite repeat attempts) were not successfully analysed and so are omitted from the main results section. Nevertheless a number of tests will still be included and discussed where it was evident that the sample remained between the rheometer plates throughout the analysis.

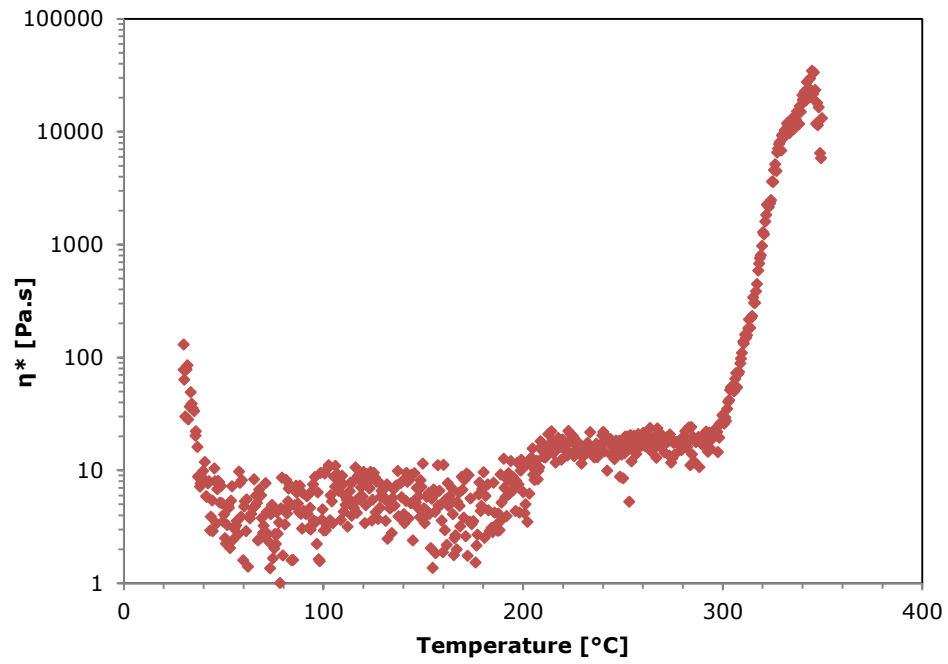


Figure 4-9: η^* , as a function of temperature for PIBSA (75 %) and MicroCB (25 %), using a heating rate of $3\text{ }^\circ\text{C min}^{-1}$ in nitrogen ($\gamma = 0.05$, $\omega = 1\text{ Hz}$). (TA-2000 instrument).

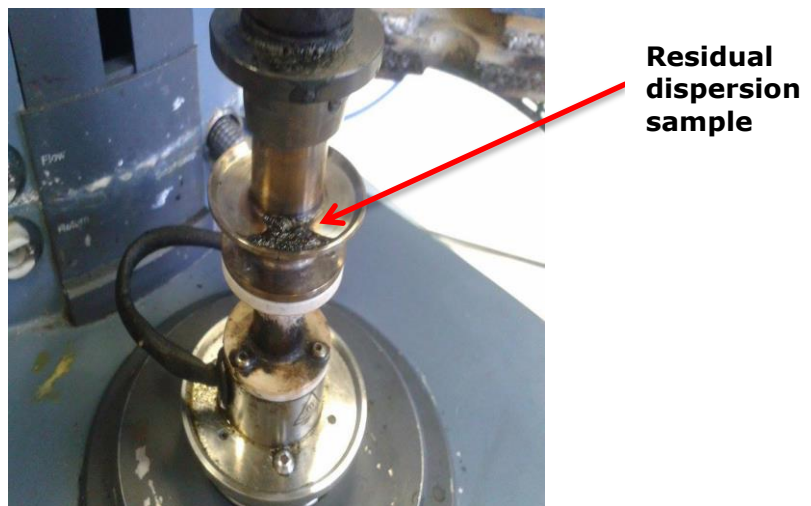


Figure 4-10: Image showing residual PIBSA MicroCB dispersion material post heating. (TA AR-2000 rheometer).

4.2.5 Effect of increasing carbon loading on viscoelastic behaviour

Figure 4-11 shows the effect of particle concentration on the viscoelastic properties using various PIBSI-A and MicroCB weight percentages. The PIBSI-A (75 %) MicroCB (25 %) sample (which remained between the plates throughout the test) was analysed on the TA AR-2000 rheometer due to the low viscosity of the sample while all other concentrations were measured on the Rheometrics RDA-III high torque instrument. It can be seen that the overall η^* trends increases with increasing MicroCB loading %. The trends are characterised by lower η^* values at low temperatures followed by a drastic increase in complex viscosity from around 60 °C onwards. The complex viscosity of all the samples is then relatively constant. The solid loading was not increased beyond 55 % because, when attempting to lower the top plate to a 1 mm gap the initial force that was measured was very high (almost 2000 g) and risked damaging the instrument. A wider initial starting plate gap may have affected the results as the initial volume of sample may have been altered.

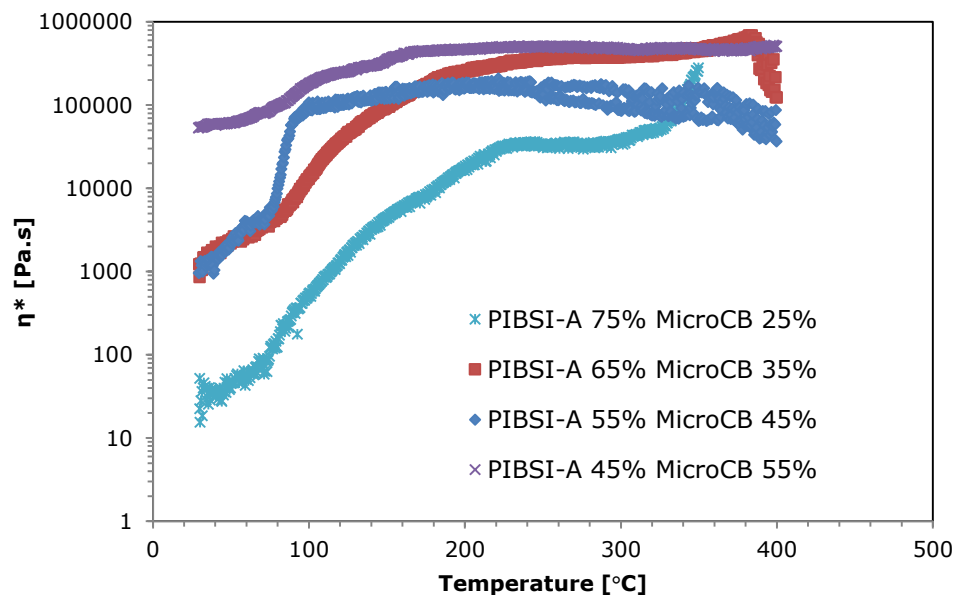


Figure 4-11: Complex viscosity (η^*) as a function of temperature for various PIBSI-A (75 – 45 %) and MicroCB (25 – 55 %) dispersions, using a heating rate of 3 °C min⁻¹ in nitrogen ($\gamma = 0.05$, $\omega = 1$ Hz).

To ensure that the sample was still operating in the linear viscoelastic region at higher solid loadings strain sweep tests were performed for samples of PIBSI-A (45 %) MicroCB (55 %) at 100, 250 and 350 °C, the results of which can be found in Appendix B. It was again found that the G' and G'' moduli remained fairly constant at strains below 0.1 % and that a strain of 0.05 % is acceptable throughout the concentration range studied.

4.3 OPTIMISATION CONDITIONS FOR CHARACTERISATION OF POLYMER CARBON

DISPERSIONS- HIGH TEMPERATURE ^1H NMR

Initial ^1H NMR peak half width ($\Delta H_{1/2}$) measurements were performed on a high-temperature Doty 200 MHz NMR probe in conjunction with a Bruker MSL300 instrument. The high temperature ^1H NMR analyses were carried out as described in section 3.12.1. A PIBSI-A (85 %) MicroCB (15 %) was used to investigate repeatability, reproducibility and the effect of leaving out the ultra-sonication step. Various samples with different PIBSI-A / MicroCB loadings were also analysed to attempt to correlate with rheometer measurements.

4.3.1 Temperature range

The samples were heated from ambient temperature to the final temperature at approximately 3 °C min⁻¹. This heating rate was chosen as it allowed sufficient time for the temperature to increase between each acquisition of the spectra. The samples could not be sealed air tight within the ceramic capsule as this risked exploding the capsules due to devolatilisation of the polymers. For the majority of the tests it was decided not to exceed temperatures of more than 250 °C. This was done to prevent degradation of the polymer leading to contamination of the NMR probe which was a time consuming process to clean.

4.3.2 ^1H NMR peak graph fitting

Once the free induction decay signal had been obtained for a typical analysis Fourier transformation was used to convert the free induction decay signal into a single peak. A numerical programme was then used to allow the spectra obtained to be fitted to Lorentzian and Gaussian components. It was found that the spectra of the dispersions were composed of almost entirely of Lorentzian distribution functions. The peak width at half height ($\Delta H_{1/2}$) was therefore measured as function of temperature to investigate the mobility of the fluid ^1H of the polymer constituents. An example of one such spectrum is shown in **Error! Reference source not found.** and displays the experimental and calculated (Lorentzian) components for a PIBSI-A (85 %) MicroCB (15 %) sample at 250 °C. Again, no contribution from a Gaussian distribution function (i.e. hydrogens associated with the rigid phase) was observed therefore the peak fitting was carried out using the Lorentzian parameters only.

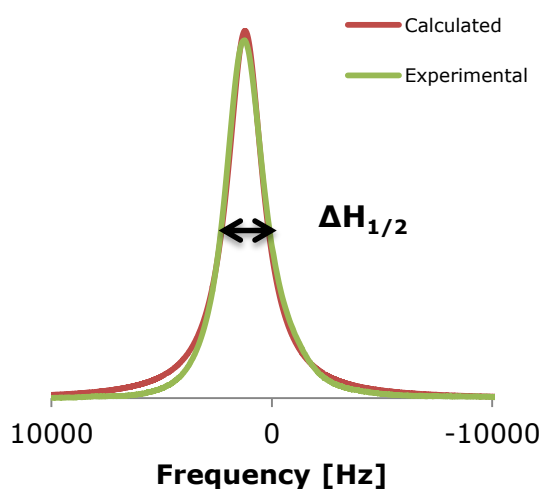


Figure 4-12: ^1H NMR spectra of PIBSI-A (85 %) MicroCB (15 %) dispersion at 250°C with Calculated and Experimental components.

For the PIBSI-A (85 %) MicroCB (15 %) sample described above the $\Delta H_{1/2}$ was measured and plotted as a function of temperature (Figure 4-13). The lines between each data point representing each $\Delta H_{1/2}$ measurement are strictly there

as a guide for the eye. To reiterate variation in $\Delta H_{1/2}$ is representative of a change of fluidity of a system i.e. increasing $\Delta H_{1/2}$ implies decreasing mobility (as well as shorten the spin-spin relaxation time (T_2)). Figure 4-13 therefore shows that for this dispersion, the mobility of the H atoms decreased with increasing temperature. A full description of the $\Delta H_{1/2}$ trend and explanations for the differences in the viscoelastic behaviour in comparison with PIB and PIBSA dispersions is presented in chapter 5.

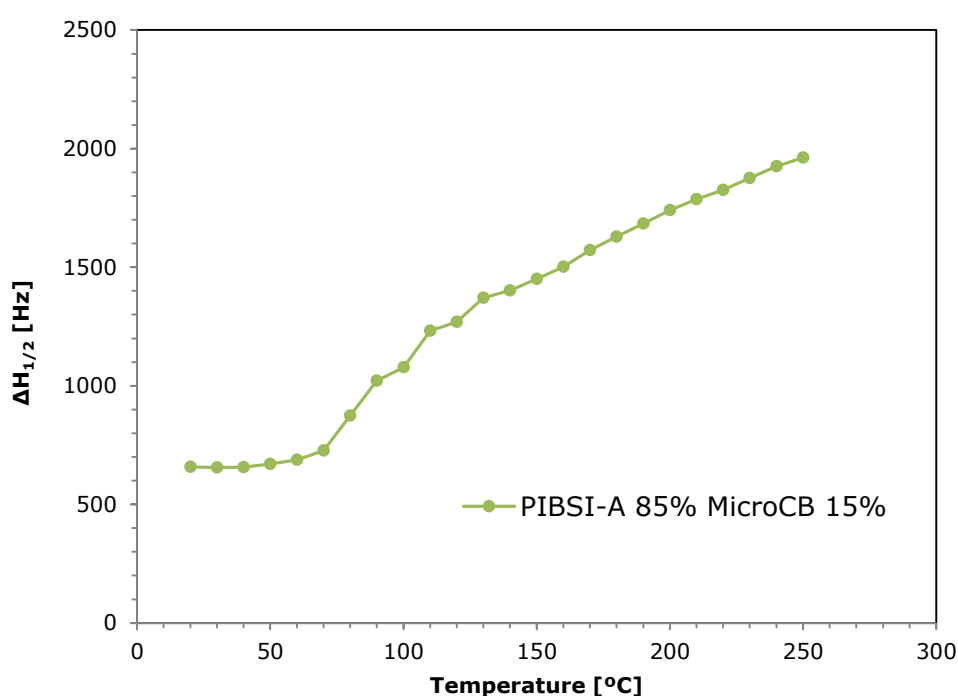


Figure 4-13: Evolution of the ^1H NMR $\Delta H_{1/2}$ with temperature for a PIBSI-A (85 %) MicroCB (15 %) dispersion

4.3.3 ^1H NMR repeatability

Repeat analysis of the sample was shown in Figure 4-13 in order to investigate the level repeatability of a typical dispersion. Potential sources of error include error arising from manually controlling the heating rate, possibility of non-uniformity of a typical sample, and variation in the amount of sample in the

ceramic capsule. Figure 4-14 shows the ^1H NMR $\Delta H_{1/2}$ for 3 repeat tests of a PIBSI-A (85 %) MicroCB (15 %) sample as a function of temperature. Figure 4-15 shows the mean of these tests with error bars to one standard deviation of the sample mean. The greatest deviation from the mean was between 70 to 100 °C with the greatest deviation from the mean having a value of ± 118 Hz at 90°C. The deviation from the mean at higher temperatures was less with a standard error of ± 22 Hz at 250 °C.

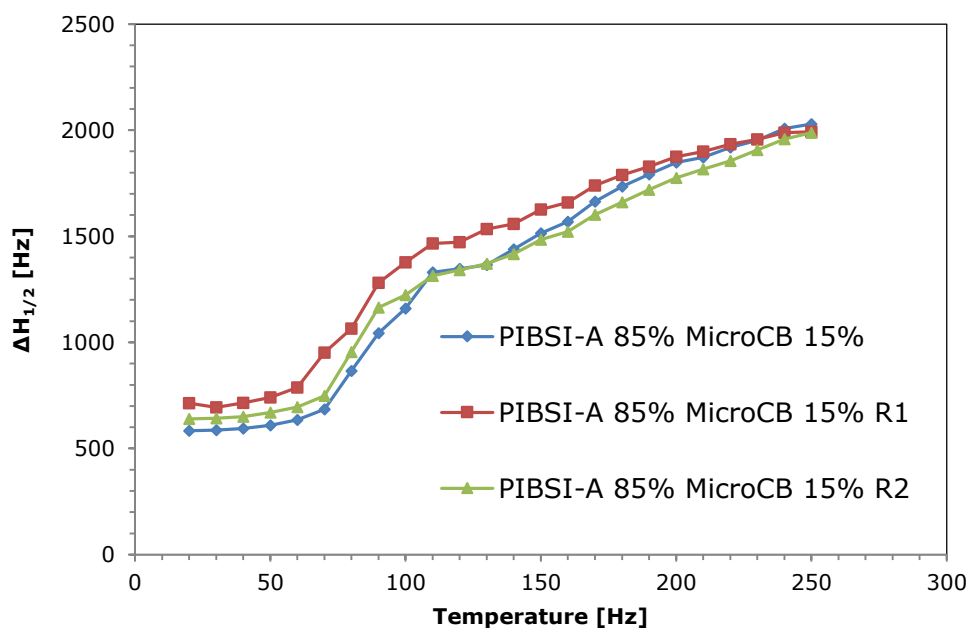


Figure 4-14: Evolution of the ^1H NMR $\Delta H_{1/2}$ with temperature for repeat analysis of a PIBSI-A (85 %) Micro CB (15 %) dispersion

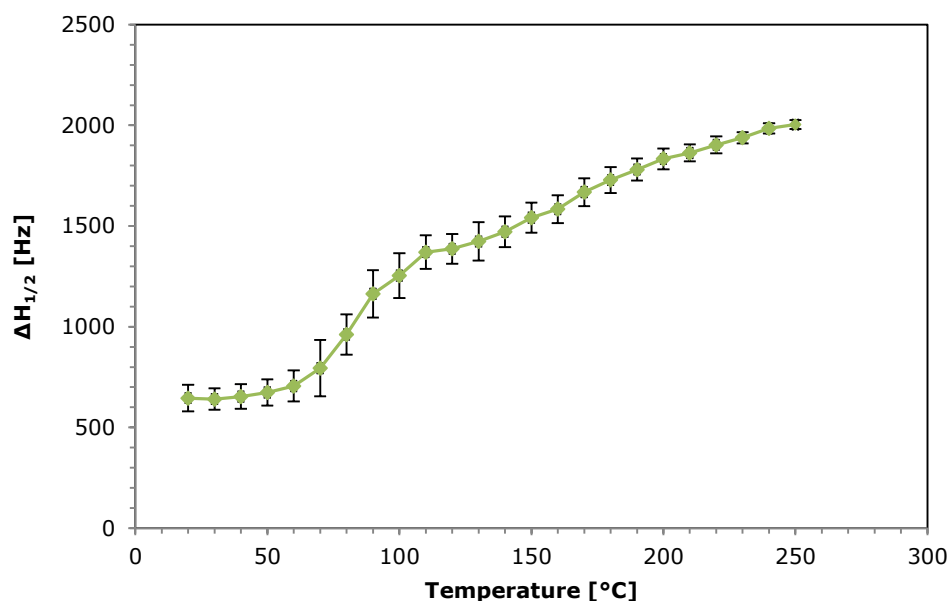


Figure 4-15: Evolution of the mean ^1H NMR $\Delta H_{1/2}$ with temperature for repeat analysis of a PIBSI-A (85 %) Micro CB (15 %) dispersion

4.3.4 ^1H NMR reproducibility

Duplicate samples of PIBSI-A (85 %) MicroCB (15 %) were made to ensure good reproducibility. Figure 4-16 shows the ^1H NMR $\Delta H_{1/2}$ for 3 duplicate samples of MicroCB dispersions with PIBSI-A as a function of temperature. A weight percentage of 85 % polymer 15 % MicroCB was chosen to test reproducibility as it was believed a more fluid sample would most likely yield the largest error in the mobility measurement of each sample. The mean of these tests are shown in Figure 4-17. Error bars to one standard deviation of the sample mean are also included. The graphs show that the largest range in error occurred between 60 – 100 °C with the greatest deviation from the mean of ± 274 Hz at 90°C. This error is most likely associated with differences in the conformational changes in the polymer chains for each sample as described by Won et al. (2005) and possibly due to residual hexane evaporation that had become encapsulated by the polymer (this is discussed in more detail in chapter 5). The deviation from the mean at higher temperatures was less with a standard error of ± 61 Hz at 250 °C. This

shows analysis of these dispersions at high temperatures shows good reproducibility.

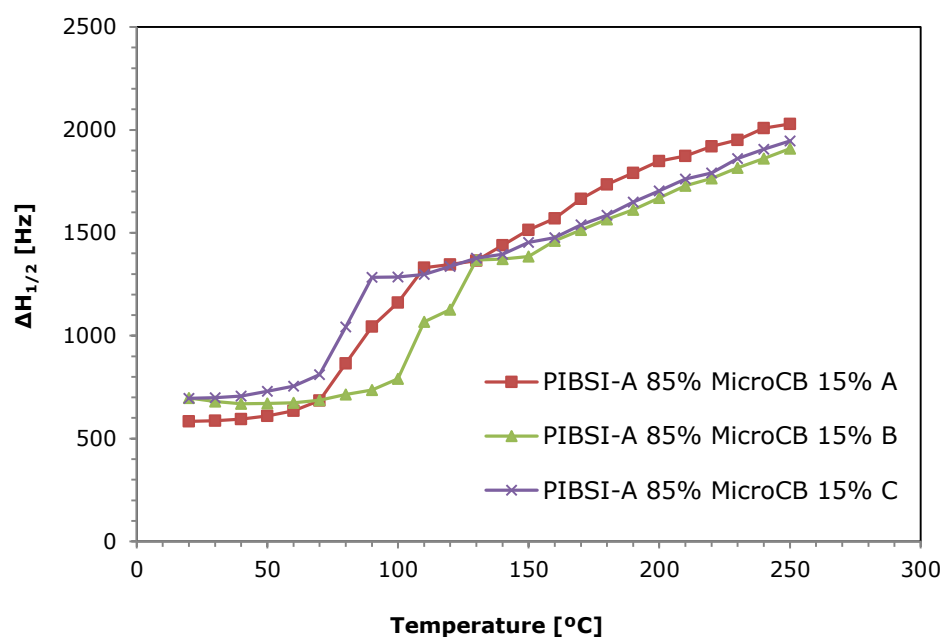


Figure 4-16: Evolution of the ^1H NMR $\Delta H_{1/2}$ with temperature for 3 duplicate PIBSI-A (85 %) Micro CB (15 %) dispersions (A, B, C) with sonication

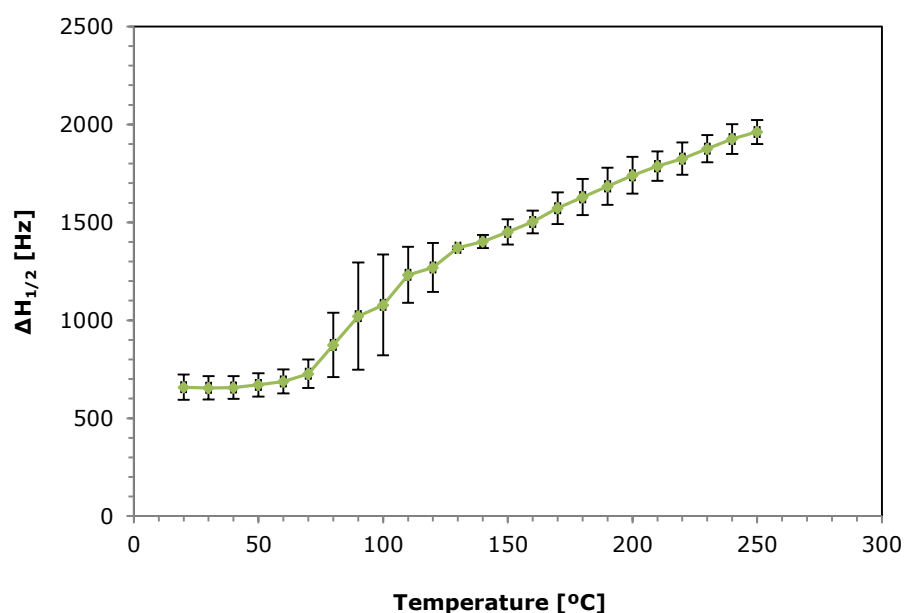


Figure 4-17: Evolution of the mean ^1H NMR $\Delta H_{1/2}$ with temperature for 3 duplicate PIBSI-A (85 %) Micro CB (15 %) dispersions (A, B, C). Error bars are to 1 standard deviation of the sample mean.

4.3.5 Effect of removing sonication step

Figure 4-18 shows the $\Delta H_{1/2}$ measurements for similar set of samples as in Figure 4-16 but this time the sonication step was left out. Sonication is used in the preparation of the dispersions for three reasons; to help the polymer dissolve in the hexane faster, to break down any aggregates of the carbon particles and to facilitate the interaction between the polymer and the particles. The technique has been used in various studies involving similar PIB dispersions. However, sonication is widely known in polymer chemistry to alter the structural configuration of polymers (Price & Smith, 1991). As is demonstrated however in Figure 4-16 and Figure 4-18 there is little difference between $\Delta H_{1/2}$ trends of A,B and C samples (with sonication step) and D,E and F samples (without sonication step). D, E and F show a mean trend (shown in Figure 4-19) that is slightly less than A, B and C although this is just outside the experimental error. The reproducibility appeared to be better with sonication as shown by the lower error at high temperatures. The sonication step will therefore remain in the preparation of the dispersions.

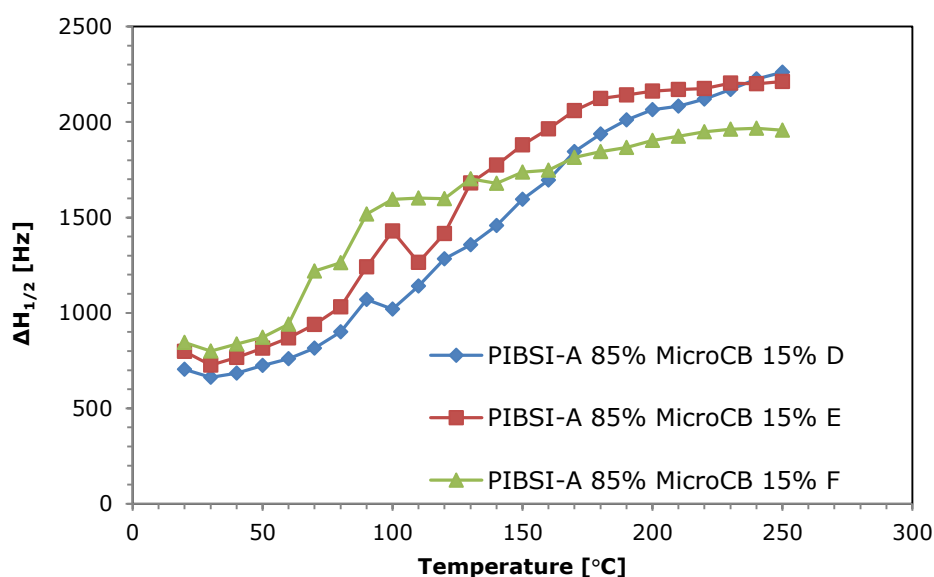


Figure 4-18: Evolution of the ^1H NMR $\Delta H_{1/2}$ with temperature for 3 duplicate PIBSI-A (85 %) Micro CB (15 %) dispersions (D, E, F) without sonication.

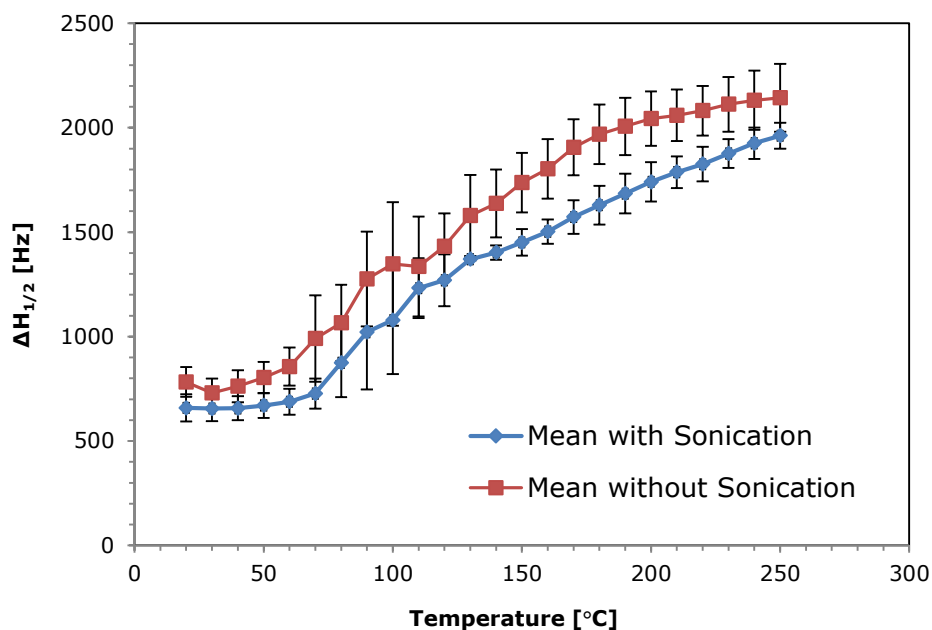


Figure 4-19: Evolution of the mean ^1H NMR $\Delta H_{1/2}$ with temperature for 6 duplicate PIBSI-A (85 %) Micro CB (15 %) dispersions with (A, B, C) and without (D, E, F) sonication step. Error bars are to 1 standard deviation of the sample mean.

4.3.6 Error measurement of data processing

Figure 4-20 shows the mean data set for a particular sample that has been processed from the FID 4 separate times. As there was a subjective element to processing in terms of baseline correction etc. there was the possibility of an additional error. From the mean of the data set including error bars to one standard deviation of the sample mean (shown in Figure 4-21) it is clear that this error is minimal enough to ignore when distinguishing different polymers using $\Delta H_{1/2}$ measurements.

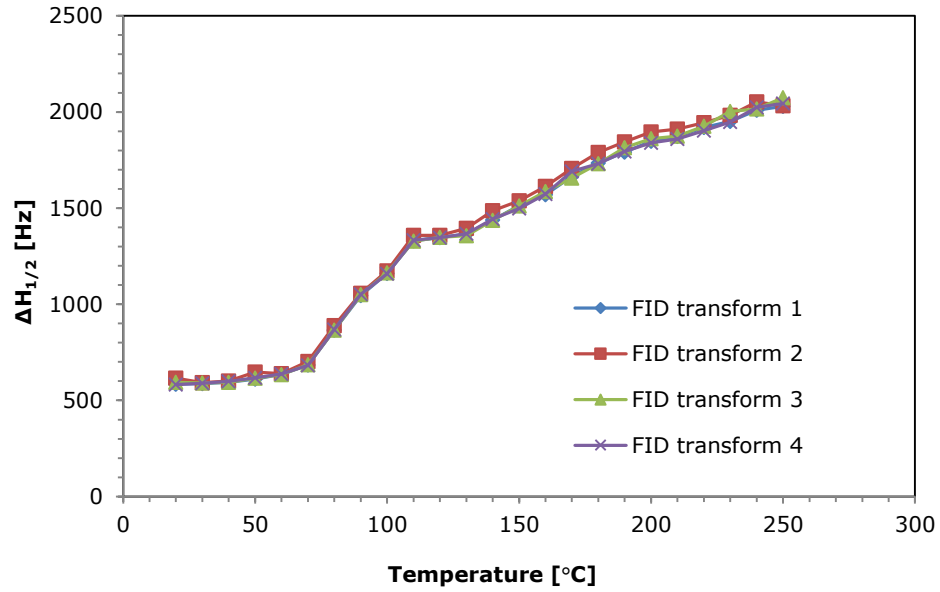


Figure 4-20: Evolution of the ^1H NMR $\Delta H_{1/2}$ with temperature for a PIBSI-A (85 %) MicroCB (15 %) dispersion showing the FID transformed and processed 4 separate times.

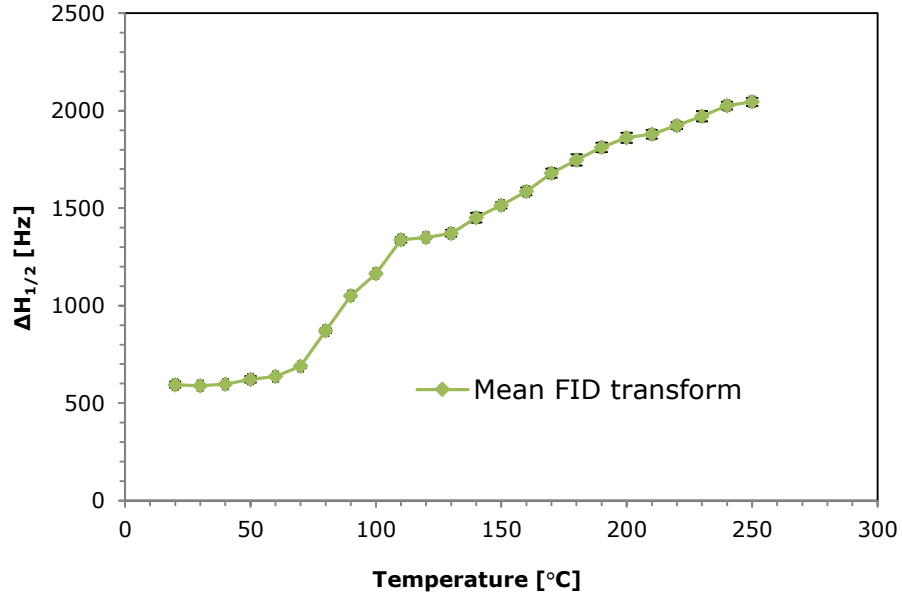


Figure 4-21: Evolution of the mean ^1H NMR $\Delta H_{1/2}$ with temperature for a PIBSI-A (85 %) MicroCB (15 %) dispersion transformed from the FID and processed 4 separate times. Error bars are to 1 standard deviation of the sample mean.

4.3.7 Effect of increasing solid loading on ^1H NMR mobility measurements

The effect of particle concentration on the $\Delta H_{1/2}$ trend was investigated (Figure 4-22). The trends show that as the particle concentration increases the overall $\Delta H_{1/2}$ trend appeared to increase particularly between 15 and 20 % solid loading. As the particle concentration is increased further the difference between the trends appears to be less and particularly at high temperatures the $\Delta H_{1/2}$ values are more similar. The PIBSI-A (55 %) MicroCB (45 %) dispersion is the only sample that starts out with a decreasing $\Delta H_{1/2}$ trend. This could possibly have been due to the high particle concentration restricting the mobility of the H atoms; as the temperature was increased the sample may have softened which allowed the H atoms to become more mobile.

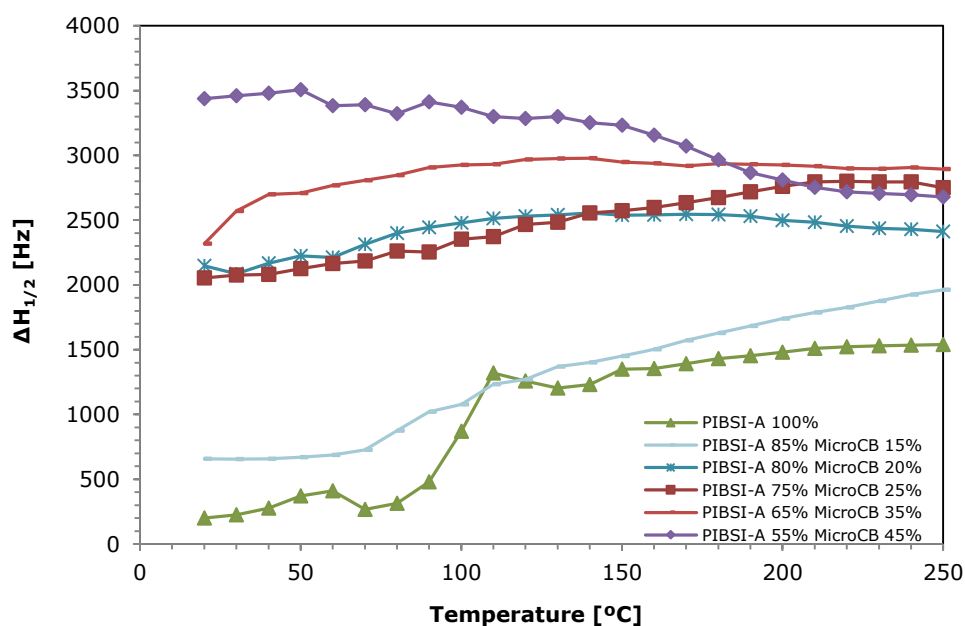


Figure 4-22: Evolution of the ^1H NMR $\Delta H_{1/2}$ with temperature for PIBSI-A (100 – 55 %) MicroCB (0 –45 %) dispersions

As has been stated the ^1H NMR spectra were comprised almost entirely of Lorentzian distribution functions that arise from the mobility of the fluid H atoms. As the solid loading was increased however a small number of Gaussian

distribution functions associated with rigid H atoms were observed at various temperatures. These were largely minimal and seemed to appear and disappear at random (most likely arising from the numerical programme attempting to pick out Gaussian peaks that were not really there). Therefore to ensure the best peak fitting and for consistency, only Lorentzian parameters (associated with mobile H atoms) were applied to the peak fitting. In order to confirm, however, that the random occurrence of Gaussian distribution functions had no effect on the measurement of the $\Delta H_{1/2}$ a number of spectra were processed both with and without Gaussian distribution functions. An example is shown in Figure 4-23 and displays the variation in $\Delta H_{1/2}$ with temperature for a PIBSI-A (75 %) MicroCB (25 %) sample. The figure shows that exclusively peak fitting the Lorentzian components is justified as there is very little difference ($< \pm 2$ Hz) when the Gaussian component was taken into account. This was found to be the case even up to temperatures of 400 °C as shown Figure 4-23.

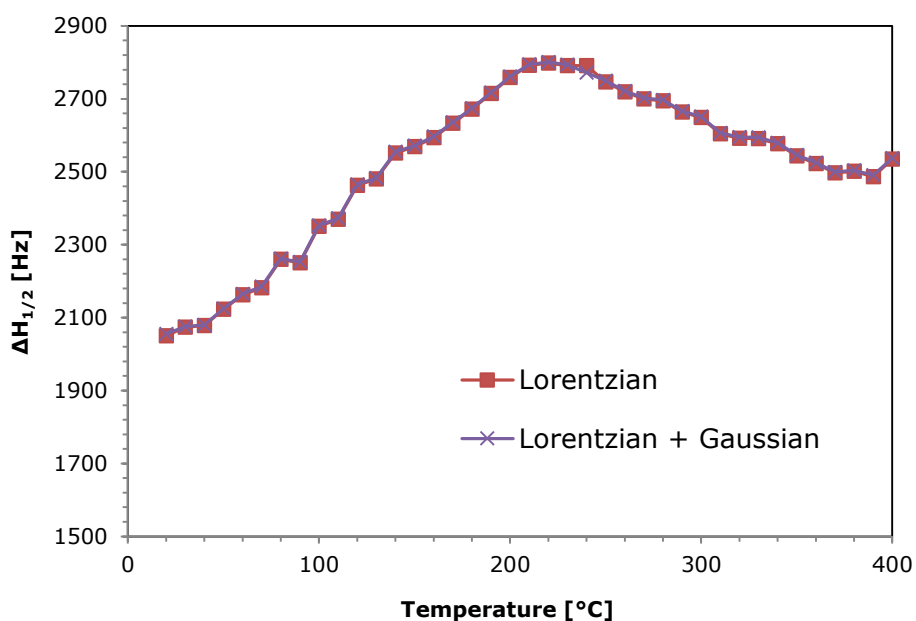


Figure 4-23: Evolution of the ^1H NMR $\Delta H_{1/2}$ with temperature for PIBSI-A (75 %) MicroCB (25 %) dispersion fitted with and without Gaussian components.

4.3.8 Contribution from the carbon black to the ^1H signal

A ^1H NMR test was run to investigate if there was any contribution from MicroCB to the ^1H NMR signal by analysing the carbon black in isolation. No discernible peak was found throughout the temperature range (20 – 400 °C) studied.

4.4 CHAPTER SUMMARY

Conditions for the characterisation of dispersions of PIBSI and a MicroCB using rheometry and ^1H NMR at high temperatures for both the sample preparation and analytical methodologies has been carried out and the following key outcomes have been found:

- Rheometer tests using the RDA III instrument with a fixed plate gap showed mostly linear behaviour and very high viscosity values which amplified the η^* measurements at high temperatures. The rheometer plate gap therefore had to be allowed to expand as the viscosity of a sample increased otherwise additional forces would have affected the results. This was achieved by carrying out the tests with the auto tension on. The samples needed to be initially viscous enough otherwise the plates would squash the sample with this setting therefore minimum solid loading of 35 % was required to obtain a successful analysis on the RDA-III instrument.
- A PIBSI-A (65 %) MicroCB (35 %) sample was duplicated and analysed a number of times using rheometry with the auto tension on. The η^* trends were reproducible. The error for these samples varied along the temperature range. The error at 250 °C was ± 75000 Pa.s. This may be appear to be a very high margin of error however it will be investigated in the next chapter if this is sufficient to distinguish various PIBSIs.
- Strain-sweep tests showed the behaviour of the PIBSI MicroCB dispersions were within the linear viscoelastic region and not affected by strains of

0.05 %. This was the case both within the temperature range studied and at the different PIBSI/MicroCB loadings employed.

- A low viscosity sample measured on a TA-2000 rheometer instrument showed to correspond well with the results from the RDA-III instrument. However on occasion samples were lost from the plate top meaning certain tests were unsuccessful.
- It was found that increasing the solid loading of the dispersions led to an increase in the η^* values although the overall viscoelastic trend remained the same.
- High temperature ^1H NMR was used to analyse a number of PIBSI-A MicroCB dispersions up to 250 °C. The resultant spectra were composed of Lorentzian distribution functions. The $\Delta H_{1/2}$ was measured to obtain information about the mobility of the polymer constituents.
- Duplicate $\Delta H_{1/2}$ measurements of samples of PIBSI (85 %) MicroCB (15 %) showed good reproducibility and repeatability. The largest error occurred between 60 and 100 °C in both cases. The error in $\Delta H_{1/2}$ for the duplicate samples at 250 °C was ± 60 Hz. For three repeat analysis of the same sample the error at 250 °C was ± 22 Hz and the error in processing was ± 20 Hz at 250 °C.
- The effect of leaving out the sonication had little effect on $\Delta H_{1/2}$ trend. However the error at 250 °C was slightly greater than samples where the sonication step remained. It is therefore concluded that the sonication step should remain in the sample preparation as it appears to increase the level of reproducibility.
- Increasing the solid loading of the dispersions led to an increase in the overall $\Delta H_{1/2}$ values.
- There was found to be no contribution from any hydrogen atoms in the carbon black to the ^1H NMR signal.

5 Characterisation of Polyisobutylene-Carbon Black Dispersions

This chapter presents the characterisation of dispersions of a carbon black (MicroCB) with polyisobutylene (PIB), polyisobutylene succinic anhydride (PIBSA) and two similar derivatives of polyisobutylene succinimide (PIBSI-A and PIBSI-B) using high temperature rheometry and ^1H NMR spectroscopy. The chapter investigates how using the techniques can demonstrate that the viscoelastic and molecular mobility behaviour of a sample can be an indication of the strength of the interaction between the polymer and the carbon black particles.

5.1 EXPERIMENTAL

5.1.1 Materials

A summary of the polymers used in this chapter is shown in Table 5-1. The polymer polar head groups are displayed as is the number average molecular weight of the PIB backbone (PIB- M_n) from which the polymers are derived. Also presented is the number average molecular weight (M_n), weight average molecular weight (M_w) and polydispersity values (PD) of the final polymer products obtained from GPC analysis as described in section 3.12.6. All polymers with (the exception of PIBSI-B) were synthesised via thermal synthetic route (ENE type reaction). PIBSI-B was synthesised via chlorine synthetic route (Dies Alder type reaction).

Table 5-1: Head groups, average molecular weights, polydispersity and functionality of polymer samples.

Polymer reference	Polymer Head group	PIB- M_n (g/mol)	M_n (g/mol)	M_w (g/mol)	PD	PIB Funct.
PIB	N/A	750	771	1075	1.4	N/A
PIBSA(-A)	Succinic Anhydride	750	904	1170	1.3	<i>mono</i>
PIBSI-A	TEPA	750	1253	2049	1.6	<i>mono</i>
PIBSI-B*	TEPA	1000	1740	2648	1.5	<i>mono</i>

*Refer to section 3.10.1 for head group abbreviations

A commercial carbon black (MicroCB) with an average particle size of 45 μm and surface area of 205 m^2g^{-1} was used. A description of this carbon can be found in section 3.10.2. Hexane (Aldrich 95% was used) was used as a solvent.

5.1.2 Sample preparation

The polymer carbon black dispersions were prepared as described in section 3.11.

5.1.3 Summary of analytical methods used

Thermogravimetric analysis (TGA) was used to investigate the thermal degradation of the polymers using the method outlined in section 3.12.3. The polymer-MicroCB dispersions were analysed via high temperature rheometry on the two separate rheometer instruments and via ^1H NMR as outlined in sections 3.12.3 and 3.12.1 respectively.

5.2 RESULTS AND DISCUSSION

5.2.1 Thermogravimetric analysis (TGA) of PIB, PIBSA, PIBSI-A, PIBSI-B

Figure 5-1 shows the weight percentage loss of PIB, PIBSA, PIBSI-A and PIBSI-B measured by thermogravimetric analysis (TGA). It can be seen that PIB begins to gradually devolatilise at around 100 $^{\circ}\text{C}$. The rate of volatile release increases with increasing temperature as the polymer begins to thermally degrade and reaches a maximum rate of weight loss at around 330 $^{\circ}\text{C}$. This is consistent with Lehrle et al., (2002) who found for similar PIB samples the majority of degradation was found to occur between 270 – 360 $^{\circ}\text{C}$ where the most likely mechanism of degradation is described as end-initiated depropagation of the double bonds at the end of the PIB chains. At approx. 360 $^{\circ}\text{C}$ the rate of weight loss decreases significantly and at 400 $^{\circ}\text{C}$ there is < 1 % residual PIB remaining. PIBSA did not begin to devolatilise until around 200 $^{\circ}\text{C}$. At 300 $^{\circ}\text{C}$ the rate of weight loss increases substantially and reaches a maximum rate loss at around 360 $^{\circ}\text{C}$. The

higher degradation temperature of PIBSA compared with PIB was probably not due to molecular weight since the polymers both have quite similar M_n/M_w values (see Table 4-1). A more likely explanation could be due to substitution of the PIB vinylidene chain ends with the maleic anhydride groups which can increase the thermal stability of the polymer. This can be attributed to either increased steric bulk around the end radicals around the PIBSA restricting chain-end initiated depropagation, or loss of the most unstable hydrogen atoms in the starting PIB due to oxidation during the conversion of PIB to PIBSA (Lehrle et al. 2002). At around 410 °C the residual amount of PIBSA is < 1 %. PIBSI-A and PIBSI-B both begin devolatilising at around 60 °C and around 10 % weight has been lost by ~200 °C. This was most likely due to presence of solvent in each of the polymer samples. The rapid thermal degradation of PIBSI-A and PIBSI-B both begins at around 280 °C although the trends do diverge slightly with PIBSI-A degrading at slightly lower temperatures reaching a maximum rate of weight loss at around 340 °C and the PIBSI-B at around 365 °C. A residual amount of each of polymer is obtained at 450 °C and is below 4 % of the initial weight for each polymer. An explanation for the slightly higher temperature at which the maximum rate of degradation occurred for PIBSI-B can be explained by the higher molecular M_w/M_n values of the PIBSI-B sample.

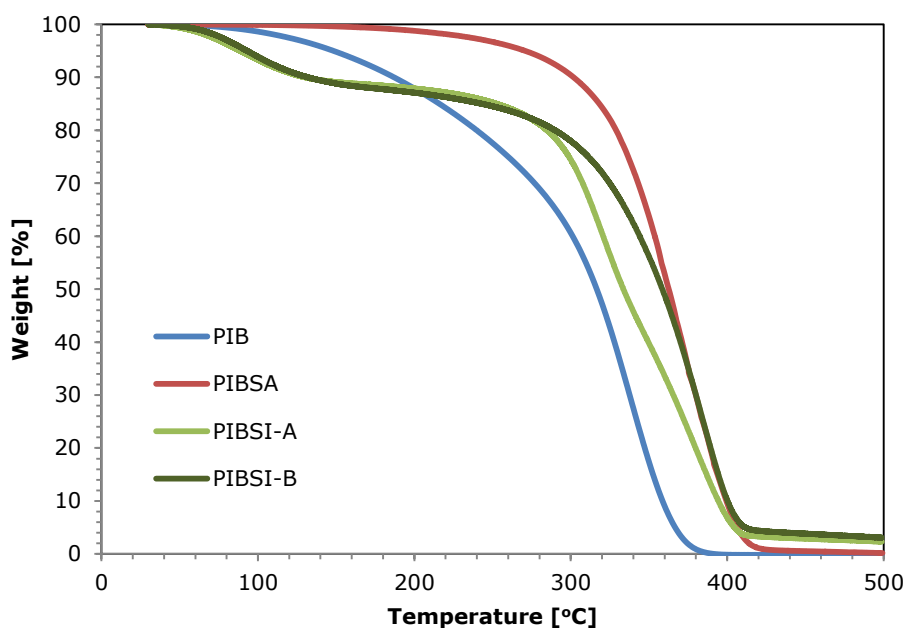


Figure 5-1: Weight percentage loss of PIB, PIBSA, PIBSI-A and PIBSI-B with temperature using a heating rate of 3 °C min⁻¹ in nitrogen.

5.2.2 High temperature rheological measurement of polyisobutylene

Although the conditions for high temperature rheological analysis of PIBSI MicroCB dispersions were optimised in the previous chapter, attempts were made to characterise the PIB, PIBSA and PIBSIs in isolation. However, the results showed values that were almost entirely below the detection limit of both rheometer instruments (Rheometrics RDA-III instrument minimum $\eta^* \sim 10^3$ Pa.s, TA-AR-2000 instrument minimum $\eta^* \sim 10^1$ Pa.s). For example, Figure 5-2 (Rheometrics RDA-III instrument) and Figure 5-3 (TA AR-2000 instrument) show the complex viscosity (η^*) data as a function of temperature of PIB to be in both cases largely scattered. This meant that the polymers could not be successfully characterised in isolation using rheometry on these instruments.

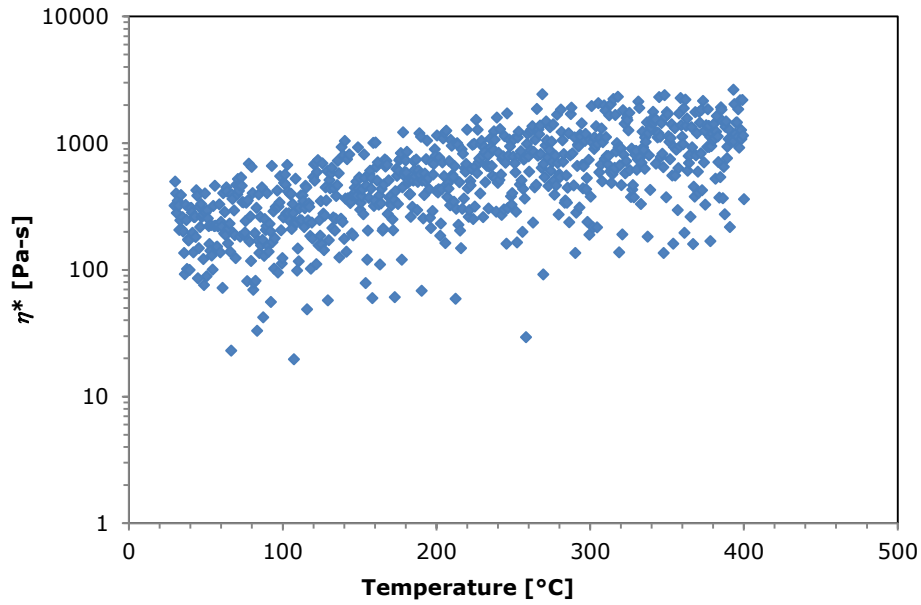


Figure 5-2: η^* as a function of temperature for PIB using a heating rate of $3\text{ }^\circ\text{C min}^{-1}$ ($\gamma=0.05\%$, $\omega=1\text{ Hz}$) measured on Rheometrics RDA-III high torque controlled strain rheometer.

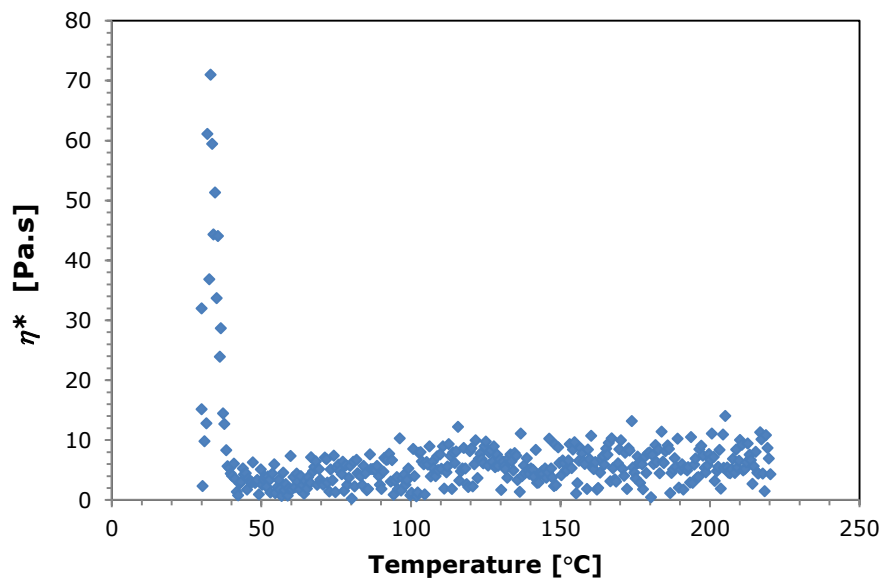


Figure 5-3: η^* as a function of temperature for PIB using a heating rate of $3\text{ }^\circ\text{C min}^{-1}$ ($\gamma=0.05\%$, $\omega=1\text{ Hz}$) measured on TA AR-2000 Controlled Stress rheometer.

5.2.3 Rheological characterisation of PIB, PIBSA, PIBSI-A, PIBSI-B /MicroCB dispersions

Figure 5-4 presents the viscoelastic properties of the dispersion of PIB (65 %) and MicroCB (35 %) as a function of temperature under a nitrogen atmosphere using a heating rate of 3 °C min⁻¹, a strain of 0.05 % and a frequency of 1 Hz. It is clear that the viscoelastic trend can be differentiated into a number of regions.

The first region begins at 30 °C and ends at around 100 °C and shows an increase in complex viscosity (η^*) from 230 Pa.s to 4000 Pa.s. This increase in this temperature region has been observed previously by Won et al. (2005) and Yang et al. (2007), and is ascribed to conformational changes in the polymer chains affecting the dispersancy efficiency leading to aggregation of the carbon particles. Evaporation of residual hexane (BP. 69°C) that had become trapped within the polymer sample may have also indirectly contributed to the increase in η^* . The second region (100 °C – 320 °C) may be characterised by relatively constant η^* values which would suggest the aggregation of the particles has yielded a network structure. Formation of a network structures at lower temperatures (<100 °C) was observed by Won et al. (2005) and Yang et al. (2007) for carbon black and nanotube dispersions respectively although in both cases the concentrations of the carbon were much less (typically 5 % carbon). In Yang et al. (2007) a dispersion stabilised by a long PIBSI chain (1000) showed an increase in viscosity at 60 °C which was attributed to flocculation of the carbon particles via the PIBSI chains. A network structure was said to form by around 80 °C between the nanotubes with contributions from the long polymer chains which then collapsed, shown by a decrease in the storage and loss moduli. Here, unlike the dispersion trend observed by Yang et al. (2007) the network does not appear to collapse and the η^* values are relatively constant up to around 320 °C. This was most likely due to the higher loading of MicroCB with the close proximity of the carbon particles preventing the network from collapse. Region three (320 °C – 375 °C)

shows a drastic increase in η^* from around 1000 Pa.s to around 3×10^5 Pa.s which was most likely due to degradation of free polymer causing an increase in the solid fraction of sample. This corresponds quite well with the TGA results for PIB (see Figure 5-1) which showed the majority of the PIB weight loss between 280 to 360 °C. Degradation of the PIB may have occurred at slightly higher temperatures in the presence of the MicroCB due to the carbon black enhancing the thermal stability of the polymer as described by Jakab & Omastova et al., (2005). From 375 – 400 °C the data becomes scattered which could be due to collapse of the network brought about from degradation of any remaining PIB that was trapped between the carbon particles.

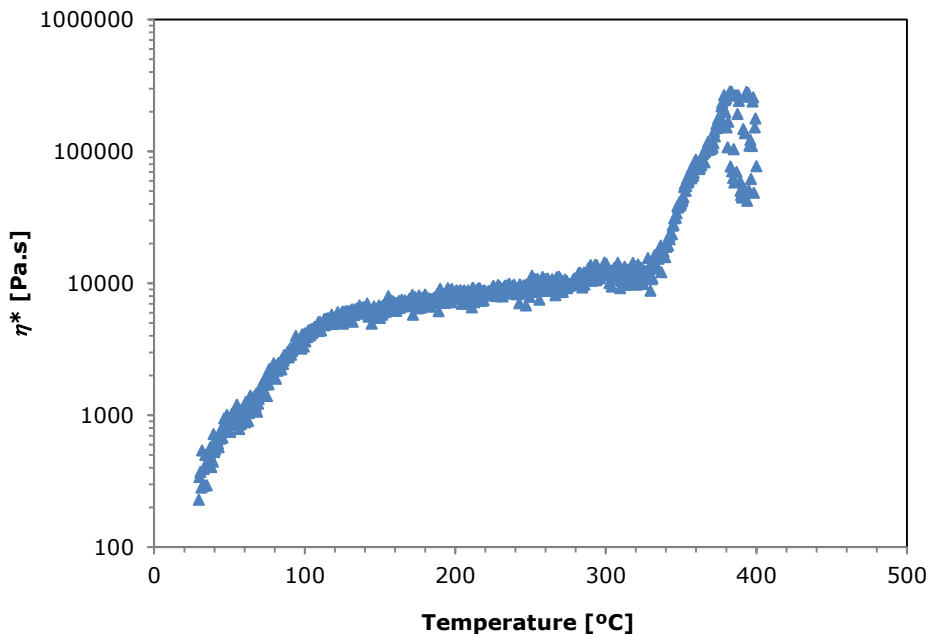


Figure 5-4: η^* as a function of temperature for a PIB (65 %) MicroCB (35 %) dispersion, using a heating rate of $3 \text{ }^\circ\text{C min}^{-1}$ in nitrogen ($\gamma = 0.05$, $\omega = 1 \text{ Hz}$). (RDA-III instrument)

Figure 5-5 shows a comparison of the viscoelastic trend for PIB (65 %) MicroCB (35 %) and the corresponding PIBSI-A (65 %) MicroCB (35 %) dispersion that was utilised for optimisation in the previous chapter. Both samples begin with

similarly low η^* values at temperatures around 90 °C. However, it is clear from examination of Figure 5-5 that the PIBSI-A dispersion sample shows markedly higher η^* values than the corresponding PIBSI-A sample between 90 and 370 °C. This cannot be due to the thermal degradation of the PIBSI-A as TGA results showed that both PIBSI and PIB begin to thermally degrade above 250 °C. A likely explanation for this behaviour corresponds with the expected level of interaction between the polymer and the MicroCB particles. PIB, which is made up of a hydrocarbon tail, does not have a polar head group and so the level of adsorption onto the carbon surface should be low. This means that during formation of the network (after the conformation changes of the polymer chains, hexane evaporation and aggregation of the particles) less of the polymer contributes to the network. PIBSI-A on the other hand is a polymer containing a polar head group with multiple amines therefore its level of interaction with the MicroCB should be greater. This would cause more of the polymer to become encapsulated within the network, increasing the effective solid fraction of the sample leading to higher η^* values at high temperatures. A similar effect has been observed previously in studies of polymer nanocomposites in which the viscoelastic response can serve as an indirect qualitative measure of the dispersion state of nanotubes in polymer composites where a higher G' can be an indication of a better dispersion (Moniruzzaman & Winey, 2006).

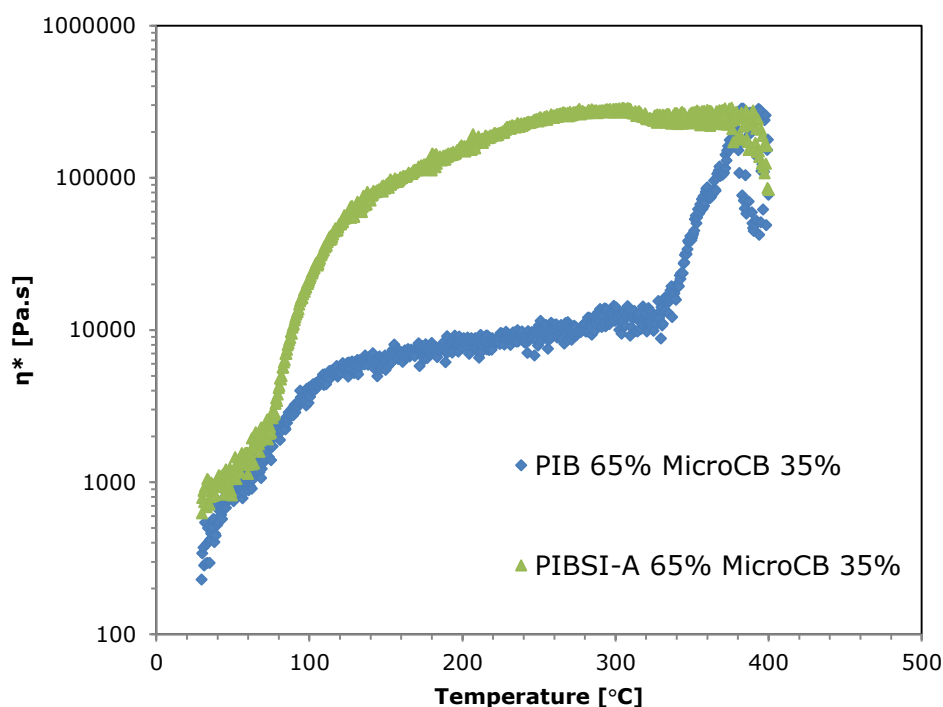


Figure 5-5: η^* as a function of temperature for PIB (65 %) and MicroCB (35 %) and PIBSI-A (65 %) and MicroCB (35 %) using a heating rate of $3\text{ }^\circ\text{C min}^{-1}$ in nitrogen ($\gamma = 0.05$, $\omega = 1\text{ Hz}$). (RDA-III instrument)

As PIBSA is an intermediate in the synthetic route from PIB to PIBSI it seems logical to suggest it will have an intermediate level of interaction with the carbon black particles. A PIBSA (65 %) MicroCB (35 %) dispersion was therefore analysed via rheometry and is shown in Figure 5-6. The corresponding PIB and PIBSI viscoelastic trends are also shown for comparison. The viscoelastic trend for the PIBSA sample is similar to that of PIB but mostly exhibits higher η^* values throughout heating. In the first stage (30 – 100 °C) there is an increase in η^* from 230 Pa.s to around 20000 Pa.s. Stage two extends from 100 to around 300 °C and shows η^* to be relatively constant. The third stage (300 – 400 °C) shows an increase in η^* to similar values for PIB and PIBSI-A dispersions followed by a scattering of the data, which as confirmed by the TGA results is most likely due to degradation of the polymer with the MicroCB remaining.

From examining the trends for each polymer in Figure 5-6 it is apparent that the polymers are the most distinguishable in the second region where the η^* values are relatively constant (100 – 300 °C) associated with the formation of a polymer – carbon network. PIB has the lowest η^* values (~ 10000 Pa.s) in this region, followed by PIBSA (~ 100000 Pa.s) and PIBSI-A (~ 300000 Pa.s). As has been stated, it would be expected since PIBSA as an intermediate between PIB and PIBSI-A should have intermediate η^* values in the network region and the viscoelastic trends of the polymers support this.

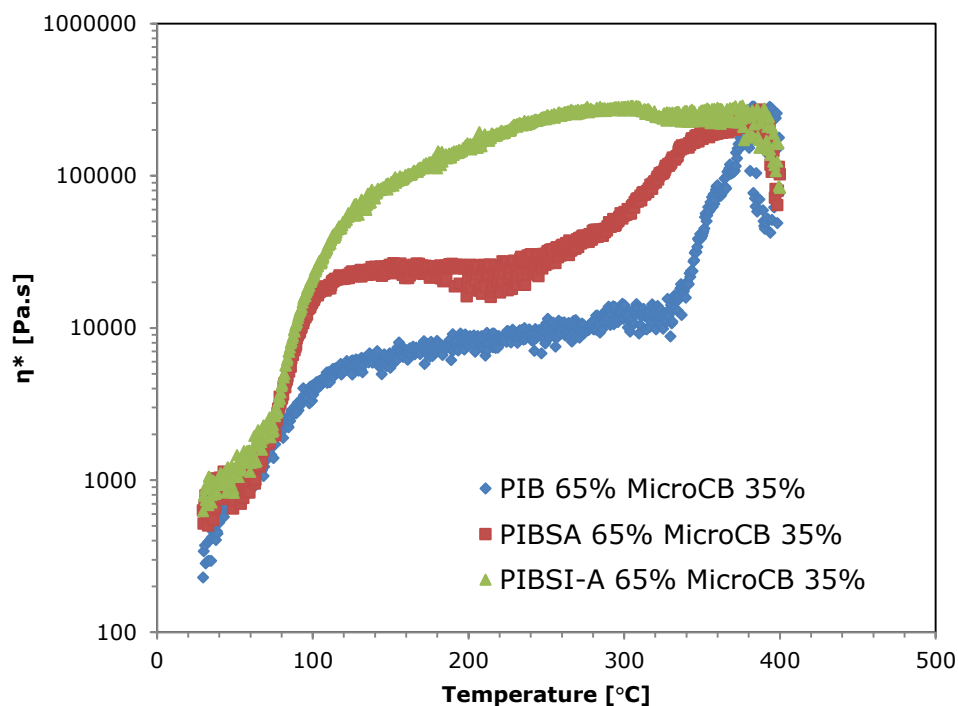


Figure 5-6. η^* as a function of temperature for PIB, PIBSA, PIBSI-A and PIBSI-B (65 %) - MicroCB (35 %) dispersions using a heating rate of $3\text{ }^\circ\text{C min}^{-1}$ in nitrogen ($\gamma = 0.05$, $\omega = 1\text{ Hz}$). (RDA-III instrument)

The suggestion that the most efficient dispersant yields the highest viscosity may seem to be in contrast to various studies of polymer / carbon dispersions such as Won et al., (2005), Yang et al. (2007) and Yasin et al., (2013) that demonstrate that the most effective stabilisers produce dispersions of generally lower viscosities. However many of these studies used carbon concentrations (typically

< 5 % carbon) that were much lower than used in this study (to more accurately reflect the low deposit to fuel ratio as would be found in the proper application of the additive). However due to the high carbon content employed to characterise the dispersions the results could indicate that, at high solid loading, higher η^* values could reflect a more efficient dispersant due to, as stated, more of a contribution from the polymer to the network. It also appears that due to the high solid loading the network does not collapse (unlike in the study by Yang et al., (2007)) shown by constant η^* values up until the polymer begins to degrade from around 250 °C onwards.

The viscoelastic trends in Figure 5-6 show that the PIB, PIBSA and PIBSI-A polymer dispersions are distinguishable via high temperature rheometry. However it was necessary to investigate whether it was possible to distinguish PIBSIs that are chemically similar to each other to demonstrate the techniques potential. A second PIBSI (PIBSI-B) was therefore analysed which has the same structure as PIBSI-A but synthesised via a different method (via a chlorine synthetic route as opposed to thermal). Figure 5-7 shows the η^* of a dispersion of PIBSI-B (65 %) and MicroCB (35 %) as function of temperature. The corresponding PIBSI-A sample is shown for comparison. The overall viscoelastic trends of the two polymers are similar although PIBSI-B does show lower η^* values up until above 300 °C where the polymers would have been degrading (as shown in the TGA results). This could not have been directly due to molecular weights of the polymers since the PIBSI-A has a lower molecular weight ($M_n = 1253$, $M_w = 2049$) than PIBSI-B ($M_n = 1740$, $M_w = 2648$). Also the TGA results showed that rate of weight loss of the two polymers was the same up until around 300 °C so the higher PIBSI-A η^* values are unlikely to be due to differences in the devolatilisation rate of the two polymers. More likely, the PIBSI-A polymer has a slightly higher level of interaction with the MicroCB particles than the PIBSI-B which increases the viscosity of the sample. An explanation for this is difficult to

establish although one possible explanation could be due to differences in the synthetic routes of the polymers. PIBSI-B was synthesised using an older method/technology (now largely defunct) where the PIB basic structure is prepared cationically using AlCl_3 as a catalyst. This process means that the PIB chains have a smaller proportion of vinylidene end groups that are less reactive to the maleic anhydride used in the synthetic route to form the PIBSA intermediate and additives of this type are thought to have a lower level of engine performance than additives derived from thermal routes (Rivera-Tirado, Aaserud, & Wesdemiotis, 2012). It is possible therefore, that the use of this older technology means there are less reactive head groups on the polymer chains in the PIBSI-B sample to adsorb onto the surface of the MicroCB particles and therefore less polymer contributes to the formation of the network. Nevertheless, the result demonstrates that high temperature rheometry can be used to distinguish similar PIBSI dispersions and that the molecular weight of the polymer used in dispersions with similar solid loading does not necessarily lead to the highest η^* values at high temperatures.

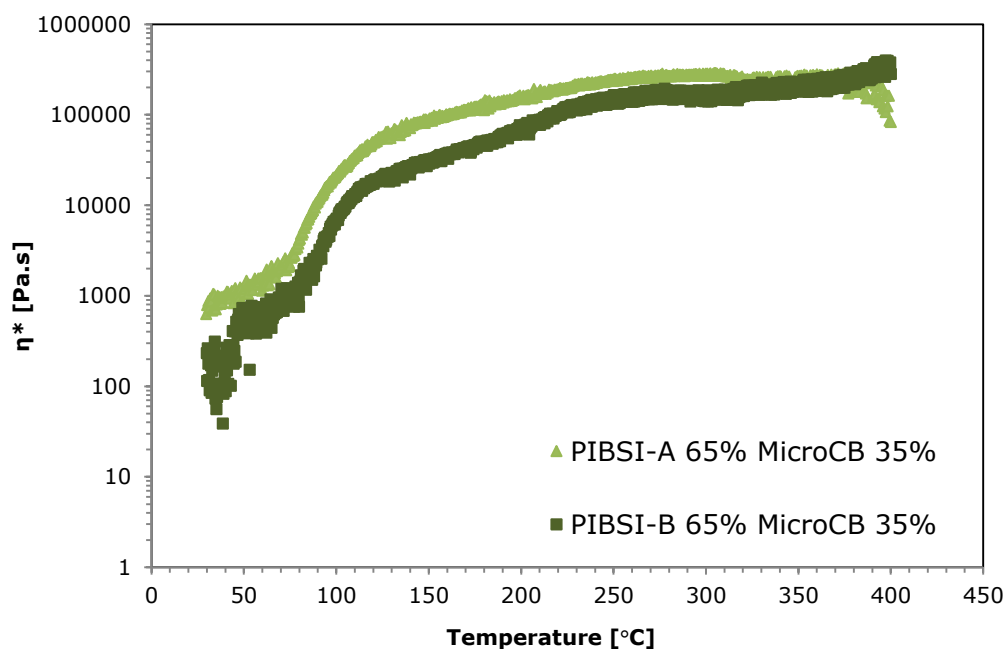


Figure 5-7 η^* as a function of temperature for PIBSI-A (65 %) and MicroCB (35 %), PIBSI-B (65 %) and MicroCB (35 %) dispersions using a heating rate of $3\text{ }^\circ\text{C min}^{-1}$ in nitrogen ($\gamma = 0.05$, $\omega = 1\text{ Hz}$). (RDA-III instrument)

Although the reproducibility for a PIBSI-A sample was established in the previous chapter the PIB, PIBSA and PIBSI-B dispersions were also duplicated three to four times to ensure good reproducibility and distinguishability. The η^* data for each duplicate can be found in the Appendix C. The mean of these analyses is shown in Figure 5-8. Error bars to one standard deviation of the sample mean are included. The graph demonstrates that the viscoelastic trends of the various polymers are distinguishable within experimental error. Although the higher η^* measurements subsequently led to a larger experimental error (for example PIBSI-A dispersion at $250\text{ }^\circ\text{C}$ had mean η^* value of $252710 \pm 47899\text{ Pa.s}$), the different polymer dispersions η^* are still distinguishable between 200 and $300\text{ }^\circ\text{C}$, post conformational changes and residual hexane evaporation and prior to degradation of the polymers.

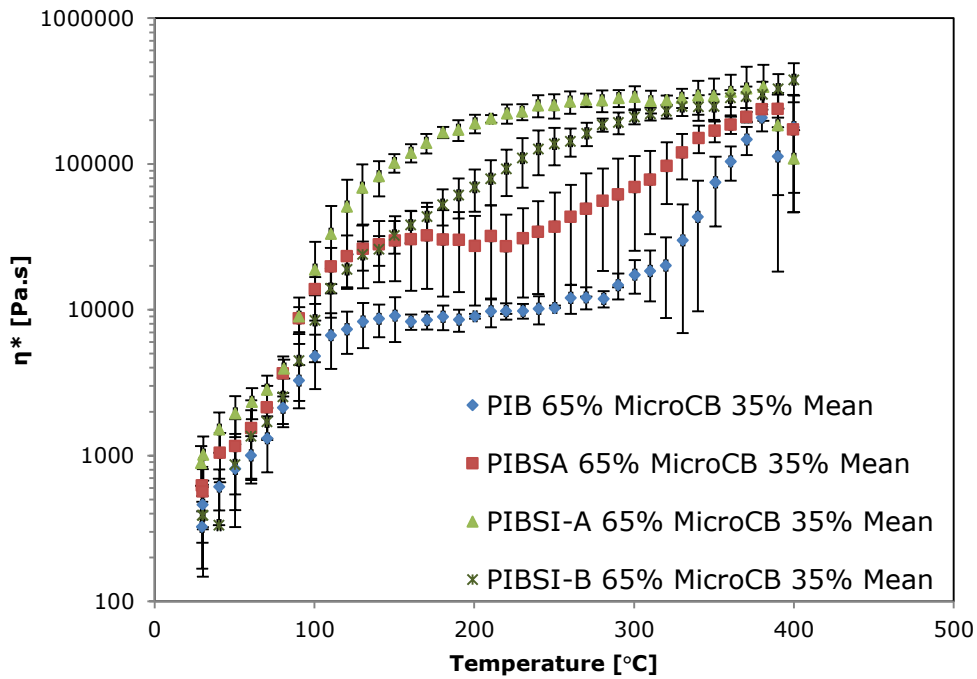


Figure 5-8: Mean η^* as a function of temperature for duplicate samples for PIB, PIBSA, PIBSI-A and PIBSI-B (65 %) and MicroCB (35 %) dispersions using a heating rate of $3\text{ }^\circ\text{C min}^{-1}$ in nitrogen ($\gamma = 0.05$, $\omega = 1\text{ Hz}$). (RDA-III instrument). Error bars are to 1 standard deviation of the sample mean.

A limited number of tests were carried out in industry on a separate rheometer instrument (TA AR-2000 Controlled strain rheometer) that is more sensitive (minimum η^* measurement $\sim 10^1\text{ Pa.s}$) in order to compare viscoelastic behaviour of the dispersions studied at a lower solid loading (25 % MicroCB). As stated in the previous chapter, not all dispersions were possible to be properly analysed on this instrument due to loss of the sample from the plate during initial heating. After numerous attempts it was found to be the case for the PIBSA (75 %) MicroCB (25 %) sample. The η^* trend for this sample has therefore been omitted from the following set of results.

A summary of the PIB, PIBSI-A and PIBSI-B (75 %) MicroCB (25 %) samples are shown in Figure 5-9. For the dispersion of PIB (75 %) and MicroCB (25 %) the overall trend is similar to the corresponding PIB (65 %) MicroCB (35 %) sample

shown in Figure 5-4. The same regions can be identified although the overall η^* trend is lower in magnitude due to the lower solid loading. The PIBSI-A (75 %) MicroCB (25 %) dispersion also gave an overall η^* trend that is similar to the corresponding PIBSI-A (65 %) MicroCB (35 %) sample. Again, the same regions can be identified although the η^* values are lower in magnitude due to the lower solid loading. The PIBSI-B once again (at high temperatures) had marginally lower η^* values than PIBSI-A at higher temperatures (150 – 300 °C). There is a sudden increase in η^* for PIBSI-A and PIBSI-B at around 330 °C which is most likely due to degradation of the polymers. It is clear once again that the order of magnitude of the η^* of the different polymer dispersions once again corresponds with the expected level of interaction between the polymer and the carbon black. To reiterate, PIB which has no polar head group should have little or no interaction with the carbon particles. PIBSI-A and PIBSI-B however should have strong interactions due to the presence of the polar succinimide head groups. It may therefore be possible that the stronger the interaction between the polymer and the carbon black the more the polymer will contribute to the solid fraction of the sample and the higher the η^* values will be in the stable network region.

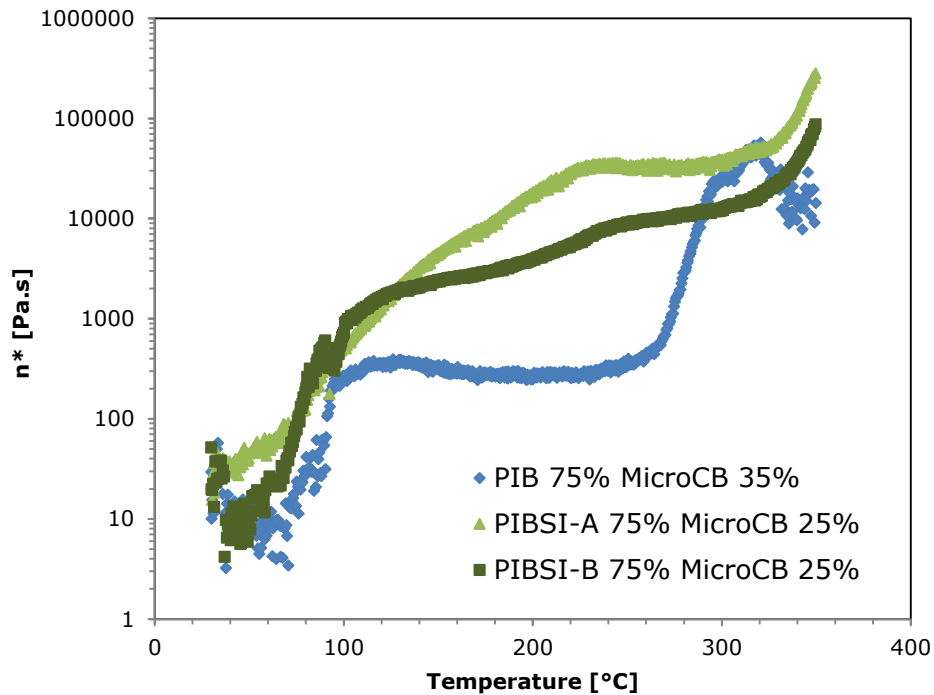


Figure 5-9: η^* as a function of temperature for PIB, PIBSI-A and PIBSI-B (75 %) - MicroCB (25 %) dispersions using a heating rate of $3\text{ }^\circ\text{C min}^{-1}$ in nitrogen ($\gamma = 0.05$, $\omega = 1\text{ Hz}$). (TA AR-2000 Instrument)

Figure 5-10 shows the η^* of dispersions of PIBSI-A and PIBSI-B (75 %) and MicroCB (25 %) samples analysed on the TA AR-2000 rheometer instrument as well as the samples measured on the less sensitive RDA-III instrument previously discussed. The graph demonstrates how two PIBSIs that are chemically very similar can be distinguished using high temperature rheometry on two separate instruments.

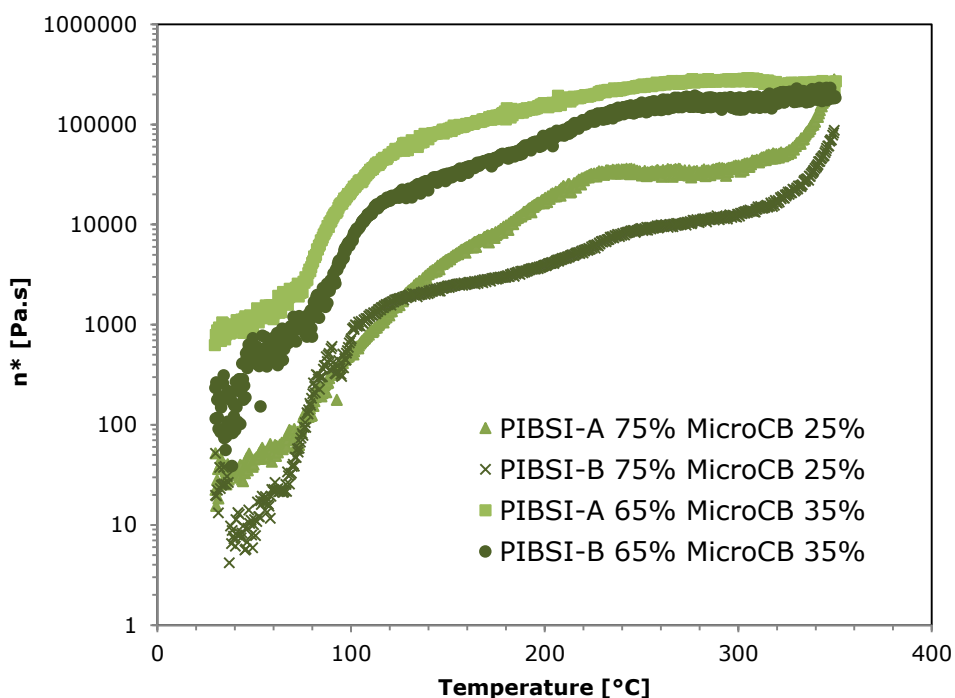


Figure 5-10. η^* as a function of temperature for PIBSI-A and PIBSI-B (65-75 %) dispersions with MicroCB (35-25 %)-(RDA-III instrument), (25 %) (TA AR-2000 instrument)

5.2.4 High temperature ^1H NMR measurement of PIB, PIBSA, PIBSI-A and PIBSI-B

Figure 5-11 shows the changes in the ^1H NMR peak half-width ($\Delta H_{1/2}$) as a function of temperature for the polymer additives. The peak width is inversely proportional to the mobility of the molecules. The mobility of PIB remains fairly constant with only a gradual increase in $\Delta H_{1/2}$ observed from 200 Hz to 970 Hz at 250 °C with the exception of a small spike at around 120 °C which may have been due to a temperature surge on the instrument since the trend returns to a similar rate of increase in $\Delta H_{1/2}$. This experiment was stopped at 250 °C. In the case of PIBSA there is an initial decrease in $\Delta H_{1/2}$ and therefore an increase in mobility from 20 °C. The mobility remains high up to around 150 °C and then decreases shown by an increase in the $\Delta H_{1/2}$ to approx. 1500 Hz remaining approximately constant

from around 190 °C up until around 390 °C where there is a slight increase. The PIBSI-A follows a similar trend to that of PIBSA although the drastic increase in $\Delta H_{1/2}$ occurs at 90 °C. These sudden changes in the $\Delta H_{1/2}$ are most likely due to conformational changes in the hydrocarbon chains at temperatures below 100 °C as reported by Won et al.(2005) as conformational changes (coil-globule transitions) have previously been shown to cause decrease in H atom mobility in polymers (Larsson, Kuckling, & Schonhoff, 2001). This may have occurred at a lower temperature for the PIBSI-A due to loss of solvent from the sample as demonstrated from the TGA results in addition to the conformational changes. The $\Delta H_{1/2}$ remains relatively constant from 100 °C onwards at around similar $\Delta H_{1/2}$ values as to the PIBSA. At around 375 °C there is another sudden increase in $\Delta H_{1/2}$ and a decrease in mobility which is most likely due to degradation of the polymer as shown by the TGA results. A possible explanation given for the similar $\Delta H_{1/2}$ higher values of the PIBSA and the PIBSI-A than the PIB could be attributed to the higher degree of interactions as the polymer forms globular structures with the polar head groups of the PIBSA and the PIBSI-A interacting with one another. The fact that PIBSA ends up with lower mobility at high temperatures than the PIB even though their weight average and number average molecular weights are similar could be due to the succinic anhydride head groups in the PIBSA dispersions interacting with each other leading to more entanglements. The PIBSI-B polymer shows the largest increase in the $\Delta H_{1/2}$ from ~ 320 Hz to 2000 Hz between 60 and 150 °C. The higher $\Delta H_{1/2}$ values of PIBSI-B than PIBSI-A at temperatures between 130 and 390 °C could be attributed to the higher molecular weight of PIBSI-B polymer ($M_n = 1740$, $M_w = 2648$) than PIBSI-A ($M_n = 1253$, $M_w = 2049$) which could have favoured the reduction in mobility due to more entanglements. The $\Delta H_{1/2}$ remains constant up until 400 °C. This therefore showed no evidence of the degradation of the PIBSI-B as there was no great change in

$\Delta H_{1/2}$ however the TGA results do show that at 400 °C there was still approx. 10 % polymer remaining so this may explain the perseverance of the mobility.

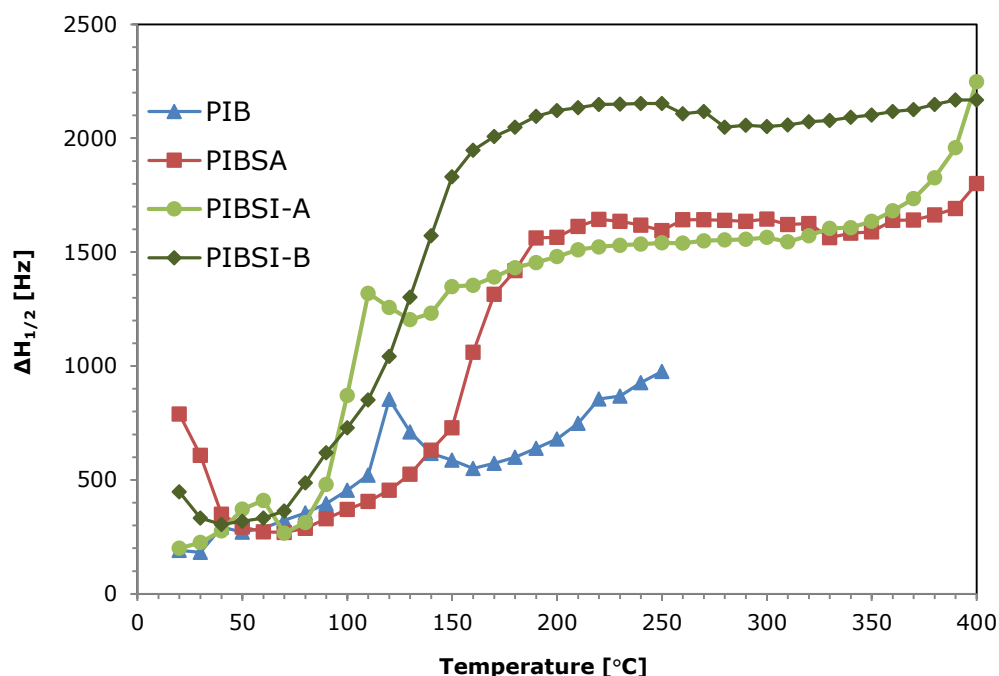


Figure 5-11: Evolution of ^1H NMR $\Delta H_{1/2}$ with temperature for PIB, PIBSA, PIBSI-A and PIBSI-B using a heating rate of $3\text{ }^\circ\text{C min}^{-1}$ in nitrogen

5.2.5 High temperature ^1H NMR peak half width ($\Delta H_{1/2}$) measurement of PIB, PIBSA, PIBSI-A, PIBSI-B – MicroCB dispersions

Figure 5-12 shows the changes in $\Delta H_{1/2}$ as a function of temperature for the PIB, PIBSA, PIBSI-A and PIBSI-B MicroCB dispersions each with 65 % polymer and 35 % MicroCB loadings. These loadings were chosen to attempt to compliment the corresponding rheometry analyses shown in Figure 5-8. The temperature was not increased beyond 250 °C to avoid devolatilised polymer contaminating the NMR probe. Although the reproducibility for a PIBSI-A sample was established in the previous chapter the PIB, PIBSA and PIBSI-dispersions at this solid loading were duplicated three times to ensure good reproducibility and to correspond to the

rheology duplicates shown in Figure 5-8. The data for each individual run can be found in the Appendix E. Error bars to one standard deviation of the sample mean are included. The graph shows that qualitatively, the $\Delta H_{1/2}$ trends of the various polymers are distinguishable within experimental error. It is clear that all of the dispersions show some sort of gradual increase in $\Delta H_{1/2}$ with increasing temperature. However none of the trends show evidence of a more substantial increase between 60 and 100 °C attributed to conformational changes in the polymer chains as observed when the polymers were analysed in isolation via ^1H NMR as well as the corresponding rheometer results. It is possible that the higher $\Delta H_{1/2}$ values brought about by the large solid loading prevented the conformational changes from being observed. The PIB (65 %) MicroCB (35 %) sample shows a gradual increase in $\Delta H_{1/2}$ from 1386 ± 196 Hz at 20 °C to 2146 ± 39 Hz at 250 °C. The PIBSA (65 %) MicroCB (35 %) sample has a $\Delta H_{1/2}$ value of 1660 ± 56 Hz at 20 °C and increases to 2450 ± 96 Hz at 250 °C. The PIBSI-A and PIBSI-B samples both show consistent $\Delta H_{1/2}$ trends which are almost parallel to one another. PIBSI-A shows consistently higher $\Delta H_{1/2}$ values than the PIBSI-B sample which is the opposite to what was observed with the 100 % polymer samples shown in Figure 5-2 which showed PIBSI-B to have the lowest mobility at higher temperatures once conformational changes had taken place. This indicates the order of the mobility/ $\Delta H_{1/2}$ of the different samples can be affected by the presence of the carbon black. Despite the lack of a large increase in $\Delta H_{1/2}$ between 60 to 100 °C that was observed in the ^1H NMR measurements of the polymers in isolation (and the viscosity measurements with 25 and 35% MicroCB) the trends in the order of mobility at high temperatures corresponds to the order of the viscoelasticity measurements at similar temperatures (PIB < PIBSA < PIBSI-B < PIBSI-A). This would correspond with the rheometry results in that there is a greater contribution to the network by the polymers that would be expected to have a strong interaction (PIBSI-A/B) with the carbon black which leads to higher

viscosities and lower mobility's and less of a contribution to the network by the polymers that have little or no interaction (PIB and PIBSA) with the carbon black leading to lower viscosities and therefore higher mobility's at high temperatures.

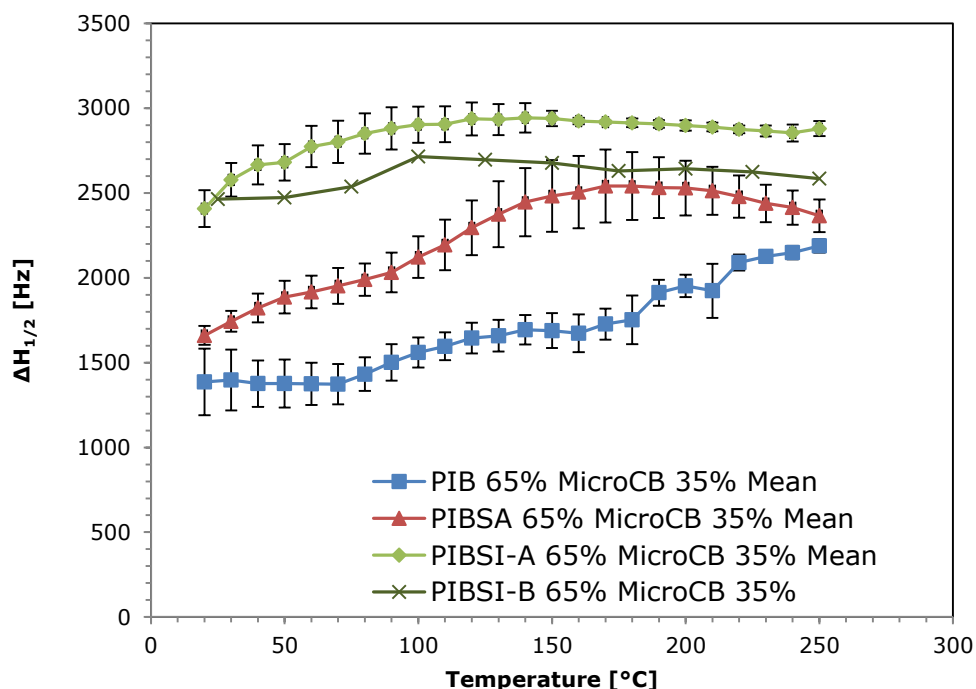


Figure 5-12: Evolution of the ^1H NMR $\Delta H_{1/2}$ with temperature for PIB, PIBSA, PIBSI-A and PIBSI-B (65 %)-MicroCB (35 %) dispersions using a heating rate of $3\text{ }^\circ\text{C min}^{-1}$ in nitrogen. Error bars are to 1 standard deviation of the sample mean.

The order of mobility (at 250 °C) is the same when the percentage of each polymer is increased to 75 % and MicroCB decreased to 25 % as shown in Figure 5-13. Again, all of the dispersions show some sort of gradual increase in $\Delta H_{1/2}$ with increasing temperature. The PIBSA sample is the only sample to show a more substantial increase in $\Delta H_{1/2}$ between 60 and 100 °C which was observed for all the polymers in isolation suggesting that the sample is initially fluid enough to allow the conformational changes to occur i.e. the carbon black did not restrict the mobility of the polymer to such an extent that the effects of the conformational changes could be observed. This may help to explain why it was possible to obtain

a rheometer analysis on the TA-AR2000 instrument for the PIB, PIBSI-A, PIBSI-B (75 %) MicroCB (25 %) dispersions and not for the PIBSA (75 %) MicroCB (25 %) dispersion: the low viscosity/high fluidity of the sample at temperatures between 20 to 60 °C allowed the polymer to flow off the rheometer plate.

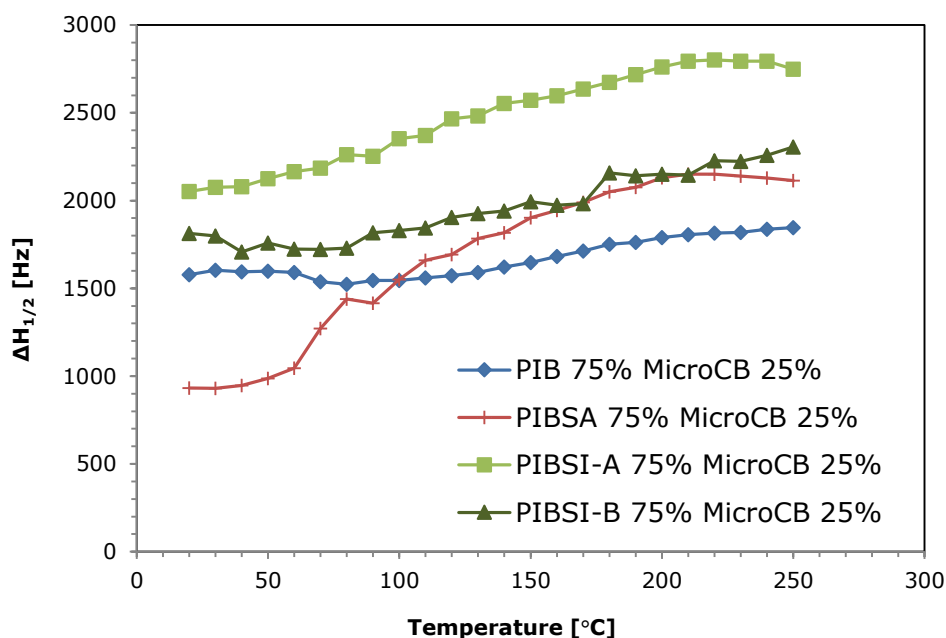


Figure 5-13: Evolution of the ^1H NMR $\Delta H_{1/2}$ with temperature for PIB, PIBSA, PIBSI-A and PIBSI-B (75 %) MicroCB (25 %) dispersions using a heating rate of $3\text{ }^\circ\text{C min}^{-1}$ in nitrogen.

Figure 5-14 shows a summary of the ^1H NMR analysis of PIBSI-A and PIBSI-B MicroCB dispersions as a function of temperature at various concentrations. The graph shows that as the solid loading of the samples are increased the $\Delta H_{1/2}$ at high temperatures also increases. A similar effect has been previously observed in solid state ^1H NMR studies of polymer/ palygorskite clay composites where the line width increased with increasing clay load (Li, et al., 2010). As mentioned above, at 35 and 25 % solid loading the PIBSI-A sample exhibits higher $\Delta H_{1/2}$ values at higher temperatures than PIBSI-B. This is possibly due to a stronger interaction with the carbon black (possibly due to the lower reactivity of the

vinylidene groups to succinic anhydride during the CI synthetic route). The 85 % polymer 15 % MicroCB samples however showed similar $\Delta H_{1/2}$ values at high temperatures. The changes in the $\Delta H_{1/2}$ between 60 and 100°C that were attributed to the conformational changes in the polymer chains observed in the ^1H NMR results of the polymers in isolation (also shown in Figure 5-14) were also observed in these samples. This indicates that the $\Delta H_{1/2}$ trends of the dispersions with $\leq 15\%$ MicroCB were not greatly affected by the carbon black. The observation that the $\Delta H_{1/2}$ trends for PIBSI-A and PIBSI-B dispersions are mostly indistinguishable at 15 % solid loading at high temperatures yet more distinguishable at 25 and 35 % solid loading suggests higher solid loadings may yield more distinguishable trends. This will be investigated in the next chapter with PIBSIs that have more variation in their chemical structure in order to examine the effects on the viscoelastic and mobility behaviour at high temperatures.

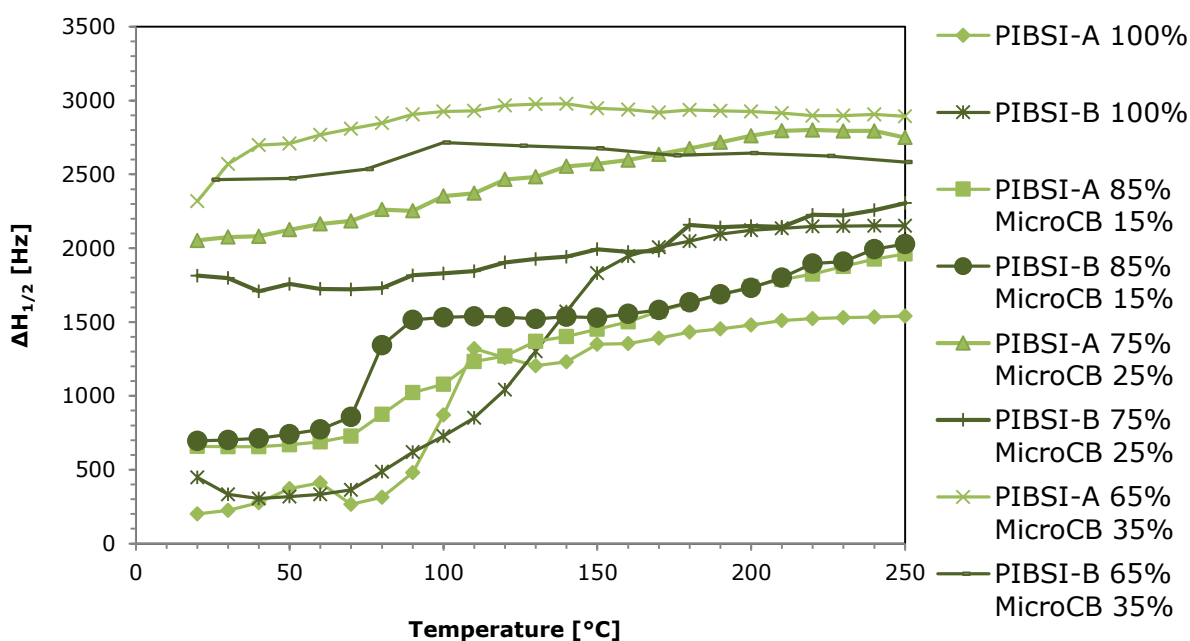


Figure 5-14: Evolution of the ^1H NMR $\Delta H_{1/2}$ with temperature for PIBSI-A and PIBSI-B MicroCB dispersions at various concentrations (polymer 100-65 %, MicroCB (0-35 %)).

5.3 CHAPTER SUMMARY

- High temperature rheometry and ^1H NMR have been used to characterise dispersions of carbon black and PIB, PIBSA and two derivatives of PIBSI PIBSI-A and PIBSI-B, up to temperatures of 350 and 250 °C respectively.
- Attempts to analyse polymer surfactants in isolation were unsuccessful due to the low sensitivity of the rheometer instruments (10^3 Pa.s for RDA-III instrument, 10^1 Pa.s for TA AR-2000 instrument).
- It has been demonstrated that PIB, PIBSA and PIBSIs could be distinguished using high temperature rheometry and ^1H NMR at 65 % polymer 35 % MicroCB. Various viscoelastic stages have been identified. The first is the initial dispersion stage where the particles are dispersed in the polymer. Secondly, it is likely that the conformational changes in the polymer chains lead to aggregation of the particles with each other (PIB) or the adsorbed polymer chains (PIBSA and PIBSIs) creating entanglements which cause an increase in the viscosity. Loss of hexane that is contained within the sample may also contribute to the increase in viscosity around 69 °C. The process leads to a formation of a stable network characterised by relatively constant η^* values up to temperatures associated with polymer degradation. For the PIB sample the network formation yielded lower η^* values than any of the polymers most likely due to the low interaction with the carbon particles. For the PIBSI-A and PIBSI-B samples, the η^* reached higher values in a similar region which may be related to the greater interaction with the carbon black particles by the adsorbed PIBSI-A/ PIBSI-B molecules which causes entanglements and so there is a greater contribution from the polymer to the network. PIBSA which is the intermediate molecule in the synthesis of PIB and PIBSI-A had an intermediate η^* values at high temperatures suggesting

an intermediate level of interaction with the MicroCB particles. The final stage involved polymer degradation which reduces the amount of liquid phase increasing the viscosity further.

- A more sensitive instrument (TA-AR 2000) was used to characterise dispersions with 25 % solid loading. The results correlated well with the RDA-III results (with the exception when the polymer was lost from the rheometer plate when heating).
- ^1H NMR $\Delta H_{1/2}$ measurements of the dispersions up to temperatures 250 °C were shown to compliment well with the rheometry results at high temperatures. The $\Delta H_{1/2}$ measurements, an indication of the mobility and therefore viscosity of a system at high temperatures were the same order of magnitude for the polymers (PIB<PIBSA<PIBSI-A) as the η^* trends at high temperatures (250 °C). Two similar PIBSIs analysed using high temperature rheometry and ^1H NMR both showed higher $\Delta H_{1/2}$ measurements for PIBSI-A indicating it has a stronger interaction with MicroCB than PIBSI-B. This may be attributed differences in the polymers respective synthetic routes.

6 Effect of Polymer Structure on Dispersion Behaviour

This chapter attempts to explore the relationship between the structure of the PIB derivative dispersants and the effect on the viscoelastic behaviour and molecular mobility via high temperature rheometry and ^1H NMR. This includes the effects of the number of amines in the head group, the length of the PIB chain and the number of PIB chains. The first half of this chapter primarily deals with rheometry and ^1H NMR measurements at high polymer loading while the second half primarily concerns mobility behaviour at low polymer loadings using exclusively high temperature ^1H NMR.

6.1 EXPERIMENTAL

6.1.1 Materials

The commercial polymers used were supplied by Innospec Inc. A summary of the properties of the polymers used in this chapter is shown in Table 6-1. The number average molecular weight of the PIB backbone (PIB- M_n) from which the polymers are derived is presented as is the number average molecular weight (M_n) and weight average molecular weight (M_w) and polydispersity values (PD) of the final products obtained from GPC analysis as described in section 3.12.6. The PIB functionality (PIB Func.) or the number of PIB hydrocarbon tails is also presented. The polyisobutylene succinic anhydride (PIBSA) that was discussed in the previous chapter will henceforth be referred to as PIBSA-A.

Table 6-1: Head groups, average molecular weights, polydispersity and functionality of polymer samples

Polymer	Head group*	PIB-M_n (g/mol)	M_n (g/mol)	M_w (g/mol)	PD	PIB Funct.
PIB	N/A	750	771	1075	1.4	N/A
PIBSA(-A)	Succinic Anhydride	750	904	1170	1.3	<i>mono</i>
PIBSA-B	Succinic Anhydride	260	347	363	1.0	<i>mono</i>
PIBSA-C	Succinic Anhydride	1000	1046	1342	1.3	<i>mono</i>
PIBSI-A	TEPA	750	1253	2049	1.6	<i>mono</i>
PIBSI-B	TEPA	1000	1740	2648	1.5	<i>mono</i>
PIBSI-C	AEEA	750	748	1794	2.4	<i>mono</i>
PIBSI-D	Ethanolamine	750	1005	1352	1.3	<i>mono</i>
PIBSI-E	AEEA	750	1277	2037	1.6	<i>mono</i>
PIBSI-F	Ethanolamine	260	382	442	1.2	<i>mono</i>
PIBSI-G	TEPA	1000	1921	3473	1.8	<i>bis</i>
PIBSI-H	TEPA	1000	1858	2793	1.5	<i>bis</i>
PIBSI-I	EDA	750	1490	2055	1.4	<i>bis</i>
PIBSI-J	Ethanolamine	1000	1118	1469	1.3	<i>mono</i>
PIBSI-K	EDA	750	1653	2717	1.6	<i>mono</i>

*Refer to section 3.10.1 for head group abbreviations

A commercial carbon black (MicroCB) with an average particle size of 45 μm and surface area of 205 m^2g^{-1} was used. A description of this carbon can be found in the experimental section 3.10.2. Hexane (Aldrich 95 % was used) was used as a solvent.

6.1.2 Sample preparation

The polymer carbon black dispersions were prepared as described in section 3.11.

6.1.3 Summary of analytical methods

Thermogravimetric analysis (TGA) was used to investigate the thermal degradation of the polymers using the method outlined in section 3.12.3. The polymer-MicroCB dispersions were analysed via high temperature rheometry on the two separate rheometer instruments (RDA-III and TA-2000) and via ^1H NMR as outlined in sections 3.12.3 and 3.12.1 respectively. ^{13}C NMR analysis was

carried out as described in section 3.12.2 to analyse a number of dispersions at low polymer loading.

6.2 RESULTS AND DISCUSSION

6.2.1 Thermogravimetric analysis (TGA) results

Figure 6-1 and Figure 6-2 display the weight percentage loss of PIB, PIBSA (A-C) and PIBSI (A-K) measured by TGA respectively. The rate of weight loss trends for PIB, PIBSA-A, PIBSI-A and PIBSI-B have already been described in chapter 5 section 5.2.1. PIBSA-A and PIBSA-C have similar rates of weight loss with the higher molecular weight PIBSI-C having a maximum rate of weight loss at a slightly higher temperature (370 °C). The low molecular weight PIBSA-B devolatilises at much lower temperatures reaching maximum rate of weight loss at approx. 220 °C and by 300 °C there is < 3 % of the polymer remaining. PIBSI-F which has the lowest molecular weight of any of the PIBSI samples ($M_n = 382 \text{ g mol}^{-1}$, $M_w = 442 \text{ g mol}^{-1}$) begins to devolatilise at around 100 °C and from then on the rate of weight loss increases substantially with around 60 % weight remaining at 250 °C and 13 % remaining at 300 °C. PIBSI-C, PIBSI-E and PIBSI-G all show similar weight loss profiles with all three beginning to devolatilise from initial heating and around 20 % weight is lost by approx. 200 °C. This was most likely due to loss of solvent in each of the polymer samples. PIBSI-D, PIBSI-H, PIBSI-I also showed evidence of devolatilisation of solvent with weight losses of 17 %, 10 % and 13 % respectively at 200 °C. These polymers (including PIBSI-C, E and G) all show a maximum rate of weight loss associated with degradation between 320 and 400 °C. PIBSI-J and PIBSI-K show slower rates of devolatilisation with weight loss of 7 % and 5 % respectively at 250 °C and are also shown to thermally degrade between 320 to 400 °C.

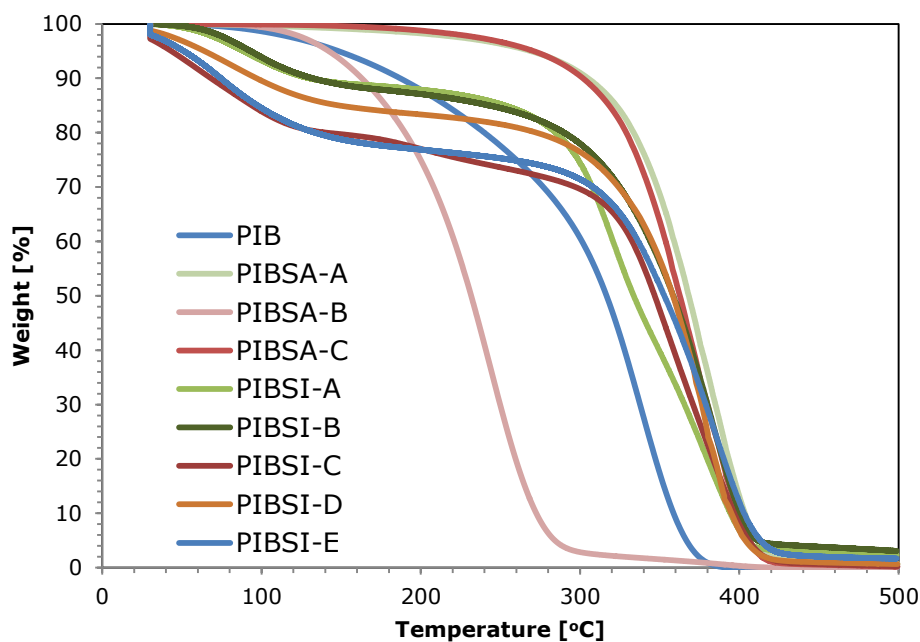


Figure 6-1: Weight percentage loss as a function of temperature using a heating rate of 3 °C min⁻¹ for PIB, PIBSA (A-C), PIBSI (A-E) in nitrogen.

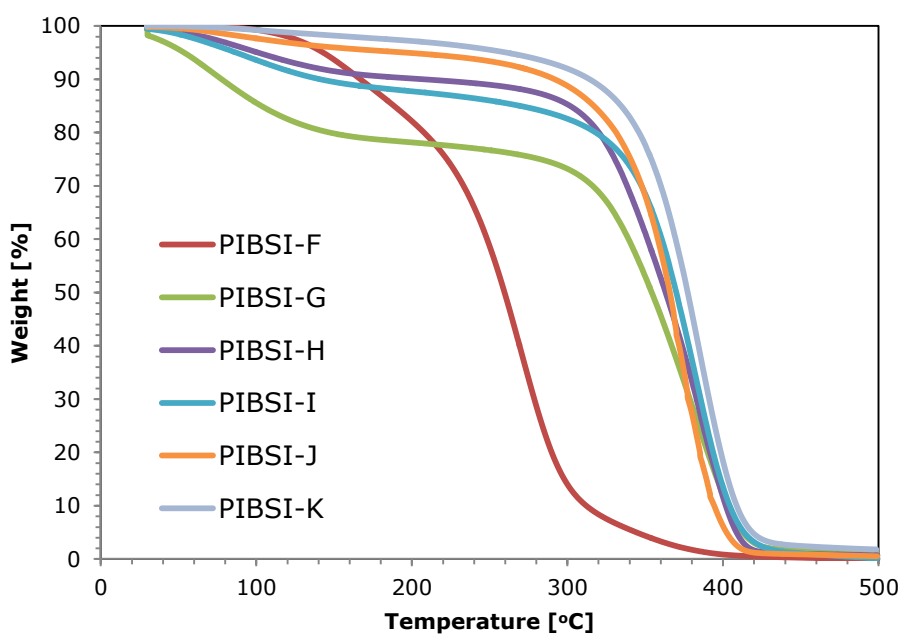


Figure 6-2: Weight percentage loss as a function of temperature using a heating rate of 3 °C min⁻¹ for PIBSI (F-K) in nitrogen.

6.2.2 Polar surface area calculations

The polarity (or basicity) of the head groups of PIBSI type dispersants is known to effect the efficiency of dispersants in reducing the amount of carbon deposits

(Kim, et al., 2015). To determine if there is any overall relationship between the η^* and $\Delta H_{1/2}$ measurements at high temperatures the head group polar surface area which is related to the number of basic sites that interact with the carbon deposit precursors was calculated for each polymer. The polar surface area was calculated using topological polar surface area methodology (TPSA) developed by Ertl, Rohde, & Selzer, (2000) and applied recently by Kim et al. (2015) to investigate the polarity of alkyleneamine and amino ether head groups of PIBSI type dispersants. The atomic contributions of the various molecules obtained from Kim et al. (2015) is shown in Table 6-2. The calculated polar surface area for the head groups for the polymers in this work is shown in Table 6-3.

Table 6-2: Atomic contributions to TPSA (Kim et al., 2015)

Atom type Any Non-hydrogen atom (*), Single bond (-), Double bond (=), Triple bond (#)	Polar Surface Area Contribution [Å ²]
[N]#*	23.8
[NH](-*)-*	12.0
[NH ₂]-*	26.0
[O](-*)-*	9.2
[OH]-*	20.2

Table 6-3: Calculated Polar Surface area of head groups

Polymer	Head Group	Polar Surface Area [\AA^2]
PIB	N/A	N/A
PIBSA-A	Succinic Anhydride	9.2
PIBSA-B	Succinic Anhydride	9.2
PIBSA-C	Succinic Anhydride	9.2
PIBSI-A	TEPA	88.2
PIBSI-B	TEPA	88.2
PIBSI-C	AEEA	58.3
PIBSI-D	Ethanolamine	46.3
PIBSI-E	AEEA	58.3
PIBSI-F	Ethanolamine	46.3
PIBSI-G	TEPA	88.2
PIBSI-H	TEPA	88.2
PIBSI-I	EDA	52.0
PIBSI-J	Ethanolamine	46.3
PIBSI-K	EDA	52.0

6.2.3 Structure activity relationships at high polymer loadings

In order to easily compare the magnitude of the η^* values of the PIB and PIBSI-A samples at various weight percentages, the η^* values of each sample at 250 °C are taken and plotted on the same graph (the complete η^* trends for each polymer as a function of temperature at various concentrations can be found in Appendix D. The value of 250 °C is chosen because it appears to be a high enough temperature whereby the η^* exhibits the most relatively constant values (indicative of stable network formation) but is low enough to avoid the effects of polymer degradation for the majority of the polymers as shown by the TGA measurements. Figure 6-3 therefore shows the η^* values taken at 250 °C of PIB and PIBSI-A dispersions with MicroCB at various weight percentages as an example. The polymer (75 %) MicroCB (25 %) samples were run on the TA-2000 rheometer due to the low viscosity of the samples while all other concentrations

were run on the RDA-III instrument. The graph shows that at various concentrations PIBSI-A consistently exhibits higher η^* values than PIB. As discussed in the previous chapter this indicates that the PIBSI-A has a stronger interaction with the particles (at the various concentrations) since there is a greater contribution from the polymer to the network due to greater polymer adsorption.

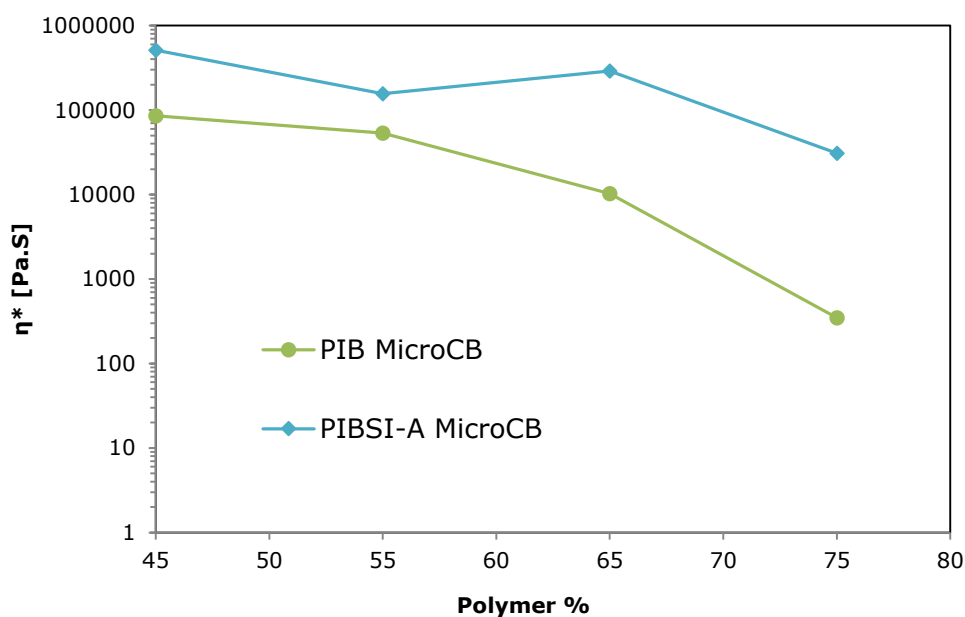


Figure 6-3: η^* values at 250 °C as a function of polymer % for various PIB and PIBSI-A MicroCB dispersions.

In a similar manner, the ^1H NMR $\Delta H_{1/2}$ values for PIB and PIBSI-A dispersions are also taken at 250 °C and plotted on the same graph as shown in Figure 6-4. The graph shows that at various concentrations PIBSI-A consistently exhibits higher $\Delta H_{1/2}$ values than PIB at various concentrations which is indicative of a stronger interaction.

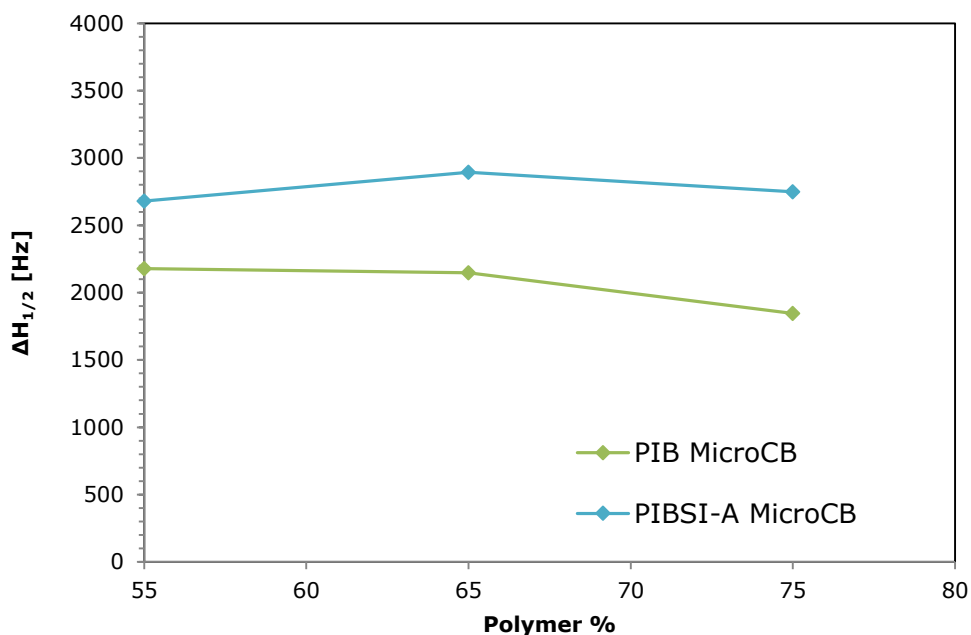


Figure 6-4: ^1H NMR $\Delta H_{1/2}$ values at 250 °C as a function of polymer % for various PIB and PIBSI-A MicroCB dispersions.

Despite the clear discrepancy between the PIB and PIBSI-A η^* and $\Delta H_{1/2}$ measurements it is clear that PIB and PIBSI-A are markedly different samples and so it is difficult to definitively ascribe the differences to one particular structural aspect of the polymers. A number of other polymers were therefore analysed that contain closer variation between the structures in order to gain a better insight into the structural activity relationships. Comparisons are made between polymers that contain only one or two differences so that an explanation for the effect can be attempted to be established. This subsequently leads to dispersions whose trends are (not unexpectedly) more similar. Nevertheless an attempt to characterise and distinguish these polymers is presented. As with the previous graph (Figure 6-3) the η^* measurements will be presented and discussed using the η^* values taken at 250 °C and as a function of polymer %. Again in all cases the polymer (75 %) MicroCB (25 %) samples were analysed on the TA-2000 instrument whereas all other samples were analysed on the RDA-III instrument. The full η^* data for each dispersion at each concentration can be found in

Appendix D. Summaries of the ^1H NMR mobility measurements at 250 °C of the dispersions at similar concentrations are also presented (as in Figure 6-4) in conjunction with rheometer results. The full $\Delta H_{1/2}$ trends as a function of temperature at various concentrations can also be found in Appendix E.

Figure 6-5 shows a summary of the η^* values at 250 °C as a function of polymer % for dispersions of *mono*-PIB (750) with AEEA (PIBSI-C) and *mono*-PIB (750) with ethanolamine (PIBSI-D) with MicroCB at various weight percentages as a function of temperature. The polymers therefore mainly differ in nature of the head groups. The η^* values of the PIBSI-D samples increases linearly with decreasing polymer loading whereas the PIBSI-C samples show a more drastic increase to 55 % PIBSI-C followed by a drop in η^* at 45% loading. The graph shows that at each concentration the PIBSI-C dispersions exhibit greater η^* values than PIBSI-D at 250 °C with the largest η^* difference at 55 % polymer.

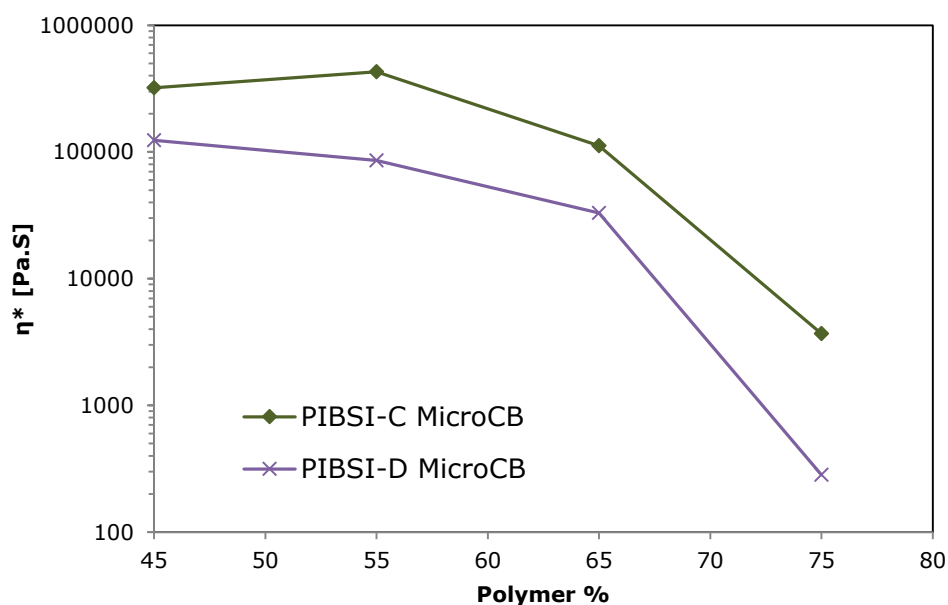


Figure 6-5: η^* values at 250 °C as a function of polymer % for various PIBSI-C and PIBSI-D MicroCB dispersions.

Figure 6-6 shows a summary of the $\Delta H_{1/2}$ values at 250 °C as a function of polymer % for the same PIBSI-C and PIBSI-D dispersions at similar concentrations. The

$\Delta H_{1/2}$ values correspond well with the rheometry results where the $\Delta H_{1/2}$ values are consistently greater for PIBSI-C than PIBSI-D. The difference between the two polymer dispersion $\Delta H_{1/2}$ measurements at 250 °C appears to increase with decreasing polymer concentration.

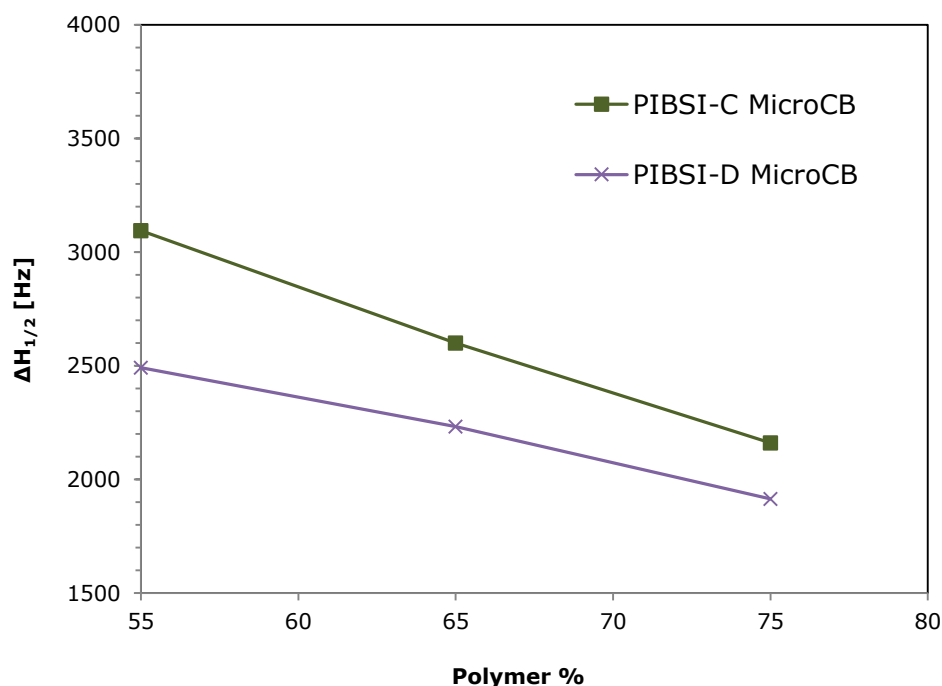


Figure 6-6: 1H NMR $\Delta H_{1/2}$ values at 250 °C as a function of polymer % for various PIBSI-C and PIBSI-D MicroCB dispersions.

The greater η^* and $\Delta H_{1/2}$ values at 250 °C of PIBSI-C compared with PIBSI-D dispersions is most likely representative of a stronger interaction of PIBSI-C with the MicroCB. Both PIBSI-C and PIBSI-D were both synthesised using 750 PIB- M_n basic structure and both are *mono* functional. However PIBSI-C possesses greater polarity of the head group with the presence of an additional secondary amine. Kozak, Moreton, & Vincent, (2009) found that PIBSI adsorption increased in the presence of additional primary and secondary amines in dispersant head groups, increasing the stability of the carbon black suspensions. Also, Kim et al. (2015) observed that a PIBSI with a head group with a larger polar surface area can lead to a reduction in the amount of carbon deposits that precipitates out of fuel at

high temperatures and pressures and this was ascribed to greater adsorption amounts. PIBSI-C has a greater polar surface area (PSA=58.3 Å²) than PIBSI-D (PSA= 46.3 Å²) which could have led to an increase in the level of interaction between the polymer and the carbon surface therefore a greater contribution from the polymer to the network. The effect may have been amplified by the PIBSI-C having slightly higher M_w ($M_w = 1794 \text{ g mol}^{-1}$) than PIBSI-D ($M_w = 1352 \text{ g mol}^{-1}$) but as these polymers are derived from the same PIB backbone it is unlikely to have made a large effect.

A summary of the η^* values at 250 °C of *mono*-PIB (1000) with AEEA (PIBSI-C) and *mono*-PIB (750) with AEEA (PIBSI-E) with MicroCB at various weight percentages are shown in Figure 6-7. The actual viscoelastic trends can be found in the Appendix D. These polymers therefore have the same head group, PIB molecular weight and the same number of PIB tails, differing with only the GPC results with PIBSI-E having higher M_n and M_w values. It is therefore interesting to see if there are any major differences in the viscoelastic behaviour of these polymers. The η^* values for both polymers are similar which would be expected. The polymer (55 %) MicroCB (45 %) samples show PIBSI-C to have higher η^* values than PIBSI-E.

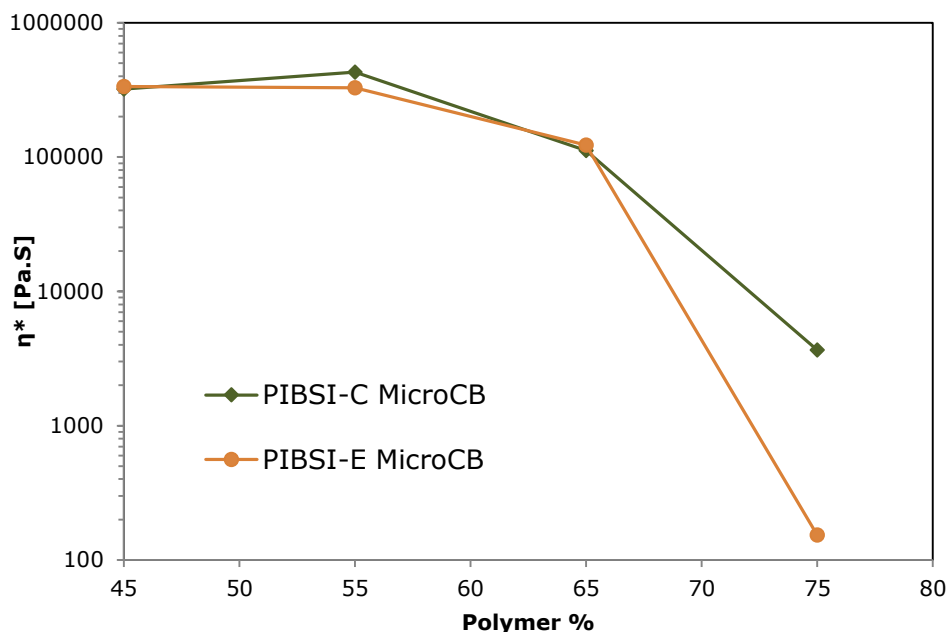


Figure 6-7: η^* values at 250 °C as a function of polymer % for various PIBSI-C and PIBSI-E MicroCB dispersions.

Figure 6-8 shows the $\Delta H_{1/2}$ values at 250 °C as a function of polymer % for the same PIBSI-C and PIBSI-E dispersions at similar concentrations. The individual $\Delta H_{1/2}$ trends can be found in Appendix F. The $\Delta H_{1/2}$ values trend for the two sets of dispersions are quite similar with the PIBSI-C $\Delta H_{1/2}$ values consistently marginally higher than PIBSI-E. This may have been due to the higher molecular weight of PIBSI-E ($M_n = 1277 \text{ g mol}^{-1}$, $M_w = 2037 \text{ g mol}^{-1}$) compared with PIBSI-C ($M_n = 748 \text{ g mol}^{-1}$, $M_w = 1794 \text{ g mol}^{-1}$) with more polymer contributing to the formation of the network. TGA analysis of the free polymers showed both to have similar solvent contents with very similar rates of weight loss. Both show an increase in $\Delta H_{1/2}$ with decreasing polymer %.

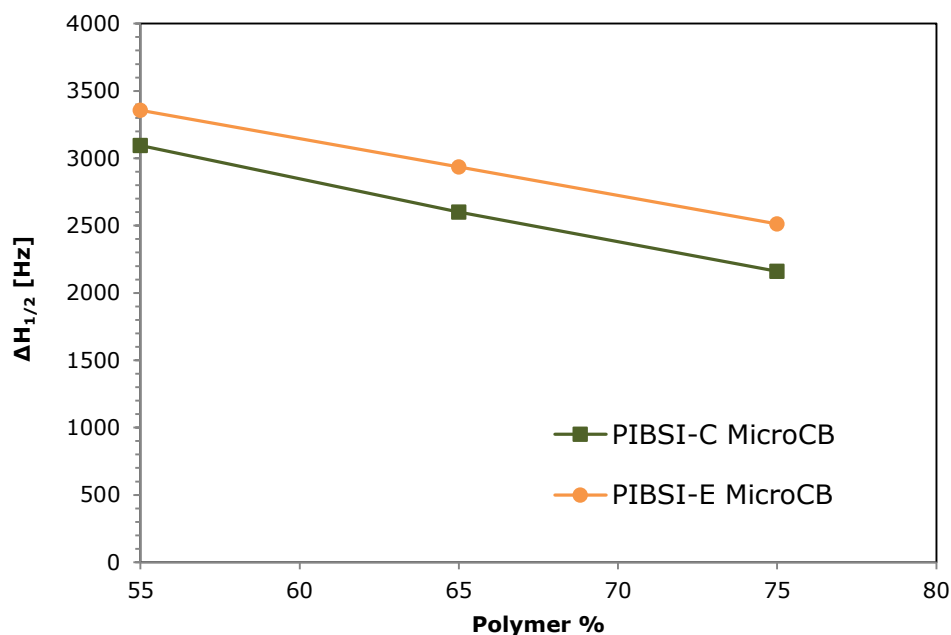


Figure 6-8: ^1H NMR $\Delta H_{1/2}$ values at 250 °C as a function of polymer % for various PIBSI-C and PIBSI-E MicroCB dispersions.

A summary of the η^* values taken at 250 °C for *bis*-PIB (1000) with TEPA (PIBSI-G) and *bis*-PIB (750) with TEPA (PIBSI-H) is presented in Figure 6-9. The full η^* trends with increasing temperature can be found in Appendix D. These polymers differ only in the length of the PIB backbones: PIBSI-H (PIB- $M_n = 1000 \text{ g mol}^{-1}$), PIBSI-G (PIB- $M_n = 750 \text{ g mol}^{-1}$). The effect of the length of the PIB chain on the rheological response has previously been investigated by Yang et al., (2007) who compared the storage and loss moduli of two dispersants up to 100 °C. It was found in that study that the dispersion with the longer chain (PIB- $M_n = 1000$) had higher moduli than the dispersion containing the shorter chain (PIB- $M_n = 550$). It was suggested that the long chain polymer contributed more to the agglomeration of the dispersing system at high temperature. As conformational changes occurred as the temperature was increased the entanglement of the polymer chains that had adsorbed onto the surface of the nanotubes helped to cause the network structure. From the result in Figure 6-9 it is clear that the η^* values at 250 °C are quite similar. The largest difference in η^* was at 55 % polymer

concentration which showed PIBSI-H to have a markedly higher η^* value (approx. 78400 Pa.s) than PIBSI-G. However at 65 % and 75 % the PIBSI-G sample has the higher η^* values. It is therefore difficult to fully establish the effect of the length of the PIB backbone given the inconsistency of the results. The lower difference in the lengths of the PIB backbones in this case may have made for more similar values. Also, given that PIBSI-G has the higher overall molecular weight as obtained from the GPC results ($M_n = 1921 \text{ g mol}^{-1}$, $M_w = 3473 \text{ g mol}^{-1}$) than PIBSI-H despite having the shorter PIB backbone makes an explanation even more difficult to establish.

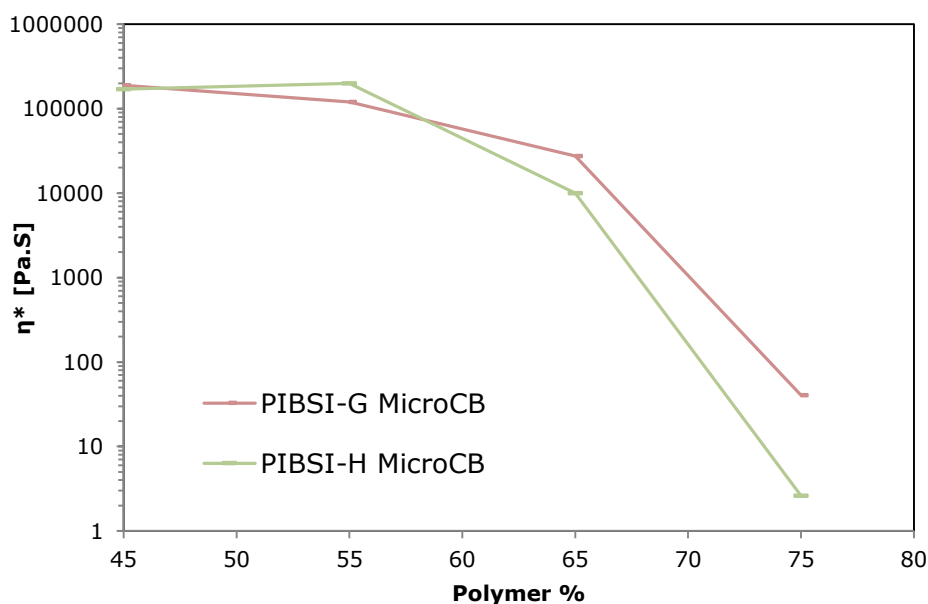


Figure 6-9: η^* values at 250 °C as a function of polymer % for various PIBSI-G and PIBSI-H MicroCB dispersions.

Figure 6-10 shows the $\Delta H_{1/2}$ values at 250 °C as a function of polymer % for the same PIBSI-G and PIBSI-H dispersions at similar concentrations. The graph shows that the polymer dispersions are almost indistinguishable up to 75 % polymer. The general similarity in both the rheometry and ^1H NMR measurements indicates that both polymers have a similar interaction with the MicroCB. This is to be expected since both polymers have the same TEPA head group and so the same

polar surface areas (88.2 \AA^2). The fact that the trends are similar despite differing in molecular weight in both the PIB backbones and in the M_n and M_w values obtained from the GPC molecular weights indicates that molecular weight is not having a substantial effect on the resulting trends. Although Forbes & Neustadter, (1972) found that PIBs with the molecular weight range of 900-1000 gave the best “performance” in terms of stabilisation it maybe that the difference in molecular weights of the polymers is not great enough to show major differences in the η^* and $\Delta H_{1/2}$ measurements and that the strong interaction of the TEPA head groups is the dominant property that ultimately leads to similarly high η^* and $\Delta H_{1/2}$ values.

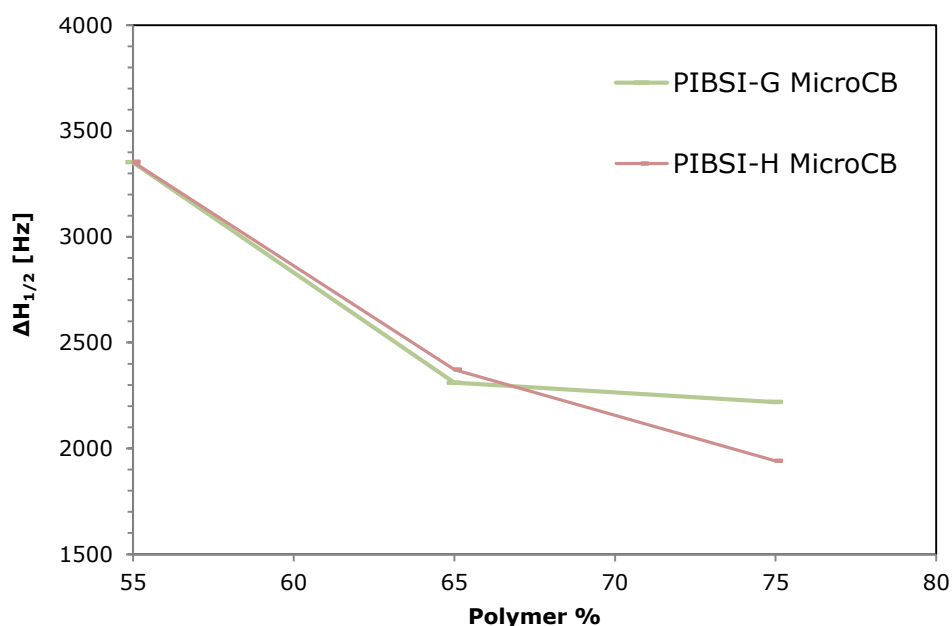


Figure 6-10: ^1H NMR $\Delta H_{1/2}$ values at 250 °C as a function of polymer % for various PIBSI-G and PIBSI-H MicroCB dispersions.

A summary of the η^* values at 250 °C for *mono*-PIB (750) with ethanolamine (PIBSI-D) and *mono*-PIB (260) with ethanolamine (PIBSI-F) is shown in Figure 6-11. The η^* trends may be found in Appendix D. These polymers differ only in the length of the PIB backbones. It is clear that PIBSI-F exhibits higher values than PIBSI-D at each concentration studied. This is unexpected since PIBSI-F has

a shorter PIB tail and so it would be expected (as described by Yang et al., (2007)) to exhibit lower η^* values because less polymer should contribute to the network. The high η^* values of PIBSI-F dispersions at 250 °C may be explained by the low molecular weight of PIBSI-F which could have led to lower temperature degradation which caused an increase in the solid fraction of the sample causing an increase in η^* . The TGA results showed that PIBSI-F degrades at lower temperatures (at 250 °C there was a 40 % weight loss for a 10 mg free PIBSI-F sample).

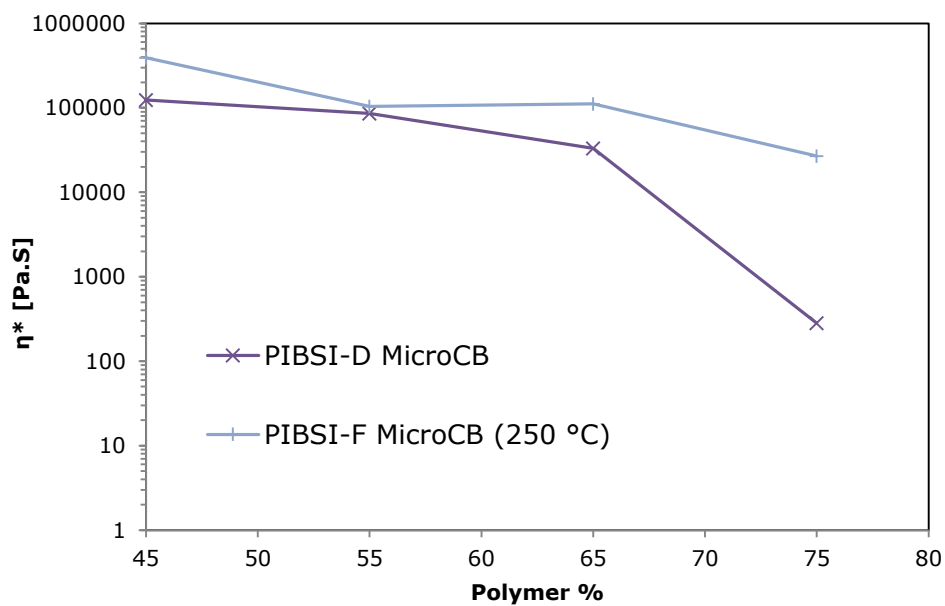


Figure 6-11: η^* values at 250 °C as a function of polymer % for various PIBSI-D and PIBSI-F MicroCB dispersions.

While the η^* data at various concentrations can be found in Appendix D the 75% polymer 25% MicroCB samples measured on the TA Rheometer is interesting and is displayed in Figure 6-12. There is initial scattering between 50 °C to 80 °C followed by a sharp increase to around 300 Pa.s at around 100 °C. Both PIBSI-D and PIBSI-F samples have similar and approximately constant η^* values up until around 220 °C where the PIBSI-F sample has a sudden increase in η^* up to around 4500 Pa.s, most likely due to polymer degradation. The same sudden increase does not occur for the PIBSI-D sample until around 300 °C. The trend indicates

that the molecular weight of the polymers does not greatly affect the viscosity of the network until the polymers begin to degrade. This therefore explains why taking the values at 250 °C of lower molecular weight polymers can lead to misinterpretation of the results in this case.

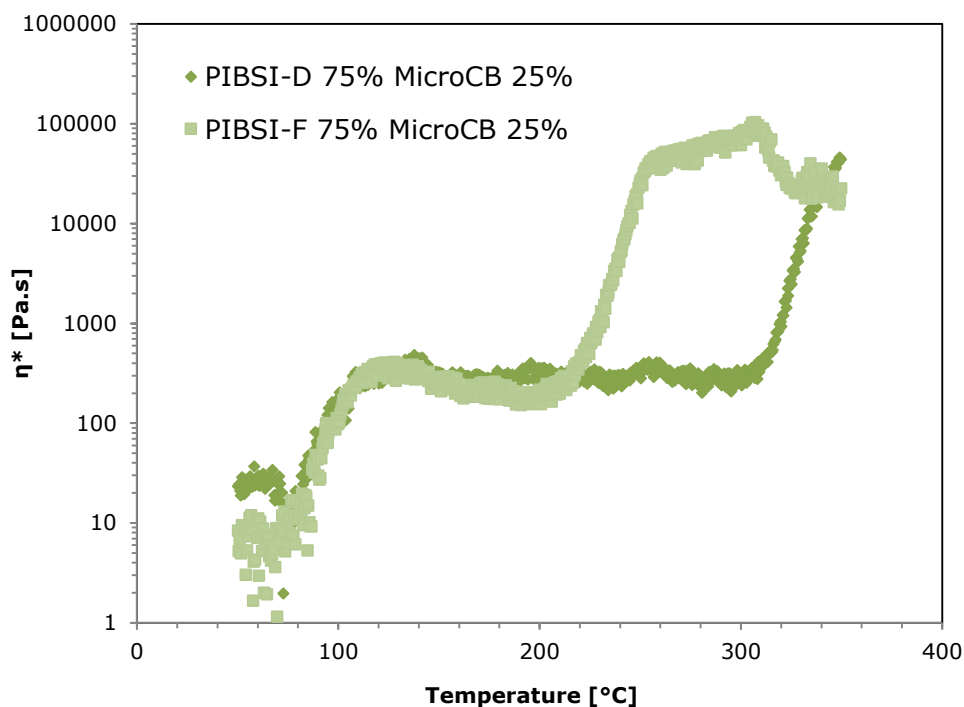


Figure 6-12: η^* as a function of temperature for PIBSI-D and PIBSI-F (75%) MicroCB (25%) dispersions, using a heating rate of $3\text{ }^\circ\text{C min}^{-1}$ in nitrogen ($\gamma = 0.05$, $\omega = 1\text{ Hz}$). (TA-2000 instrument).

A summary of the η^* values at 200 °C for PIBSI-D and PIBSI-F is shown in Figure 6-13. The greater similarity in the η^* trends of the two sets of polymer dispersions at 200 °C suggests that despite the longer PIB chain of PIBSI-D than PIBSI-F, there is not substantial impact on the magnitude of the η^* measurements until, crucially, the polymers begin to degrade after which the measurements can vary substantially.

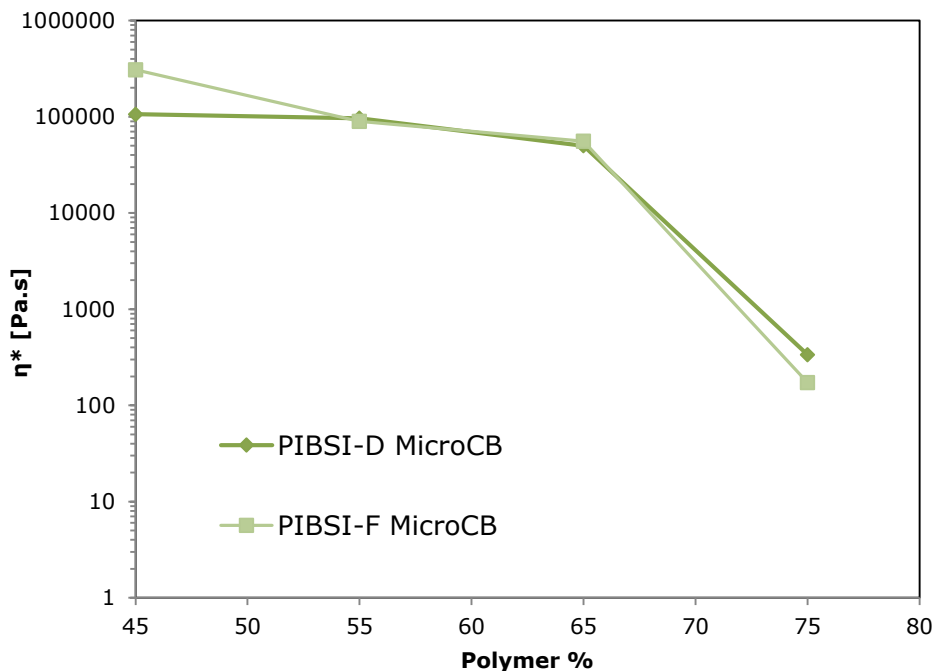


Figure 6-13: η^* values at 200 °C as a function of polymer % for various PIBSI-D and PIBSI-F MicroCB dispersions.

Figure 6-14 displays the $\Delta H_{1/2}$ values at 250 °C as a function of polymer % for the same PIBSI-D and PIBSI-F dispersions at similar concentrations. Due to the low degradation temperature of PIBSI-F the $\Delta H_{1/2}$ values at 200 °C are also displayed in Figure 6-15. The individual $\Delta H_{1/2}$ trends for the polymer MicroCB dispersions can be found in Appendix F. The two graphs show almost identical values as the $\Delta H_{1/2}$ did not vary much with temperature. TGA measurements showed that at 200 °C, 20 % of PIBSI-F had devolatilised whereas at 250 °C around 40 % of the total weight had been lost. The ^1H NMR mobility measurements are not greatly affected by the degradation of some of the PIBSI-F from the sample. The fact that the corresponding rheometer trends are highly affected by degradation of the polymer could be due to a greater amount of free polymer that was contained within the sample due to the larger sample volume that was used for the analysis. The two graphs show (both at 200 °C and at 250

°C) PIBSI-F has higher $\Delta H_{1/2}$ values with 75 and 65 % polymer loading than PIBSI-D while at 55 % the $\Delta H_{1/2}$ values for PIBSI-F are lower. It therefore appears that at lower polymer loadings PIBSI-F samples go to lower $\Delta H_{1/2}$ values (this is found to be the case and is discussed later in this chapter). It is unknown why at 65 % and 75 % PIBSI-F samples exhibit such high $\Delta H_{1/2}$ values even at 200 °C.

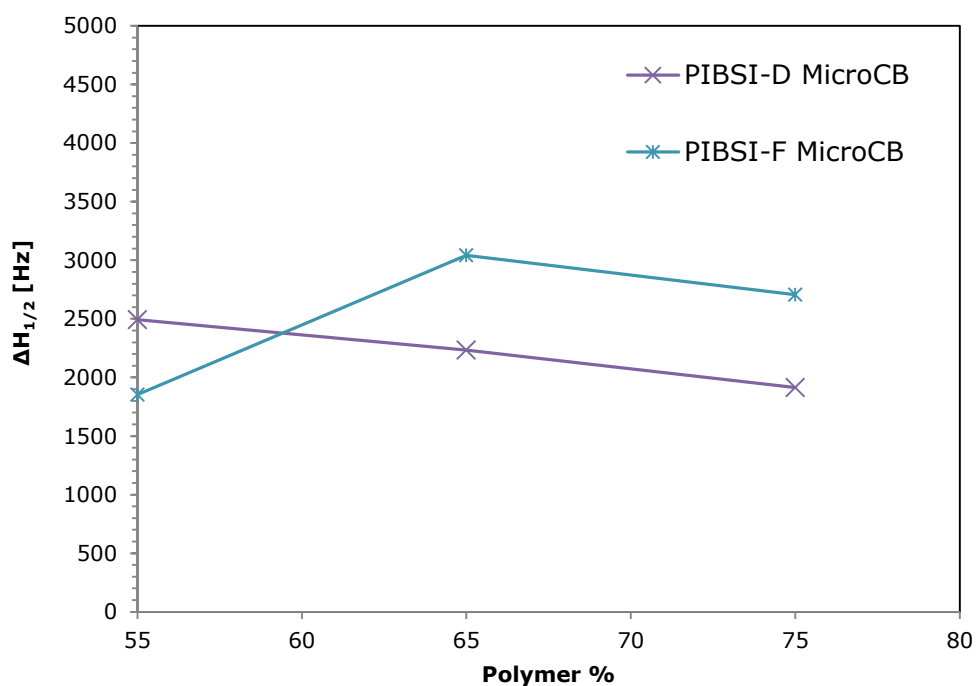


Figure 6-14: ^1H NMR $\Delta H_{1/2}$ values at 250 °C as a function of polymer % for various PIBSI-D and PIBSI-F MicroCB dispersions.

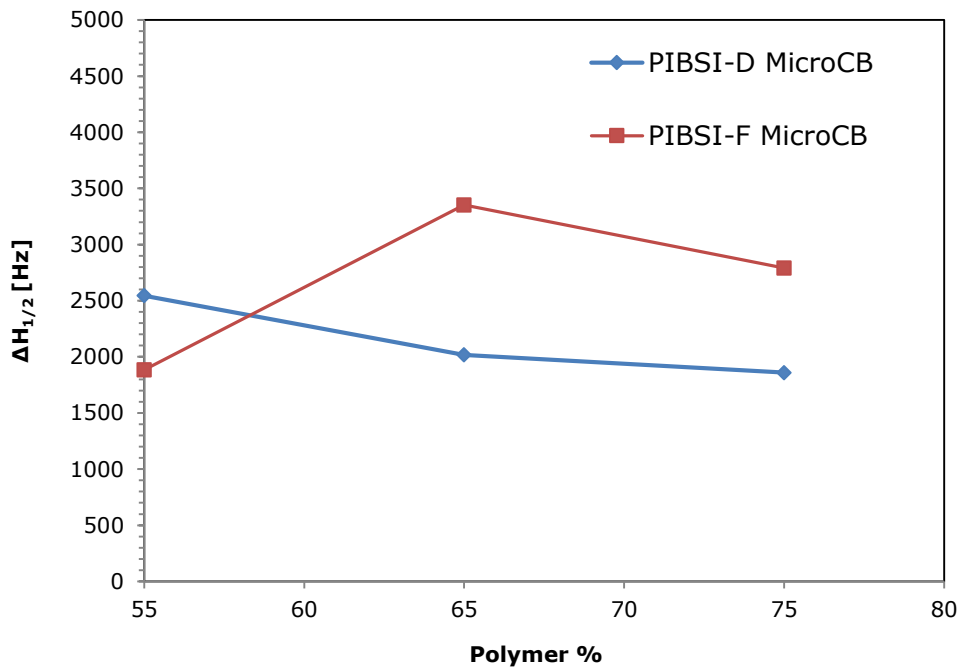


Figure 6-15: ^1H NMR $\Delta H_{1/2}$ values at 200 °C as a function of polymer % for various PIBSI-D and PIBSI-F MicroCB dispersions.

Figure 6-16 and Figure 6-17 shows a summary of the η^* and ^1H NMR $\Delta H_{1/2}$ values at 250 °C as a function of polymer % for PIB, PIBSI-A,C,D and E MicroCB dispersions respectively. The two graphs highlight that the two techniques complement each other quite well. Dispersions containing polymers where it would be expected to exhibit weaker interactions with the MicroCB due to the lack of or smaller amine head groups (PIB and PIBSI-D) do indeed have the lower η^* / $\Delta H_{1/2}$ measurements at different concentrations whereas the polymer dispersions containing the polymers with the larger head groups generally have the greater η^* / $\Delta H_{1/2}$ values.

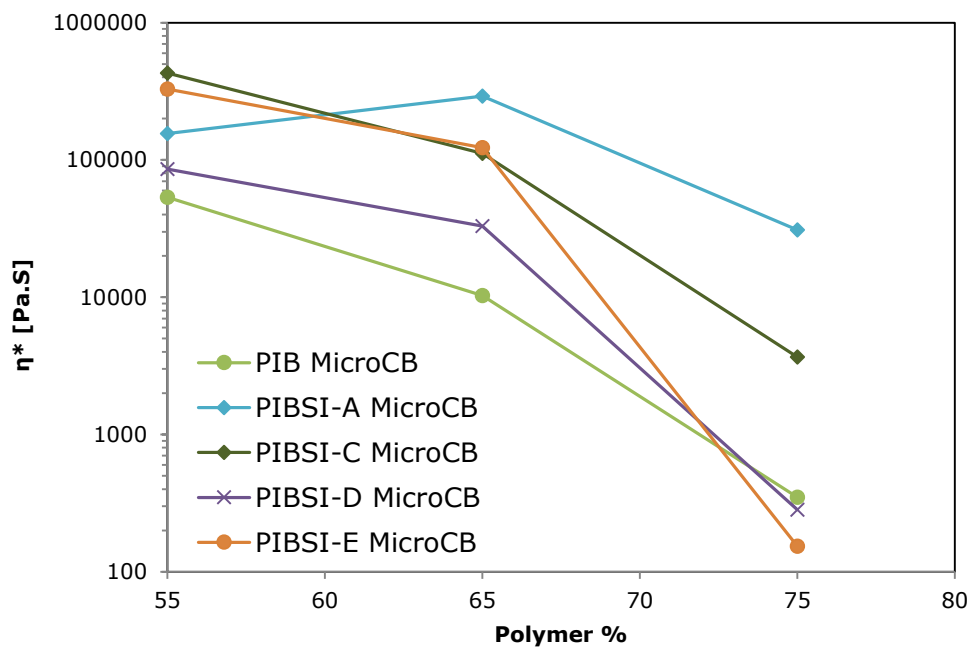


Figure 6-16: η^* values at 250 °C as a function of polymer % for various polymer MicroCB dispersions.

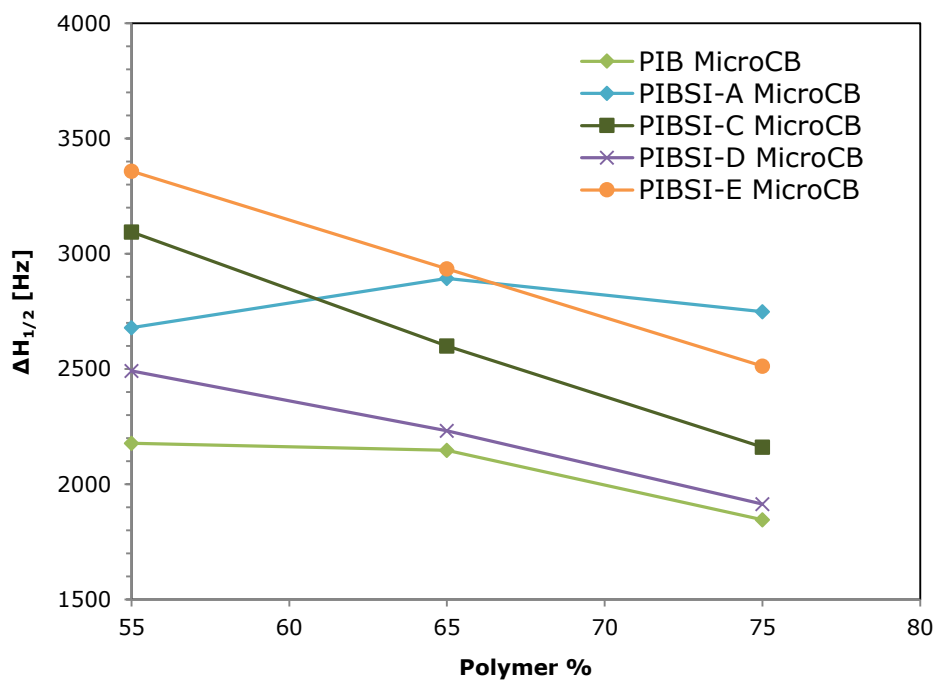


Figure 6-17: ^1H NMR $\Delta H_{1/2}$ values at 250 °C as a function of polymer % for various polymer MicroCB dispersions.

Figure 6-18 shows a summary of the remaining polymers with the η^* values at 250 °C as a function of polymer % for PIBSI-F, G and H MicroCB dispersions. The corresponding ^1H NMR $\Delta H_{1/2}$ values for the same dispersions at the concentrations are shown below in Figure 6-19 for comparison. Values at 200 °C for PIBSI-F samples are also included on both graphs. It can be seen that generally these trends correspond well to one another although it is unknown why PIBSI-F displays higher η^* and $\Delta H_{1/2}$ values than PIBSI-G and PIBSI-H even below degradation temperatures (< 200 °C). It is clear that the relative shortness of the PIB chain of PIBSI-F has had some effect at higher polymer %.

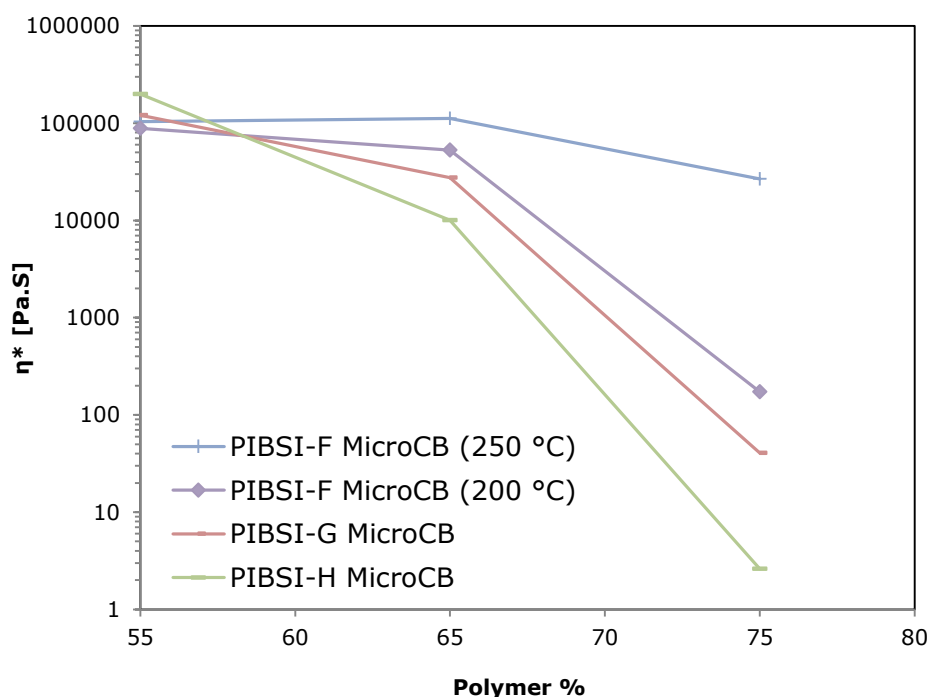


Figure 6-18: η^* values at 250 °C as a function of polymer % for various polymer MicroCB dispersions.

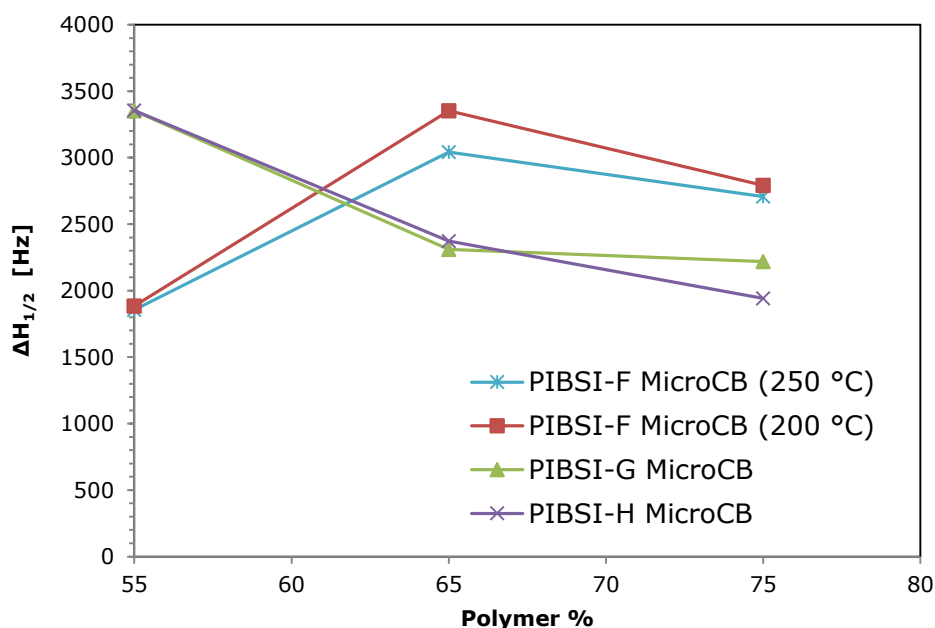


Figure 6-19: ^1H NMR $\Delta H_{1/2}$ values at 250 °C as a function of polymer % for various polymer MicroCB dispersions.

6.2.4 Structure activity relationships at low polymer loadings

Despite the generally good correlation between the rheometry and ^1H NMR results it has found that it is still difficult distinguish between similar, albeit different, polymer dispersions and to accurately ascribe the magnitude of the relevant trends to the chemical structures. It was therefore decided to investigate if the various dispersions maybe better distinguished at higher solid loadings. The remainder of this chapter will therefore focus on investigating samples at low polymer content/high solid content. Only high temperature ^1H NMR analysis was carried out due to the increased difficulty in distinguishing the rheological trends at high solid content with rheometry. One advantage of ^1H NMR is that the $\Delta H_{1/2}$ trends appear to be unaffected by partial degradation of the polymers (for example PIBSI-F) characterised by relatively constant $\Delta H_{1/2}$ values up to 250 °C. The solid loadings of dispersions of PIB and PIBSI-A was increased up to 97.5 % MicroCB. Figure 6-20 shows a summary of the $\Delta H_{1/2}$ values of PIB and PIBSI-A

MicroCB dispersions at 250 °C Vs polymer percentage. The graph shows that at higher solid loading the $\Delta H_{1/2}$ values at 250 °C for both PIB and PIBSI-A remain approximately constant up to 20 % polymer loading. At this point the PIBSI-A $\Delta H_{1/2}$ values at 250 °C drastically increase from around 3000 Hz at 20 % to 6200 Hz at 10 % polymer. At 5 % PIBSI-A the $\Delta H_{1/2}$ is around 6000 Hz whereas the 5 % PIB sample gave a much lower $\Delta H_{1/2}$ value at around 2500 Hz. The most likely explanation for this increase in the $\Delta H_{1/2}$ of the PIBSI-A and not the PIB is that this is the point, at around 20 % polymer loading, at which the PIBSI-A achieves monolayer coverage of the MicroCB particles. This corresponds quite well with an approximate theoretical concentration of monolayer coverage (~ 30 % polymer) as calculated in Appendix I. At >20 % PIBSI-A in addition to the molecules that are bound to the particle surface (the monolayer coverage) there is also a fraction of unadsorbed polymer which without being anchored is more mobile and therefore yields a lower $\Delta H_{1/2}$. At < 20 % PIBSI-A all of the polymer in the sample is adsorbed onto the surface of the carbon and so this leads to a reduction in the average mobility of the sample since all of the polymer is now anchored. A similar saturation effect has been observed recently by Gao, et al. (2014) who observed a sudden decrease in the T_2 (therefore a decrease in the mobility) when decreasing the polymer % in a carboxyl terminated polybutadiene / organo-clay composite system. The increase in $\Delta H_{1/2}$ may have also been affected by the entry of the polymer into the mushroom regime at low surface coverage as described by Dubois-Clochard et al. (2001) due to loss of lateral interactions. At 5 % PIB, because of the lack of interaction between the polymer and the carbon surface, the PIB molecules are still free to move and so the H atoms remain highly mobile resulting in lower $\Delta H_{1/2}$ values.

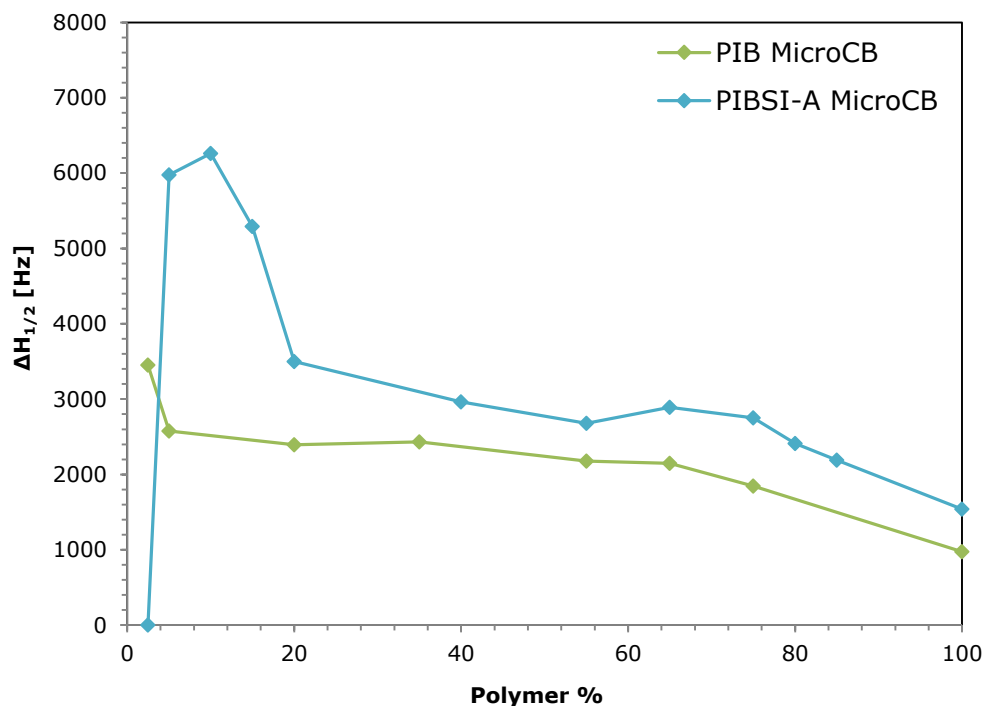


Figure 6-20: ^1H NMR $\Delta H_{1/2}$ values at 250 °C as a function of polymer % for various PIB and PIBSI-A MicroCB dispersions.

The polymer % was decreased further to 2.5 % loading. As is shown in Figure 6-20 the PIB $\Delta H_{1/2}$ increased from approx. 2500 to 3400 Hz. This increase could be due to the lack of free PIB leaving behind only (weakly) adsorbed PIB chains on the surface of the carbon which are less mobile. For the PIBSI-A (2.5 %) sample, the signal is lost under background “noise” and was undetectable. This loss of signal at 2.5 % PIBSA-A while still present with 2.5 % PIB further supports the suggestion that it is because of the stronger interaction between the PIBSI-A and the carbon surface that leads to stronger anchorage of the polymer chains, leading to a reduction in mobility which at <5 % is below the detection levels of the instrument while the PIB which has little or no interaction with the carbon is still partially mobile and gives a small yet detectable signal even with very low polymer content.

To investigate this further various PIBSI-A (5, 15, 25 %) MicroCB (95, 85, 75 %) samples were analysed through solid-state ^{13}C NMR. A 100 % MicroCB sample was also analysed. The results can be found in Figure 6-21. The peak position at 3.5 ppm corresponds to the internal standard TKS (tetrakistrimethylsilane). The substantially broad range of peaks between 75 – 300 ppm is most likely associated with the graphitic carbon black (Freitas, Cunha, & Emmerich, 2012). The broad peak in the 10 – 50 ppm region that originates for the 25 % PIBSI-A sample most likely corresponds to the PIB hydrocarbon chain (McGrath, Ngai, & Roland, 1992). It is interesting that this peak appears at 25 % and is hardly present for the other samples. This corresponds well to the ^1H NMR results which saw a sudden broadening of the peak width with < 20 % polymer in the samples. In this case the polymer peak becomes broad so that it is beyond detection of the ^{13}C analysis. This would again indicate that with < 20 % polymer there is no longer any free PIBSI-A in the sample.

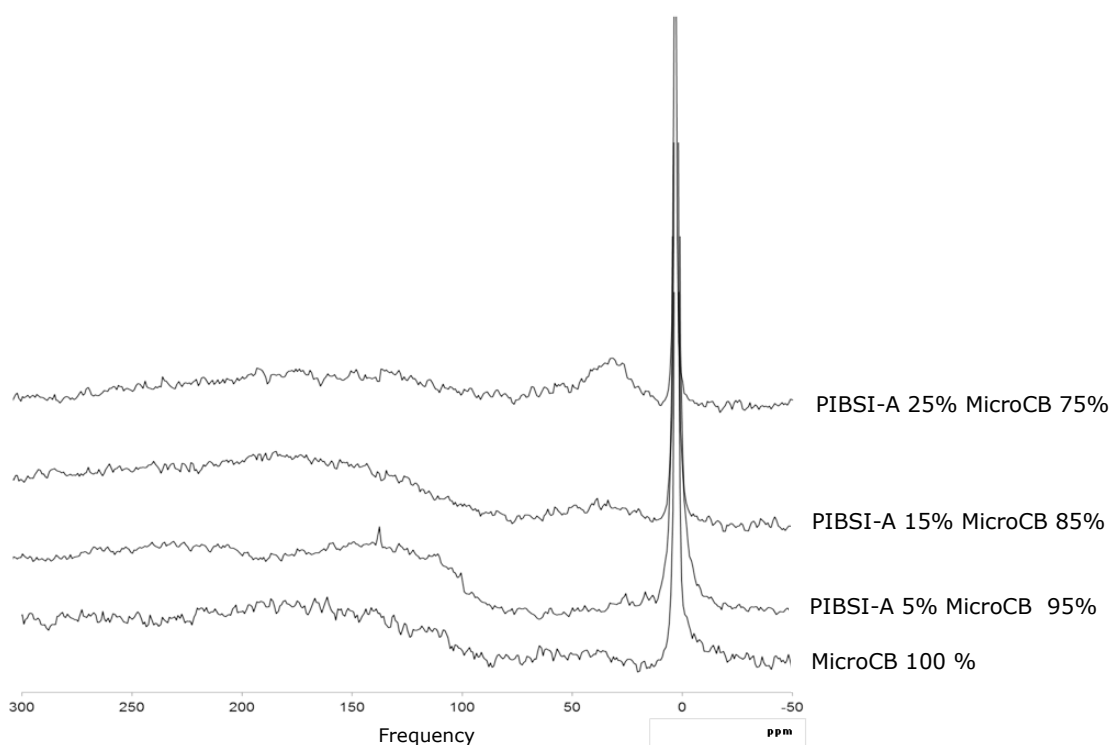


Figure 6-21: ^{13}C NMR spectra of various PIBSI-A MicroCB dispersions (ambient temperature).

Due to the greater discrepancy in the $\Delta H_{1/2}$ measurements between PIB and PIBSI-A dispersions in region 5 – 20 % it was decided to investigate the structure activity relationships of various dispersions within this region in order to investigate whether the polymers could be better distinguished. Again polymers are compared that have differences in as few structural properties as possible to attempt to investigate the structure activity effect on the resulting $\Delta H_{1/2}$ measurements. Only the values at 250 °C are presented. The full $\Delta H_{1/2}$ trends as a function of temperature for each sample can be found in Appendix F. Prior to this however duplicate samples of PIBSI-A (5 %) MicroCB (95 %) were prepared to provide an indication of the level reproducibility of the $\Delta H_{1/2}$ results at the low polymer loading region. Figure 6-22 shows the ^1H NMR $\Delta H_{1/2}$ for 3 duplicate samples of MicroCB dispersions with PIBSI-A as a function of temperature. Figure 6-23 shows the evolution of the mean ^1H NMR $\Delta H_{1/2}$ with temperature for the duplicate analysis. The error measurement at all three concentrations is substantial up to 200 °C (> 1000 Hz). The increased level in error in this region could have due to the high solid loading in the sample which may have been less homogenous due to pockets of residual polymer and/or hexane leading to residual mobility. At higher temperatures (> 200 °C) the error reduces as the volatiles reach similar levels for each sample. The standard error at 250 °C for the PIBSI-A (5 %) MicroCB (95 %) samples is ± 153 Hz. Although the level of error appears to increase with decreasing polymer % this value will be assumed to be the maximum error at all three concentrations studied (5, 15, 25 %) at 250 °C for the following set of results.

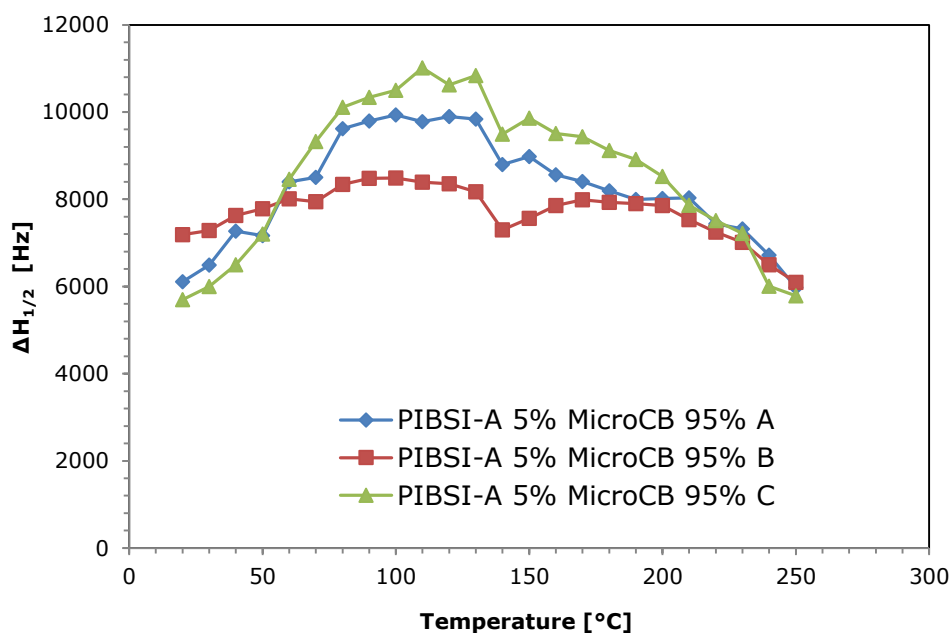


Figure 6-22: Evolution of the ^1H NMR $\Delta H_{1/2}$ with temperature for 3 duplicate PIBSI-A (5 %) Micro CB (95 %) dispersions (A, B, C).

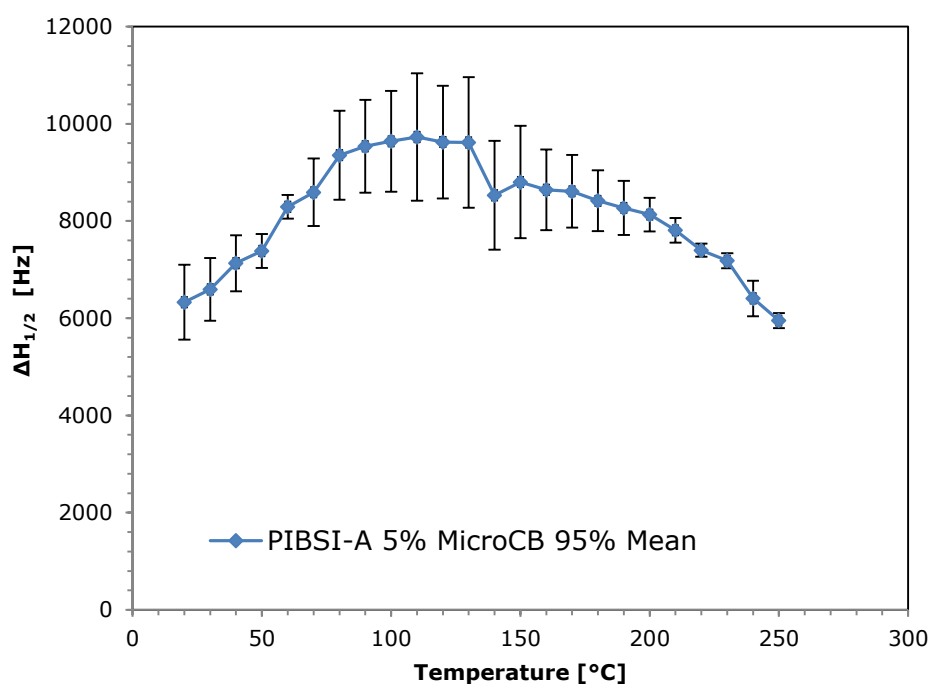


Figure 6-23: Evolution of the mean ^1H NMR $\Delta H_{1/2}$ with temperature for duplicate analysis of PIBSI-A (5 %) Micro CB (95 %) dispersions (A, B, C). Error bars are to 1 standard deviation of the sample mean.

Figure 6-24 shows the $\Delta H_{1/2}$ values at 250 °C for PIBSI-C and PIBSI-D dispersions. As both the polymers are derived from a 750 PIB backbone and are both *mono* functional the graph highlights the effect of increasing the head group length to include an additional secondary amine group. Since PIBSI-C and PIBSI-E differ only in their GPC results both are used to compare with PIBSI-D. The graph shows that the PIBSI-C has higher $\Delta H_{1/2}$ values at 250 °C at each concentration. The values are much more distinguishable in this concentration region (5, 15, 25 % polymer) with an average difference between the two polymers of 2229 Hz as opposed to 405 Hz in the high polymer % region (55, 65, 75%). This would again indicate that, as shown by Kozak, Moreton, & Vincent (2009), the presence of additional amine groups can lead to an increase in the level of interaction between the polymer and the carbon particle. PIBSI-E also shows higher $\Delta H_{1/2}$ values than PIBSI-D although at 5 % polymer the $\Delta H_{1/2}$ value of PIBSI-E was lower than PIBSI-C. This may have been due to the increased error associated at 5 % polymer loading.

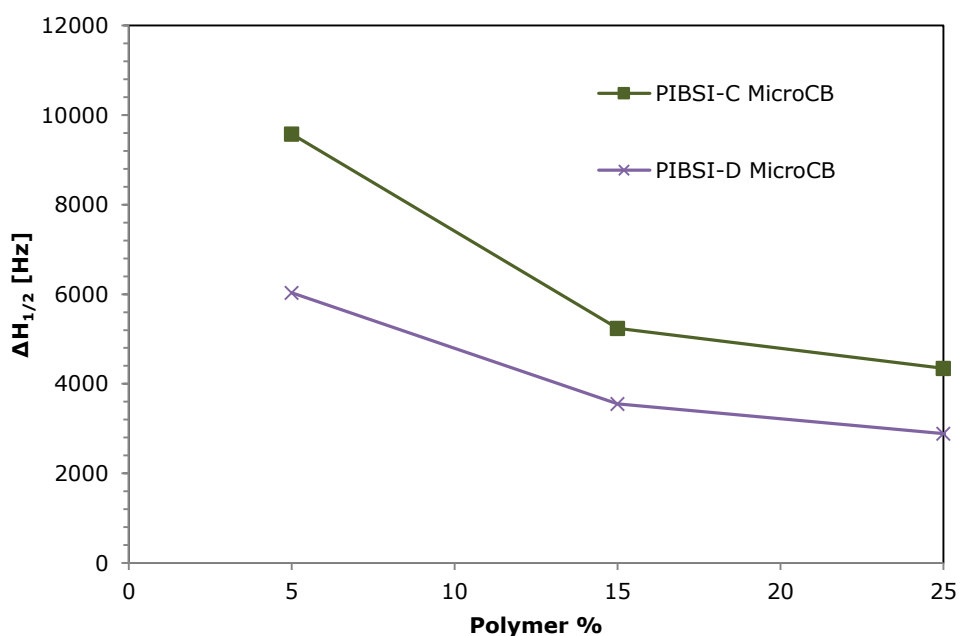


Figure 6-24: ^1H NMR $\Delta H_{1/2}$ values at 250 °C as a function of polymer % for various PIBSI-C and PIBSI-D MicroCB dispersions.

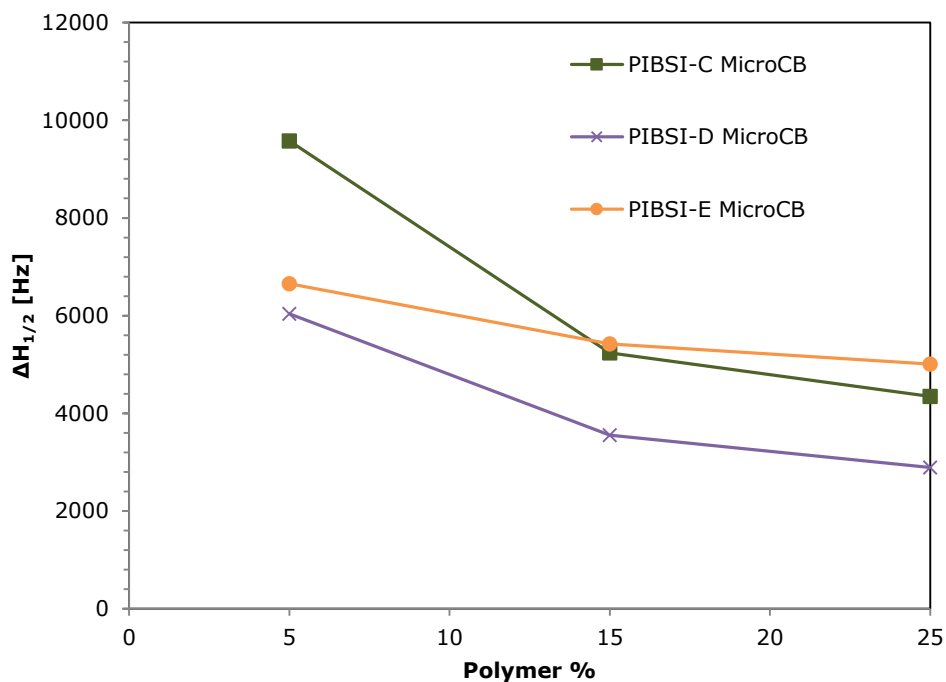


Figure 6-25: ^1H NMR $\Delta H_{1/2}$ values at 250 °C as a function of polymer % for various polymer MicroCB dispersions.

Figure 6-26 shows the effect of changing the end alcohol group to an amine group, displaying the $\Delta H_{1/2}$ measurements for PIBSI-D and *mono*-PIB with EDA (PIBSI-K). As PIBSI-K has an additional amine group and higher calculated PSA it would be expected to display the higher $\Delta H_{1/2}$ measurements. At 15 and 25 % polymer PIBSI-K does indeed show the higher $\Delta H_{1/2}$ values than PIBS-D and the trends are more distinguishable at these polymer loadings. At 5 % polymer however PIBSI-D and PIBSI-K have quite similar $\Delta H_{1/2}$ values with 6036 ± 153 Hz and 5686 ± 153 Hz respectively. This could be a result of the line broadening associated with the decreasing polymer % for the PIBSI-D even though the PIBSI-D should have a weaker interaction.

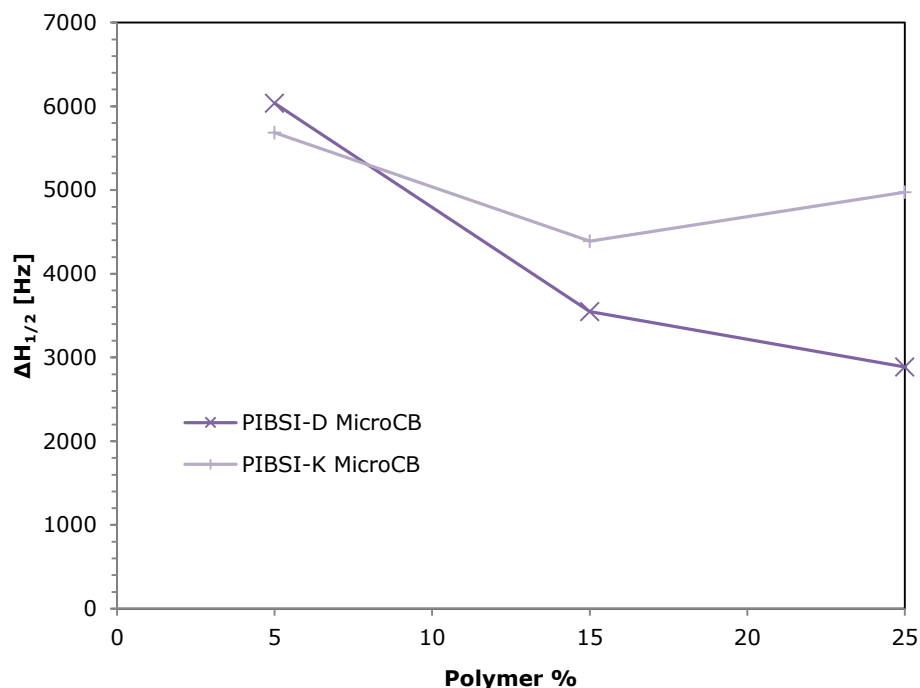


Figure 6-26: ^1H NMR $\Delta H_{1/2}$ values at 250 °C as a function of polymer % for various polymer (PIBSI-D, K) MicroCB dispersions.

Figure 6-27 once again shows the effect of extending the number of amines in the polar head group. *Bis*-PIB (750) with EDA (PIBSI-I) contains two secondary amines while PIBSI-G has four. Both polymers are *bis* functional therefore contain two PIB hydrocarbon tails on either side of the head group. The graph shows that PIBSI-G has consistently higher $\Delta H_{1/2}$ values at 250 °C at each concentration although the gap does narrow from 2766 ± 153 Hz at 5 % polymer to 936 ± 153 Hz at 25 % polymer. These large differences in $\Delta H_{1/2}$ would strongly indicate the additional amine groups had the effect of decreasing the mobility of the PIBSI-G chains due to an increased level of interaction between the polymer head group and the carbon surface. Although the two polymers are derived from 750 PIB backbone PIBSI-G does have higher molecular weight ($M_n = 1921 \text{ g mol}^{-1}$, $M_w = 3473 \text{ g mol}^{-1}$) than PIBSI-I ($M_n = 1490 \text{ g mol}^{-1}$, $M_w = 2055 \text{ g mol}^{-1}$) which may have increased the $\Delta H_{1/2}$ further as more polymer contributed to the network, further restricting the mobility of the PIBSI-G chains.

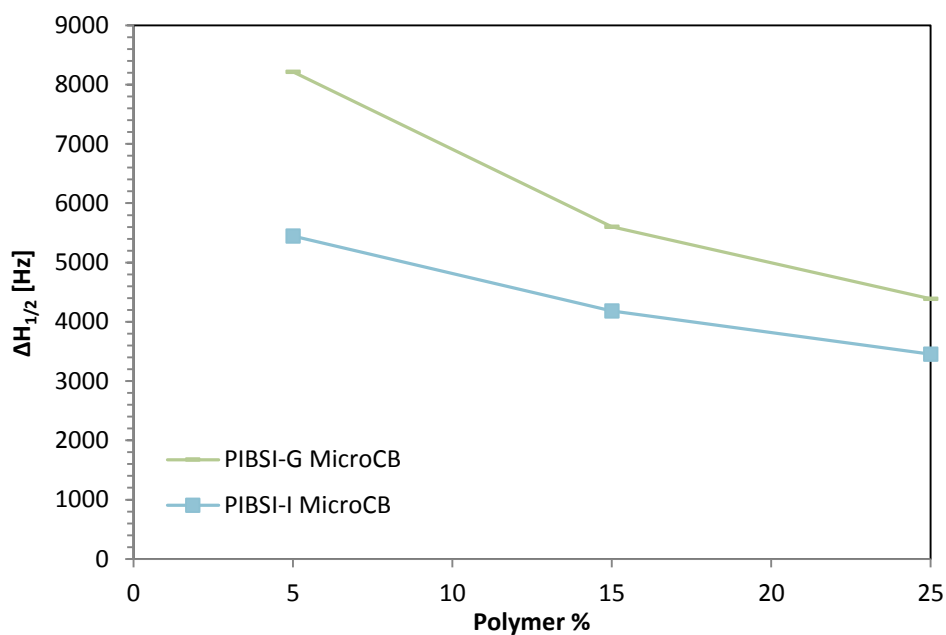


Figure 6-27: ^1H NMR $\Delta H_{1/2}$ values at 250 °C as a function of polymer % for various polymer (PIBSI-G, I) MicroCB dispersions.

Figure 6-28 shows the effect of increasing the polymer tail length. PIBSI-G (derived from 750 PIB- M_n) and PIBSI-H (derived from 1000 PIB- M_n) both show quite similar $\Delta H_{1/2}$ values at 250 °C at each concentration and there is no discernible trend as was also found at higher polymer % (see Figure 6-10). Given that both polymers have four secondary amines in the head groups it would be expected that both polymers should have a strong interaction with the particles. Again, this may have made the effect of differences in molecular weight to have a more negligible due to the strength of the head group being the most dominant structural property.

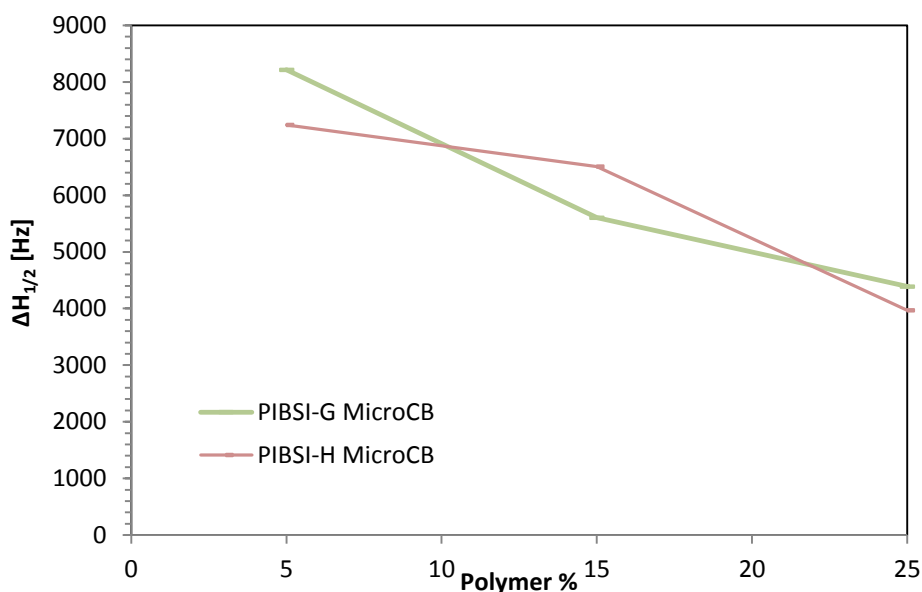


Figure 6-28: ^1H NMR $\Delta H_{1/2}$ values at 250 °C as a function of polymer % for various polymer (PIBSI-G, H) MicroCB dispersions.

The effect of the PIB chain length on the $\Delta H_{1/2}$ value at 250 °C for polymers with smaller head groups is presented in Figure 6-29. This includes PIBSI-D, *mono*-PIB (1000) with ethanolamine (PIBSI-J) as well as PIBSI-F which, while being shown to partially devolatilise as a free polymer at low temperatures (see TGA results, Figure 6-1), displays a $\Delta H_{1/2}$ trend as a function of temperature that remains largely unaffected at least upto 250 °C (see appendix F). PIBSI-F (PIB- $M_n = 260$) clearly gives the lowest $\Delta H_{1/2}$ values at 250 °C at each concentration than both PIBSI-J (PIB- $M_n = 1000 \text{ g mol}^{-1}$) and PIBSI-D (PIB- $M_n = 750 \text{ g mol}^{-1}$) the results of which are both similar except at 5 % polymer where the $\Delta H_{1/2}$ of PIBSI-D is greater. This shows that the two dispersions with the polymers containing the largest PIB backbones (PIBSI-D and PIBSI-J) gave the largest $\Delta H_{1/2}$ measurements at all concentrations indicating that the longer chains lead to more viscous networks that reduce the mobility of the chains as observed by Yang et al. (2007).

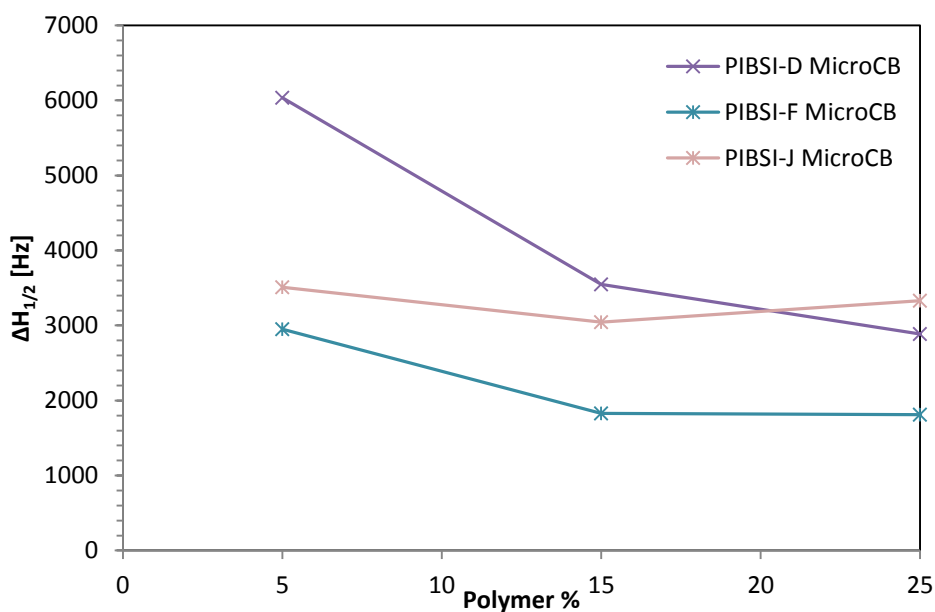


Figure 6-29: ^1H NMR $\Delta H_{1/2}$ values at 250 °C as a function of polymer % for various polymer (PIBSI-D, F, J) MicroCB dispersions.

The effect of the length of the PIB chain for weakly interacting polymers is also demonstrated in Figure 6-30 which shows the effect of PIB chain length on the values of $\Delta H_{1/2}$ at 250 °C for three PIBSAs, PIBSA-A (PIB- $M_n = 750 \text{ g mol}^{-1}$), PIBSA-B (PIB- $M_n = 260 \text{ g mol}^{-1}$) and PIBSA-C (PIB- $M_n = 1000 \text{ g mol}^{-1}$). The overall $\Delta H_{1/2}$ trend as a function of temperature for each polymer may be found in Appendix F. PIBSA-C which has the highest PIB chain length displays the higher $\Delta H_{1/2}$ values at 5 and 15 % polymer which would be expected, since more polymer would contribute to the network increasing viscosity. At 25 % polymer loading however the PIBSI-A sample shows a similar $\Delta H_{1/2}$ to PIBSA-B which due to its low PIB- M_n was expected to have lower $\Delta H_{1/2}$. The 5 and 15 % PIBSA-B samples also gave higher $\Delta H_{1/2}$ values than PIBSA-A which was also unexpected since PIBSA-A has a higher PIB- M_n . Any degradation of PIBSA-B did not appear to affect the $H_{1/2}$ trend at least up to 250 °C so that would not explain the high $\Delta H_{1/2}$ values of PIBSA-B. It is therefore difficult to explain the effect of the length of the PIB backbone from these results. What is clear however is that these three PIBSAs, for which it would be expected to have weaker interactions with the MicroCB

compared with the PIBSIs (due to lack of amine head groups), all exhibit similarly low $\Delta H_{1/2}$ values.

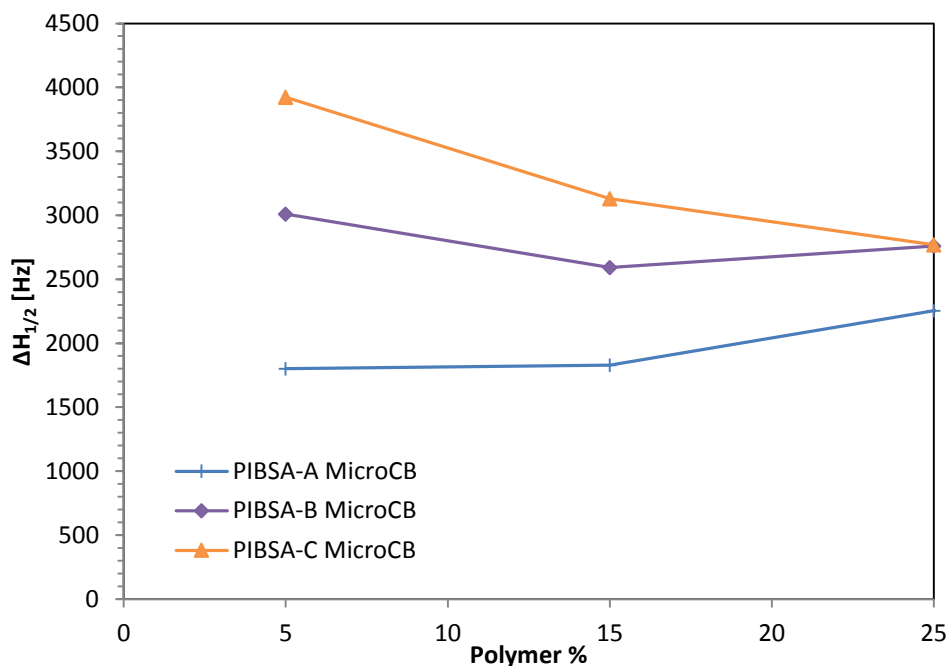


Figure 6-30: ^1H NMR $\Delta H_{1/2}$ values at 250 °C as a function of polymer % for various polymer (PIBSA-A, B, C,) MicroCB dispersions.

Figure 6-31 displays the $\Delta H_{1/2}$ measurements at 250 °C for PIBSI-I and PIBSI-K and so describes the effect of the addition of an extra PIB backbone. There is very little difference in the $\Delta H_{1/2}$ values at 250 °C of the two polymers at 5 and 15 polymer % except that the PIBSI-K sample is slightly higher in both cases although at 25 % polymer the PIBSI-K has a substantially greater $\Delta H_{1/2}$. Cox et al. (2001) found that *bis*-PIB derivatives to be more efficient than *mono* or *tris* derivatives in the stabilisation of carbon blacks whereas Tomlinson et al., (2000) found that the *mono* compounds did not appear to show greater affinity than more highly substituted *bis* and *tris* compounds. These results indicate that the PIBSI-K has a stronger interaction with the carbon black which would disagree with both of these studies. It may be possible that the lack of a primary amine with PIBSI-I due to the presence of the extra PIB tail is responsible for the lower $\Delta H_{1/2}$ and the effect is more pronounced with a greater proportion of polymer present.

Alternatively despite the polymers being derived from the same 750 PIB- M_n backbone the molecular weight values for PIBSI-K are greater ($M_n = 1653 \text{ g mol}^{-1}$, $M_w = 2717 \text{ g mol}^{-1}$) for PIBSI-K than PIBSI-I ($M_n = 1490 \text{ g mol}^{-1}$, $M_w = 2055 \text{ g mol}^{-1}$) and this may have been the cause of the higher $\Delta H_{1/2}$. It is difficult therefore to establish the exact effect of the additional PIB tail has on the mobility measurements from these results.

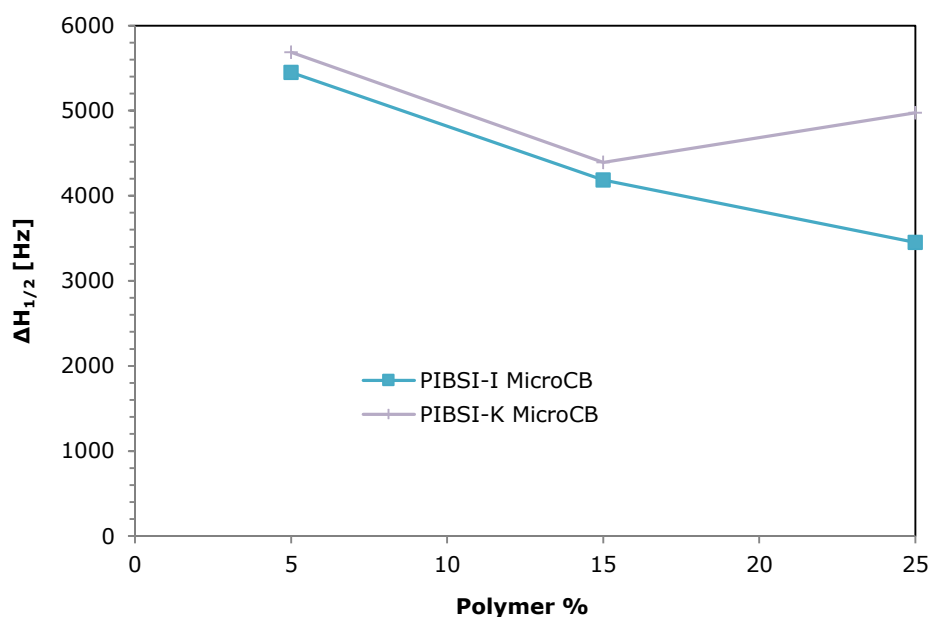


Figure 6-31: ^1H NMR $\Delta H_{1/2}$ values at 250 °C as a function of polymer % for various polymer (PIBSI-I, K) MicroCB dispersions.

6.2.5 Summary of structure activity relationships at low polymer loadings

The direct comparison of two to three dispersions of different polymers indicates that the various sample mobility behaviour can be related to their individual structural properties although it is difficult in some cases to fully distinguish between polymers with similar structures. The final section of this chapter therefore provides more of an overview of the polymer dispersion $\Delta H_{1/2}$ values at 250 °C to attempt to discover if there are any general trends relating to these

structural properties. Figure 6-32 shows the $\Delta H_{1/2}$ values for all of the dispersions studied between 5 – 25 % polymer loadings. While it is difficult to distinguish between every individual trend it is apparent that the results can be generally separated into two groups (labelled group 1 and 2). The polymers and their properties with the assigned group number are summarised in Table 6-4.

It is clear from examination of Figure 6-32 and Table 6-4, that the polymers with lower polar surface areas which would be expected to have a weaker interaction with the MicroCB generally fall into group 1 and the polymers with higher polar surface area and would be expected to have a stronger interaction generally fall into group 2. The polymers in group 1 have more consistent $\Delta H_{1/2}$ measurements at each concentration due to the higher mobility of the more weakly adsorbed polymer. Group 2 polymers exhibit more of an increase in the $\Delta H_{1/2}$ values with decreasing polymer % attributed to the decrease in mobility as there becomes less free polymer in the sample due to stronger adsorption. Although PIBSI-D exhibits a high $\Delta H_{1/2}$ at 5 % loading the 15 and 25 % samples are markedly lower. It therefore may be assigned to either group 1 or 2.

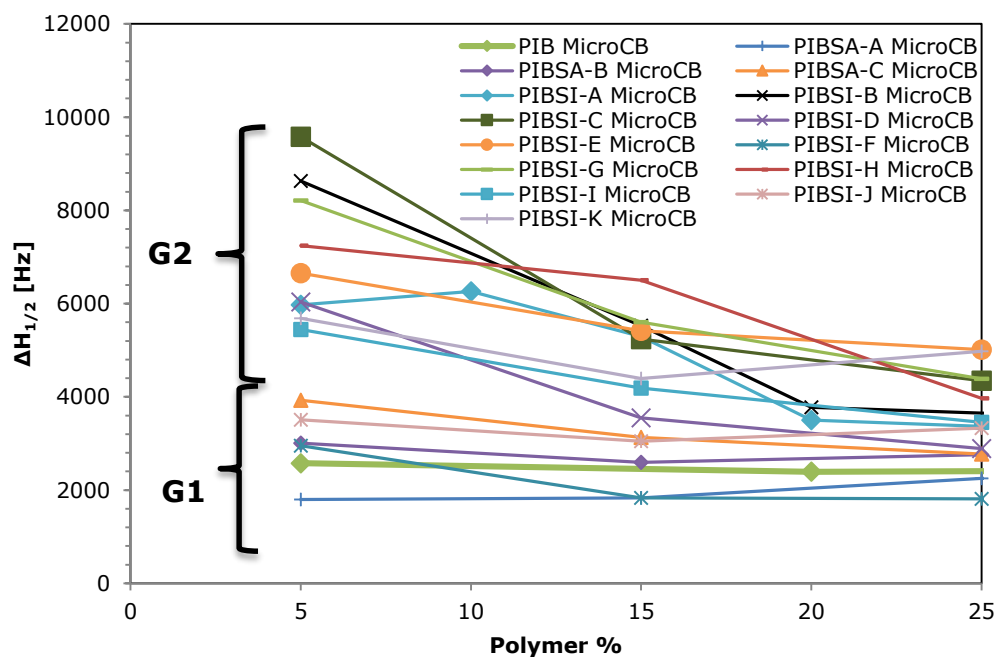


Figure 6-32: ^1H NMR $\Delta H_{1/2}$ values at 250 °C as a function of polymer % for various polymer MicroCB dispersions.

Table 6-4: Summary of polymer properties with assigned group number

Polymer	Head Group	Polar Surface Area [\AA^2]	PIB- M_n [g mol^{-1}]	Group
PIB	N/A	N/A	750	1
PIBSA-A	Succinic Anhydride	9.2	750	1
PIBSA-B	Succinic Anhydride	9.2	260	1
PIBSA-C	Succinic Anhydride	9.2	1000	1
PIBSI-A	TEPA	88.2	750	2
PIBSI-B	TEPA	88.2	1000	2
PIBSI-C	AEEA	58.3	750	2
PIBSI-D	Ethanolamine	46.3	750	1 or 2
PIBSI-E	AEEA	58.3	750	2
PIBSI-F	Ethanolamine	46.3	260	1
PIBSI-G	TEPA	88.2	1000	2
PIBSI-H	TEPA	88.2	1000	2
PIBSI-I	EDA	52.0	750	2
PIBSI-J	Ethanolamine	46.3	1000	1
PIBSI-K	EDA	52.0	750	2

Figure 6-33 shows the ^1H NMR $\Delta H_{1/2}$ values at 250 °C as a function of the polar surface area of the polymer head groups for various polymer (5, 15, 25 %) MicroCB (95, 85, 75 %) dispersions. Linear trend lines have been fitted to each concentration and presented with the coefficient of determination (R^2) values. The graph shows that there is positive correlation at all three concentrations studied and a weak to medium correlation (increase in polar surface area led to an increase in the $\Delta H_{1/2}$ at 250 °C) indicating that this could be a contributing factor to the mobility of the H atoms in the sample. This is in indirect agreement with Dubois-Clochard et al. (2001) and Kozak, Moreton, & Vincent, (2009) who found that the amount of polymer adsorbed increased with an increase in the number of primary and secondary amines in the polyamine head group as well as with Kim et al. (2015) who related the ability of PIBSI to prevent deposit formation through increased adsorption to the calculated polar surface areas of similar PIB derivatives. The relationship is most prominent at 5 and 15 % polymer loading with R^2 values of 0.64 and 0.72 respectively. At 25 % the linear trend line has a lower gradient with a lower R^2 value (0.37) suggesting a weaker relationship at this concentration.

In order to give a more categorical description on the level of correlation of variables an F-test will be used. Briefly, the F-observed value is used to determine whether the observed relationship between the variables occurs by chance (Kennedy & Neville, 1986). If the F-observed value exceeds the critical value (which is determined from the number of data points in the data set and can be found in the relevant published F-distribution tables) then the probability that the two variances occurred by chance alone is smaller than a specified probability and the rejection of a null hypothesis is justified (i.e. that there is a relationship between the known x and y values) (Kennedy & Neville, 1986). This test will be used henceforth to categorise whether the correlation is statistically significant or not. The specified probability (alpha value) will be 0.05 or 5 % in all cases.

For the 5 % polymer data set in Figure 6-33, assuming an alpha value of 0.05 the F critical value is 4.67 (Kennedy & Neville, 1986). The F-observed value is calculated as 22.67. As F-observed > F critical value then the rejection of the null hypothesis is justified and correlation maybe regarded as statistically significant. The 15 and 25 % samples also have F-observed values (34.25 and 7.78 respectively) above the F critical value and so their correlation is also statistically significant.

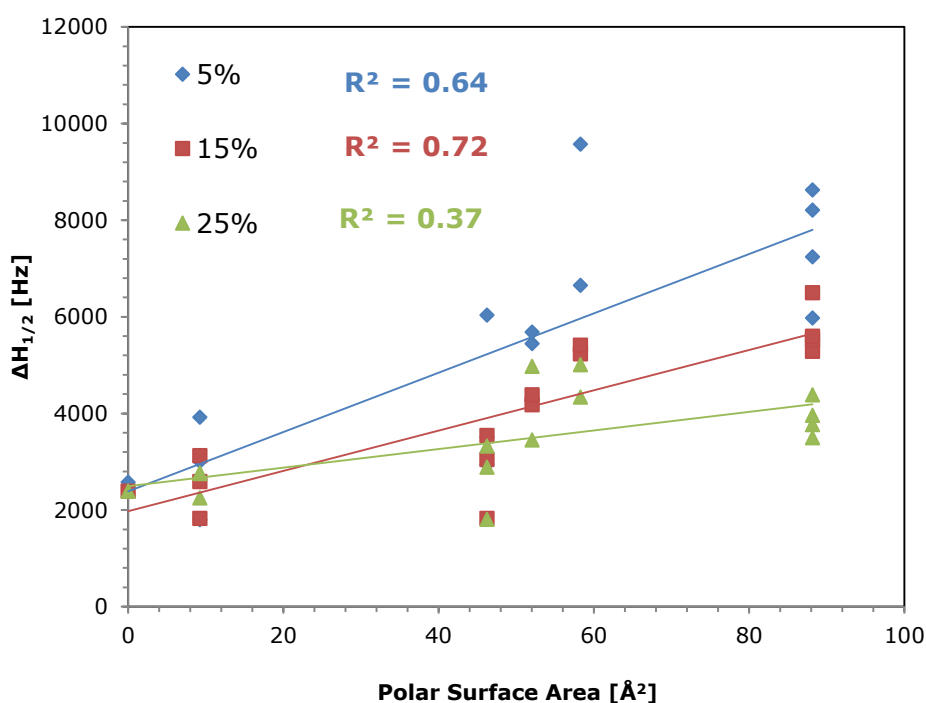


Figure 6-33: ¹H NMR ΔH_{1/2} values at 250 °C as a function of the polar surface area of the polymer head groups for various polymer MicroCB dispersions.

Figure 6-34 shows the ΔH_{1/2} values at 250 °C as a function of the PIB-M_n for various polymer (5, 15, 25 %) and MicroCB (95, 85 and 75 %) dispersions. A linear trend line has been added to each data set of data. The samples that gave the best correlation were the 15 % samples which overall have an R² value of

0.22. Although this sample had the highest F-observed value (3.76) of the three data sets this is still below the F critical value (4.67). All three data sets therefore show that the correlation is insufficient to prove that the distribution was not caused by chance alone and therefore indicates there to be no relationship between the PIB- M_n and the $\Delta H_{1/2}$ at 250° C indicating that this is not a factor in effecting the mobility.

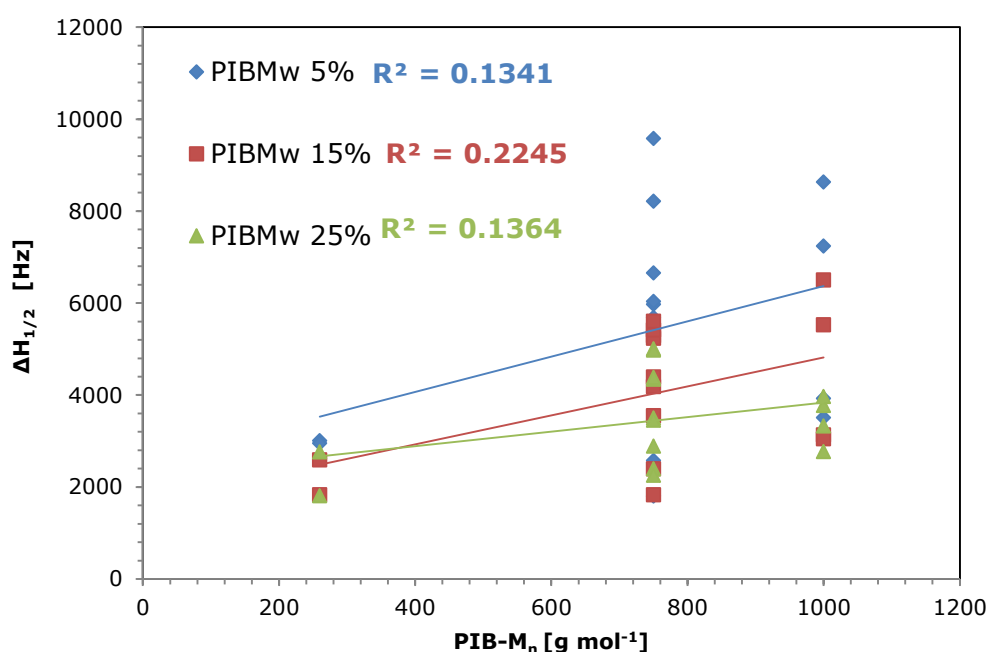


Figure 6-34: 1H NMR $\Delta H_{1/2}$ values at 250 °C as a function of the molecular weight of the PIB backbone (PIB- M_n) for various polymer MicroCB dispersions.

Figure 6-35 shows the $\Delta H_{1/2}$ values at 250 °C as a function of the M_n for various polymer (5, 15, 25 %) and MicroCB (95, 85 and 75 %) dispersions. A linear trend line has been added to each data set of data. The 25 % data set trend line generally have the lowest set of $\Delta H_{1/2}$ values as well as the lowest gradient. This is clearly as a result of similar $\Delta H_{1/2}$ values at this concentration where the polymer samples are not very distinguishable with higher molecular mobility. The 15 % data set shows a steeper gradient indicating a stronger correlation between the $\Delta H_{1/2}$ and the M_n . The 5 % data set also shows positive correlation between the

$\Delta H_{1/2}$ and the M_n although the data is more scattered ($R^2= 0.36$) than the 15 % ($R^2=0.58$) or the 5 % ($R^2= 0.45$). All of the data sets have F-observed values (7.22, 18.26, 10.63 for 5, 15 and 25 % samples respectfully) greater than the F critical value (4.67) which shows the correlations to have some statistical significance and therefore it may be possible that the polymer M_n may have some effect on the magnitude of the $\Delta H_{1/2}$ values.

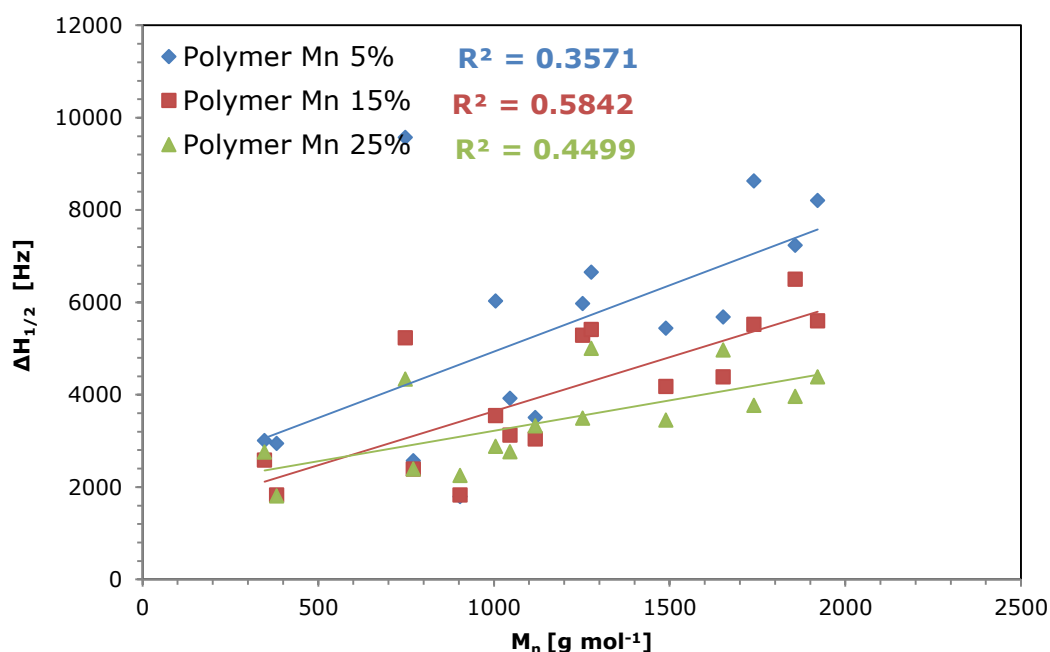


Figure 6-35: ^1H NMR $\Delta H_{1/2}$ values at 250 °C as a function of the number average molecular weight (M_n) for various polymer MicroCB dispersions.

Figure 6-36 shows the $\Delta H_{1/2}$ values at 250 °C as a function of M_w for various polymer (5, 15, 25 %) and MicroCB (95, 85 and 75 %) dispersions. A linear trend line has been added to each data set of data. Similarly to Figure 6-35 the 25 % data set shows the lower $\Delta H_{1/2}$ values as well as the lowest gradient. Again, this is most likely due to the high polymer content leading to an increase in mobility of a sample and as well as making the polymers less distinguishable. The 15 % data set shows stronger correlation between the $\Delta H_{1/2}$ and the M_w and shows the next highest linear trend line and is also quite linear ($R^2= 0.72$). The 5 % polymer

data set shows the highest average trend line and the strongest gradient however the data is a more scattered ($R^2 = 0.56$) than the 15 % data set ($R^2 = 0.72$). All of the data sets have F-observed values (16.51, 33.66, 21.15 for 5, 15 and 25 % samples respectfully) greater than the F critical value (4.67) which means the null hypothesis can be rejected and the correlation is statistically significant.

Despite some low R^2 values in the data sets in Figure 6-35 and Figure 6-36 in all cases there appears to be some positive correlation between the M_n and M_w of the $\Delta H_{1/2}$ and the resulting $\Delta H_{1/2}$ at high temperature. It therefore seems likely that with a polymer with a higher M_n or M_w ; there is a greater amount of polymer that can contribute to the network on heating which leads to lower mobility and broader $\Delta H_{1/2}$ values at high temperatures. However Figure 6-35 and Figure 6-36 does not necessarily mean there is direct relationship between the molecular weight and the $\Delta H_{1/2}$ for one important reason. The polymers that were analysed that contain large head groups and therefore high polar surface areas generally also have large M_n and M_w values. This therefore means that if some correlation is found between the size of the head group and the $\Delta H_{1/2}$ measurements it should come as no surprise that there is also an apparent relationship between molecular weight as well. Also the M_n and M_w values will undoubtedly increase with larger head group sizes making a direct cause of the relationship more difficult to establish. As displayed in Table 6-4, group 1 contains polymers with only lower PSA values ($\leq 46.3 \text{ \AA}^2$) and group 2 contains polymers with only higher PSA values ($\geq 46.3 \text{ \AA}^2$). However, given that both groups contain PIBSIs synthesised with high molecular weight PIB backbones (1000 PIB- M_n) it is therefore tentatively concluded that increasing the size of the PIBSI head group is most likely the dominant factor in the observed increases in the $\Delta H_{1/2}$ measurements. This is not to say that the molecular weight of the polymer cannot have an effect on the $\Delta H_{1/2}$ measurements and a longer PIB backbone may still lead to an increase in the measured $\Delta H_{1/2}$.

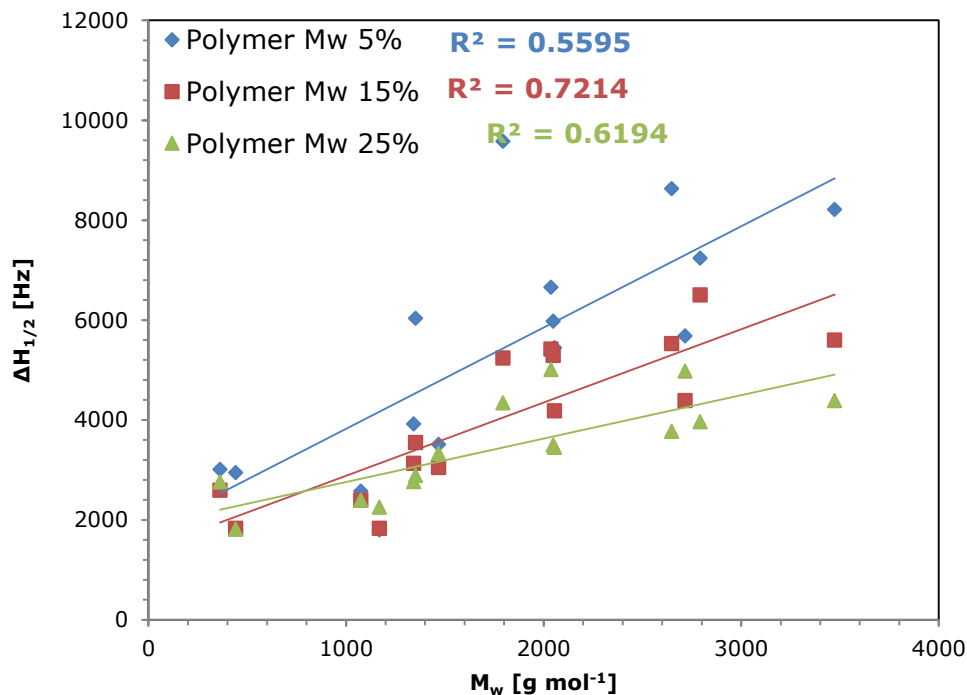


Figure 6-36: ¹H NMR $\Delta H_{1/2}$ values at 250 °C as a function of the weight average molecular weight (M_w) for various polymer MicroCB dispersions.

6.3 CHAPTER SUMMARY

It has been demonstrated that changing the PIB derivative used in a dispersion sample can significantly affect the viscoelastic behaviour and measured mobility of the sample. This has been achieved using a number of polymers of varying head groups, PIB tail lengths and functionality. This chapter has been separated into two sections, high polymer, low solid which includes ¹H NMR and rheology analysis and low polymer, high solid samples analysed mainly via ¹H NMR.

- It was found that the η^* values increased with increasing MicroCB content for PIB samples. PIBSI-A samples were found to be more consistent with increasing MicroCB content. The values for the η^* at 250 °C of PIB and PIBSI-A MicroCB samples were compared. It was found that PIBSI-A consistently exhibited higher η^* values than PIB. This was attributed to the stronger interaction of PIBSI-A with the MicroCB particles than PIB.

- It has been demonstrated that increasing the length of the head-group (including adding additional amines) and therefore the polar surface area can have some effect on the viscoelastic behaviour at low polymer loading and on the molecular mobility at both low and high polymer content. This is in agreement with a number of studies which described an increase in the level of interaction between a succinimide type dispersants when increasing the number of amines in the polar head group. This was most prominent at 5 and 15 % polymer samples and it is postulated this most likely due to surface coverage effects reducing the mobility of strongly adsorbing polymers.
- The effect of the PIB tail length and on the number of tails has been investigated. The effect of increasing the PIB chain length proved difficult to characterise. A comparison with the M_n and M_w of each polymer from GPC data showed there to be some relationship between the molecular weight and the $\Delta H_{1/2}$ although the exact effect remains unclear. Polymers with dissimilar yet high molecular weights proved difficult to distinguish in both the η^* and $\Delta H_{1/2}$ indicating that the polymer molecular weight does not have as substantial effect on the resulting trends. However for lower molecular weight polymers (such as PIBSI-F), degradation effects must be taken into consideration when comparing polymer η^* trends as degradation has been shown to cause a drastic increase in the magnitude of the η^* . In ^1H NMR the $\Delta H_{1/2}$ trends are largely unaffected by partial degradation of the polymers.

7 Possible effects of deposit surrogate properties on dispersion behaviour at high temperatures

The effect of the polymer structure on the rheology and ^1H NMR results with the same carbon black has previously been investigated. This chapter aims to show the effect that changing the carbon type has on the ^1H NMR peak half width ($\Delta H_{1/2}$) measurements. Several forms of commercially available carbons were tested which have been utilised previously by Barker et al. (2010) as reference carbons in comparison with actual fuel injector deposits.

7.1 EXPERIMENTAL

7.1.1 Materials

The commercial polymers used were supplied by Innospec Inc. A summary of the properties of the polymers used in this chapter are shown in Table 7-1. The number average molecular weight of the PIB backbone (PIB- M_n) from which the polymers are derived is also presented as is the number average molecular weight (M_n) and weight average molecular weight (M_w) and polydispersity values (PD) of the final products obtained from GPC analysis as described in section 3.12.6. The PIB functionality (PIB Func.) or the number of PIB hydrocarbon tails is also presented.

Table 7-1: Polymer properties

Polymer	Head group*	PIB- M_n (g/mol)	M_n (g/mol)	M_w (g/mol)	PD	Func.
PIBSI-C	AEEA	750	748	1794	2.4	<i>mono</i>
PIBSI-D	Ethanolamine	750	1005	1352	1.3	<i>mono</i>
PIBSI-F	Ethanolamine	260	382	442	1.2	<i>mono</i>
PIBSI-G	TEPA	1000	1921	3473	1.8	<i>bis</i>
PIBSI-H	TEPA	1000	1858	2793	1.5	<i>bis</i>
PIBSI-I	EDA	750	1490	2055	1.4	<i>bis</i>
PIBSI-K	EDA	750	1653	2717	1.6	<i>Mono</i>

*Refer to section 3.10.1 for head group abbreviations

The majority of the commercial carbons used in this chapter were supplied by Innospec Inc. and are originally sourced from Asbury Carbons and Degussa. These

carbons have been used previously in a study by Barker et al. (2010) as reference carbons in comparison with actual engine deposits. The small particle mesoporous carbon black adsorbent (MicroCB) was sourced from Sigma Aldrich. A description of the carbons may be found in the materials section 3.10.2. A summary of the properties of the carbons are shown in Table 7-2. Unless stated otherwise the nominal average particle sizes and surface areas were obtained from the product data sheets supplied with the samples.

Hexane (95%, Aldrich) was used as a solvent in the preparation of the dispersions.

Table 7-2: Carbon Properties

Carbon Black	Average Particle size μm	Surface Area m^2/g
Mesoporous Carbon Black Adsorbent (MicroCB)	45	205
Degussa Carbon Black (DegCB)	43 D[4,3] (From particle size analysis, section 3.12.9)	417 (From BET analysis, section 3.12.8)
Flake graphite146 (Micro146)	21	6
Flake graphite850 (Micro850)	5	13
Synthetic graphite450 (Micro450)	5	17
Green Coke (GreenCoke)	2	10
Calcined Coke (CalCoke)	6	20

7.1.2 Sample Preparation

The polymer carbon black dispersions were prepared as described in section 3.11.

7.1.3 Summary of Analytical Methods

The polymer-MicroCB dispersions were analysed using high temperature by ^1H NMR as outlined in section 3.12.1. X-ray photoelectron spectrum (XPS) measurements were carried out to determine the surface elemental composition of the carbon samples as described in section 3.12.7. Temperature programmed oxidation (TPO) was used to provide a measure of the level amorphicity and

graphicity of the carbons as outlined in section 3.12.5. These values were obtained from a study by Barker et al. (2010) with the exception of the MicroCB and the DegCB samples which were carried out in industry specifically for this study as described in section 3.12.5.

7.2 RESULTS AND DISCUSSION

7.2.1 ¹H NMR spectroscopy results

Although a number of polymers could be differentiated with the MicroCB samples as discussed in chapter 5 and 6 more ¹H NMR tests were carried out with a number of different carbons in order to investigate the effects of the carbons various properties on the $\Delta H_{1/2}$ measurements. The polymers PIBSI-F and PIBSI-H were selected for this set of tests because the two polymers gave some of the largest differences in $\Delta H_{1/2}$ values between each other with the MicroCB samples. PIBSI-F gave low $\Delta H_{1/2}$ values at 250 °C thought to be mainly due to low polar head group surface area and short PIB- M_n while PIBSI-H gave high $\Delta H_{1/2}$ values at 250 °C thought to be mainly due to a large polar surface area and long PIB- M_n . Figure 7-1 shows the $\Delta H_{1/2}$ values of various polymer carbon dispersions at 250 °C as a function of polymer percentage. The overall $\Delta H_{1/2}$ trend as a function of temperature for each polymer may be found in Appendix G. It can be seen that for all of the polymers studied the 25 % and 15 % polymer loadings gave the most consistent results. At 5 % polymer loading the $\Delta H_{1/2}$ at 250 °C became highly variable with even a number of the PIBSI-F samples exhibiting high $\Delta H_{1/2}$ values. This is most likely due to the low amount of polymer in the samples causing further broadening of the peaks and may have even been related to the low degradation temperature of PIBSI-F (as shown by the TGA measurements in chapter 6 section 6.2.1) affecting the magnitude of the $\Delta H_{1/2}$ values with 5% polymer loading. In all cases at 15 % and 25 % polymer content the PIBSI-F samples yields consistently lower $\Delta H_{1/2}$ values at 250 °C (at least <2500 Hz) with all of the

carbons. This shows that the PIBSI-F samples are more mobile at high temperatures which is most likely due to the lack of interaction between the polymer and any of the carbons due to the lack of primary and secondary amines in the polar head group. Figure 7-1 also shows that PIBSI-H dispersions with different carbons gave much greater $\Delta H_{1/2}$ values at 250 °C than the corresponding PIBSI-F dispersions. The carbons Micro850 and Micro450 (as well as MicroCB which was described in chapter 6) all yield significantly higher $\Delta H_{1/2}$ values at 250 °C than their corresponding PIBSI-F samples. The remaining carbons that were analysed with PIBSI-H (with the possible exception of DegCB) show lower $\Delta H_{1/2}$ values that are in the same region and not dissimilar to the corresponding PIBSI-F samples which indicates that there is less of an interaction between the PIBSI-H and those carbons. How the various properties of the carbons that could be affecting the $\Delta H_{1/2}$ values will now be discussed using the polymer (15 %) carbon (85 %) sample $\Delta H_{1/2}$ measurements.

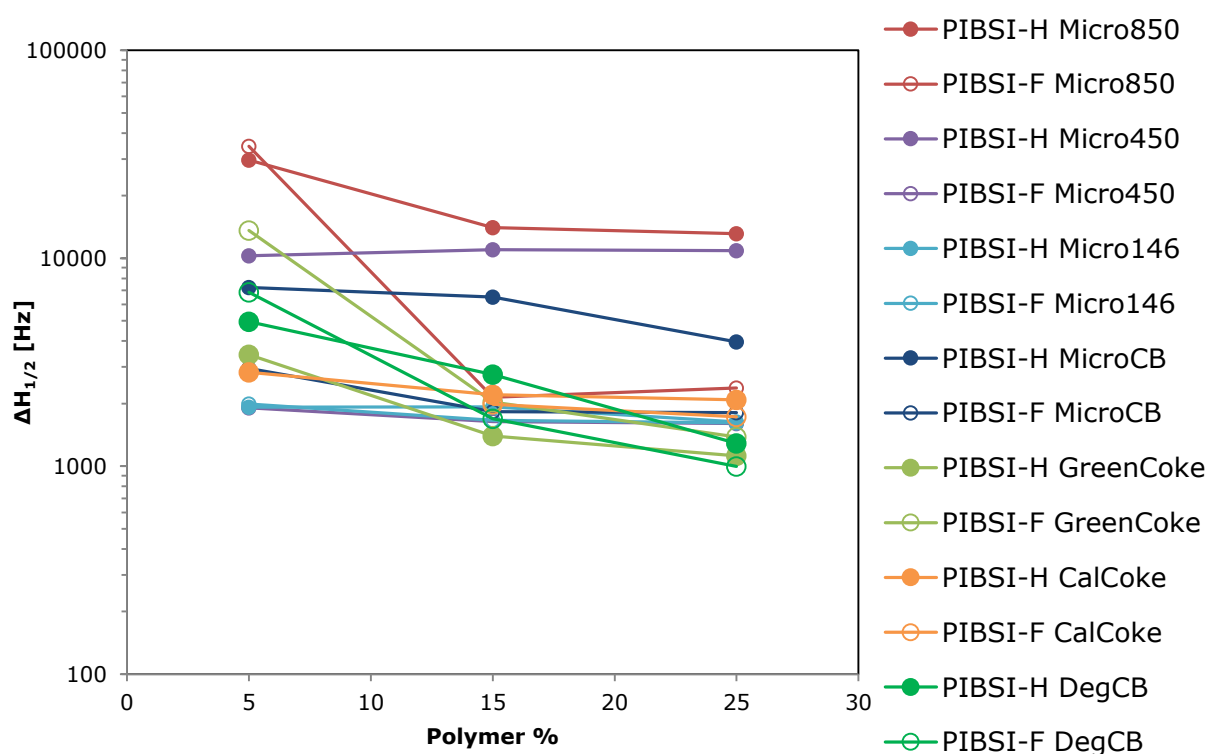


Figure 7-1: ^1H NMR $\Delta H_{1/2}$ values at 250 °C as a function of polymer % for various polymer (PIBSI-F, H) -Carbon dispersions.

7.2.2 Potential effect of carbon particle size on high temperature ^1H NMR $\Delta H_{1/2}$ measurements

Figure 7-2 shows the $\Delta H_{1/2}$ values at 250 °C of PIBSI-H and PIBSI-F (15 %) carbon (85 %) samples as a function of the average particle size of each carbon. The particle size for the DegCB sample was measured on a laser scattering based particle sizer (Mastersizer) as there was no product data sheet available. All other values were obtained from the relevant product data sheets and are nominal values. The PIBSI-F samples all exhibit low $\Delta H_{1/2}$ values at 250 °C thought to be due to the lack of particle interaction with each carbon and are shown for comparison only. The PIBSI-H samples are more significant since these showed more variation in values of the $\Delta H_{1/2}$. The data set indicates that there is no correlation between the $\Delta H_{1/2}$ at 250 °C and average particle size. This is significant since the size of the particles could have led to differences in the amount of polymer adsorption and therefore could have affected the overall mobility of the hydrocarbon chains. The fact that there is no apparent relationship however suggests that particle size is not a significant factor in affecting the $\Delta H_{1/2}$ measurements.

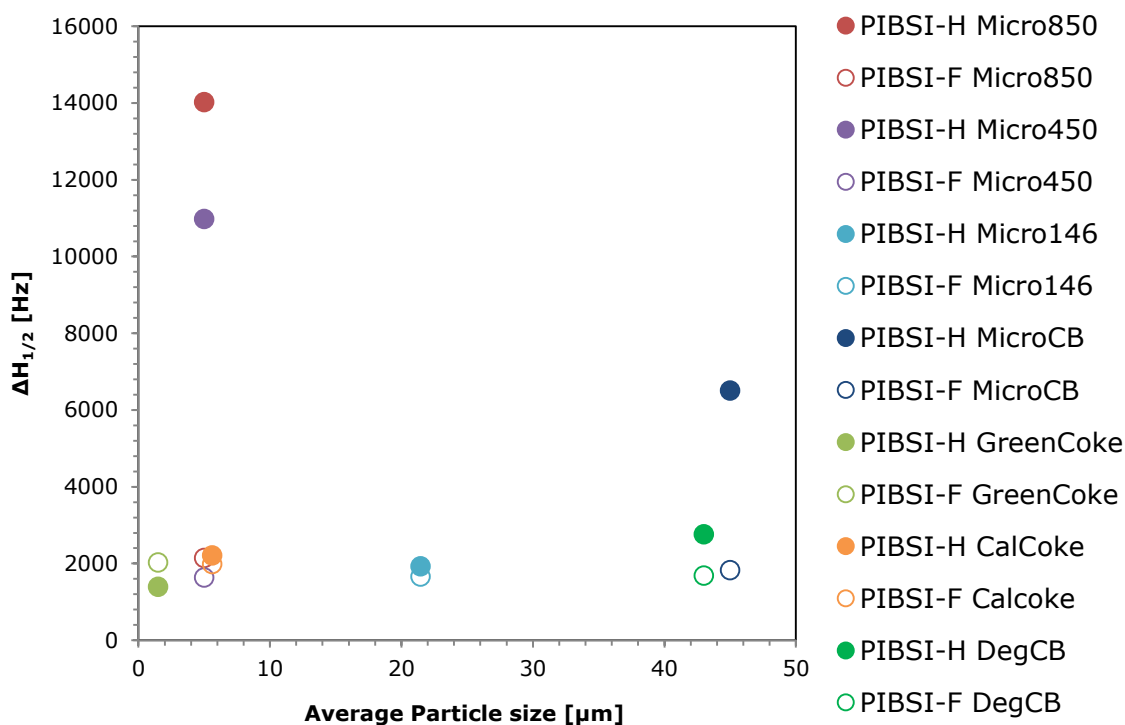


Figure 7-2: ^1H NMR $\Delta H_{1/2}$ values at 250 °C as a function of the average particle size of the carbon for various polymer (PIBSI-F,H)- carbon dispersions.

7.2.3 Potential effect of carbon surface area on high temperature ^1H NMR $\Delta H_{1/2}$ measurements

Figure 7-3 shows the $\Delta H_{1/2}$ values at 250 °C of PIBSI-H and PIBSI-F (15 %) carbon (85 %) samples against the surface area of the carbons. The surface area for the DegCB sample was measured via BET analysis as outlined in section 3.12.8 as there was no product data sheet available. All other values were obtained from the relevant product data sheets and are nominal values. Once again the PIBSI-F samples all showed low $\Delta H_{1/2}$ values at 250 °C indicating a weak or no interaction with the carbons. As for the more strongly interacting PIBSI-H samples there is little evidence that the surface area of the carbons had a significant effect on the $\Delta H_{1/2}$. This is most evident for samples with similarly low surface area ($<20 \text{ m}^2\text{g}^{-1}$) displaying different $\Delta H_{1/2}$. For instance, Micro850 and Micro450 samples had

$\Delta H_{1/2}$ values of 14026 and 10983 Hz respectively at 250 °C while Micro146, Green Coke and CalCoke all had $\Delta H_{1/2}$ values in the region of 2000 Hz. This shows that while surface area maybe a factor it is not the dominating property of the carbons that controls the $\Delta H_{1/2}$. It should be noted that it may be possible that the polymer itself had altered the overall surface area by potentially filling any micropores as was observed in the study by Zerda, Yuan, & Moore (2001) where increasing the amount of polyisobutylene amine present led to a decrease in the surface area.

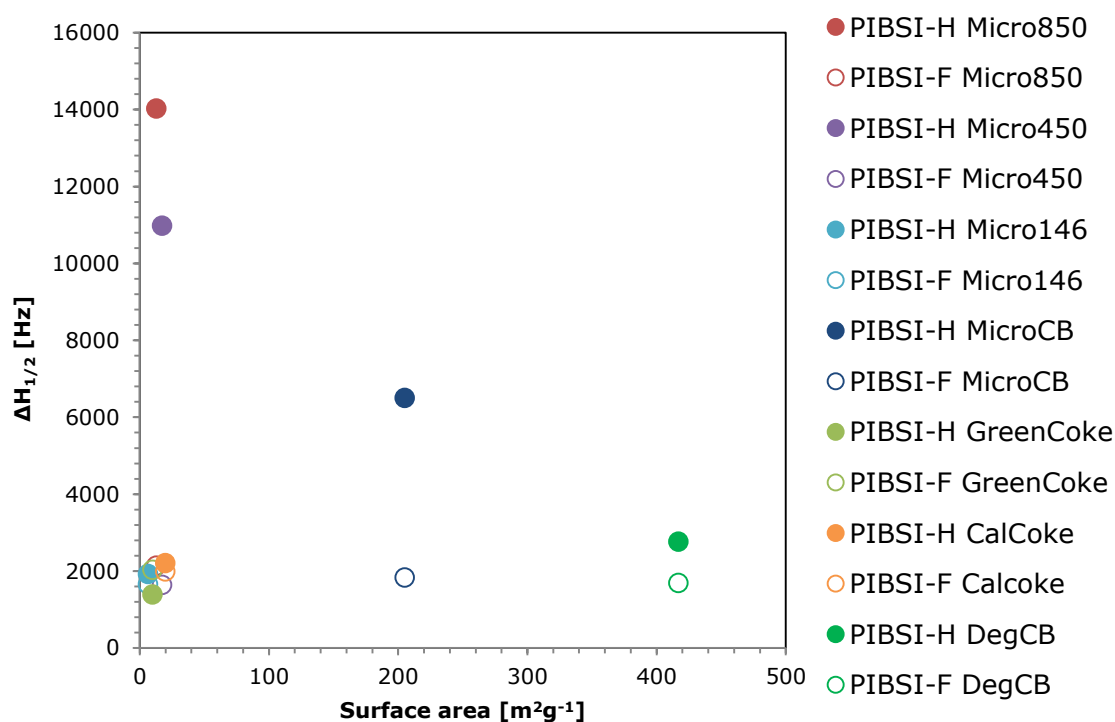


Figure 7-3: ¹H NMR $\Delta H_{1/2}$ values at 250 °C as a function of the surface area of the carbon for various polymer (PIBSI-F, H) - carbon dispersions.

7.2.4 Potential effect of carbon peak CO₂ emission temperature on high temperature ¹H NMR $\Delta H_{1/2}$ measurements

Although there has been found to be very little correlation between the average particle size / surface areas of the carbons and the $\Delta H_{1/2}$ it is possible that the surface properties of the carbons may have had more of an effect on the resulting

$\Delta H_{1/2}$ values. To investigate this the peak CO₂ emission temperatures as measured via temperature programmed oxidation (TPO) were used to provide a measure of the level amorphicity and graphicity of the carbons (as more amorphous carbon is more reactive than more structured graphitic carbon and therefore oxidises at a lower temperature) (Barker et al., 2010). These values were obtained from a study by Barker et al., (2010) with the exception of the MicroCB and the DegCB samples which were carried out in industry specifically for this study. The peak CO₂ emission temperatures of the carbons are summarised in Table 7-3.

Table 7-3: Peak CO₂ emission temperatures. *Analysis carried out for this study.

****Sourced from Barker et al., (2010)**

Carbon Black	Peak CO₂ emission temperature [°C]
*MicroCB	690
*DegCB	589
**Micro146	883
**Micro850	827
**Micro450	714
**GreenCoke	370
**Calcined Coke	574

Figure 7-4 shows the $\Delta H_{1/2}$ values of 15 % polymer 85 % carbon dispersions at 250 °C as a function of the peak CO₂ emission temperature of the carbons. Once again the PIBSI-F samples all have similarly low values of $\Delta H_{1/2}$ due to little to no interaction with the carbons and therefore do not display any discernible trend. For the PIBSI-H samples, however, there does appear to be a relationship between the $\Delta H_{1/2}$ and the peak CO₂ emission temperature. Carbons with the lower peak CO₂ emission temperatures also display lower $\Delta H_{1/2}$ values that were similar in magnitude to the PIBSI-F values suggesting little to no interaction with the carbon. As the peak CO₂ emission temperature of the various carbons increases so does the $\Delta H_{1/2}$. There is one exception to this which was the PIBSI-H Micro146 sample which had the highest peak emission temperature of all the

carbons analysed but a relatively low $\Delta H_{1/2}$ (1927 ± 153 Hz). A possible explanation for this trend is as follows. The upward trend in $\Delta H_{1/2}$ with peak CO_2 emission temperature suggests that as the carbons become more graphitic the polymers can more easily adsorb onto the carbon surface due to easier “access” onto the surfaces as they become less amorphous. There does however appear to be a point where the surface is too graphitic for the polymer to adsorb due to the total lack of surface functionality and therefore the polymer is more mobile as shown by the sudden drop in $\Delta H_{1/2}$ for PIBSI-H Micro146 sample. It has already been demonstrated in chapter 6 that the most dominating factor in controlling the mobility is the number of amines in the head group of the polymer. Figure 7-4 also suggests that the interaction between the polymer and the carbon surface is the most dominant factor in controlling the mobility of the H atoms of the polymers over physical properties such as particle size and surface area.

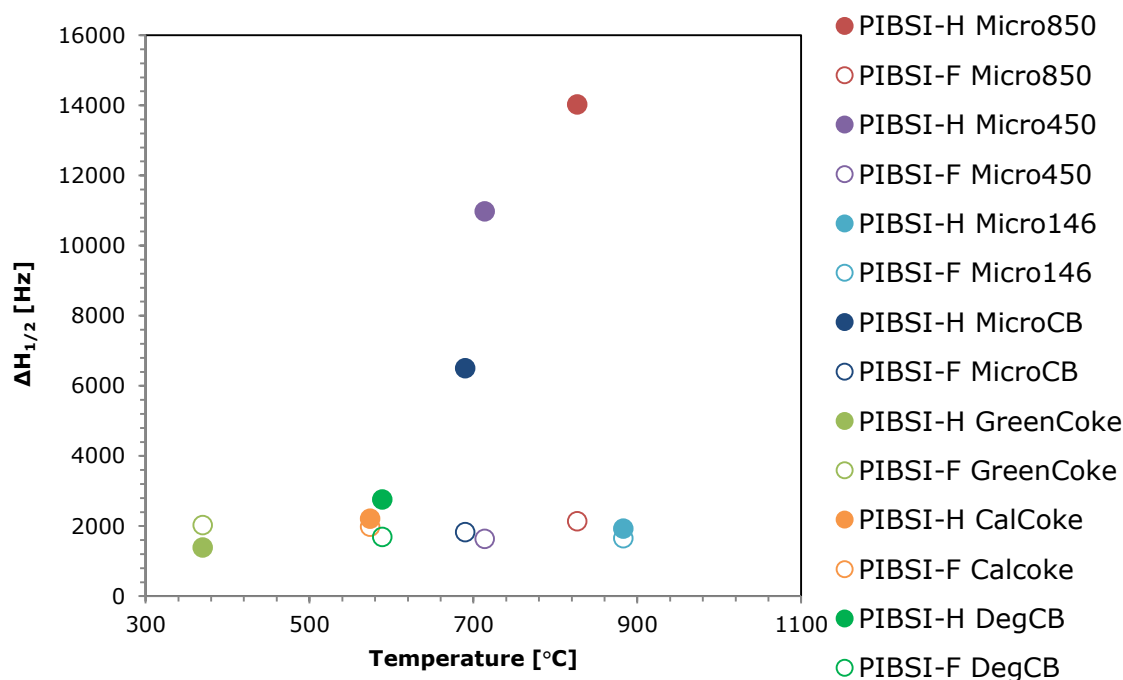


Figure 7-4: ^1H NMR $\Delta H_{1/2}$ values at 250 °C as a function of the peak CO_2 emission temperature of the carbon for various polymer (PIBSI-F,H)- carbon dispersions.

7.2.5 Potential effect of carbon elemental surface composition on high temperature ^1H NMR $\Delta H_{1/2}$ measurements

In order to investigate the effects of the surface properties of the carbons on the resulting $\Delta H_{1/2}$ values, X-ray Photon spectroscopy (XPS) characterisation was conducted to determine the elemental surface composition of each sample. The atomic concentration of the each of the carbon samples are shown in Table 7-4. The wide line XPS spectra can be found in Appendix J.

Table 7-4: Surface Composition from XPS spectra

Carbon Sample	Atomic Concentration (%)				
	C (%)	O (%)	N (%)	S (%)	Si (%)
MicroCB	99.1	0.9	0.0	0.0	0.0
DegCB	89.3	10.7	0.0	0.0	0.0
Micro146	95.5	3.7	0.0	0.0	0.8
Micro850	96.1	3.0	0.0	0.0	0.9
Micro450	97.4	2.2	0.0	0.0	0.4
GreenCoke	91.1	5.3	1.3	1.2	1.1
Calcined Coke	94.4	4.7	0.0	0.1	0.8

Figure 7-5 shows a plot of the peak CO_2 emission temperatures against the carbon surface composition. The carbon samples have been divided into amorphous carbon and graphitic carbon as in Barker et al., (2010) in which the percentage of carbon was obtained according to the dynamic flash combustion of the sample (from a ThermoQuest Flash EA 1112 series CHN-O Analyzer) in order to compare the total carbon content % of a sample, whereas here carbon surface composition as obtained by XPS analysis has been plotted. Similar to Barker et al., (2010) there is a loose correlation between the carbon surface percentage of the carbon samples and the temperature at which they oxidise.

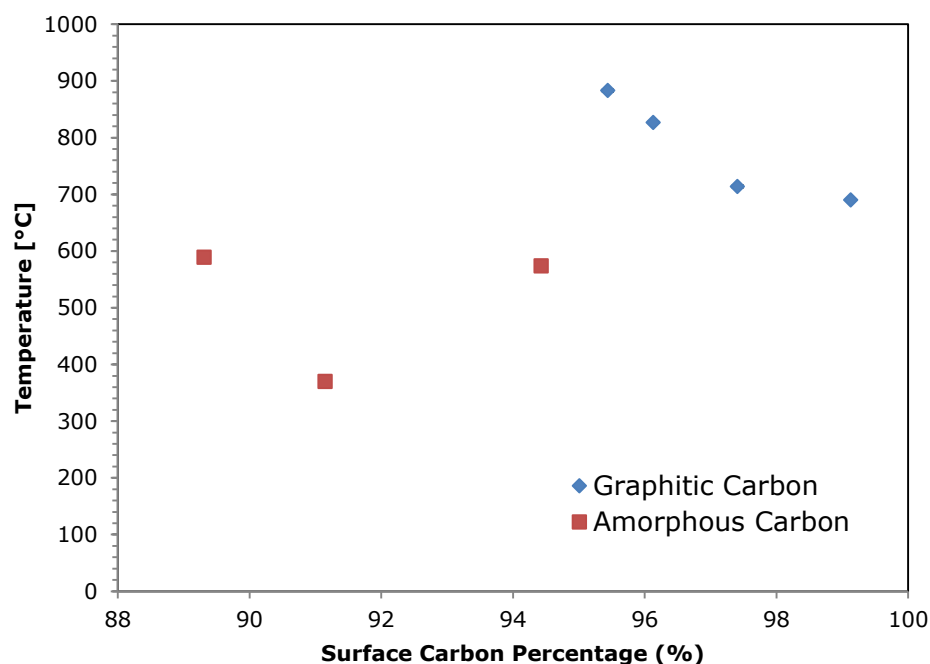


Figure 7-5: Peak CO₂ emission temperature (via TPO) against carbon surface composition (via XPS)

Figure 7-6 shows a summary of $\Delta H_{1/2}$ values of the PIBSI-H and PIBSI-F (15 % carbon (85 %) dispersions at 250 °C as a function of the carbon surface composition of each carbon sample. Once again the weakly interacting PIBSI-F results are shown for comparison. It is interesting that the three carbons which gave the highest $\Delta H_{1/2}$ values – Micro850, Micro450 and MicroCB with PIBSI-H also had the highest percentage of carbon on the surface (although between these three samples there was a decreasing trend in $\Delta H_{1/2}$ with increasing carbon surface composition amounts). This would again indicate that the most graphitic carbons provide the best condition for a strong polymer carbon interaction due to a flatter surface allowing for better adsorption. Of the three samples that gave the highest $\Delta H_{1/2}$ values the results indicate that the MicroCB is the most graphitic as it has the highest carbon surface composition and the Micro850 to be the least graphitic due to the lower carbon surface percentage. This is in contrast to the TPO measurements which showed the Micro850 to have the highest CO₂ peak

emission temperature and the MicroCB the lower CO₂ emission temperature. Also, Micro146 gave the highest CO₂ emission temperature of all the carbons indicating a high level of graphicity. However, the XPS results showed there to be 3.1 % oxygen on the surface indicating a higher level of amorphicity than the TPO measurements indicate. This may explain the relatively lower $\Delta H_{1/2}$ values for the PIBSI-H Micro146 sample.

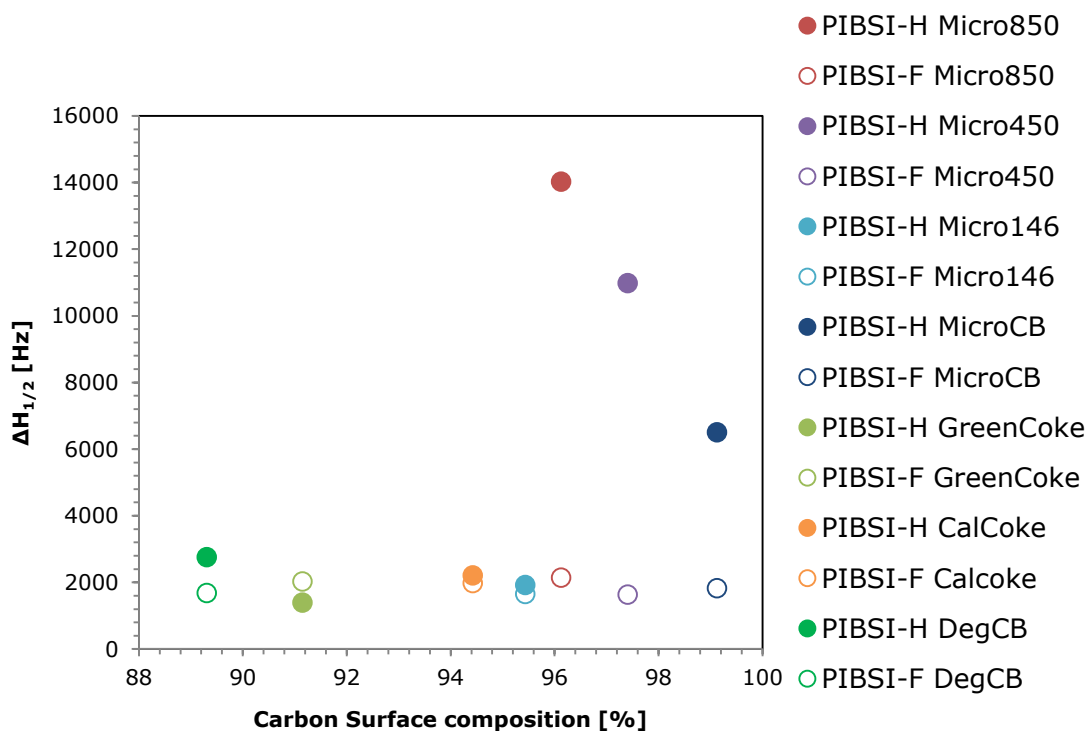


Figure 7-6: ¹H NMR $\Delta H_{1/2}$ values at 250 °C as a function of the carbon surface composition of the carbon for various polymer (PIBSI-F,H)- carbon dispersions.

Figure 7-7 shows a summary of $\Delta H_{1/2}$ values of PIBSI-H and PIBSI-F carbon dispersions at 250 °C as function of the oxygen surface composition of the carbon samples as measured by XPS. Again the PIBSI-F dispersion $\Delta H_{1/2}$ values are shown for comparison. The three samples with carbons Micro850, Micro450 and MicroCB which gave the highest $\Delta H_{1/2}$ values as well as containing the most carbon % on the surface gave the lowest oxygen surface content of all the samples. The trend between Micro850, Micro450 and MicroCB PIBSI-H samples is an increase

in $\Delta H_{1/2}$ with oxygen content. The PIBSI-H sample $\Delta H_{1/2}$ values at 250 °C are all low for the remaining samples and there is little change in $\Delta H_{1/2}$ with increasing oxygen content. Although it is difficult to fully explain from Figure 7-6 and Figure 7-7 the exact effect, if any, of the oxygen and carbon content has on the $\Delta H_{1/2}$ it is interesting to note that the three samples that gave the markedly higher $\Delta H_{1/2}$ values are at the extreme ends of the %C and %O graphs. This would indicate that it is the level of interaction between the polymer and the carbons that is the dominant property in effecting viscosity of the dispersion and therefore the mobility of the hydrogen atoms of the polymer chains.

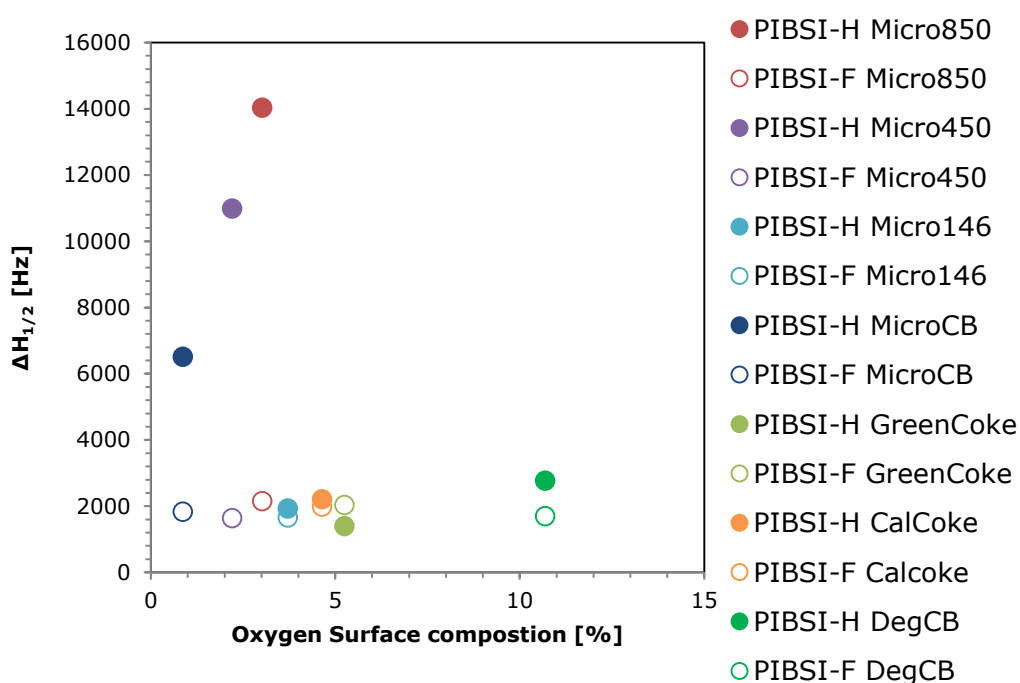


Figure 7-7: ^1H NMR $\Delta H_{1/2}$ values at 250 °C as a function of the oxygen surface composition of the carbon for various polymer (PIBSI-F,H)- carbon dispersions.

7.2.6 Polymer structure activity relationships with flake graphite (Micro850)

From observing the results in Figure 7-1 it is clear that the carbon sample that gave one of the largest differences in $\Delta H_{1/2}$ values at 250 °C between PIBSIs H

and F was flake graphite (Micro850). In order to investigate if the polymers could be distinguished further than with the MicroCB experiments, the final step of this project was to carry out a number of experiments with the Micro850 with a number of different polymers to again investigate structure activity relationships. As time was limited, only a select few of the polymers were analysed and were chosen based on key structural differences such as the calculated polar surface area of the head group, the molecular weight of the PIB tail (PIB- M_n), the overall M_n and M_w and the number of PIB tails (functionality). The full $\Delta H_{1/2}$ trends as a function of temperature can be found in Appendix H.

Figure 7-8 shows a summary of the results. It is clear that the $\Delta H_{1/2}$ values at 250 °C are much less consistent than at 15 % and 25 % loading where the data either rises or falls sharply or there is a loss of a peak signal altogether (as occurred with the PIBSI-A (2.5 %) MicroCB (97.5 %) sample discussed in chapter 6). Only the measurements at 15 and 25 % polymer loading will therefore be used in the following discussion due to the lack of consistency at 5 % polymer loadings.

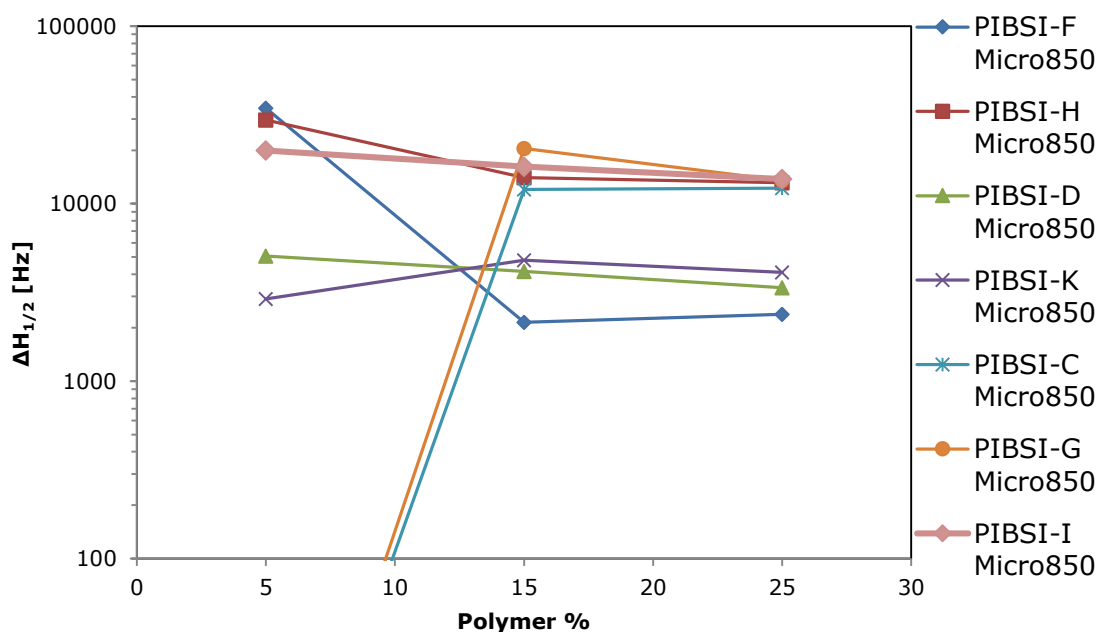


Figure 7-8: ^1H NMR $\Delta H_{1/2}$ values at 250 °C as a function of polymer % for various polymer -Micro850 dispersions.

Figure 7-9 shows the effect of increasing the PIB- M_n on the values of the $\Delta H_{1/2}$ at 250 °C. The results from the corresponding MicroCB samples for the polymers analysed are also displayed for comparison. It can be seen that at 15 and 25 % polymer loadings the trends are quite similar to that observed for MicroCB samples. At these amounts, PIBSI-D shows a higher $\Delta H_{1/2}$ than PIBSI-F does with both types of carbon. The Micro850 samples do show slightly larger overall values but the fact that they are similarly low is significant as it indicates that the polymers have a poor interaction with both types of carbon.

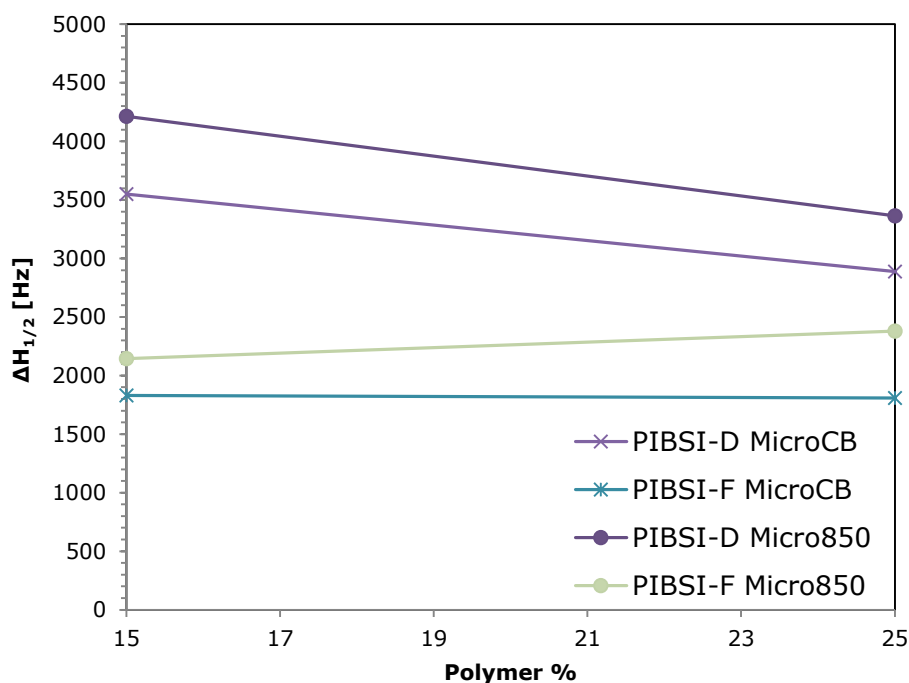


Figure 7-9: ^1H NMR $\Delta H_{1/2}$ values at 250 °C as a function of polymer % for various polymer (PIBSI-D, F) -Micro850 or MicroCB dispersions.

Figure 7-10 shows the effect of changing the end alcohol group to an amine group, displaying the $\Delta H_{1/2}$ measurements for PIBSI-D and PIBSI-K with Micro850. With the MicroCB samples PIBSI-K had overall higher $\Delta H_{1/2}$ values than PIBSI-D which was most likely due to the more polar nitrogen atom of the primary amine in

replacement of the OH group on PIBSI-D. This was indeed found to be the case for the Mico850 samples at 15 and 25% polymer loading. The values were also in a similar region (< 5000 Hz) which is another indication that weakly interacting polymers should give low $\Delta H_{1/2}$ values at high temperatures regardless of the type of carbon used.

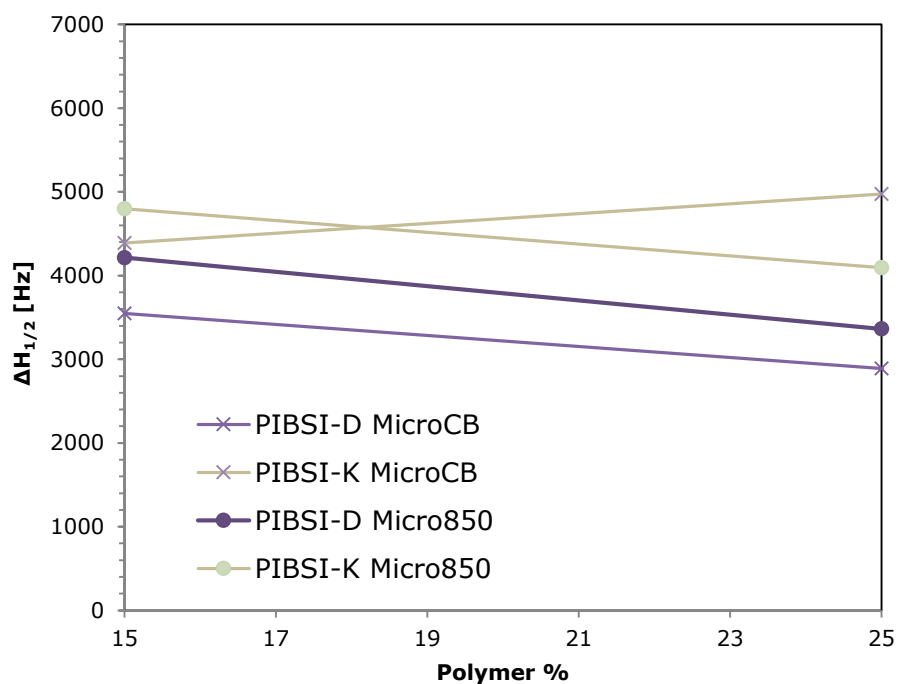


Figure 7-10: ^1H NMR $\Delta H_{1/2}$ values at 250 °C as a function of polymer % for various polymer (PIBSI-D, K) -Micro850 or MicroCB dispersions.

Figure 7-11 shows the effect of changing the molecular weight of the PIB tail for PIBSI-G (derived from 750 PIB- M_n) and PIBSI-H (derived from 1000 PIB- M_n) with both Micro850 and MicroCB. It was found previously with MicroCB samples that PIBSI-H and PIBSI-G both gave high $\Delta H_{1/2}$ values at 250 °C indicating a strong interaction with the carbon. The measurements were also difficult to distinguish suggesting that the difference in molecular weight did not have a significant effect on the mobility of the hydrogen atoms. The Micro850 samples (at 15 and 25 %) show markedly higher $\Delta H_{1/2}$ values. At 25 % polymer the two values are similarly

high at around 13000 Hz. At 15 % PIBSI-G is much higher (around 20000Hz) while PIBSI-H is around 14000 Hz. Very little can be inferred from this small data set regarding the effect of molecular weight. It is clear however that for both MicroCB and Micro850 carbons the high $\Delta H_{1/2}$ values of the PIBSI-G and PIBSI-H samples compared with other polymer dispersions showed evidence of a strong interaction and it appears the effect is more pronounced with the Micro850 samples.

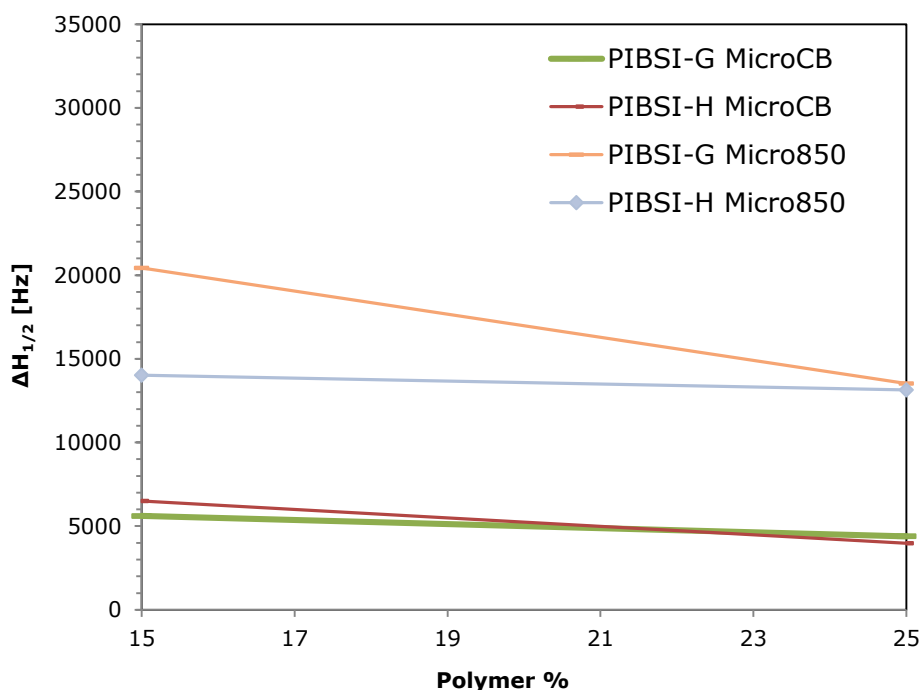


Figure 7-11: ^1H NMR $\Delta H_{1/2}$ values at 250 °C as a function of polymer % for various polymer (PIBSI-G, H) -Micro850 or MicroCB dispersions.

Figure 7-12 displays the $\Delta H_{1/2}$ measurements at 250 °C for PIBSI-I and PIBSI-K and so describes the effect of the addition of an extra PIB backbone. MicroCB-polymer samples are also shown for comparison. The PIBSI-I sample gave markedly higher $\Delta H_{1/2}$ values at 250 °C at each polymer percentage in the presence of Micro850. At 25 % polymer loadings the difference between PIBSI-I and PIBSI-K is around 9700 Hz and at 15 % around 11400 Hz. These results are

in contrast to the corresponding MicroCB samples which showed similar (albeit lower) $\Delta H_{1/2}$ values at 15 to 25 % polymer. This would therefore suggest (from a limited set of results) that the presence of the additional PIB tail has a greater effect with the Micro850 than with the MicroCB. It could be possible that the addition of the extra PIB tail led to more entanglements in the network and so a high reduction in the mobility of the polymer chains is observed.

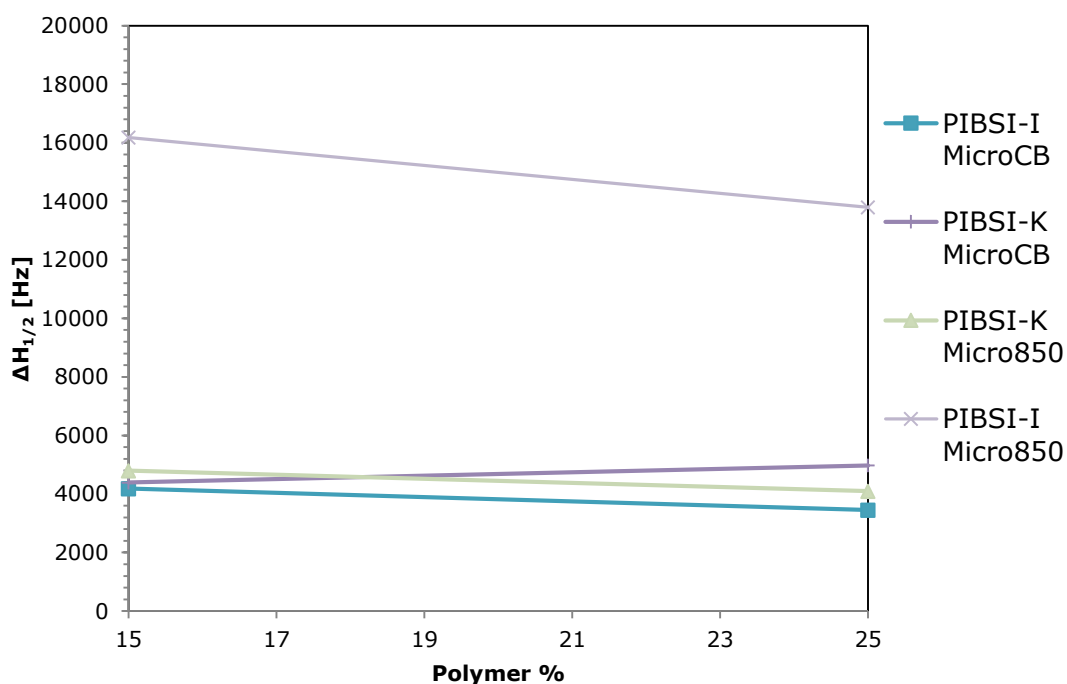


Figure 7-12: ^1H NMR $\Delta H_{1/2}$ values at 250 °C as a function of polymer % for various polymer (PIBSI-I, K) -Micro850 or MicroCB dispersions.

Figure 7-13 shows the effect of extending the number of amines in the polar head group. PIBSI-I contains two secondary amines while PIBSI-G has four. Both polymers are *bis* functional. It was previously found that with MicroCB (also shown in Figure 7-13) the PIBSI-G had slightly higher $\Delta H_{1/2}$ values at 250 °C than PIBSI-I at all three weight percentages. In the case of the dispersions containing Micro850, the $\Delta H_{1/2}$ values at 250 °C are much higher than with the corresponding MicroCB samples. The PIBSI-G Micro850 results show a larger $\Delta H_{1/2}$ value than

corresponding PIBSI-I sample at 15 % polymer. At 25 % polymer, the PIBSI-G and PIBSI-I Micro850 $\Delta H_{1/2}$ values at 250 °C are very similar. It can be tentatively said therefore that PIBSI-G exhibits a slightly greater level of interaction with both carbons because of the greater $\Delta H_{1/2}$ at 5, 15 and 25 % polymer loading with MicroCB and at 15 % polymer loading with Micro850) and that this is most likely due to more amines in the polar head group.

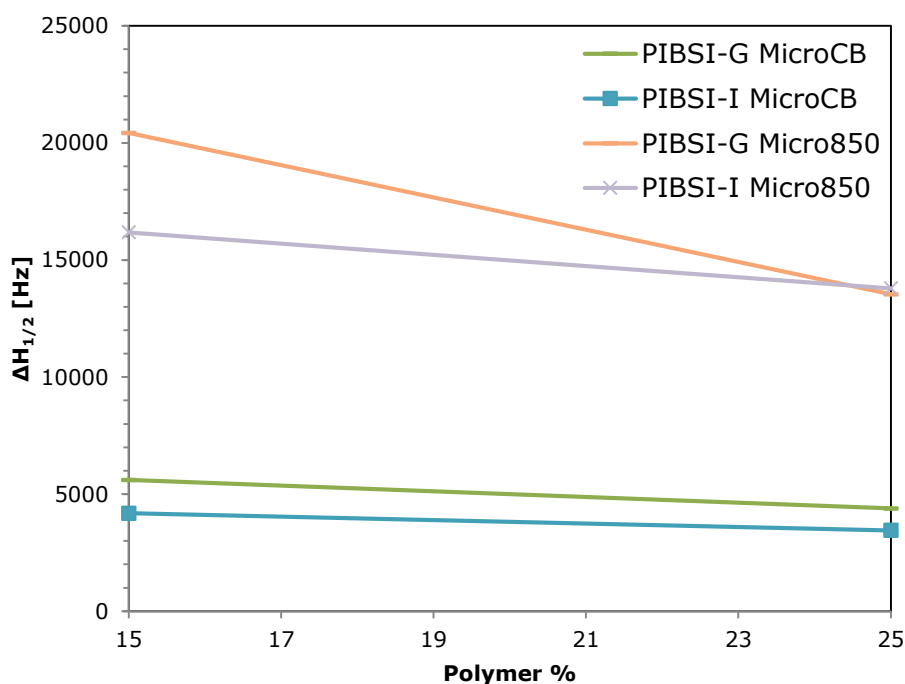


Figure 7-13: ^1H NMR $\Delta H_{1/2}$ values at 250 °C as a function of polymer % for various polymer (PIBSI-G, I) -Micro850 or MicroCB dispersions.

A summary of $\Delta H_{1/2}$ values at 250 °C of the chosen polymers with Micro850 is shown in Figure 7-14. It is clear that the values taken at 5 % polymer show inconstant results and in some cases the peaks are so broad that a $\Delta H_{1/2}$ could not be measured (PIBSI-C and PIBSI-G). This would indicate a strong interaction with the carbon since there is not enough mobile polymer in the sample to yield a measureable peak.

The remaining polymer samples at 15 and 25 % polymer loading have been separated into two groups in a similar manner to the MicroCB samples in chapter 6. The polymers and their properties with the assigned group number are summarised in Table 7-5. Figure 7-14 and Table 7-5 show the polymers assigned to group 1 generally have lower calculated polar surface areas and shorter PIB chains whereas group 2 have the higher polar surface areas and longer PIB chains. The assigned groups for each polymer correspond to the same groups for the MicroCB samples with one exception. The PIBSI-K Micro850 sample gave $\Delta H_{1/2}$ values at 250 °C values that were lower than expected particularly in comparison to PIBSI-I (although PIBSI-I was almost borderline in the MicroCB measurements). Despite this, and from the limited data set, the results indicate that the polymer dispersions are distinguishable according to their inherent structure.

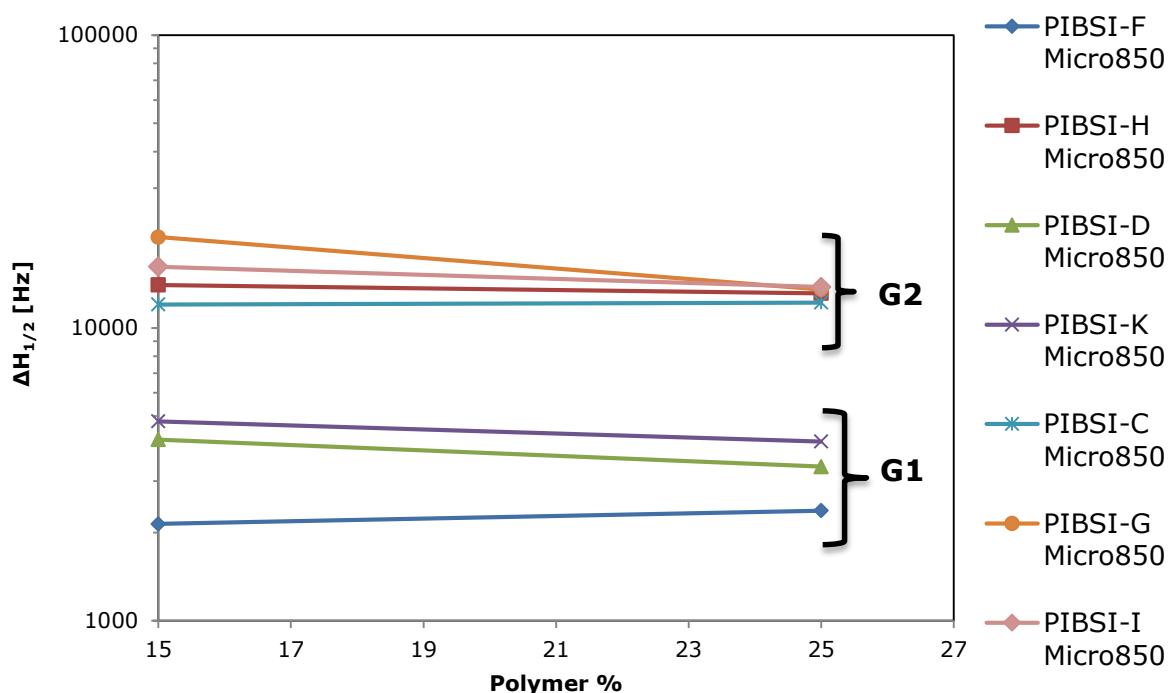


Figure 7-14: ^1H NMR $\Delta H_{1/2}$ values at 250 °C as a function of polymer % for various polymer -Micro850 dispersions.

Table 7-5: Summary of polymer properties with assigned group number

Polymer	Head Group	Polar Surface Area [\AA^2]	PIB-M_n [g mol^{-1}]	Group
PIBSI-C	AEEA	58.3	750	2
PIBSI-D	Ethanolamine	46.3	750	1
PIBSI-F	Ethanolamine	46.3	260	1
PIBSI-G	TEPA	88.2	1000	2
PIBSI-H	TEPA	88.2	1000	2
PIBSI-I	EDA	52.0	750	2
PIBSI-K	EDA	52.0	750	1

As was previously carried out in section 6.2.5 with MicroCB samples the various properties of the polymers such as the calculated polar surface area, PIB- M_n and polymer M_n and M_w were plotted with the $\Delta H_{1/2}$ values of the limited number of polymer- Micro850 samples studied at 15 and 25% polymer loading (5% samples were not included due to the loss of signal in some measurements).

Figure 7-15 shows the $\Delta H_{1/2}$ values at 250 °C for each polymer analysed with Micro850 with 15 and 25 % polymer loading as a function of the calculated polar surface area. A linear trend line has been added to each set of data. As can be seen the 15 % polymer data set R^2 value (0.53) is markedly lower than the corresponding MicroCB sample R^2 value (0.72) which was taken from a larger data set. The correlation is not strong enough to pass the F test for either data set, with F-observed values of 5.60 and 4.04 for 15 and 25 % samples respectively, with an F-critical value of 6.61 for both (Kennedy & Neville, 1986). The data sets are therefore too scattered to prove that the correlation is statistically significant and that the polar surface area has an effect on the H mobility.

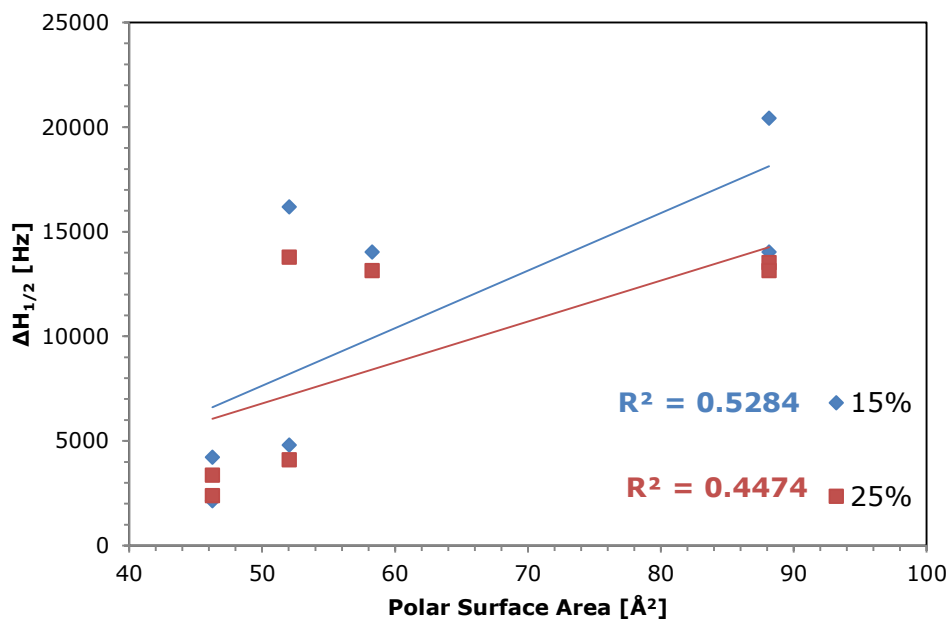


Figure 7-15: ^1H NMR $\Delta H_{1/2}$ values at 250 °C as a function of the polar surface area of the polymer head groups for various polymer MicroCB dispersions.

Figure 7-16 shows a summary of the $\Delta H_{1/2}$ values at 250 °C as a function of the PIB- M_n from which the samples were derived for various polymer (15, 25 %) and MicroCB (85 and 75 %) dispersions. The samples that gave the best correlation were the 25 % samples which overall have an R^2 value of 0.35. This data set has an F-observed value of 2.72 which is below the F-critical value (6.61 (Kennedy & Neville, 1986)) and so fails the F-test (with $\alpha = 0.05$). This could be an indication that the PIB- M_n is not a factor in effecting the mobility.

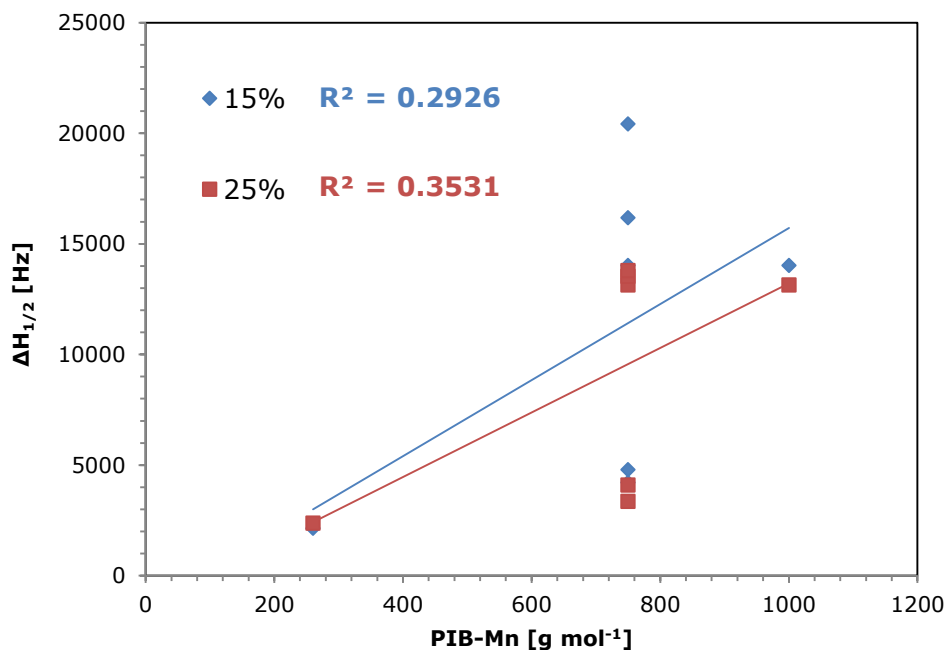


Figure 7-16: ¹H NMR $\Delta H_{1/2}$ values at 250 °C as a function of the molecular weight of the PIB backbone (PIB-M_n) for various polymer MicroCB dispersions.

Figure 7-17 and Figure 7-18 shows the $\Delta H_{1/2}$ values at 250 °C as a function of the M_n and M_w respectively for various polymer (15, 25 %) and MicroCB (85 and 75 %) dispersions. A linear trend line has been added to each data set of data. Both graphs show very loose correlation between the molecular weights and the $\Delta H_{1/2}$ values at 250 °C with low R² values. All of the data sets have F-observed values that are below the corresponding F-critical value and so the correlations cannot be said to be statistically significant. This maybe an indication of a lack of an effect of the M_n and M_w on the $\Delta H_{1/2}$ measurements. It does appear that the data sets can be separated into 2 groups as they were previously in Figure 7-14 and Table 7-5 and that within each group it appears that there is almost no gradient indicating no relationship between the $\Delta H_{1/2}$ and the M_w (this is particularly apparent in Figure 7-18 for the 25% polymer samples).

As described in chapter 6 it is difficult to separate the effects of both molecular weight and the size of the polar head groups on the $\Delta H_{1/2}$ measurements from the

range of polymers studied. As the linear trend line for the polar head group graph (Figure 7-15) had the higher R^2 values (and F-observed values that were, on average, closer to the corresponding F-critical values) than the graphs concerning molecular weight it could be somewhat tentatively concluded that the polar surface area is the more dominant parameter. However it does appear likely that a combination of the different properties of the polymers can have an effect on the magnitude of the $\Delta H_{1/2}$ values at high temperatures.

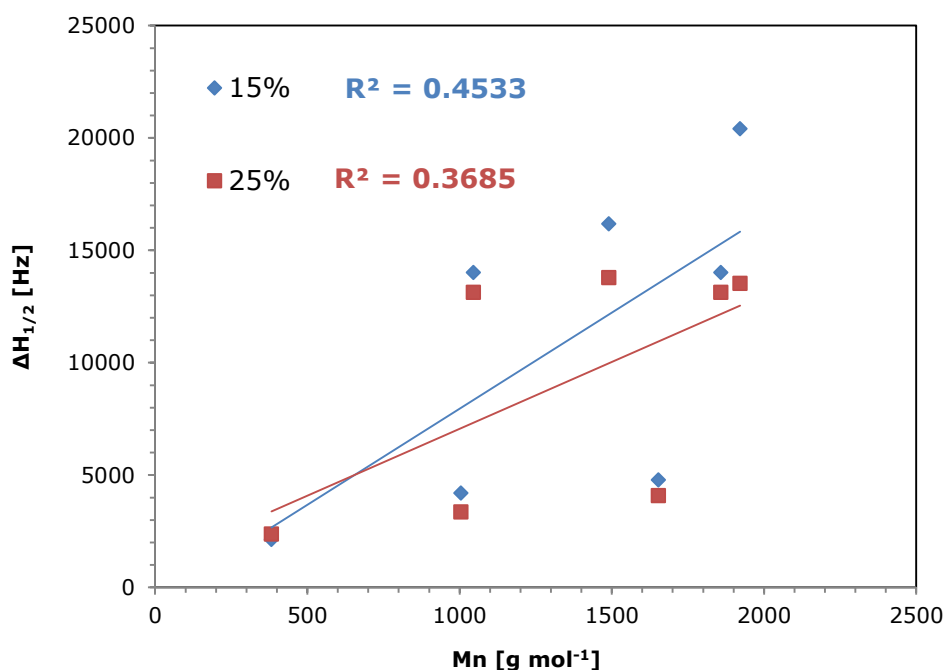


Figure 7-17: 1H NMR $\Delta H_{1/2}$ values at 250 °C as a function of the number average molecular weight (M_n) for various polymer MicroCB dispersions.

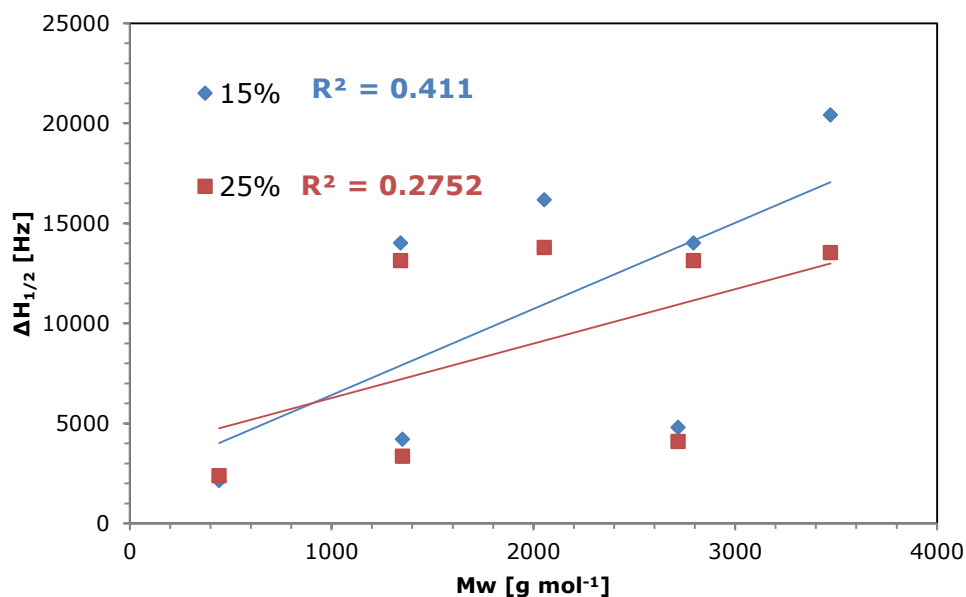


Figure 7-18: ¹H NMR $\Delta H_{1/2}$ values at 250 °C as a function of the weight average molecular weight (M_w) for various polymer MicroCB dispersions.

7.3 CHAPTER SUMMARY

It has been demonstrated that changing the type of carbon used in a dispersion sample can significantly affect the measured mobility of the sample. This has been achieved using two polymers, one which has previously been shown to give a wide $\Delta H_{1/2}$ and hence has a strong interaction (PIBSI-H) with MicroCB and one which has previously shown to give a narrow $\Delta H_{1/2}$ and hence a weaker interaction (PIBSI-F) with MicroCB.

- It was found that at 5 % polymer loading the data was much more scattered and inconsistent than at 15 and 25 % polymer content. This was most likely due to the lack of polymer sample (possibly due to degradation) causing further broadening of the $\Delta H_{1/2}$. The 5 % samples were therefore discounted. The trends in $\Delta H_{1/2}$ at 15 and 25 % were much more consistent particularly for the PIBSI-F samples.

- It was found that at 15 and 25 % polymer loading PIBSI-H samples gave much greater $\Delta H_{1/2}$ values at 250 °C than the corresponding PIBSI-F samples. The carbons Micro850 and Micro450 (as well as MicroCB which was described in chapter 6) all gave significantly higher $\Delta H_{1/2}$ values at 250 °C than their corresponding PIBSI-F samples. Most of the other carbons tested with PIBSI-H showed lower $\Delta H_{1/2}$ values that were in the same region/ not dissimilar to the corresponding PIBSI-F samples which indicated a less of an interaction between the PIBSI-H and the carbon.
- Various properties of the carbons such as surface area, particle size, peak CO₂ oxidation temperature and carbon and oxygen surface content were compared with the $\Delta H_{1/2}$ values for the PIBSI-H and PIBSI-F samples. Although there appeared to be no direct relationship between the nominal average particle size/ surface areas and the $\Delta H_{1/2}$ values there did appear to be some relationship between the $\Delta H_{1/2}$ and the carbon surface properties. As the peak CO₂ emission temperature of the various carbons increases so did the $\Delta H_{1/2}$ (with one exception - Micro146). This indicated that as graphiticity of the carbon increased the level of interaction also increased up until a point was reached whereby the carbon was too graphitic for the polymer to interact. The three carbons with the highest proportion of carbon on the surface also gave the highest $\Delta H_{1/2}$ values with PIBSI-H. The carbons with the least amount of oxygen on the carbon surface gave the highest $\Delta H_{1/2}$ values at 250 °C. These findings would reinforce the affirmation that it is the nature of the interaction between the polymer and the carbon surface that determines the magnitude of the $\Delta H_{1/2}$. It suggests that dispersions can be better distinguished with high temperature ¹H NMR with more graphitic rather than amorphous carbon.
- It was found that the largest difference in $\Delta H_{1/2}$ between the PIBSI-H and PIBSI-F samples was with the Micro850 carbon. As a result, a number of

polymers were analysed with Micro850 at high solid loading in an attempt to investigate if a number of polymer dispersions could be better distinguished than with MicroCB. The polymers were selected based on key structural differences. It was once again found that at 5 % polymer the data was much more scattered and inconsistent than at 15 and 25 % polymer content. This was most likely due to the lack of polymer sample causing a broadening of the $\Delta H_{1/2}$. The trends in $\Delta H_{1/2}$ at 15 and 25 % were much more consistent and the data set could be separated into two general groups. PIBSI-F, D and K (group 1) all have short head groups with single PIB chains whereas PIBSI-G, I, H and C all (group 2) all have longer head groups with multiple amines or have two PIB chains.

- Various properties of the polymers such as the polar surface area which relates to the size of the amine head group, the PIB- M_n and the M_n and M_w were compared to $\Delta H_{1/2}$ values for a limited number of different polymers with Micro850. Although for each structural parameter positive correlation was found the coefficient of determination values were low in each case. Also, none of these data sets passed the F-test and so it cannot be proven from these results that one property of the polymers is more dominant in controlling the mobility than any other. However the R^2 values and F-observed values were still the highest for the polar surface area on average which suggests this is could be the most dominant property affecting the $\Delta H_{1/2}$ rather than molecular weight of the polymers.

8 Conclusions and Recommendations for Future Work

This chapter summarises the conclusions of the literature review and experimental work. In addition recommendations for future work are provided.

8.1 SUMMARY OF CONCLUSIONS AND NOVELTY OF RESEARCH

Whilst there have been a number of studies with regards to PIB derivative stabilisation of carbonaceous particles at room temperature, few studies have investigated their behaviour at temperatures similar to their normal high temperature operating conditions. Although a few studies have used rheometry in combination with other techniques to study PIB type dispersions with deposit surrogates such as Won et al., (2005) and Yang et al. (2007), these were limited up to 100 °C. While these studies offered great insight into the thermal effects on the dispersions at lower temperatures the work presented here has investigated the behaviour of PIB and its derivatives at higher temperatures which are closer to the conditions in which deposit control additives normally operate.

In this work a reproducible methodology for both the sample preparation and the analysis has been established. Characterisation of PIB, and two functionalised derivatives, PIB succinic anhydride (PIBSA) and PIB succinimide (PIBSI), demonstrated that the viscoelastic and hydrogen mobility measurements of dispersion may serve as an indication of the strength of the interaction between the polymer and carbon particles. This has been achieved using dispersions with high carbon loadings ($\geq 25\%$).

The range of PIBSI type molecules was expanded to investigate the structure activity relationships which included the effects of the number of amines in the head group and the length of the PIB hydrocarbon chains. The results indicate that the size of amine head groups have the most dominant effect on the viscoelastic and molecular mobility behaviour although it has proved difficult to comprehensively establish this from the selection of polymers tested. The dispersions appeared to be the most distinguishable at low polymer loadings and

it is postulated this is most likely due to surface coverage effects reducing the mobility of the strongly adsorbing polymers.

The effect of changing the carbon type was investigated using high temperature ^1H NMR where a number of dispersions containing various types of commercially available carbons were analysed. The results showed that changing the type of carbon used in a dispersion sample can significantly affect the measured mobility of the sample. The properties of the carbon material on the surface, such as the level of carbon and oxygen surface percentage, and the level of graphiticity and amorphicity were the more dominant factors in effecting the mobility measurements as opposed to other factors such as particle size and surface area. It appeared that the polymers could be better distinguished with the more graphitic type carbons.

To the best of the author's knowledge this work presents for the first time a study of the dispersion behaviour of polyisobutylene and its derivatives at high temperatures using rheometry and ^1H NMR. This work gives additional support that this method of high temperature measurement of dispersions can provide an indication of the strength of the interaction between the polymer and deposit surrogate particles rather than simply being controlled by the inherent physical properties of the polymers or carbons themselves. Through utilisation of the high temperature techniques employed, the work demonstrates that applied methodologies have the potential (with further research) of offering a reliable and inexpensive laboratory scale screening method that may be able to accurately predict the behaviour of these dispersants without having to rely upon the expensive full scale engine testing currently employed by the fuel additives industry. Longer term direct impact on the population will be the ability to understand the properties required from the replacements for these polymers in for example the next generation of fossil fuel engine green detergents.

8.2 RECOMMENDATIONS FOR FUTURE WORK

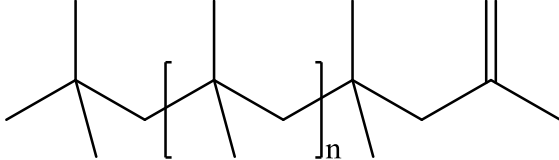
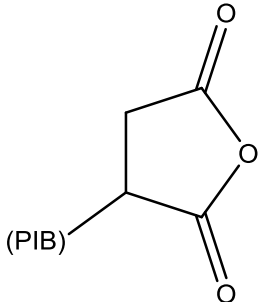
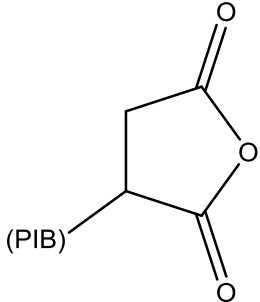
While this work has explored the potential for distinguishing various polymer /carbon dispersions using high temperature rheometry and ^1H NMR there is potential for more work to be done.

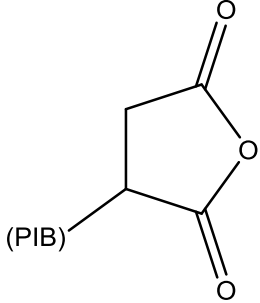
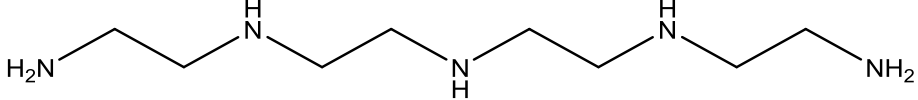
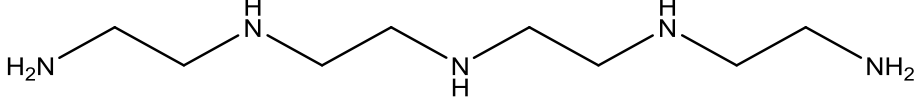
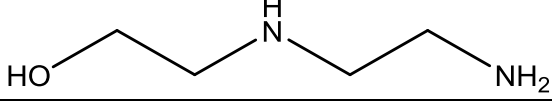
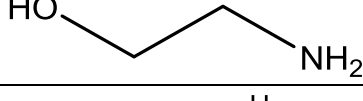
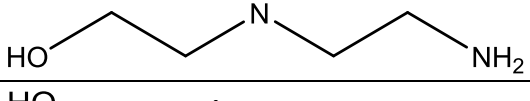
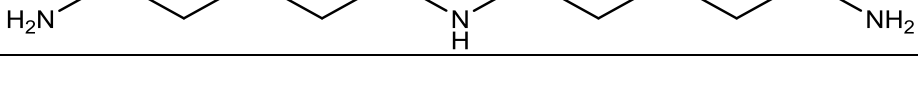
- There is ample scope for many more PIB architectures to be investigated. It would be interesting, for instance, to examine PIBSIs with amino ether head groups which, as suggested by Kim et al., (2015), have been shown to give rise to a greater affinity to carbon black. It would be interesting to analyse the comb like surfactants such as poly-PIBSI molecules as these were shown by Dubois-Chlochard et al., (2001) to have a very high affinity for carbon blacks. Also, a systematic approach to increasing the polar head group size for a greater number of polymers would allow the effects of head group size to be investigated more thoroughly.
- The exact effects of the properties of the carbons on the $\Delta H_{1/2}$ of a sample at high temperatures are still unknown. The results in chapter 7 indicate that the surface chemistry, including the levels of amorphicity and graphicity, as well as the carbon and oxygen content on the surface takes precedent over the physical properties such as surface area and particle size when establishing a relationship between carbon black and the $\Delta H_{1/2}$ measurements. A deeper investigation into the properties of the carbons looking into effects such as particle porosity and size distribution would provide further insight into these relationships.
- For every dispersion sample that has been prepared in this work hexane was used as a solvent. While the hexane was not present at high temperatures it is still unclear what effect the solvent has during the sample preparation on the polymer behaviour and therefore subsequent NMR and rheometry results. Various other solvents such as xylene and

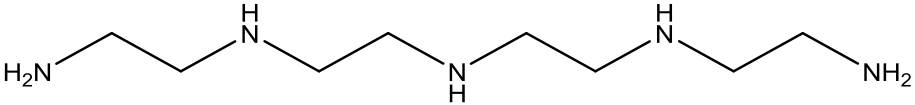
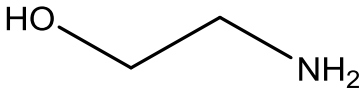
heptane could be used, as well as commercial diesel and gasolines to mimic more realistic engine conditions.

- It has been demonstrated that different PIBs could be distinguished on the RDA III rheometer instrument at carbon loadings of greater than or equal to 35 %, and that solid loading of 55 % still gave distinguishable, all be it, linear viscoelastic trends. However, work done on the more sensitive TA AR-2000 instrument was able to distinguish between polymers at solid loadings of 25 %. An issue that arose however in some instances was significant loss of the polymer as the temperature was increased which caused the data to become scattered. It is therefore recommended that for any future work which is carried out at low solid concentrations a solution to this issue be found.
- It would be advantageous to carry out analysis of dispersions using actual engine deposits as this would mimic more realistic engine conditions. Also, relating the analytical test data to real engine test data of the commercial samples would be highly useful in validating the method.

A Polymer Structures

Polymer reference	Polymer description	Structure
PIB	Polyisobutylene (PIB)	
PIBSA-A	Polyisobutylene Succinic Anhydride (PIBSA)	
PIBSA-B	Polyisobutylene Succinic Anhydride (PIBSA)	

PIBSA-C	Polyisobutylene Succinic Anhydride (PIBSA)	
Polymer reference	Polymer description	PIBSI Head group structure
PIBSI-A	Polyisobutylene Succinimide (PIBSI) with tetraethylenepentamine (TEPA)	
PIBSI-B	PIBSI with tetraethylenepentamine (TEPA). (Chlorine synthetic route)	
PIBSI-C	PIBSI with Aminoethylethanolamine (AEEA)	
PIBSI-D	PIBSI with Ethanolamine	
PIBSI-E	PIBSI with Aminoethylethanolamine (AEEA)	
PIBSI-F	PIBSI with Ethanolamine	
PIBSI-G	PIBSI with tetraethylenepentamine (TEPA)	

PIBSI-H	PIBSI with tetraethylenepentamine (TEPA)	
PIBSI-I	PIBSI with ethylenediamine (EDA)	
PIBSI-J	PIBSI with Ethanolamine	
PIBSI-K	PIBSI with ethylenediamine (EDA)	

B Strain-sweep measurements

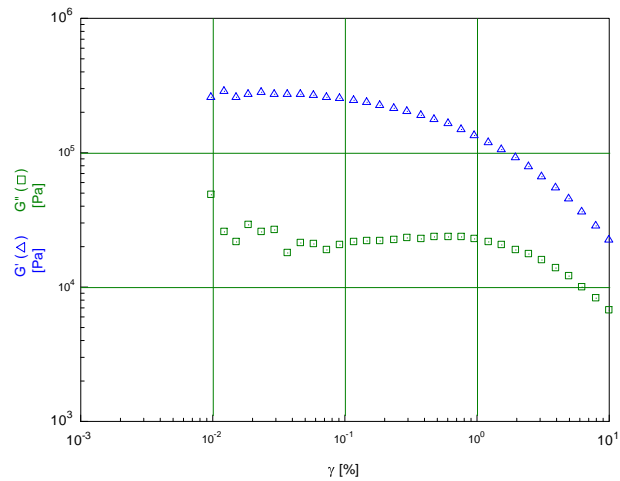


Figure B-1: Storage (G') and loss (G'') moduli as a function of strain (γ) at 100 °C for PIB 45% MicroCB 55% dispersion.

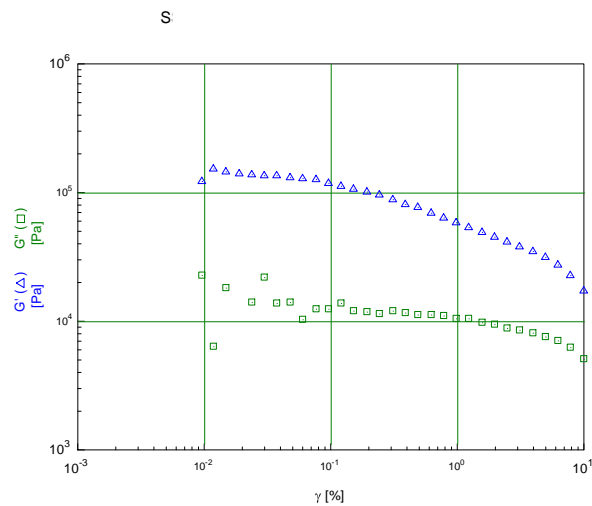


Figure B-2: Storage (G') and loss (G'') moduli as a function of strain (γ) at 250 °C for PIB 45% MicroCB 55% dispersion.

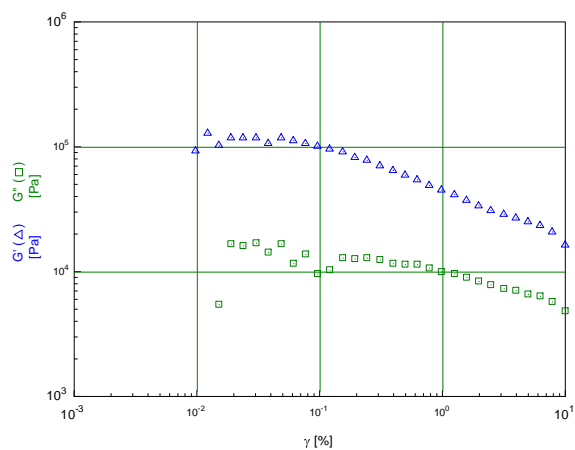


Figure B-3: Storage (G') and loss (G'') moduli as a function of strain (γ) at 350 °C for PIB 45% MicroCB 55% dispersion.

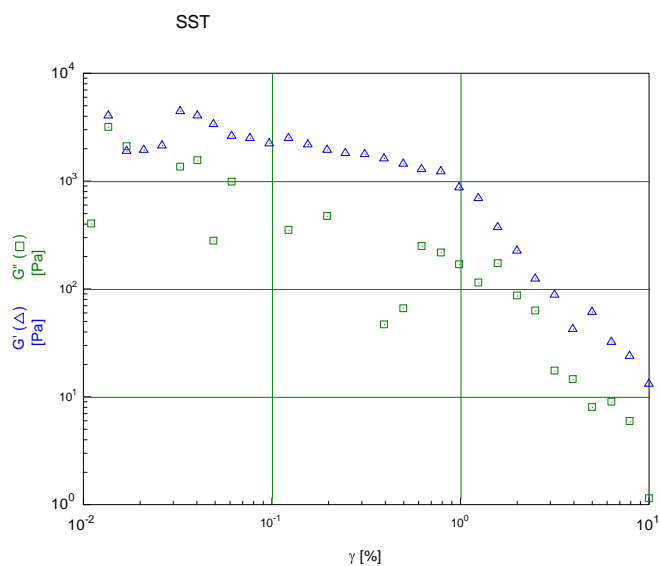


Figure B-4: Storage (G') and loss (G'') moduli as a function of strain (γ) at 100 °C for PIB 65% MicroCB 35% dispersion.

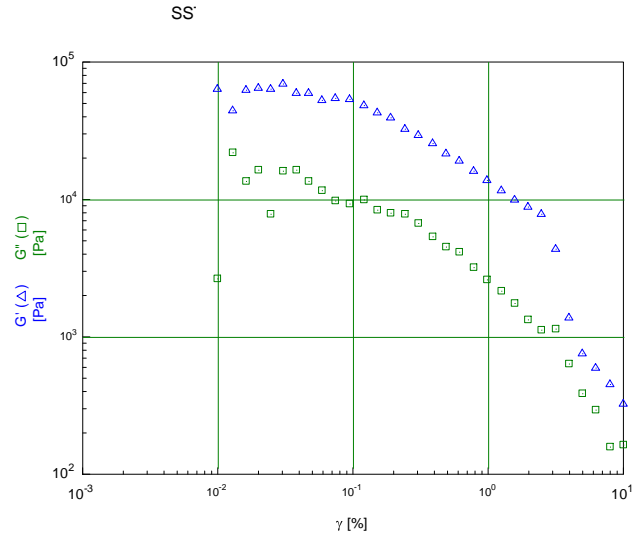


Figure B-5: Storage (G') and loss (G'') moduli as a function of strain (γ) at 250 °C for PIB 65% MicroCB 35% dispersion.

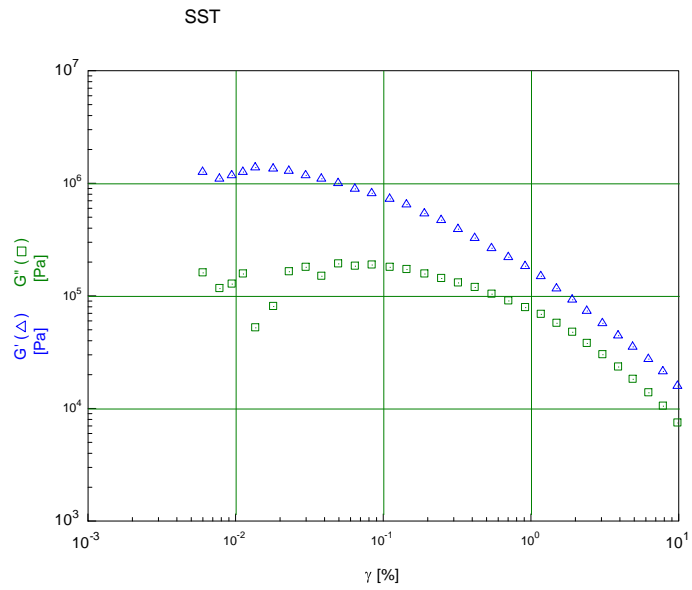


Figure B-6: Storage (G') and loss (G'') moduli as a function of strain (γ) at 350 °C for PIB 65% MicroCB 35% dispersion. (350°C)

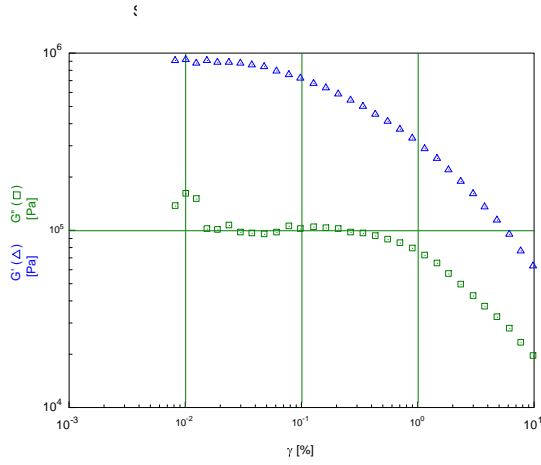


Figure B-7 : Storage (G') and loss (G'') moduli as a function of strain (γ) at 100 °C for PIBSI-A 45% MicroCB 55% dispersion.

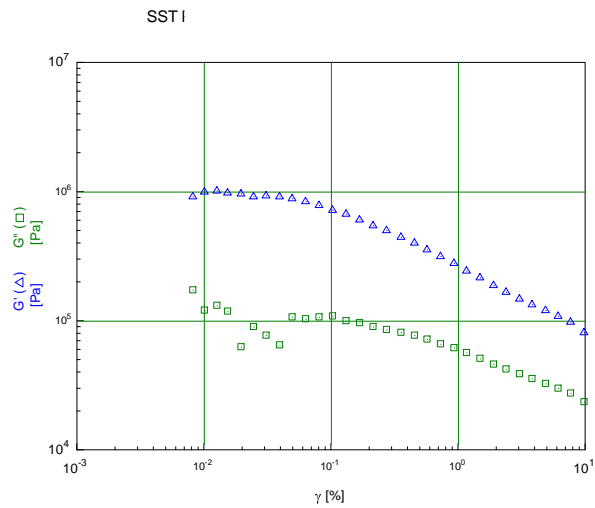


Figure B-8: Storage (G') and loss (G'') moduli as a function of strain (γ) at 250 °C for PIBSI-A 45% MicroCB 55% dispersion.

S9

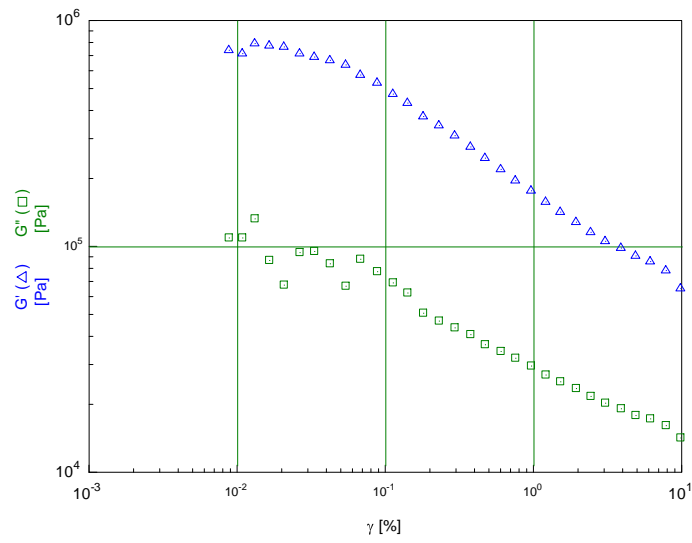


Figure B-9: Storage (G') and loss (G'') moduli as a function of strain (γ) at 350 °C for PIBSI-A 45% MicroCB 55% dispersion.

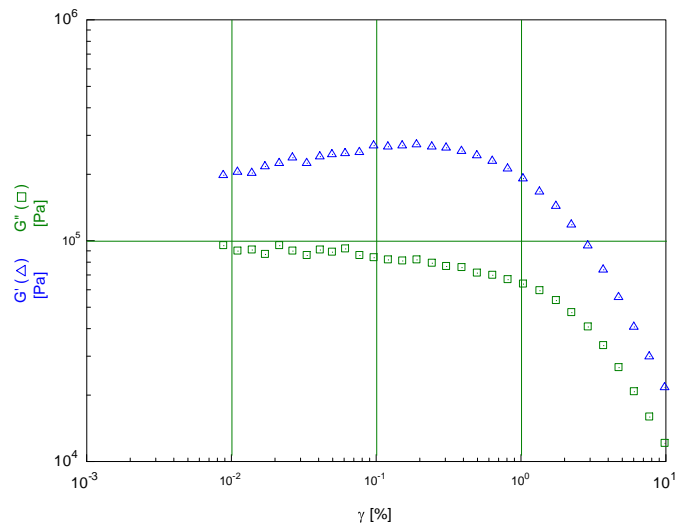


Figure B-10: Storage (G') and loss (G'') moduli as a function of strain (γ) at 100 °C for PIBSI-A 65% MicroCB 35% dispersion.

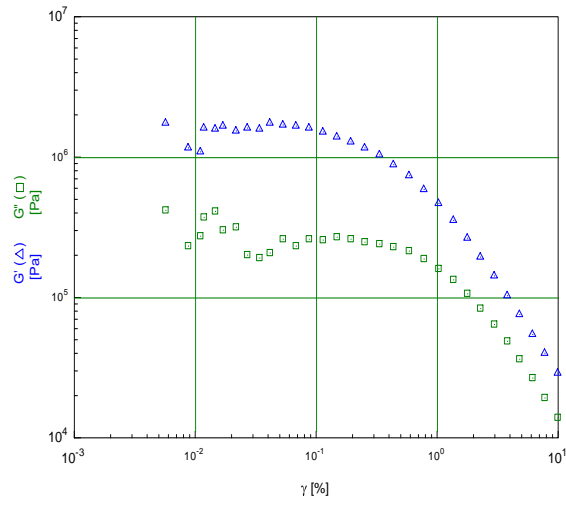


Figure B-11: Storage (G') and loss (G'') moduli as a function of strain (γ) at 250 °C for PIBSI-A 65% MicroCB 35% dispersion.

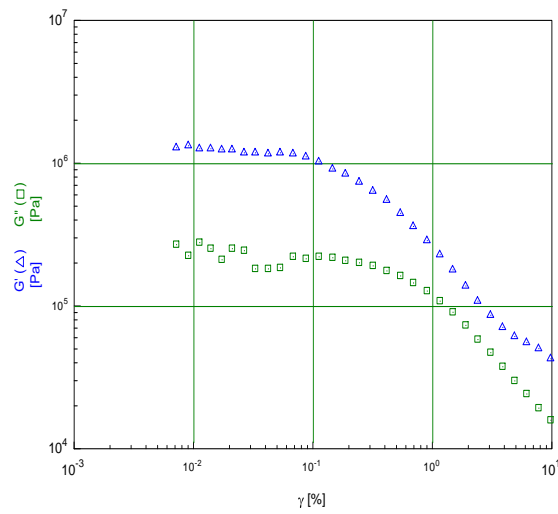


Figure B-12: Storage (G') and loss (G'') moduli as a function of strain (γ) at 350 °C for PIBSI-A 65% MicroCB 35% dispersion.

C Duplicate η^* measurements of PIB, PIBSA, PIBSI-A, PIBSI-B (65 %) MicroCB (35 %) dispersions

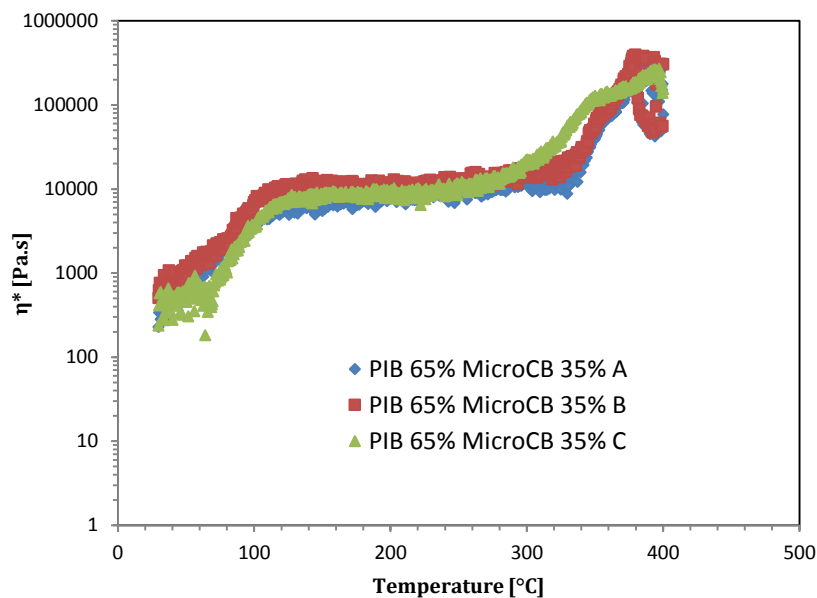


Figure C-1: Duplicate samples of PIB (65 %) and MicroCB (35 %) (A, B, C) using a heating rate of $3\text{ }^\circ\text{C min}^{-1}$ in nitrogen ($\gamma = 0.05$, $\omega = 1\text{ Hz}$). (RDA-III instrument).

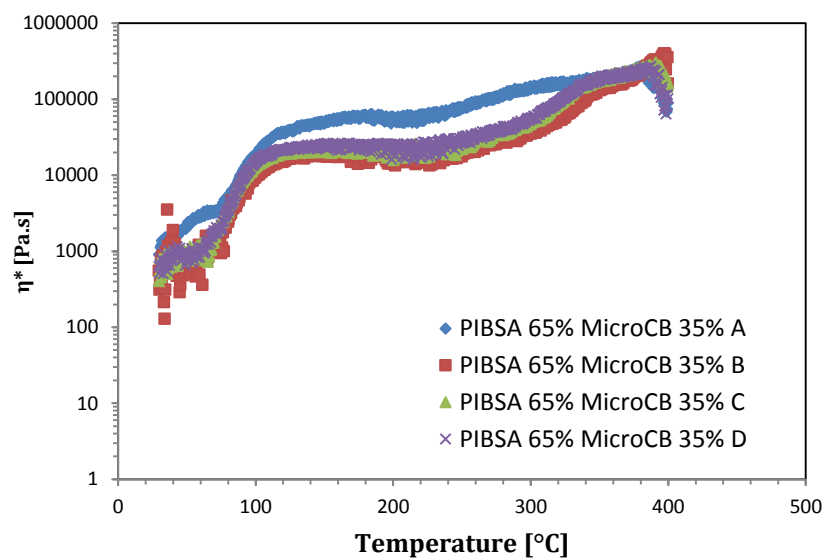


Figure C-2: Duplicate samples of PIBSA-A (65 %) and MicroCB (35 %) (A, B, C, D) using a heating rate of $3\text{ }^\circ\text{C min}^{-1}$ in nitrogen ($\gamma = 0.05$, $\omega = 1\text{ Hz}$). (RDA-III instrument).

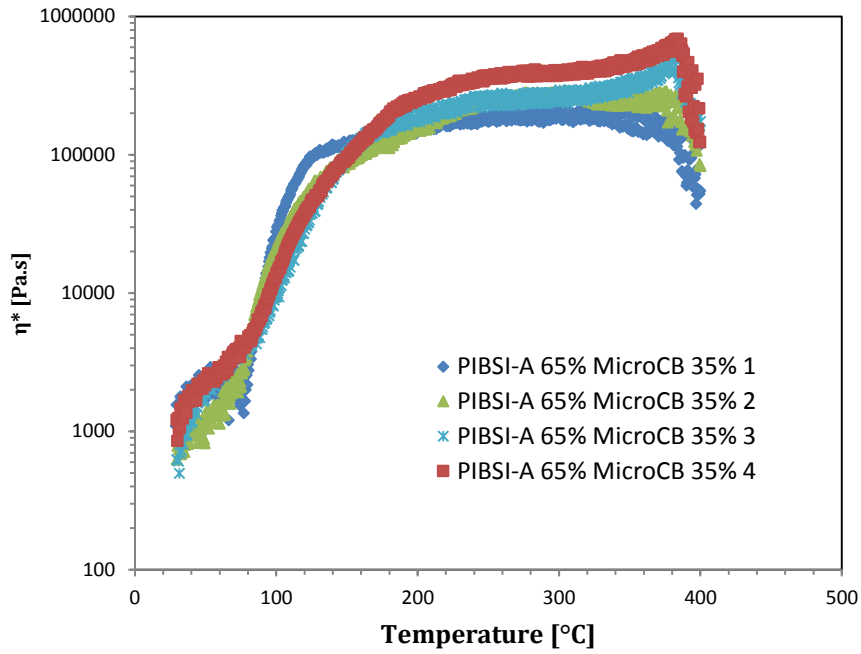


Figure C-3: Duplicate samples of PIBSI-A (65 %) and MicroCB (35 %) (1-4) using a heating rate of $3 \text{ }^\circ\text{C min}^{-1}$ in nitrogen ($\gamma = 0.05$, $\omega = 1 \text{ Hz}$). (RDA-III instrument).

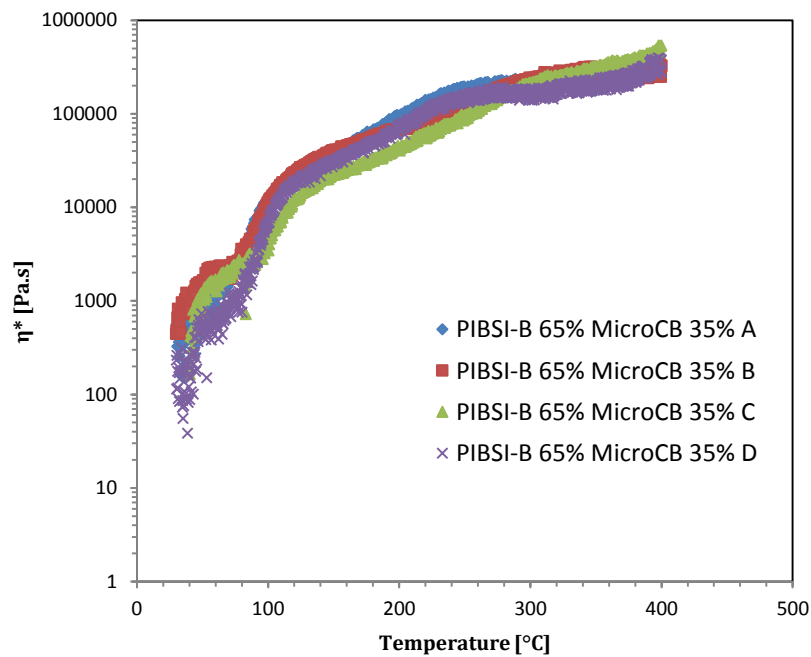


Figure C-4: Duplicate samples of PIBSA-B (65 %) and MicroCB (35 %) (A, B, C, D) using a heating rate of $3 \text{ }^\circ\text{C min}^{-1}$ in nitrogen ($\gamma = 0.05$, $\omega = 1 \text{ Hz}$). (RDA-III instrument).

D η^* measurements of various polymer MicroCB dispersions

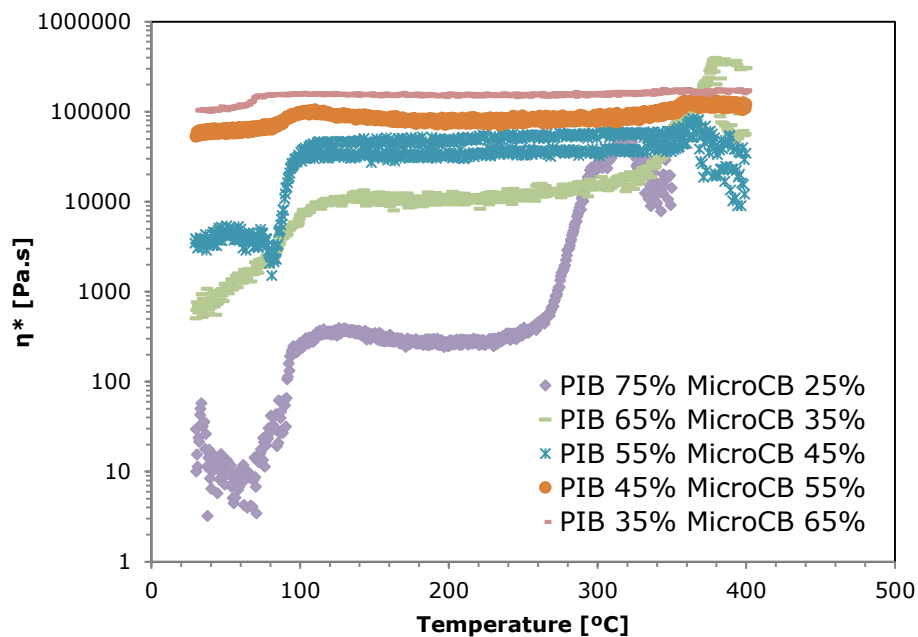


Figure D-1: η^* as a function of temperature for various PIB and MicroCB dispersions, using a heating rate of $3\text{ }^\circ\text{C min}^{-1}$ in nitrogen ($\gamma = 0.05$, $\omega = 1\text{ Hz}$).

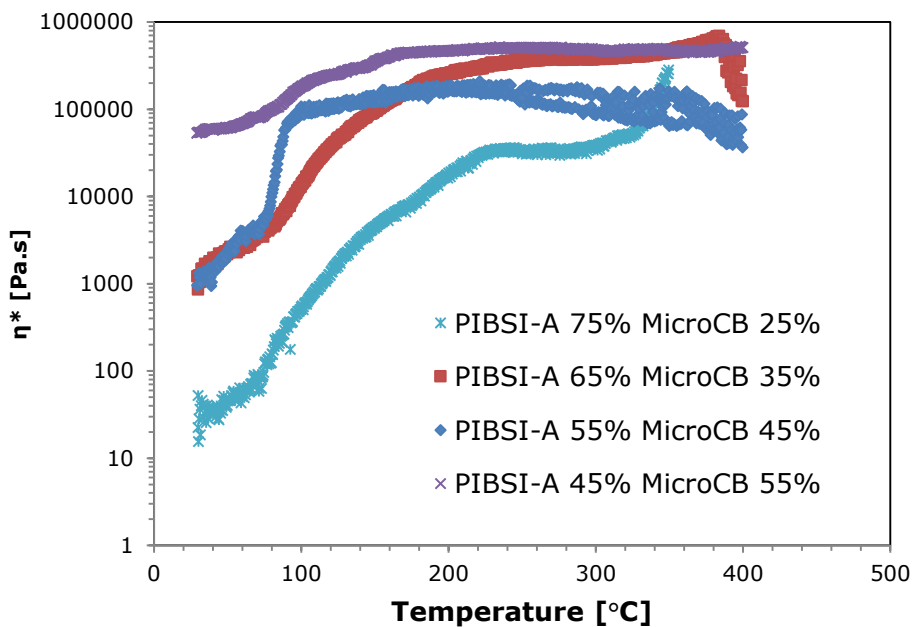


Figure D-2: Complex viscosity (η^*) as a function of temperature for various PIBSI-A and MicroCB dispersions, using a heating rate of $3\text{ }^\circ\text{C min}^{-1}$ in nitrogen ($\gamma = 0.05$, $\omega = 1\text{ Hz}$).

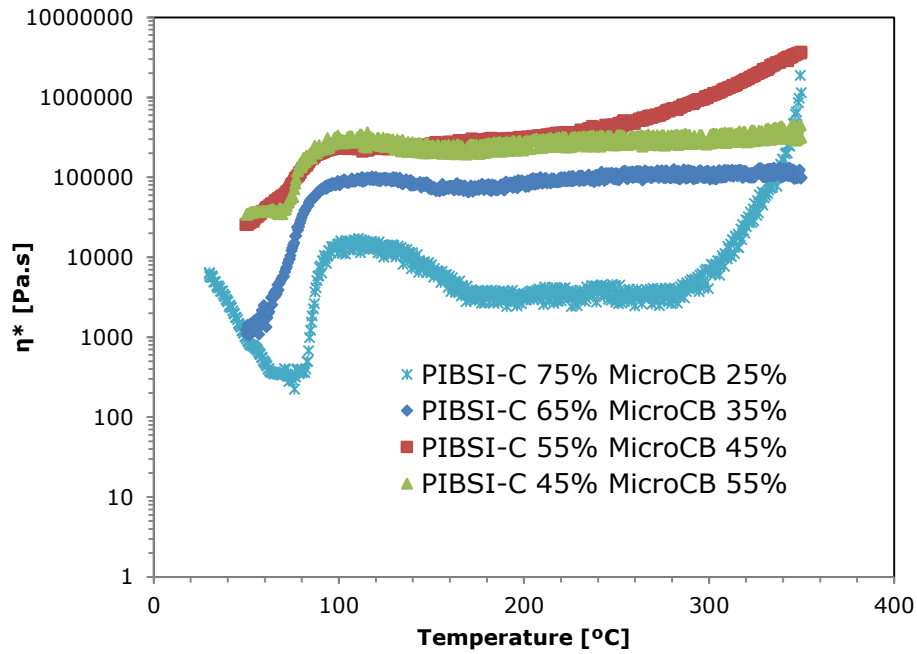


Figure D-3: η^* as a function of temperature for various PIBSI-C MicroCB dispersions, using a heating rate of $3\text{ }^\circ\text{C min}^{-1}$ in nitrogen ($\gamma = 0.05$, $\omega = 1\text{ Hz}$).

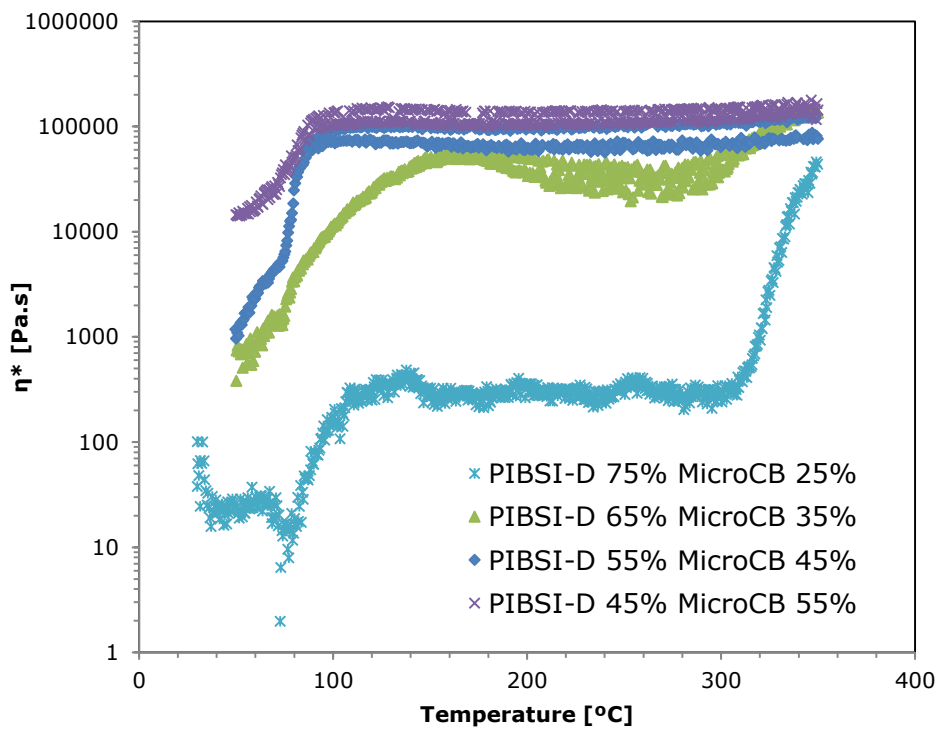


Figure D-4: η^* as a function of temperature for various PIBSI-D MicroCB dispersions, using a heating rate of $3\text{ }^\circ\text{C min}^{-1}$ in nitrogen ($\gamma = 0.05$, $\omega = 1\text{ Hz}$).

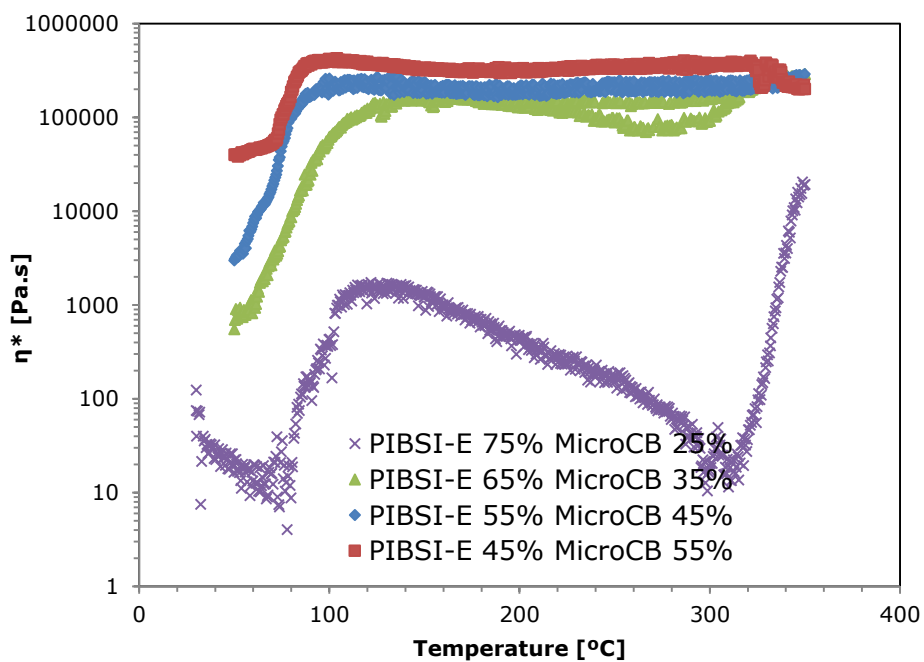


Figure D-5: η^* as a function of temperature for various PIBSI-E MicroCB dispersions, using a heating rate of $3\text{ }^\circ\text{C min}^{-1}$ in nitrogen ($\gamma = 0.05$, $\omega = 1\text{ Hz}$).

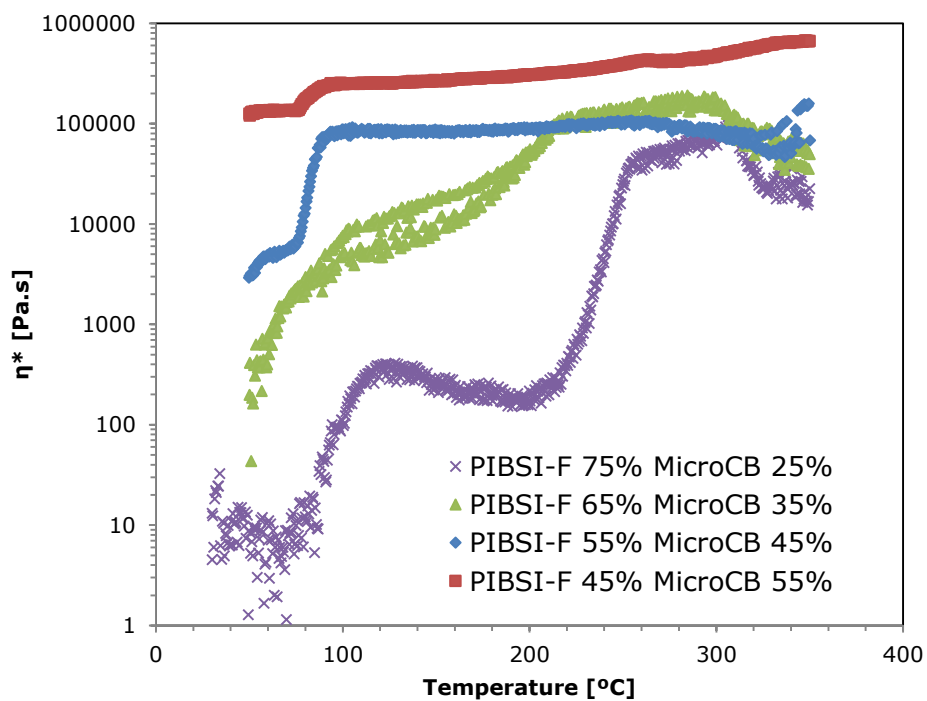


Figure D-6: η^* as a function of temperature for various PIBSI-F MicroCB dispersions, using a heating rate of $3\text{ }^\circ\text{C min}^{-1}$ in nitrogen ($\gamma = 0.05$, $\omega = 1\text{ Hz}$).

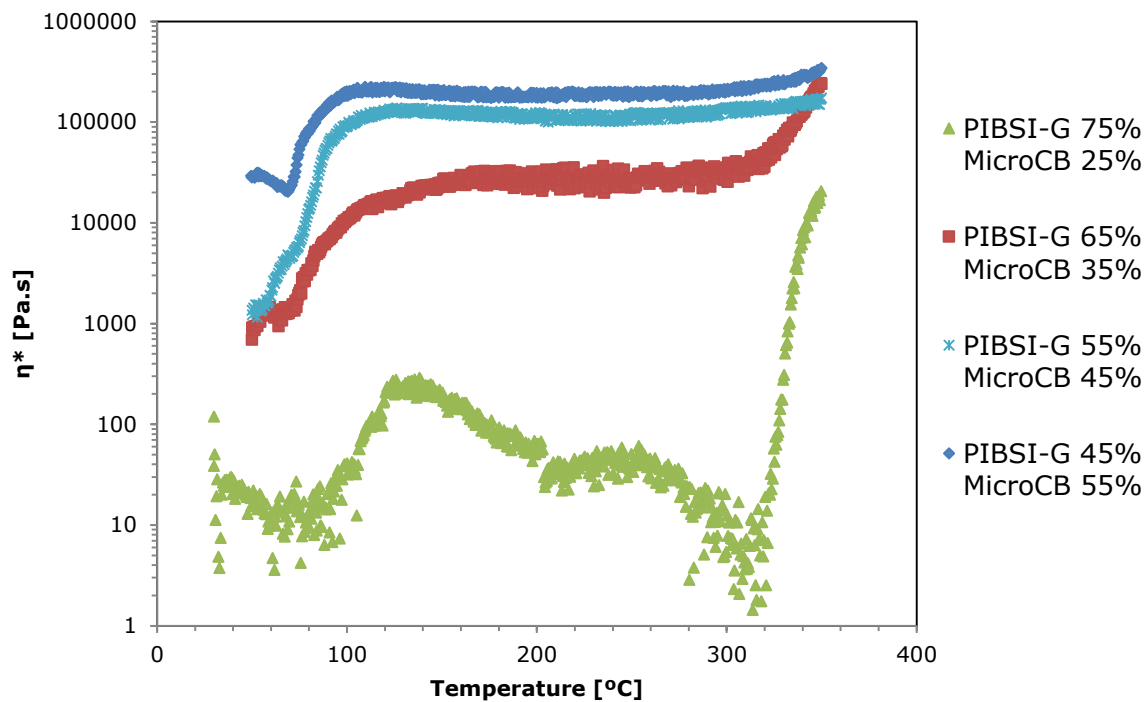


Figure D-7: η^* as a function of temperature for various PIBSI-G MicroCB dispersions, using a heating rate of $3\text{ }^\circ\text{C min}^{-1}$ in nitrogen ($\gamma = 0.05$, $\omega = 1\text{ Hz}$).

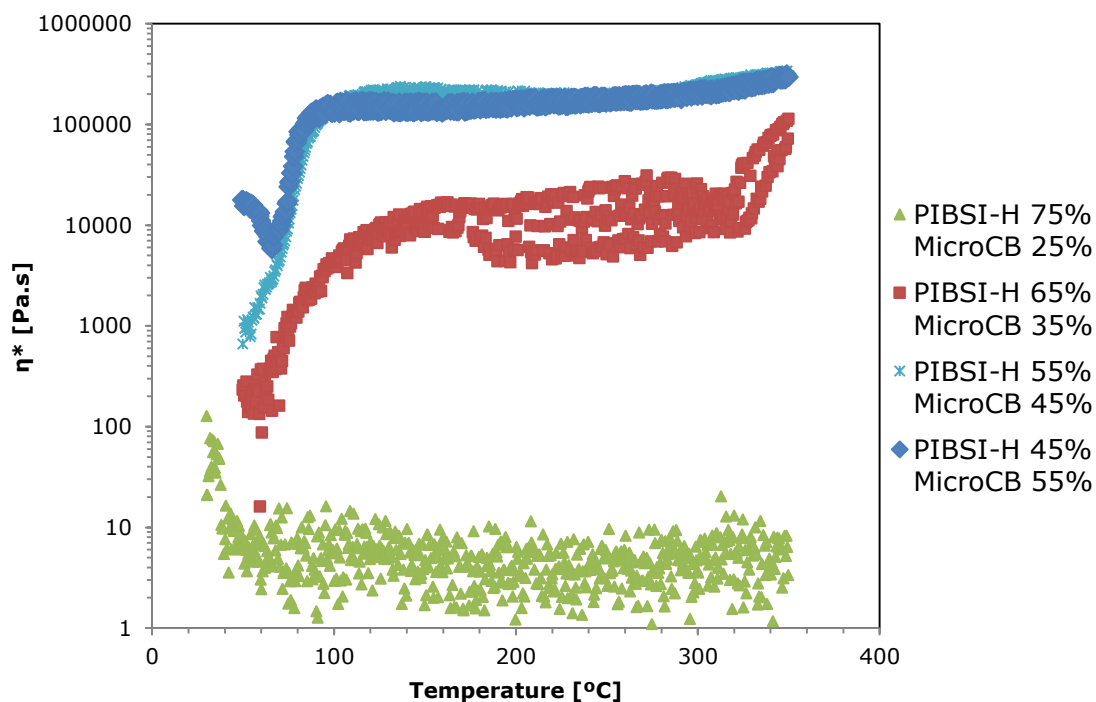


Figure D-8: η^* as a function of temperature for various PIBSI-H MicroCB dispersions, using a heating rate of $3\text{ }^\circ\text{C min}^{-1}$ in nitrogen ($\gamma = 0.05$, $\omega = 1\text{ Hz}$).

E Duplicate $\Delta H_{1/2}$ measurements of PIB, PIBSA, PIBSI-A (65 %) MicroCB (35 %) dispersions

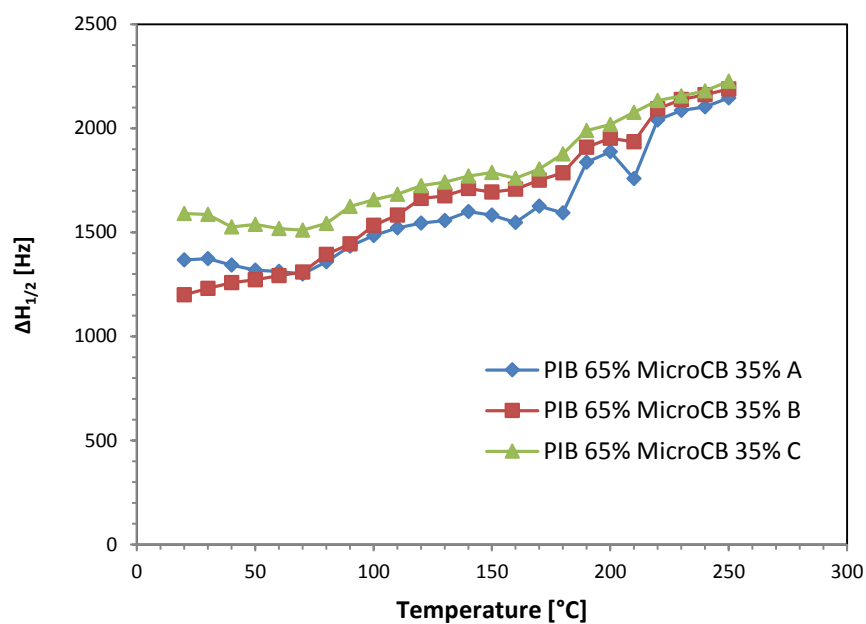


Figure E-1: Evolution of the ^1H NMR $\Delta H_{1/2}$ with temperature for 3 duplicate PIB (65 %) Micro CB (35 %) dispersions (A, B, C)

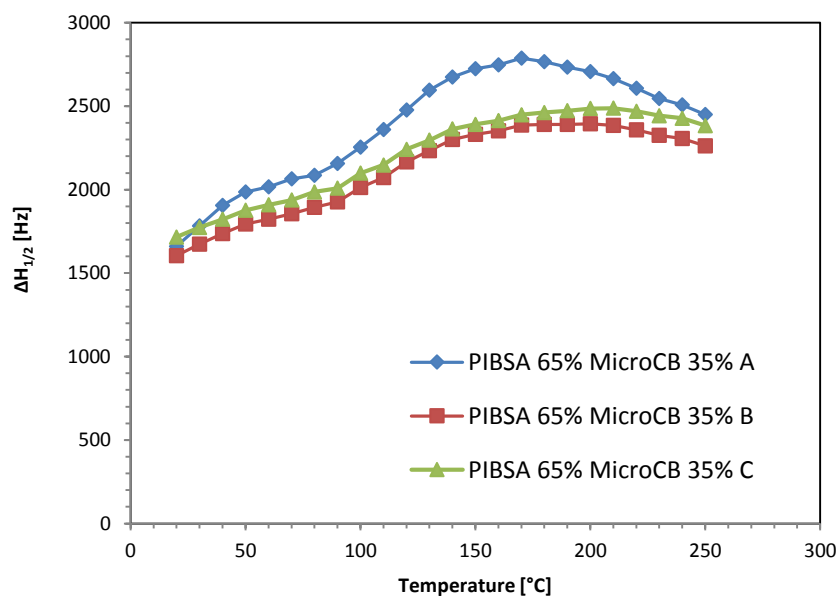


Figure E-2: Evolution of the ^1H NMR $\Delta H_{1/2}$ with temperature for 3 duplicate PIBSA-A (65 %) Micro CB (35 %) dispersions (A, B, C)

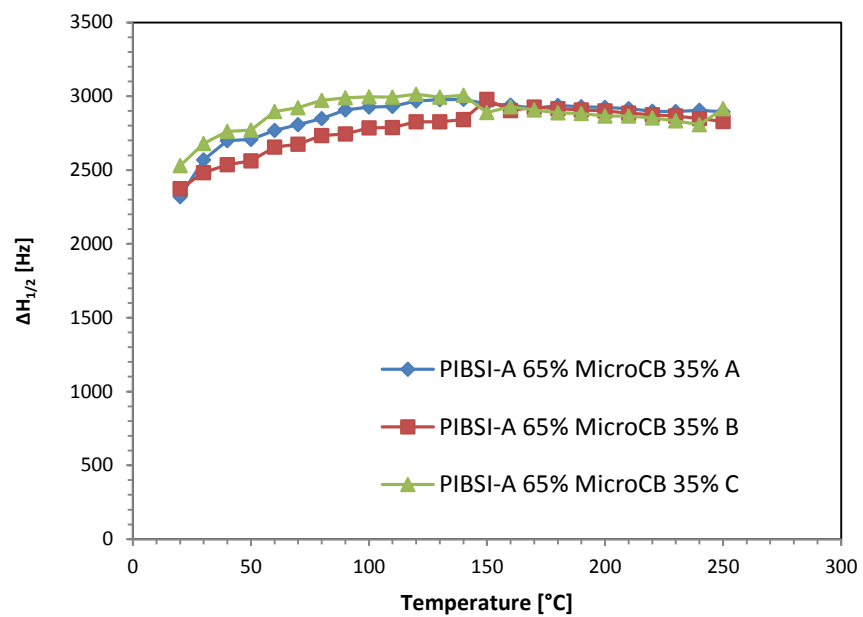


Figure E-3 Evolution of the ^1H NMR $\Delta H_{1/2}$ with temperature for 3 duplicate PIBSI-A (65 %) Micro CB (35 %) dispersions (A, B, C)

F $\Delta H_{1/2}$ measurements of various polymer MicroCB dispersions

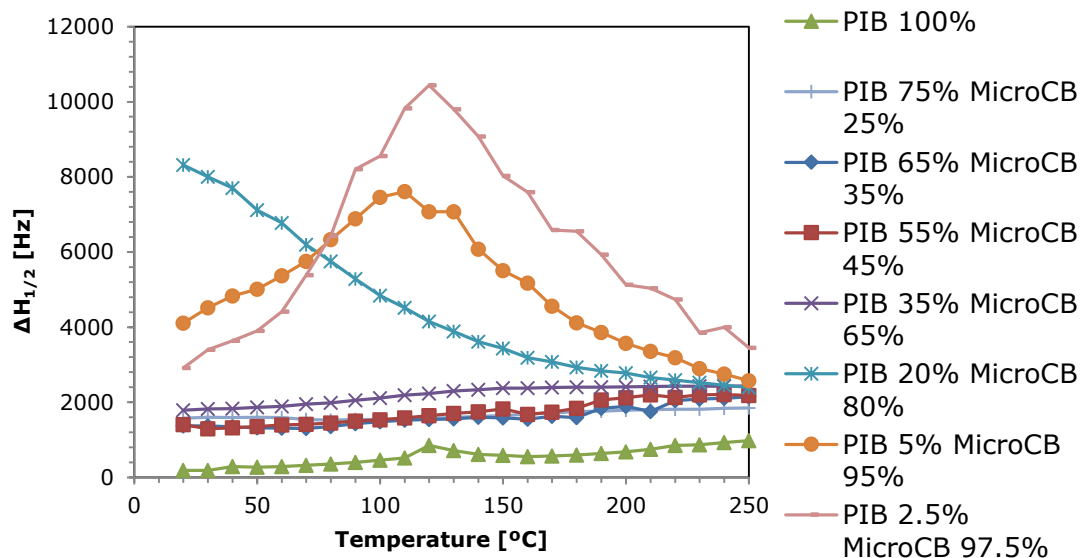


Figure F-1: Evolution of the 1H NMR $\Delta H_{1/2}$ with temperature for PIB (100 - 2.5 %) MicroCB (0 -97.5 %) dispersions

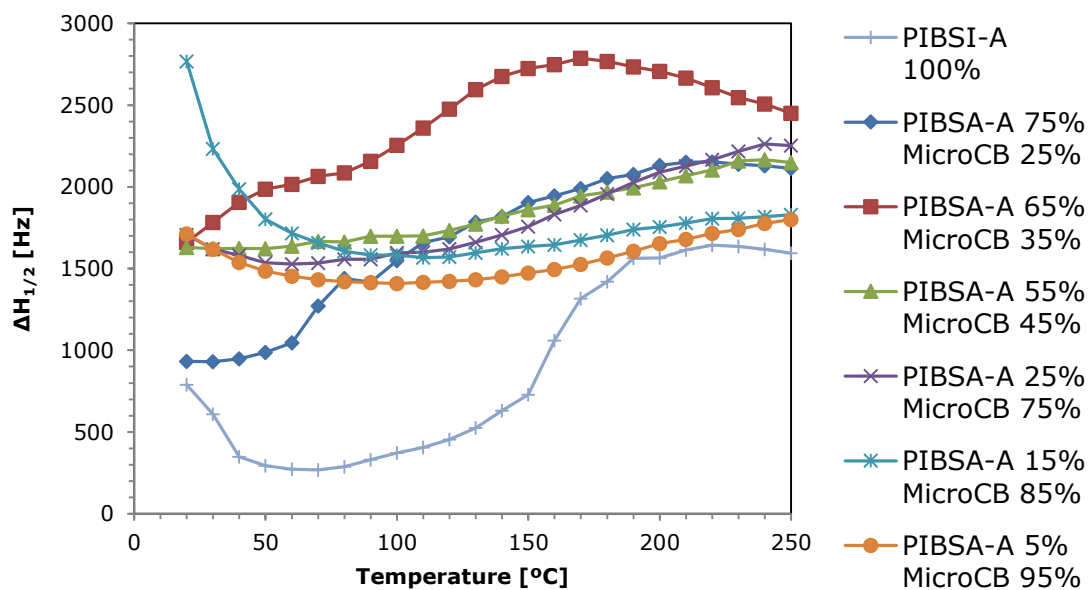


Figure F-2: Evolution of the 1H NMR $\Delta H_{1/2}$ with temperature for PIBSA-A (100 - 5 %) MicroCB (0 -95 %) dispersions

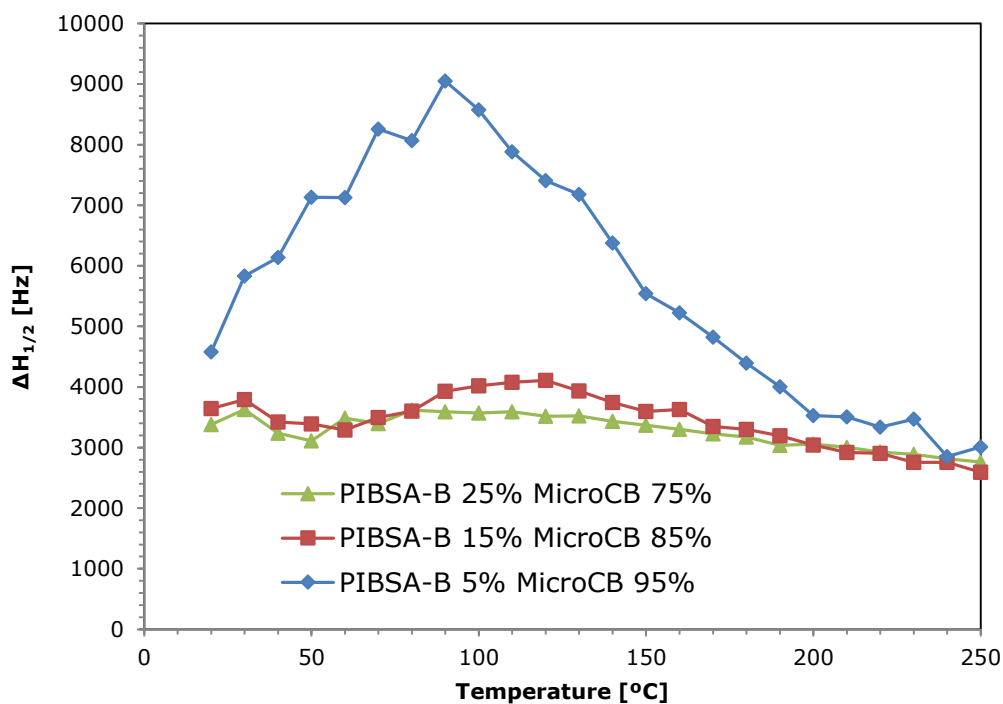


Figure F-3: Evolution of the ^1H NMR $\Delta H_{1/2}$ with temperature for PIBSA-B (25 – 5 %) MicroCB (75 -95 %) dispersions

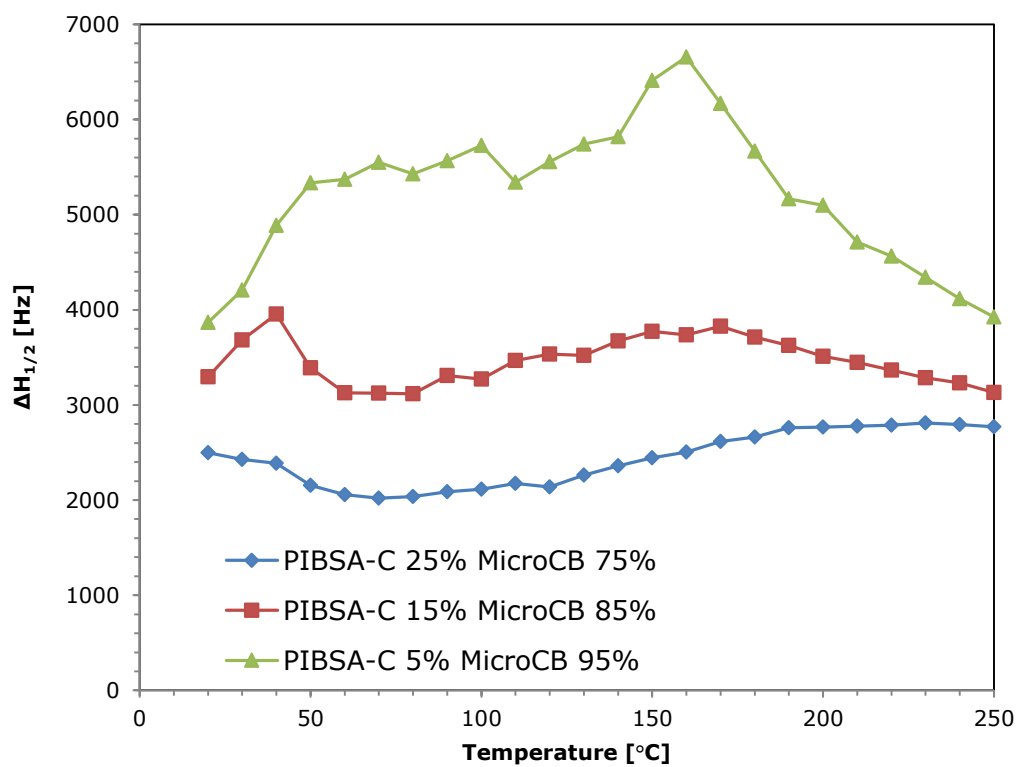


Figure F-4: Evolution of the ^1H NMR $\Delta H_{1/2}$ with temperature for PIBSA-C (25 – 5 %) MicroCB (75 - 95 %) dispersions

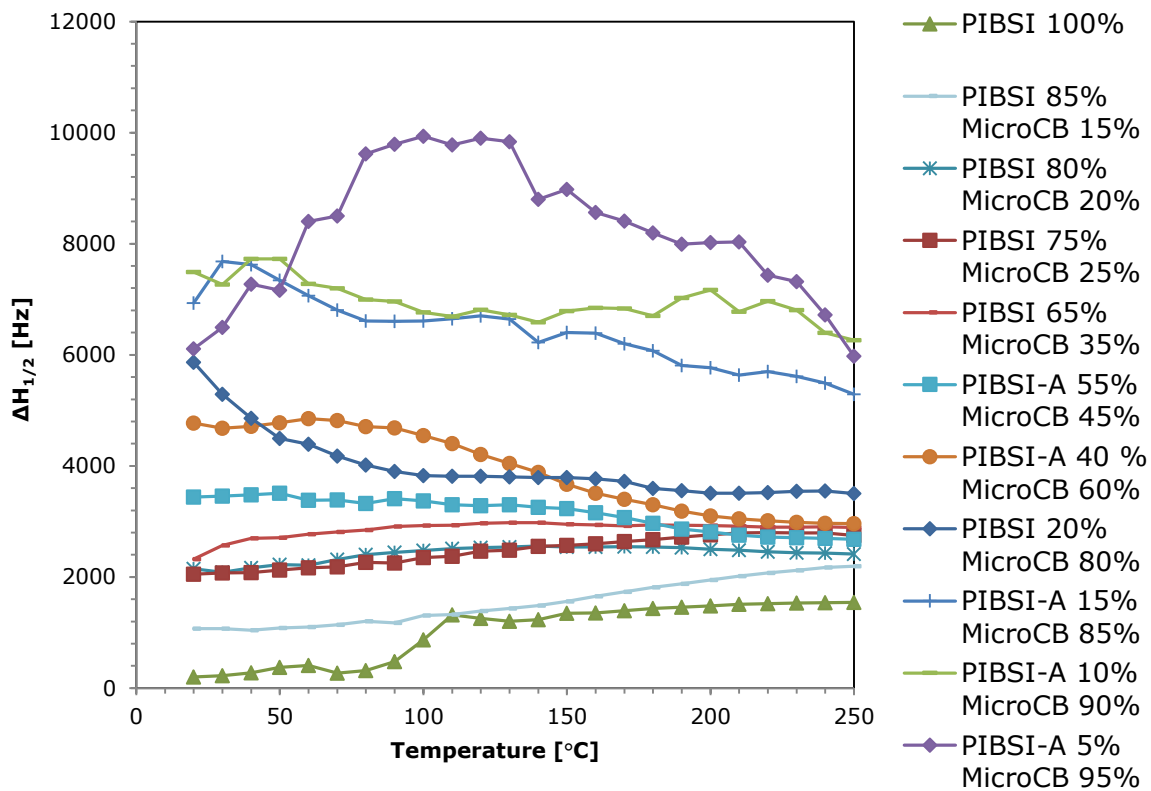


Figure F-5: Evolution of the ^1H NMR $\Delta H_{1/2}$ with temperature for PIBSI-A (100 - 5 %) MicroCB (0 - 95 %) dispersions

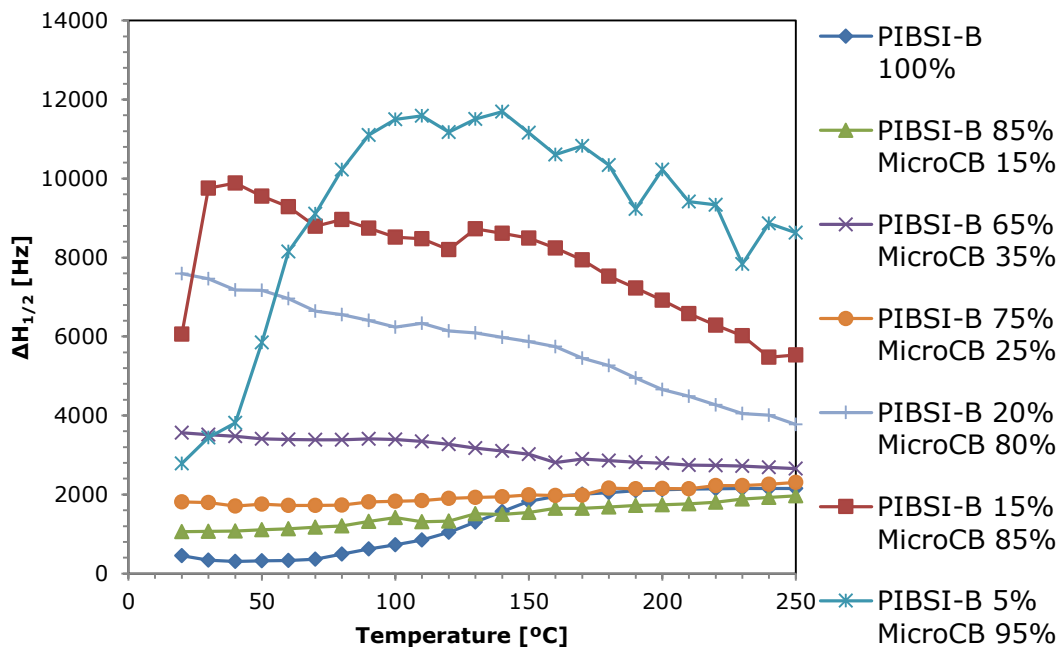


Figure F-6: Evolution of the ^1H NMR $\Delta H_{1/2}$ with temperature for PIBSI-B (100 - 5 %) MicroCB (0 - 95 %) dispersions

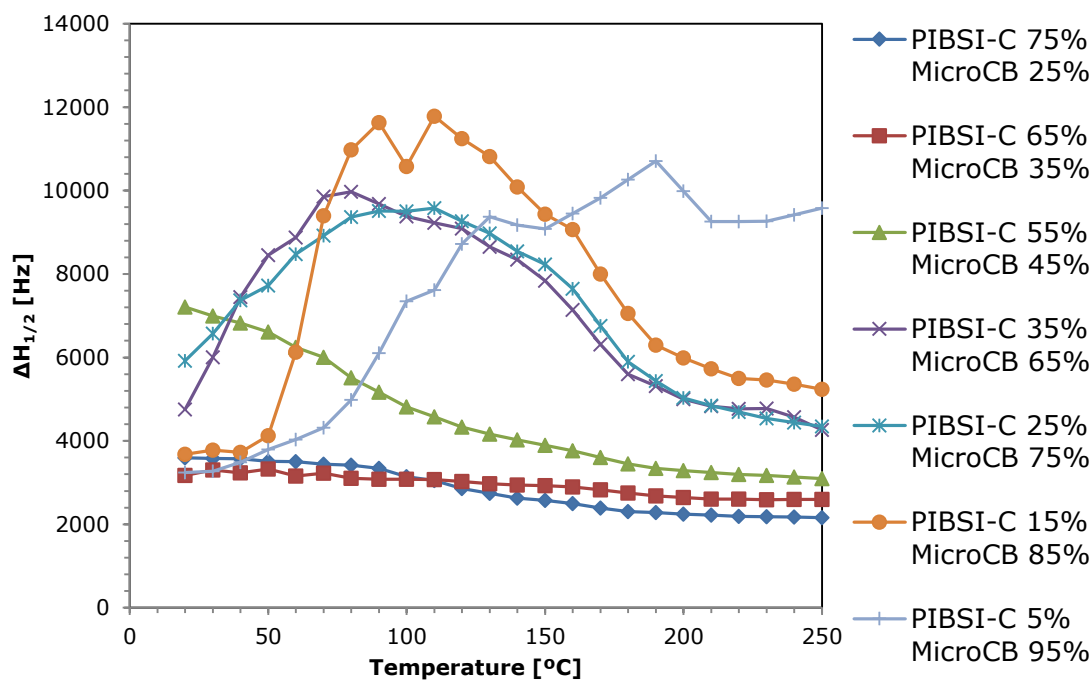


Figure F-7: Evolution of the ^1H NMR $\Delta H_{1/2}$ with temperature for PIBSI-C (75 - 5%) MicroCB (25 - 95%) dispersions

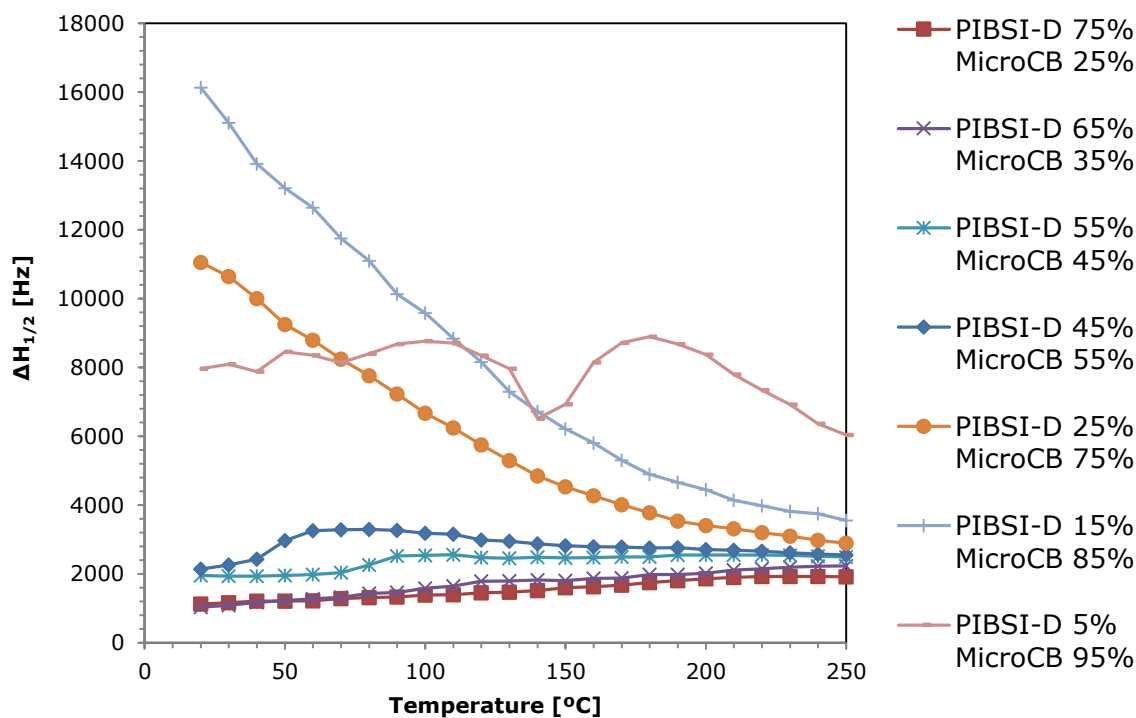


Figure F-8: Evolution of the ^1H NMR $\Delta H_{1/2}$ with temperature for PIBSI-D (75 - 5%) MicroCB (25 - 95%) dispersions

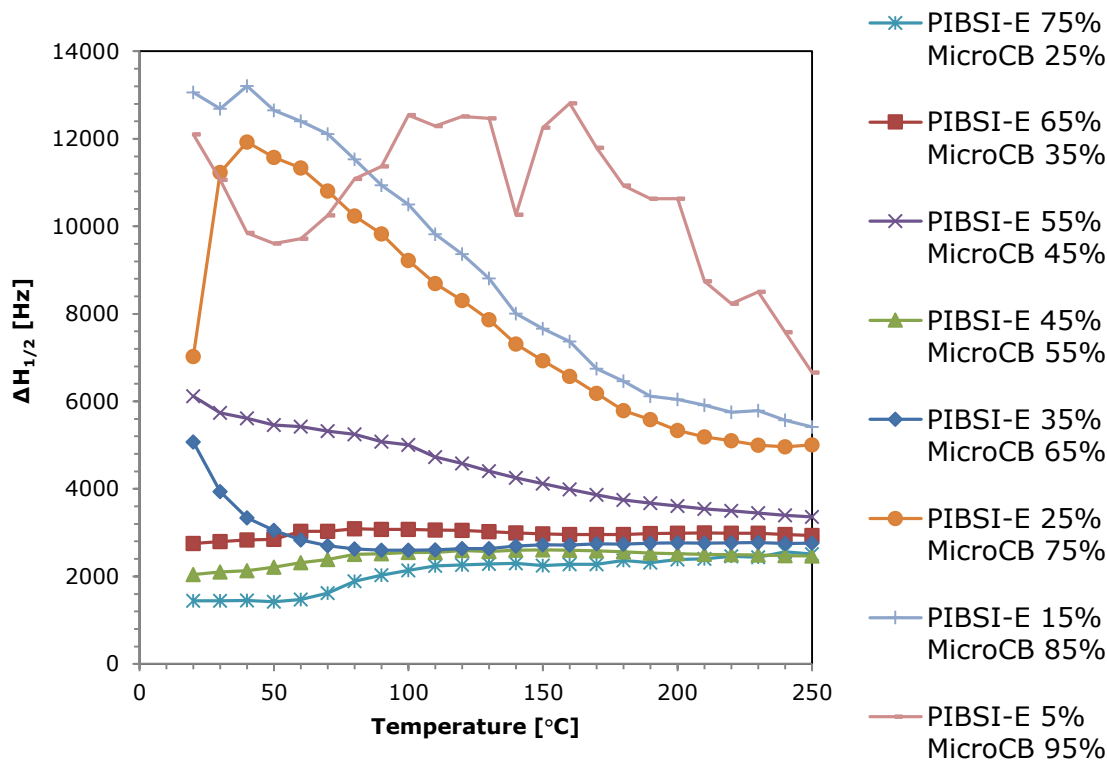


Figure F-9: Evolution of the ^1H NMR $\Delta H_{1/2}$ with temperature for PIBSI-E (75 - 5 %) MicroCB (25 - 95 %) dispersions

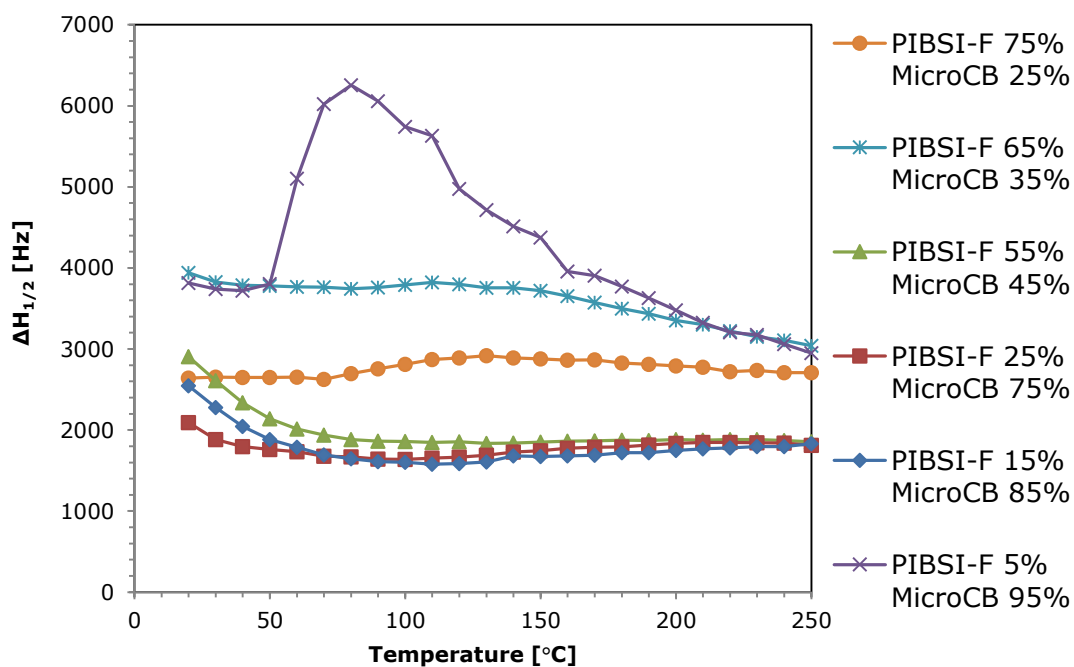


Figure F-10: Evolution of the ^1H NMR $\Delta H_{1/2}$ with temperature for PIBSI-F (75 - 5 %) MicroCB (25 - 95 %) dispersions

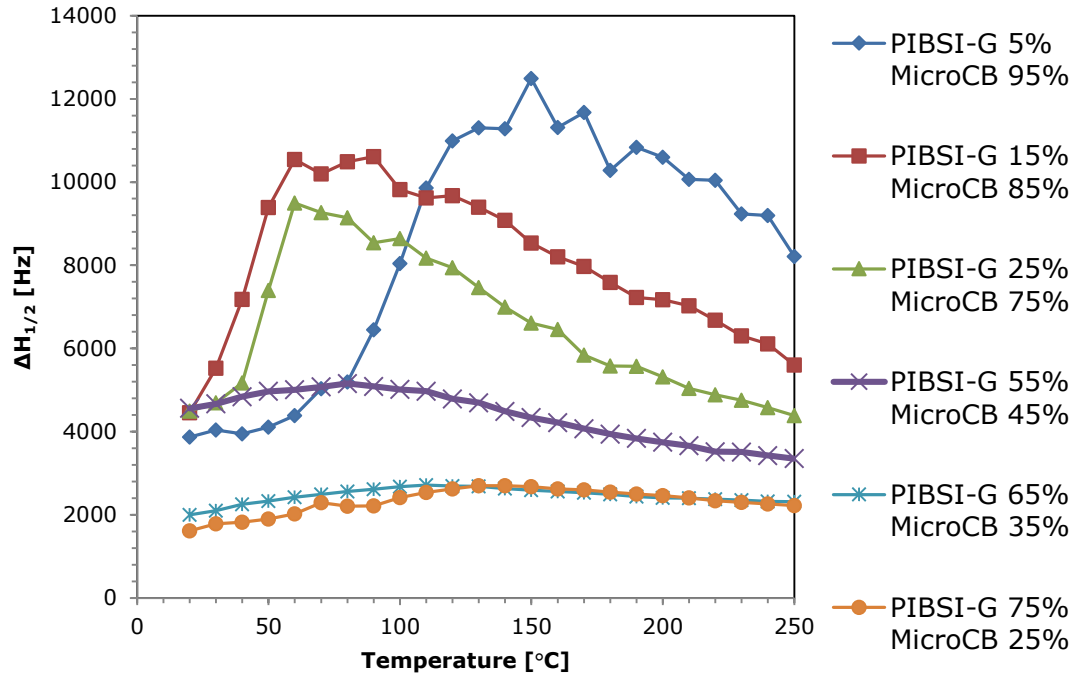


Figure F-11: Evolution of the ^1H NMR $\Delta H_{1/2}$ with temperature for PIBSI-G (75 - 5%) MicroCB (25 - 95%) dispersions

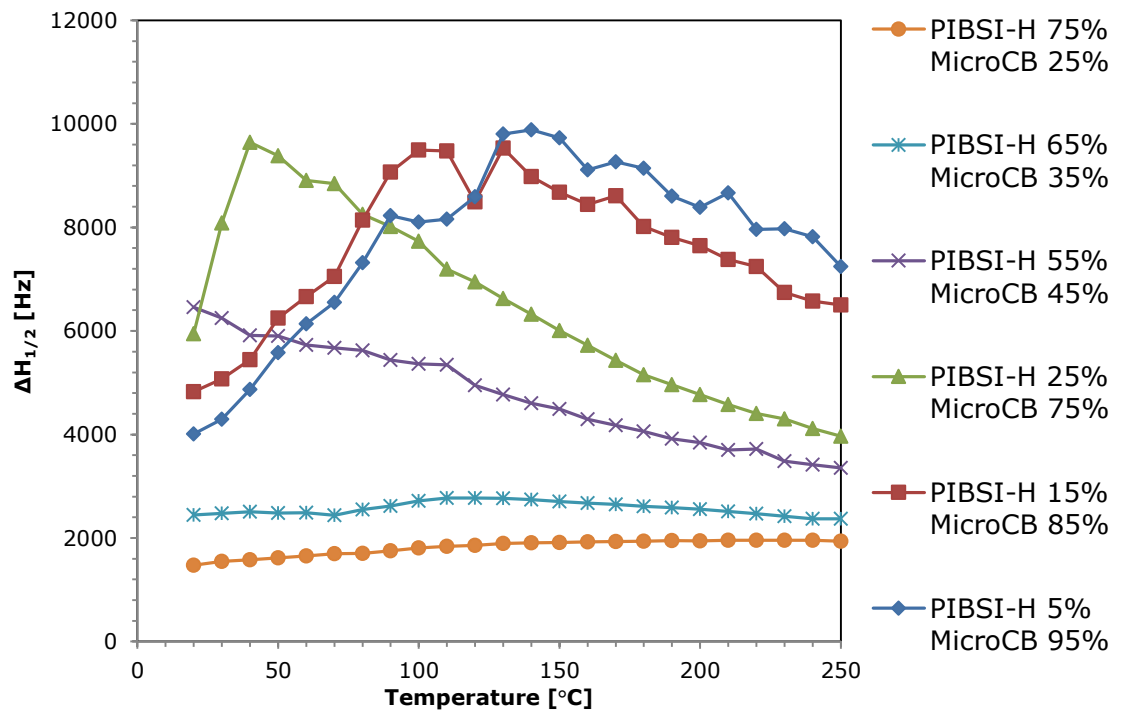


Figure F-12: Evolution of the ^1H NMR $\Delta H_{1/2}$ with temperature for PIBSI-H (75 - 5%) MicroCB (25 - 95%) dispersions.

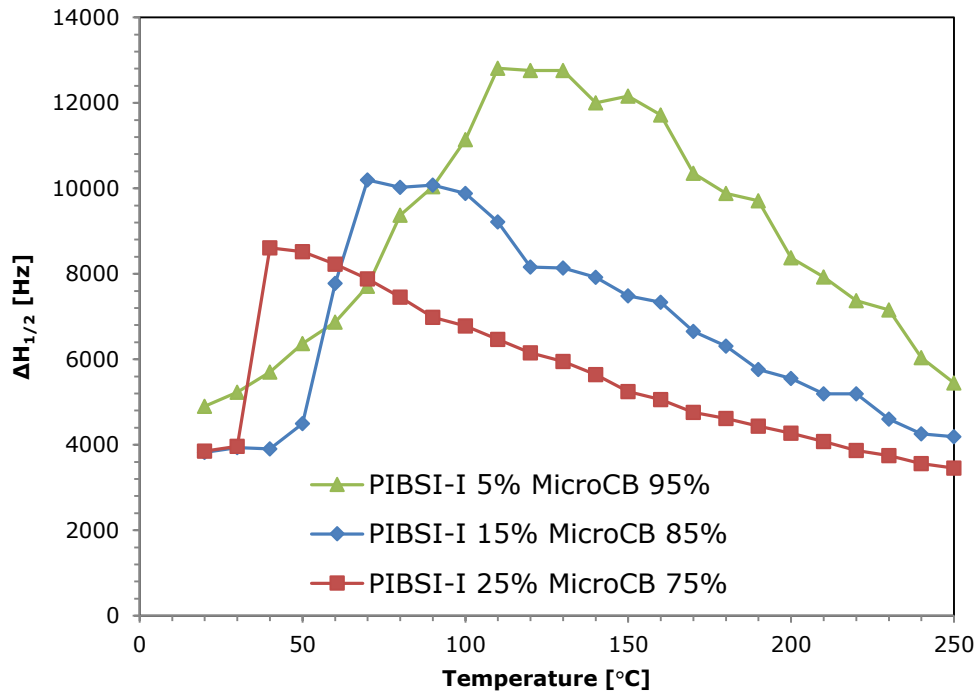


Figure F-13: Evolution of the ^1H NMR $\Delta H_{1/2}$ with temperature for PIBSI-I (25 – 5 %) MicroCB (75 - 95 %) dispersions

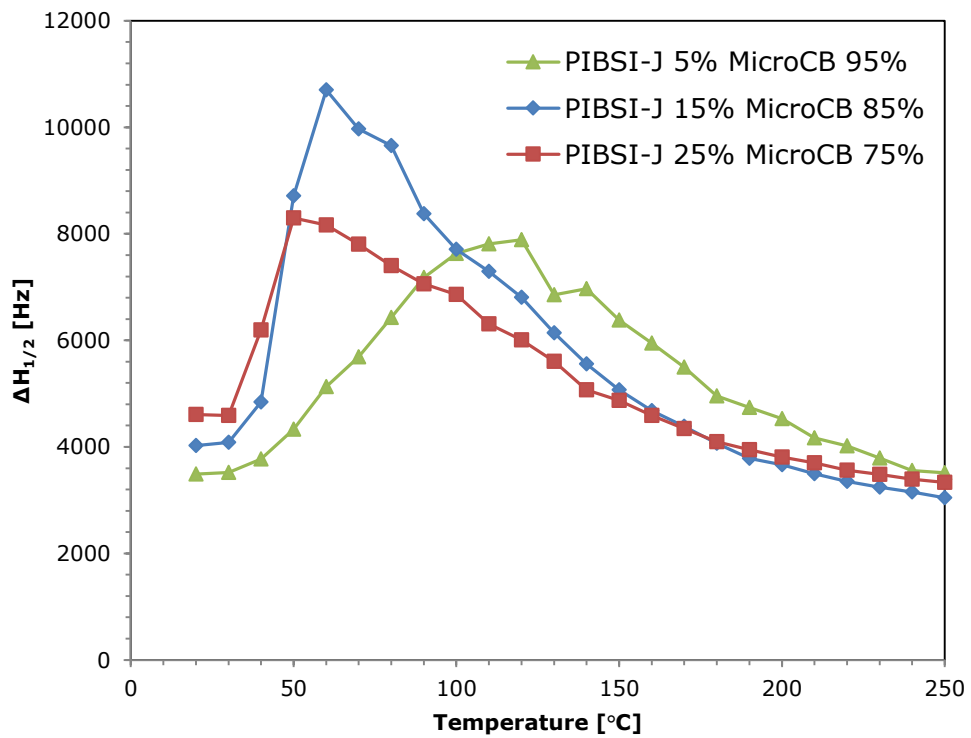


Figure F-14: Evolution of the ^1H NMR $\Delta H_{1/2}$ with temperature for PIBSI-J (25 – 5 %) MicroCB (75 - 95 %) dispersions

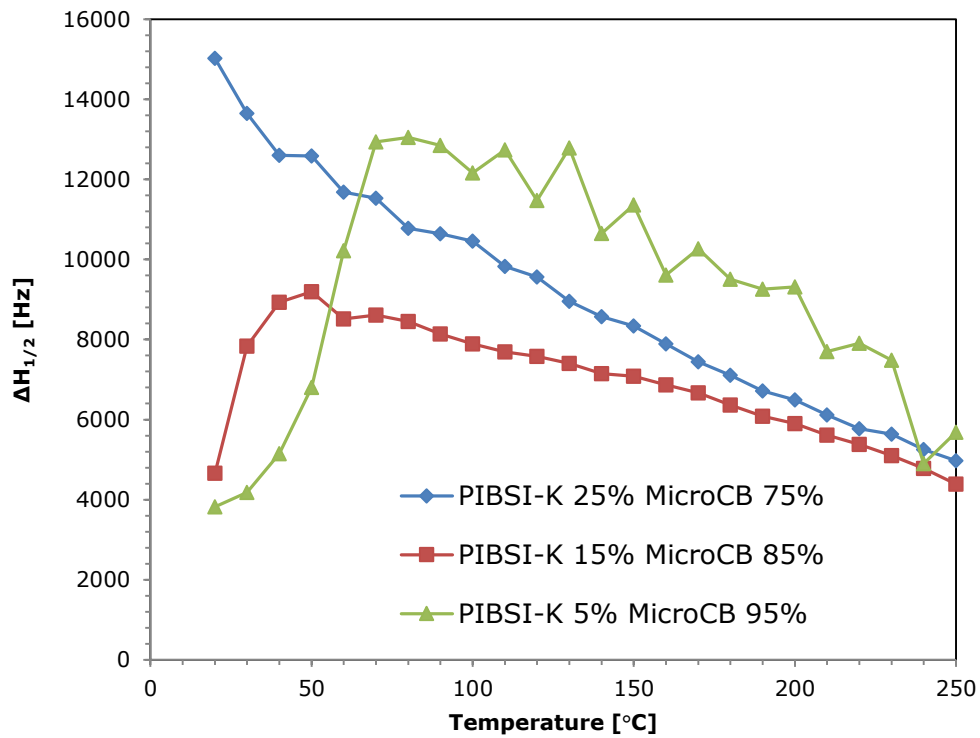


Figure F-15: Evolution of the ^1H NMR $\Delta H_{1/2}$ with temperature for PIBSI-K (25 – 5 %) MicroCB (75 - 95 %) dispersions

G $\Delta H_{1/2}$ measurements of PIBSI-H and PIBSI-F dispersions with various carbons

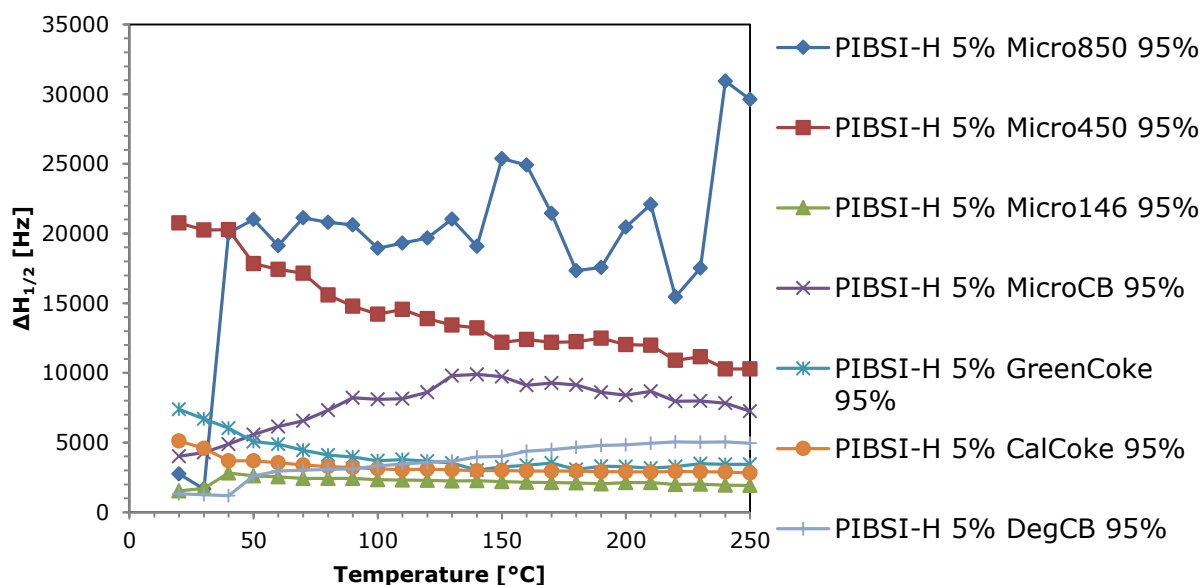


Figure G-1: Evolution of the ^1H NMR $\Delta H_{1/2}$ with temperature for various PIBSI-H (5 %) carbon (95 %) dispersions

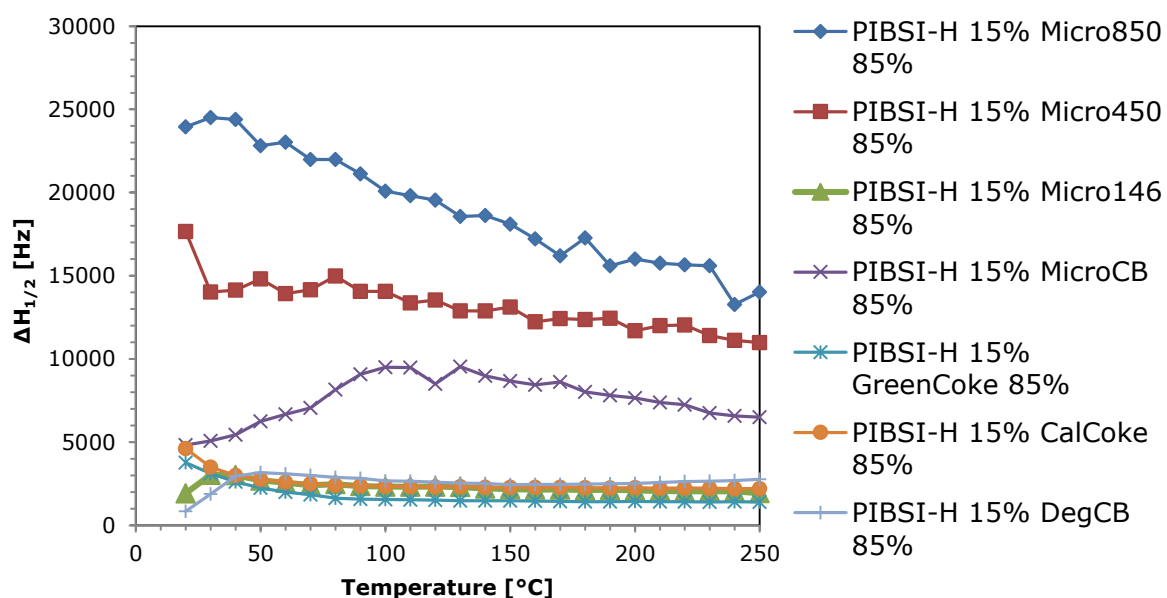


Figure G-2: Evolution of the ^1H NMR $\Delta H_{1/2}$ with temperature for various PIBSI-H (15 %) carbon (85 %) dispersions

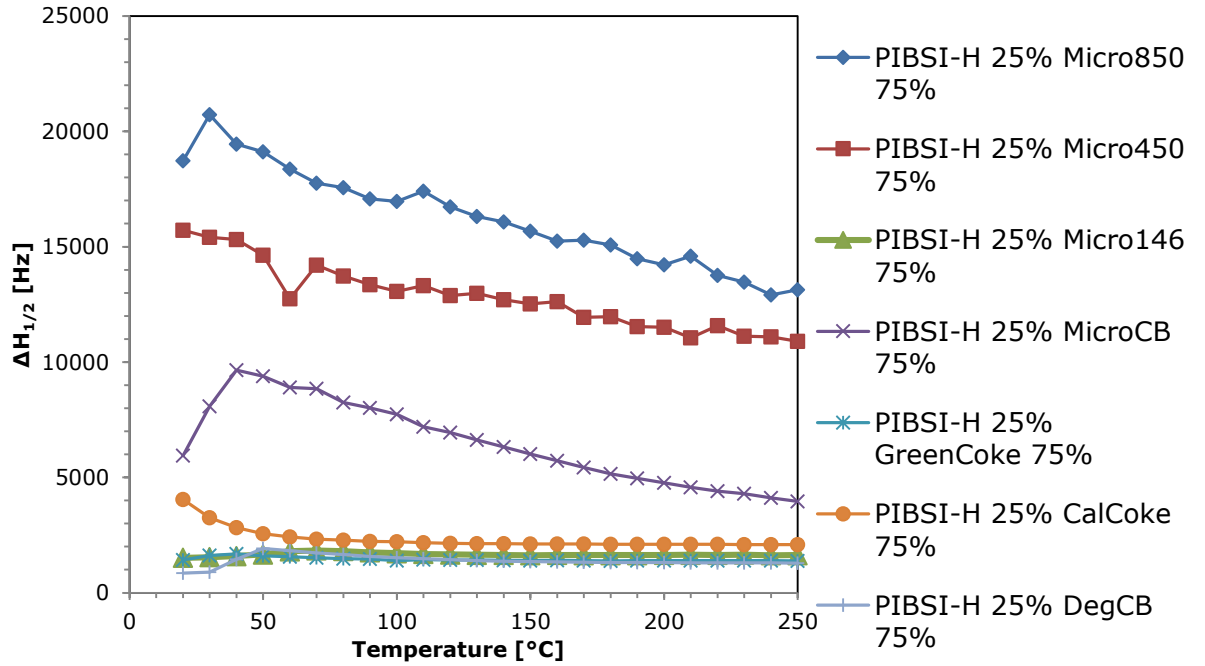


Figure G-3: Evolution of the ^1H NMR $\Delta H_{1/2}$ with temperature for various PIBSI-H (25 %) carbon (75 %) dispersions

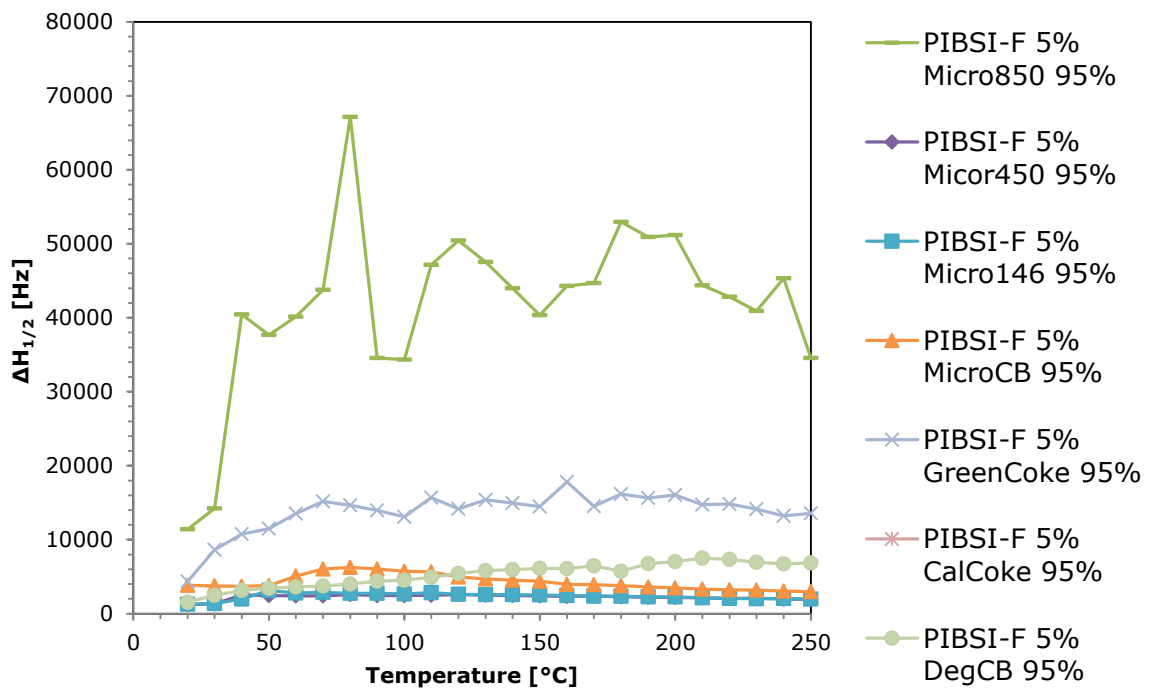


Figure G-4: Evolution of the ^1H NMR $\Delta H_{1/2}$ with temperature for various PIBSI-F (5 %) carbon (95 %) dispersions

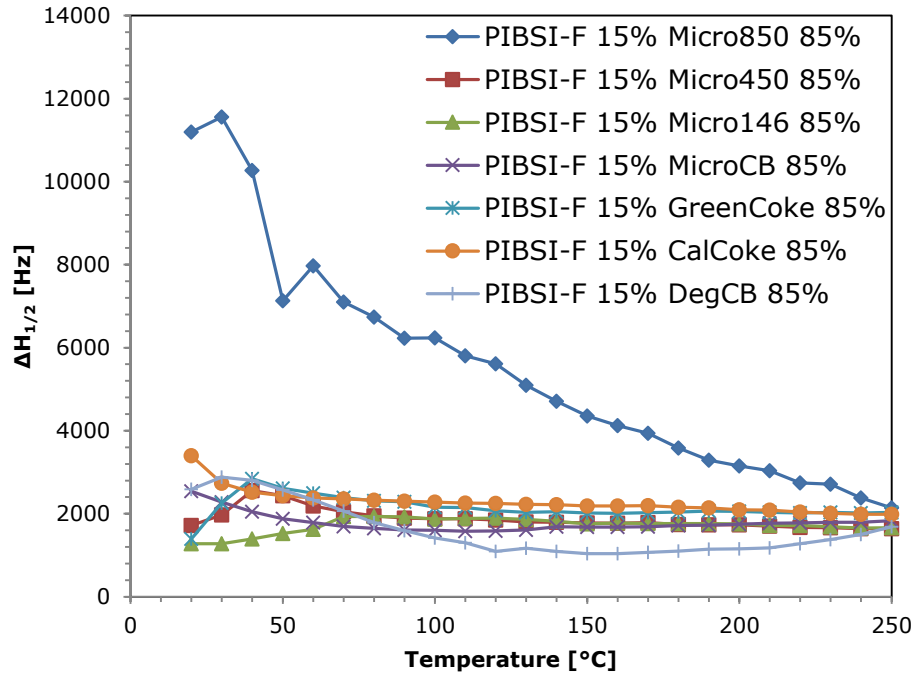


Figure G-5: Evolution of the ^1H NMR $\Delta H_{1/2}$ with temperature for various PIBSI-F (15 %) carbon (85 %) dispersions

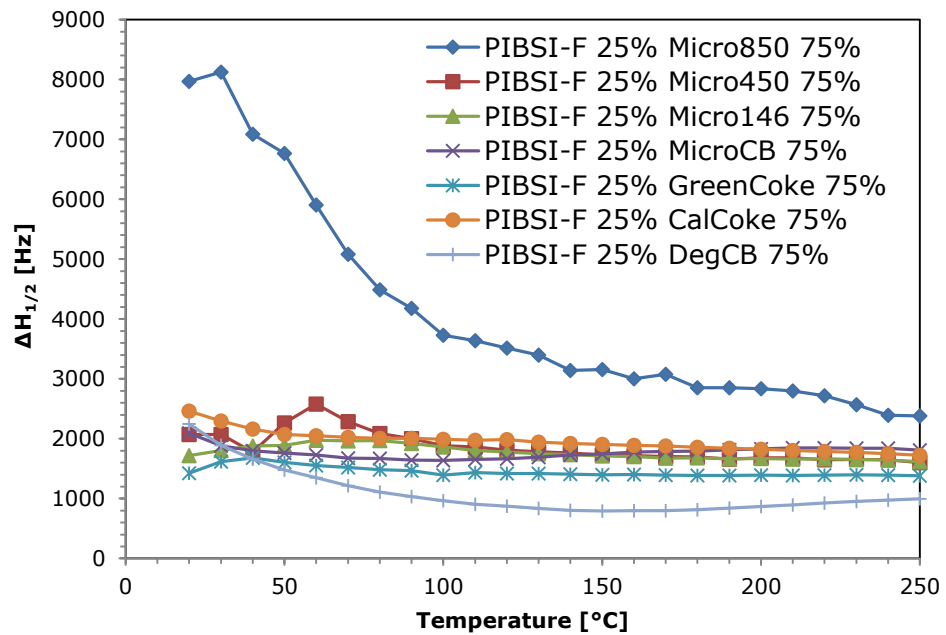


Figure G-6: Evolution of the ^1H NMR $\Delta H_{1/2}$ with temperature for various PIBSI-F (25 %) carbon (75 %) dispersions

H $\Delta H_{1/2}$ measurements for various polymer Micro850 dispersions

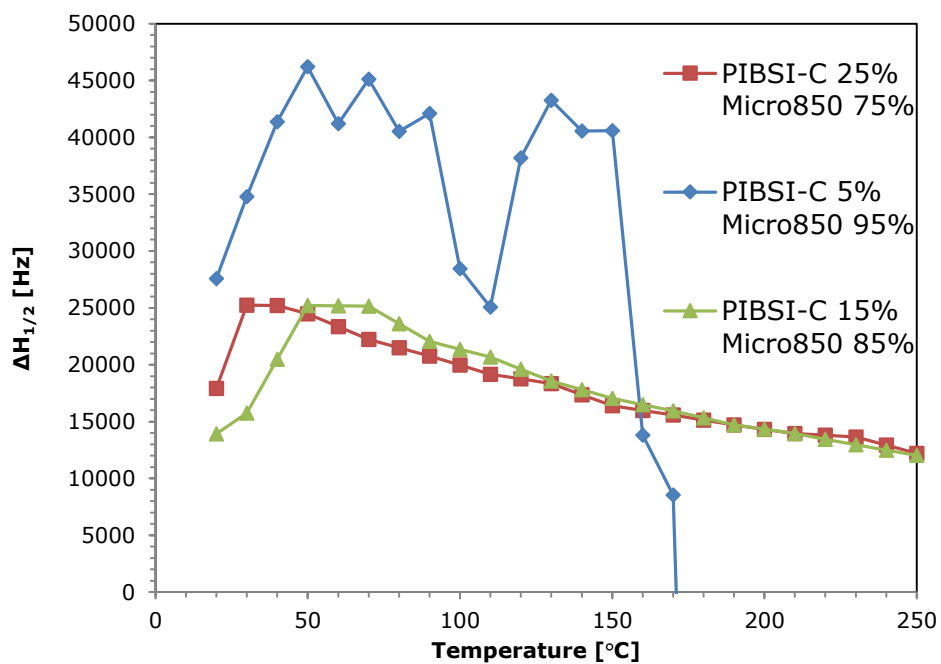


Figure H-1: Evolution of the ^1H NMR $\Delta H_{1/2}$ with temperature for PIBSI-C (25 – 5 %) Micro850 (75 - 95 %) dispersions

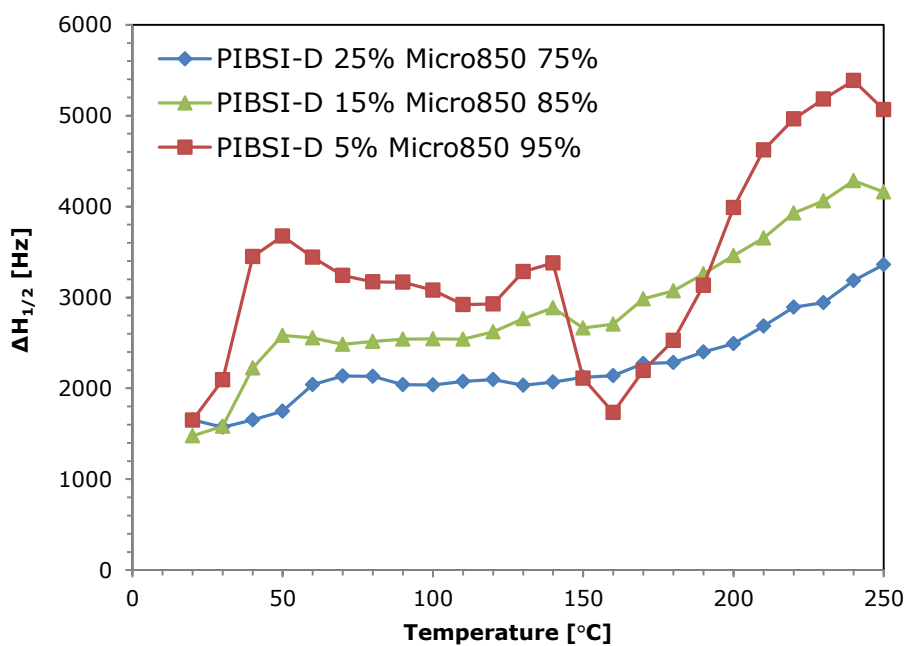


Figure H-2: Evolution of the ^1H NMR $\Delta H_{1/2}$ with temperature for PIBSI-D (25 – 5 %) Micro850 (75 - 95 %) dispersions

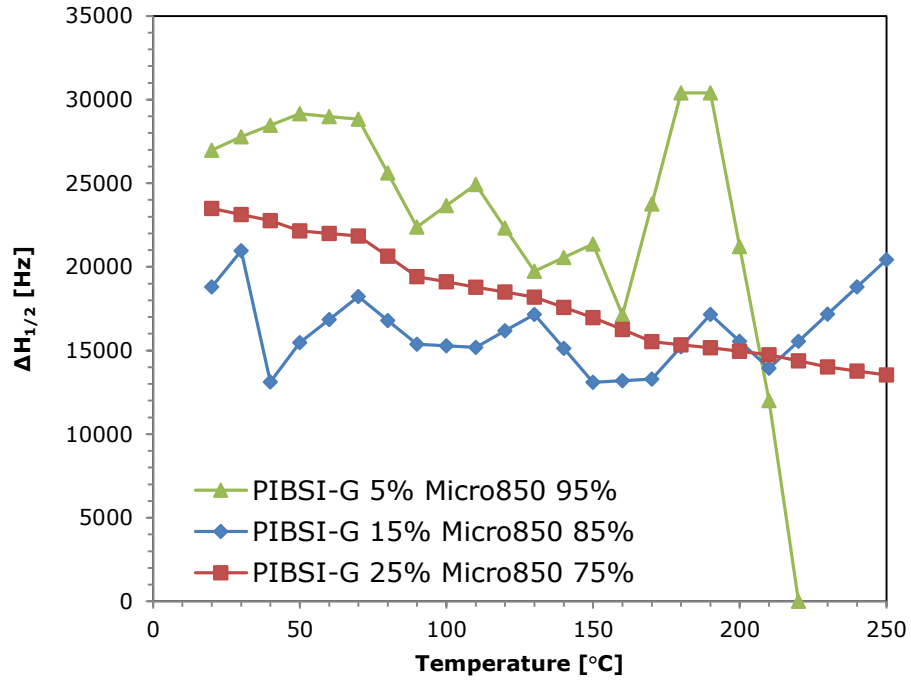


Figure H-3: Evolution of the ^1H NMR $\Delta H_{1/2}$ with temperature for PIBSI-G (25 – 5 %) Micro850 (75 - 95 %) dispersions

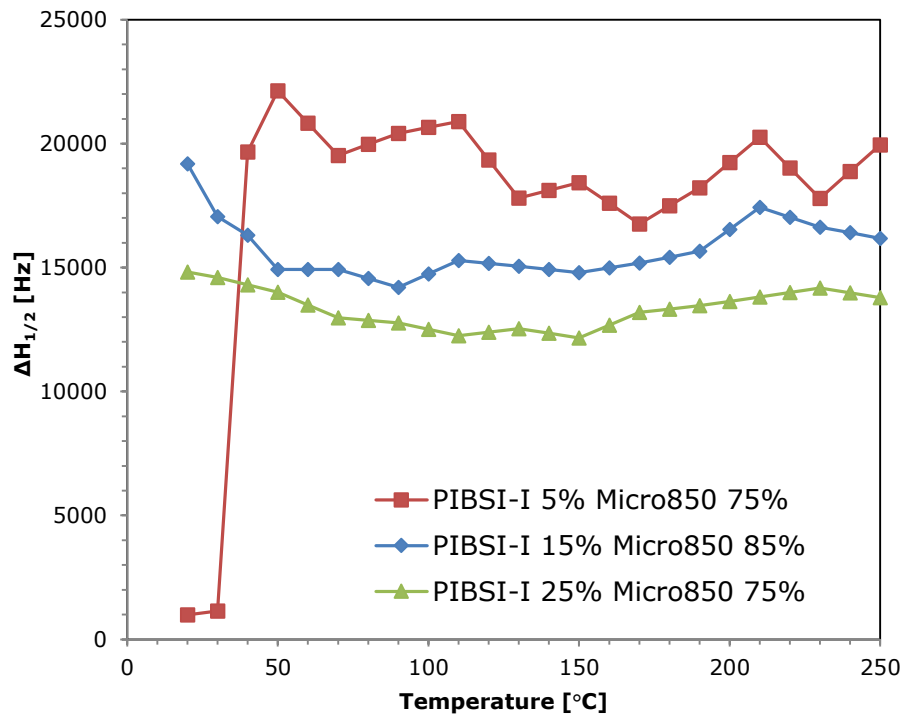


Figure H-4: Evolution of the ^1H NMR $\Delta H_{1/2}$ with temperature for PIBSI-I (25 – 5 %) Micro850 (75 - 95 %) dispersions

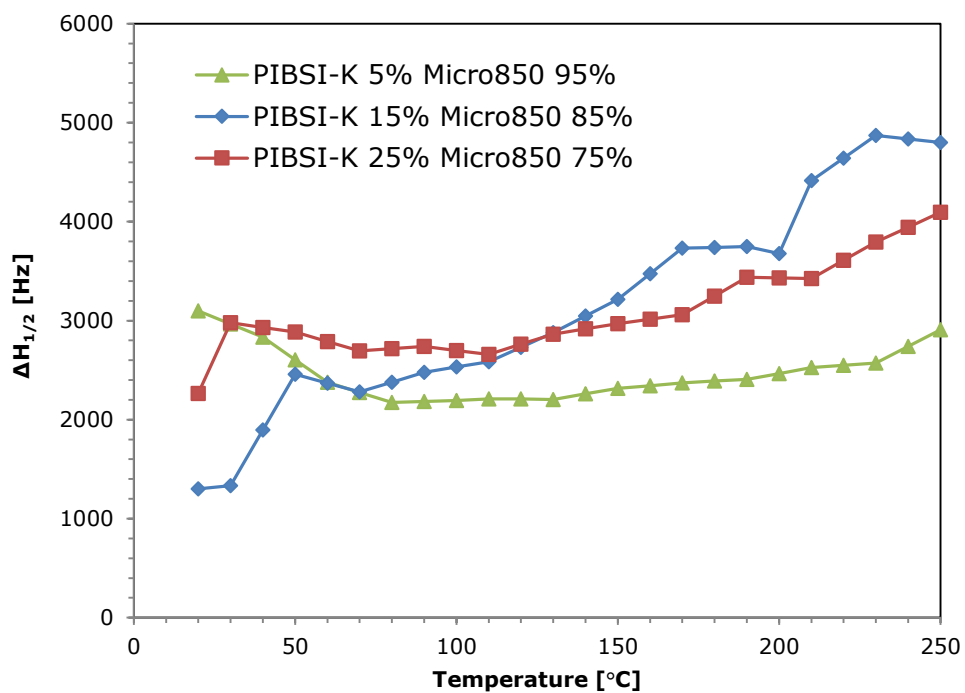


Figure H-5: Evolution of the ^1H NMR $\Delta H_{1/2}$ with temperature for PIBSI-K (25 – 5 %) Micro850 (75 - 95 %) dispersions

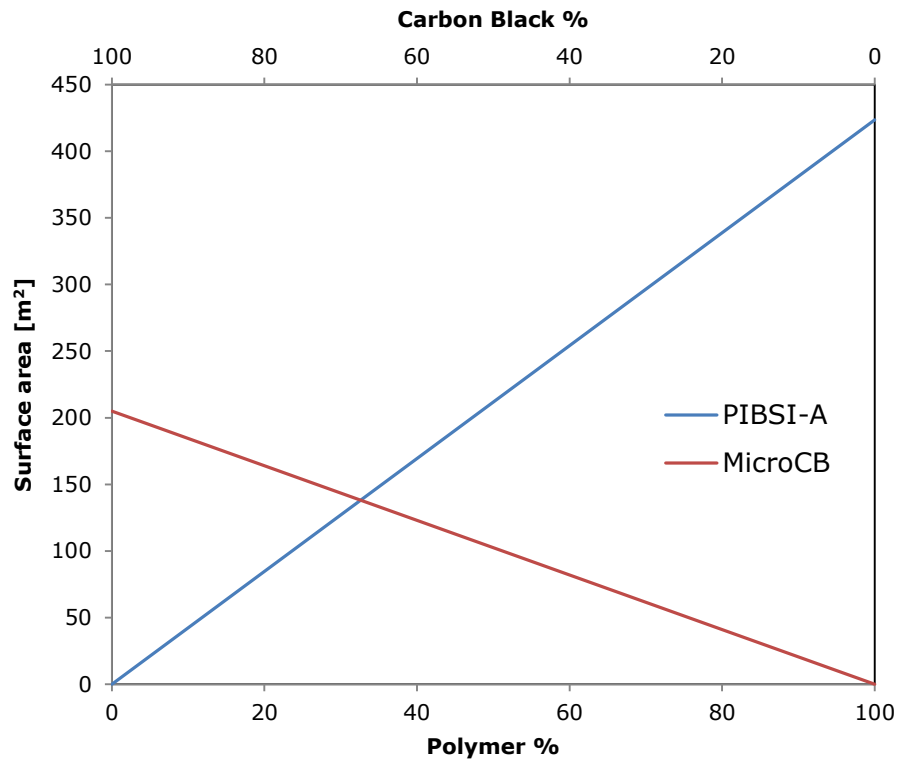
I Approximate calculation of PIBSI-A monolayer coverage of MicroCB

For a 100 % PIBSI sample (1.0 g PIBSI, 0 g carbon)

Number of PIBSI molecules = (Mass/ M_n of PIBSI-A) $\times N_A$

Total polymer surface area = Number of molecules \times calculated polar surface area
(PSA) of PIBSI head group

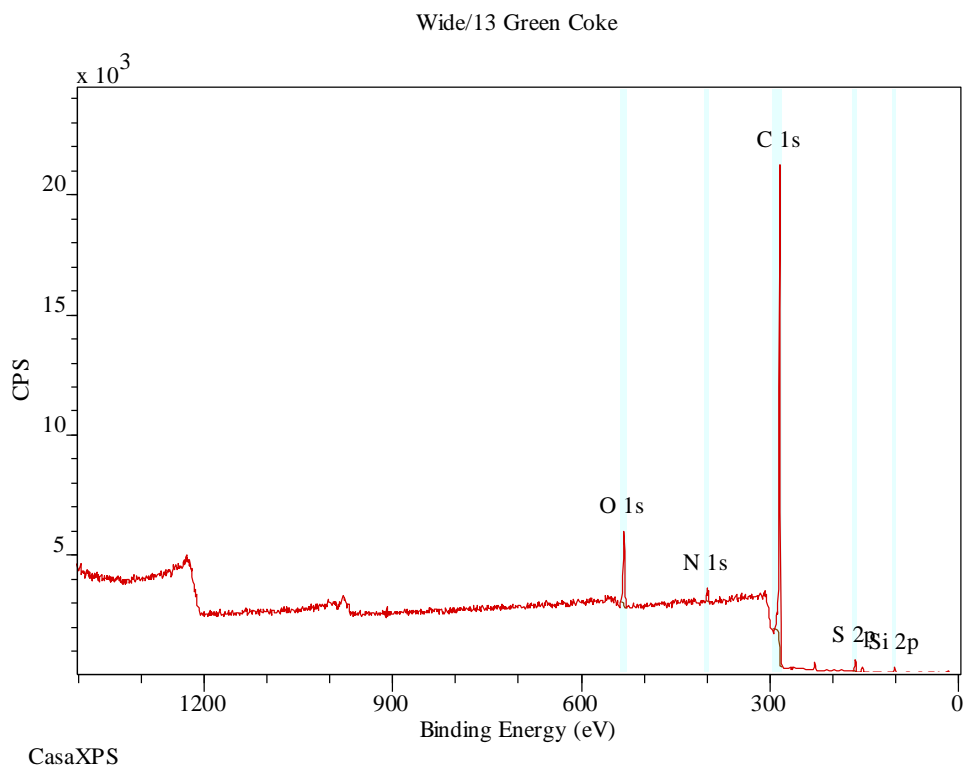
Mass of Polymer (g)	Polymer M_n (g/mol)	Polymer PSA (m^2)	No. molecules	Total Polymer Surface area (m^2)	Mass Carbon black (g)	CB surface area (m^2/g)	Total Surface area (m^2)
1.0	1253	8.8E-19	4.8E+20	423.7	0	205	0.0
0.9			4.3E+20	381.4	0.1		20.5
0.8			3.9E+20	339.0	0.2		41.0
0.7			3.4E+20	296.6	0.3		61.5
0.6			2.9E+20	254.2	0.4		82.0
0.5			2.4E+20	211.9	0.5		102.5
0.4			1.9E+20	169.5	0.6		123.0
0.3			1.4E+20	127.1	0.7		143.5
0.2			9.6E+19	84.8	0.8		164.0
0.1			4.8E+19	42.4	0.9		184.5
0.0			0.0	0.0	1.0		205.0



Theoretical calculation of PIBSI-A monolayer coverage of MicroCB therefore occurs at approx. 30 % polymer loading. Calculation highly approximate due to porosity of carbon black, particle size distribution and other effects).

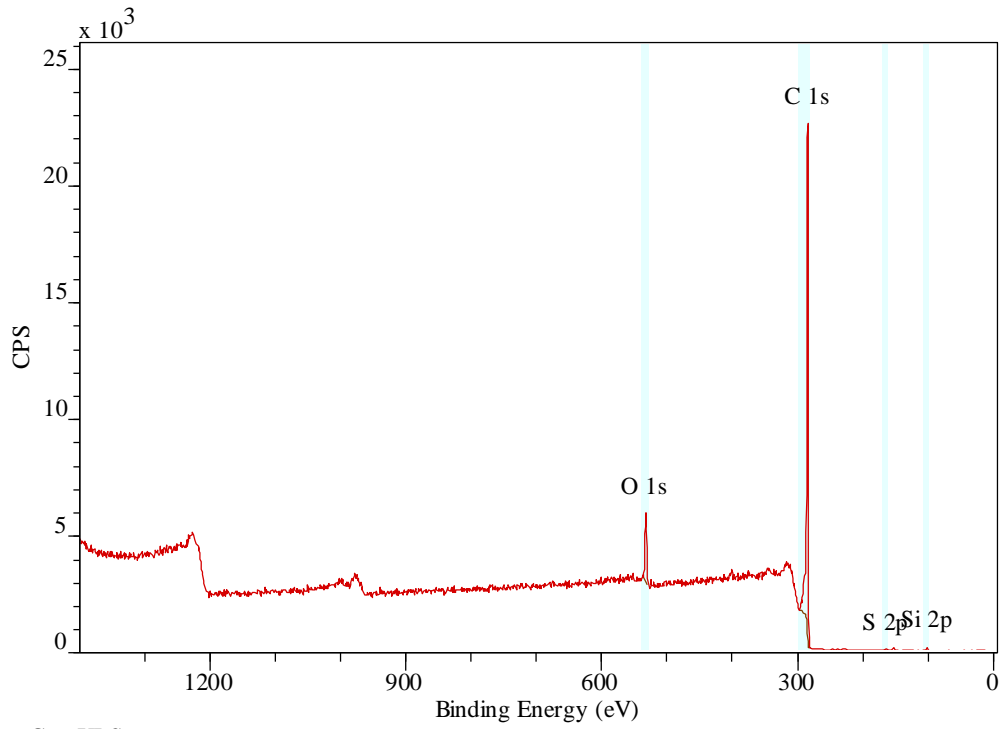
J XPS analysis results of carbon samples

Results in tables represent average of 3 analysis.



Name	Position	FWHM	Area	% Conc	% Mass Conc	Mass
O 1s	532.2	2.5	1645.3	5.3	6.6	16.0
N 1s	400.0	2.3	248.5	1.3	1.4	14.0
C 1s	284.5	1.8	10198.8	91.2	86.5	12.0
S 2p	164.0	2.2	309.1	1.2	2.9	32.1
Si 2p	102.0	1.8	151.3	1.1	2.5	28.1

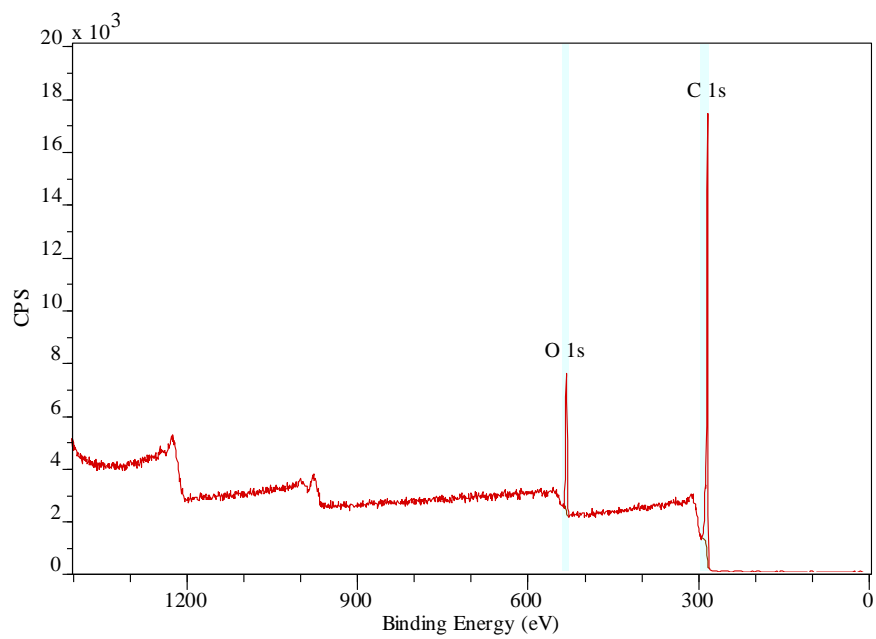
Wide/13 Calcined Coke



CasaXPS

Name	Position	FWHM	Area	% Conc	% Mass Conc	Mass
O 1s	532.0	3.0	1713.5	4.6	6.0	16.0
C 1s	284.3	1.9	12416.5	94.4	91.9	12.0
S 2p	164.2	2.1	37.3	0.1	0.3	32.1
Si 2p	101.8	2.0	124.4	0.8	1.8	28.1

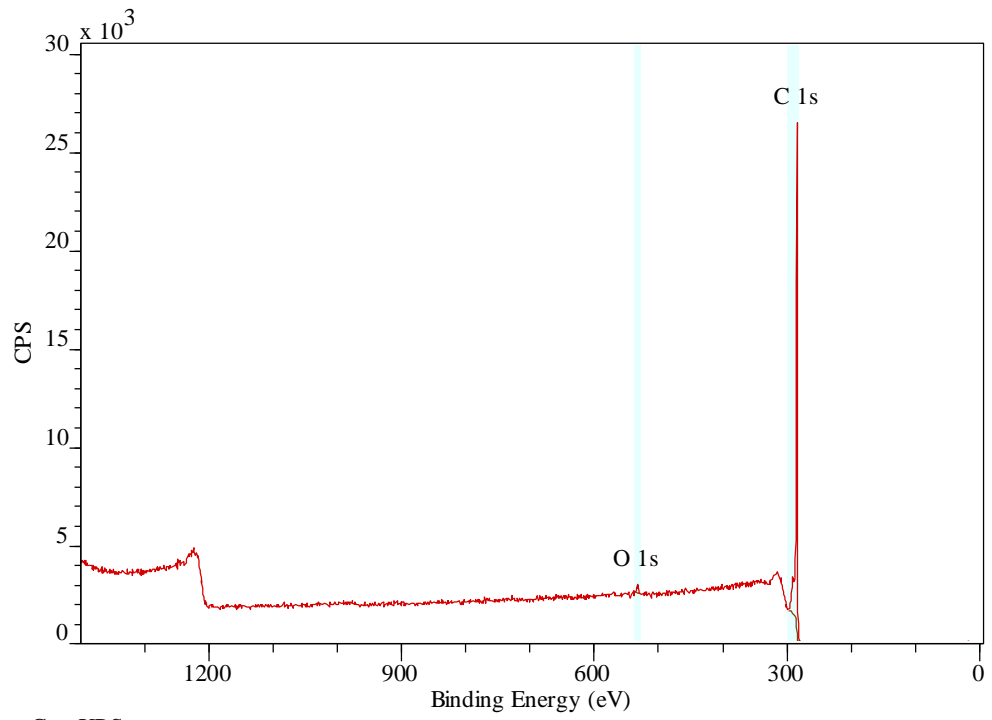
Wide/13 Carbon Black



CasaXPS

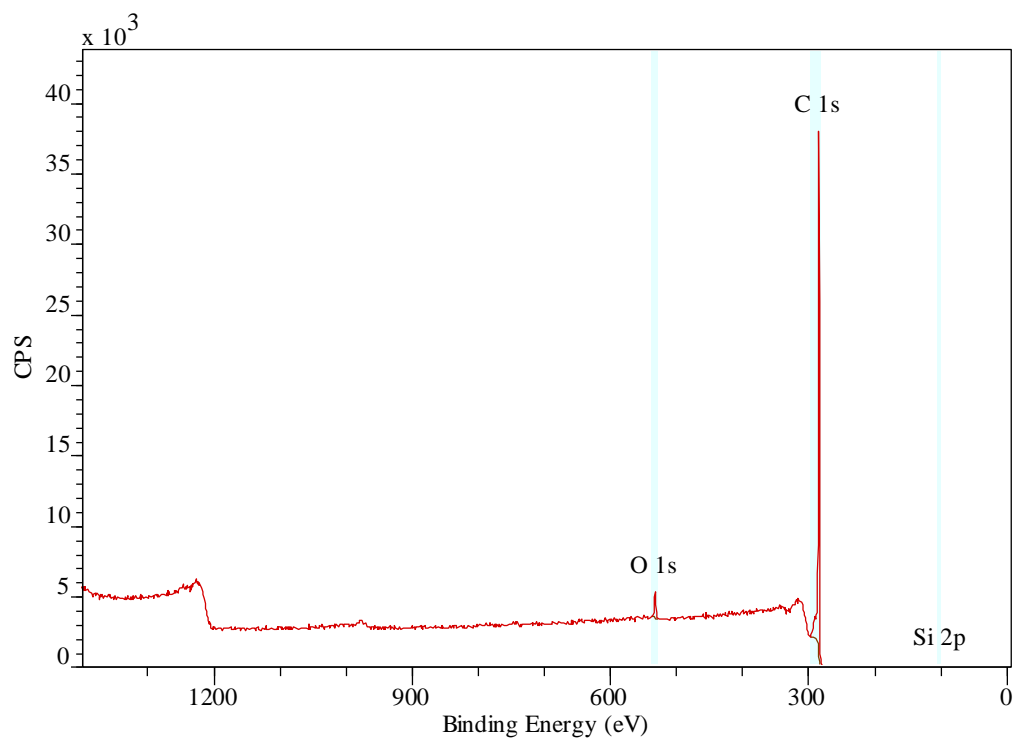
Name	Position	FWHM	Area	% Conc	% Mass Conc	Mass
O 1s	532.7	3.1	3437.0	10.7	13.8	16.0
C 1s	284.7	2.1	10235.5	89.3	86.2	12.0

Wide/13 MicroCB



CasaXPS

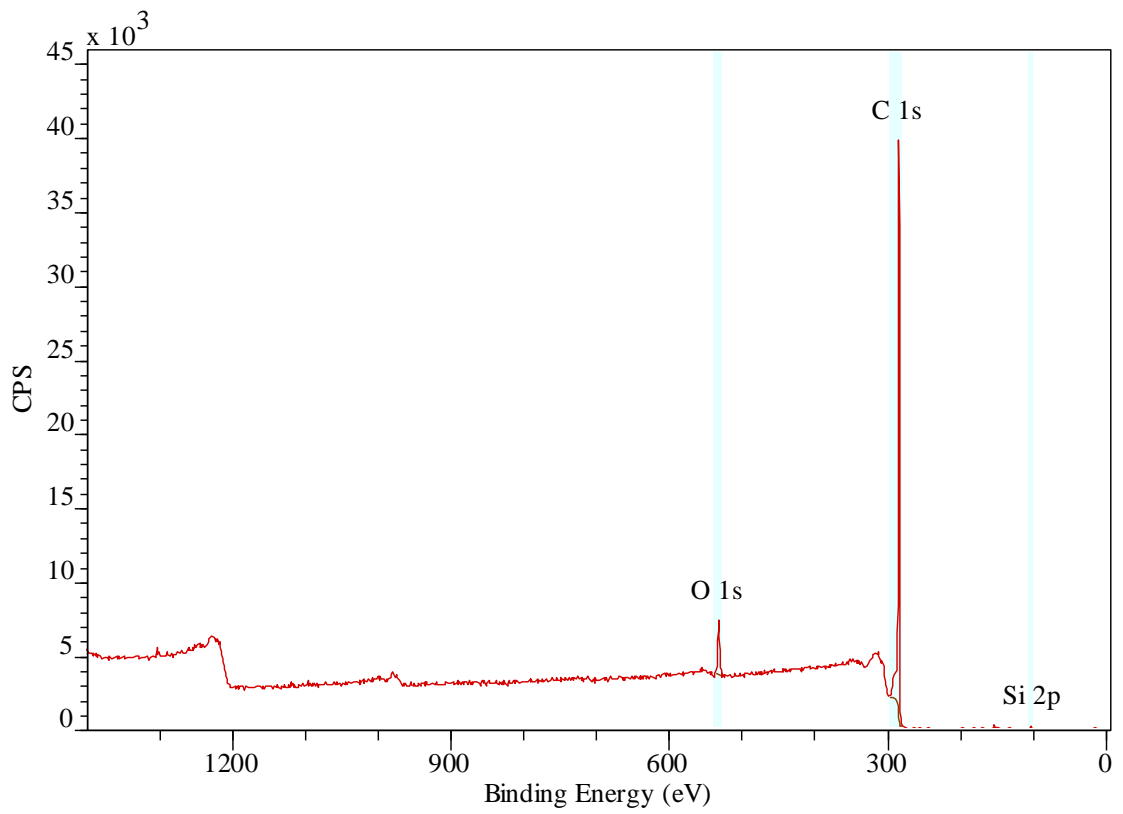
Name	Position	FWHM	Area	% Conc	% Mass Conc	Mass
O 1s	532.5	2.8	308.1	0.9	1.2	16.0
C 1s	284.5	1.5	12705.0	99.1	98.9	12.0



CasaXPS

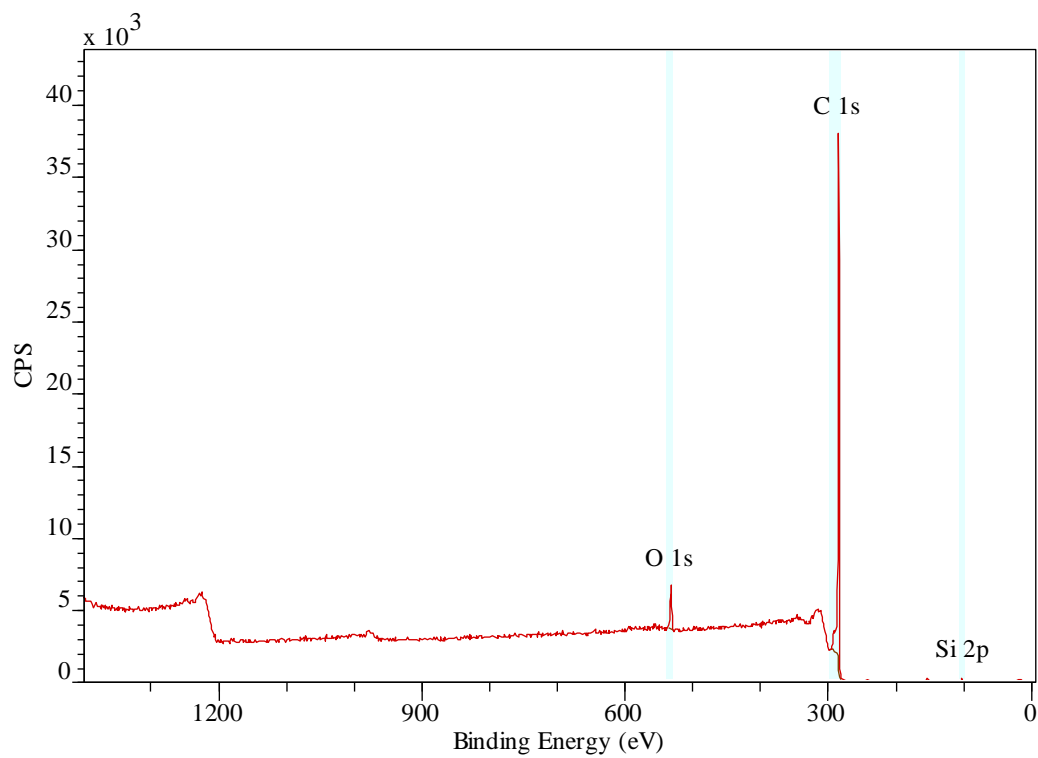
Name	Position	FWHM	Area	% Conc	% Mass Conc	Mass
O 1s	532.2	2.8	1016.7	2.2	2.9	16.0
C 1s	284.7	1.4	16038.6	97.4	96.2	12.0
Si 2p	101.5	1.9	75.5	0.4	0.9	28.1

Wide/13 Micro146



CasaXPS

Name	Position	FWHM	Area	%Conc	% Mass Conc	Mass
O 1s	532.3	2.6	2008.6	3.7	4.8	16.0
C 1s	284.8	1.4	18430.4	95.4	93.2	12.0
Si 2p	102.3	2.3	193.7	0.8	1.9	28.1



Name	Position	FWHM	Area	% Conc	% Mass Conc	Mass
O 1s	532.2	2.6	1461.4	3.0	3.9	16.0
C 1s	284.7	1.5	16577.4	96.1	94.1	12.0
Si 2p	102.2	1.8	173.5	0.9	2.0	28.1

9 References

- Akitt, J., & Mann, B. (2000). *NMR and Chemistry. An introduction to modern NMR spectroscopy*. Cheltenham: Stanley Thornes Ltd.
- Aleman-Vasquez, L., & Villagomez-Ibarra, J. (2001). Polyisobutenylsuccinimides as detergents and dispersants in fuel: infrared spectroscopy application. *Fuel*, *80*, 965.
- ATC. (2013). *ATC Document 113 - Fuel Additives and Benefits*. Retrieved from ATC Additive Technical committee Web site: <http://www.atc-europe.org/public/Doc113%202013-11-20.pdf>
- Barker, J., & Cook, S. (2013). Sodium Contamination of Diesel Fuel, its Interaction with Fuel Additives and the Resultant Effects on Filter Plugging and Injector Fouling. *SAE International*, 2013-01-2687.
- Barker, J., Langley, G., & Richards, P. (2010). Insights into Deposit Formation in High Pressure Diesel Fuel Injection Equipment. *SAE International*, 2010-01-2243.
- Barker, J., Reid, J., Snape, C., Scurr, D., & Meredith, W. (2014). Spectroscopic Studies of Internal Injector Deposits (IDID) Resulting from the Use of Non-commercial Low Molecular Weight Polyisobutylenesuccinimide (PIBSI). *SAE International*, 2014-01-2720.
- Barker, J., Richards, P., Goodwin, M., & Wooler, J. (2009). Influence of High Pressure in Diesel Fuel Stability: A study of Resultant Deposits. *SAE International*, 2009-01-1877.
- Barker, J., Richards, P., Goodwin, M., & Wooler, J. (2009a). Influence of high injection pressure on diesel fuel stability: A study of Resultant deposits. *SAE International*, 2009-01-1877.
- Barker, J., Richards, P., Pinch, D., & Cheeseman, B. (2010). Temperature Programmed Oxidation as a Technique for Understanding Diesel Fuel System Deposits. *SAE International*, 2010-01-1475.

- Barker, J., Richards, P., Snape, C., & Meredith, W. (2009b). A novel technique for investigating the nature and origins of deposits formed in high pressure fuel injection equipment. *SAE International*, 2009-01-2637.
- Barker, J., Richards, P., Snape, C., & Meredith, W. (2011). Diesel Injector Deposits - An Issue That has Evolved with Engine Technology. *SAE International*, SAE 2011-01-1923.
- Barker, J., Snape, C., & Scurr, D. (2012). A Novel Technique for Investigating the Characteristics and History of Deposits Formed Within High Pressure Fuel Injection Equipment. *SAE International*, 2012-01-1685.
- Barker, J., Snape, C., & Scurr, D. (2014). Information on the Aromatic Structure of Internal Diesel Injector Deposits From Time of Flight Secondary Ion Mass Spectrometry (ToF-SIMS). *SAE Technical Paper* , 2014-01-1387.
- Barrett, K. (1985). *Dispersion Polymerization*. John Wiley & Sons.
- Chevalier, Y., Fixari, B., Brunel, S., Marie, E., & De Guio, P. (2004). Review: The adsorption of functional polymers from their organic solutions: applications to fuel additives. *Polymer International*, 475-483.
- Clague, A., & Donnet, J. (1999). A comparison of diesel engine soot with carbon black. *Carbon*, 37, 1553.
- Cook, S., & Richards, P. (2009). Possible Influence of High Pressure on Diesel Fuel Stability: A Review and Preliminary Study. *SAE International*, 2009-01-1878.
- Cox, A., Mogford, R., Vincent, B., & Harley, S. (2001). The effect of polymer chain architecture on the adsorption properties of derivatised polyisobutylenes at the carbon / n-heptane interface. *Colloids and Surfaces A: Physicochemical and Engineering Aspects*, 181, 205.
- Denso. (2013, June 26). *What's new. Denso announces 2500 bar common rail injection system*. Retrieved August 23, 2015, from DieselNet Web site: <http://www.dieselnet.com/news/2013/06denso.php>

- Dubois Clochard, M., Durand, J., Delfort, B., Gateau, P., Barre, L., Blanchard, I., et al. (2001). Adsorption of polyisobutenylsuccinimide derivatives at a solid-hydrocarbon interface. *Langmuir*, 17, 5901.
- Dufour, A., Castro-Diaz, M., Brosse, N., Bouroukba, M., & Snape, C. (2012b). The Origin of Molecular Mobility During Biomass Pyrolysis as Revealed by In situ ¹H NMR Spectroscopy. *ChemSusChem*, 1-9.
- Dufour, A., Castro-Diaz, M., Marchal, P., Brosse, N., Olcese, R., Bouroukba, M., et al. (2012a). In Situ Analysis of Biomass Pyrolysis by High Temperature Rheology in Relations with ¹H NMR. *Energy and Fuels*, 6432-6441.
- environmental protection uk. (2015). *Car Pollution*. Retrieved June 21, 2015, from environmental protection uk: <http://www.environmental-protection.org.uk/committees/air-quality/air-pollution-and-transport/car-pollution/>
- Ertl, P., Rohde, B., & Selzer, P. (2000). Fast Calculation of Molecular Polar Surface area as a sum of Fragment-Based Contributions and Its Application to the Prediction of Drug Transport Properties. *Journal of Medicinal Chemistry*, 3715.
- European Parliament. (2007, June 20). Regulation (EC) No 715/2007 of the European Parliament and the Council of 20 June 2007 on type approval of motor vehicles with respect to emissions from light passenger and commercial vehicles (Euro 5 and Euro 6) and on access to vehicle repair and maintenance. *Official Journal of the European Union*.
- Fleer, G., Stuart, M. C., Scheutjens, J., Cosgrove, T., & Vincent, B. (1993). *Polymers at Interfaces*. London: Chapman & Hall.
- Forbes, E., & Neustadter, E. (1972). The mechanism of action of polyisobutenyl succinimide lubricating oil additives. *Tribology*.
- Freitas, J. C., Cunha, A. G., & Emmerich, F. G. (2012). Solid-State Nuclear Magnetic Resonance (NMR) Methods Applied to the Study of Carbon Materials. In L. R. Radovic, *Chemistry and Physics of Carbon* (pp. 85-170). Boca Raton: CRC Press.

- Gao, Y., Zhang, R. L., Liu, Q., Wang, X., Sun, P., Winter, H. H., et al. (2014). Critical Effect of Segmental Dynamics in Polybutadiene/Clay Nanocomposites Characterized by Solid State ¹H NMR Spectroscopy. *The Journal of Physical Chemistry*, 5606-5614.
- Georges, E., Georges, J., & Hollinger, S. (1997). Contact of two carbon surfaces covered with a dispersant polymer. *Langmuir*, 13, 3454.
- Goldansaz, H., Ruymbeke, E. v., Gohy, J.-F. F.-A., & Bailly, C. (2015). Local Molecular Dynamics and Heterogeneity in PEO-NiCl₂ Supramolecular Networks. *Macromolecules*, 2290-2298.
- Hore, P. (1995). *Nuclear Magnetic Resonance*. New York: Oxford University Press.
- Jacobsen, N. D. (2007). *NMR Spectroscopy Explained*. Hoboken: John Wiley & Sons, Inc.
- Jakab, E., & Omastova, M. (2005). Thermal decomposition of polyolefin/carbon black composites. *Journal of Analytical and Applied Pyrolysis*, 74, 204.
- Karatasos, K., Ryckaert, J., Ricciardi, R., & Laupretre, F. (2002). Methyl Dynamics and B-Relaxation in Polyisobutylene: Comparison between Experiment and Molecular Dynamics Simulations. *Macromolecules*, 1451-1462.
- Kennedy, J. B., & Neville, A. M. (1986). *Basic Statistical Methods for Engineers and Scientists, Third Edition*. New York: Harper & Row, Publishers, Inc.
- Kim, Y., Kim, J., Hyeon, D. H., Han, J. S., Chun, B.-H., Jeong, B. H., et al. (2015). Development of PIBSI type dispersants for carbon deposit from thermal oxidative decomposition of Jet A-1. *Fuel*, 91-97.
- Kornbrekke, R., Morrison, I., & Oja, T. (1992). Electrophoretic mobility measurements in low conductivity media. *Langmuir*, 8, 1211.
- Kozak, D., Moreton, D., & Vincent, B. (2009). The adsorption of non-ionic surfactants on carbon black particles in hydrocarbon media. *Colloids and surfaces A: Physicochemical and Engineering Aspects*, 347, 245.
- Larsson, A., Kuckling, D., & Schonhoff, M. (2001). ¹H NMR of thermoreversible polymers in solution and at interfaces: the influence of charged groups on the phase transition. *Colloids and Surfaces A: Physicochemical and Engineering Aspects*, 190, 185.

- Lee, Y. J., Bingol, B., Murakhtina, T., Sebastiani, D., Meyer, W. H., Wegner, G., et al. (2007). High-Resolution Solid-State NMR Studies of Poly(vinyl phosphonic acid) Proton-Conducting Polymer: Molecular Structure and Proton Dynamics. *J. Phys. Chem*, 9711-9721.
- Lehrle, R., Duncan, R., Liu, Y., Parsons, I., Rollinson, M., Lamb, G., et al. (2002). Mass spectrometric methods for assessing the thermal stability of liquid polymers and oils: study of some liquid polyisobutylenes used in the production of crankcase oil additives. *Journal of Analytical and Applied Pyrolysis*, 64, 207.
- Lepperhoff, G., & Houben, M. (1993). Mechanisms of Deposit Formation in Internal Combustion Engines and Heat Exchangers. *SAE International*, 931032.
- Li, W., Jiang, B., Buda, A., Wang, J., Blumich, B., Ang, Y. Y., et al. (2010). An NMR Investigation on the Phase Structure and Molecular Mobility of the Novel Exfoliated Polyethylene/Palgorskite Nanocomposites. *Polymer Science*, 1363-1371.
- Li, Y., Cokoja, M., & Kuhn, F. (2011). Inorganic/organometallic catalysts and initiators involving weakly coordinating anions for isobutene polymerisation. *Coordination chemistry reviews*, 225, 1541.
- Luna-Barcenas, G., Gromov, D., Meredith, J., Sanchez, I., de Pablo, J., & Johnston, K. (1997). Polymer chain collapse near the low critical solution temperature. *Chemical Physics Letters*, 278, 302.
- Malvern. (1994). *Mastersizer User Manual MAN0096*. Worcestershire: Malvern Instruments Ltd.
- Martin, S., Liggat, J., & Snape, C. (2001). In situ NMR investigation into the thermal degradation and stabilisation of PAN,(2001) Polymer Degradation and Stability. *Polymer Degradation and Stability*, 407.
- McGrath, K., Ngai, K., & Roland, C. (1992). Temperature Dependence of Segmental Motion in Polyisobutylene and Poly(vinylethylene). *Macromolecules*, 4911-4914.

- Mekewi, M. (2002). Synthesis and characterisation of antioxidants and detergent dispersant based on some polyisobutylene copolymers. *Materials Research Innovations*, 6, 214.
- Menard, K. P. (1999). *Dynamic mechanical analysis: a practical introduction*. Boca Raton: CRC Press.
- Miyazawa, K., Yokono, T., & Sanada, Y. (1979). High Temperature H-NMR study of coal and pitch at the early stages of carbonaization. *Carbon*, 223-225.
- Moniruzzaman, M., & Winey, K. I. (2006). Polymer Nannocomposites Containing Carbon Nanotubes. *Macromolecules*, 5194-5205.
- Mortier, R., & Orszulik, S. (1997). *Chemistry and Technology of Lubricants*. London: Chapman & Hall .
- Napper, D. H. (1970). Colloid Stability. *Ind. Eng. Chem. Prod. Res. Develop*, 467-477.
- Nsib, F., Ayed, N., & Chevalier, Y. (2006). Selection of dispersants for the dispersion of carbon balck in organic medium. *Progress in Organic Coatings*, 303-310.
- Omori, T., Tanaka, A. Y., & Bunne, S. (2011). Biodiesel deposit formation mechanism and improvement of Fuel Injection Equipment (FIE). *SAE International* , 2011-01-1935.
- Oswald, P. (2009). *Rheophysics*. Cambridge: Cambridge University Press.
- Owen, K. (1989). *Gasoline and Diesel Fuel Additives*. The Society of Chemical Industry.
- Parent, M. E., Yang, J., Jeon, Y., Toney, M. F., Zhou, Z.-L., & Henze, D. (2011). Influence of Surfactant Structure on Reverse Micelle Size and Charge for Nonpolar Electrophoretic Inks. *Langmuir*, 11845-11851.
- Particle Analytical. (2015). *Brunauer, Emmet and Teller (BET) Theory*. Retrieved August 16, 2015, from Particle Analytical: <http://particle.dk/methods-analytical-laboratory/surface-area-bet/surface-area-bet-theory/>
- Perkin Elmer. (2010). *Frequently Asked Questions Thermogravimetric Analysis (TGA)*. Retrieved August 16, 2015, from Perkin Elmer: http://www.perkinelmer.co.uk/CMSResources/Images/44-74556GDE_TGABeginnersGuide.pdf

- Petruzzelli, A. M. (2013). A STORY OF BREAKTHROUGH. THE CASE OF COMMON RAIL DEVELOPMENT. *35th DRUID Celebration Conference 2013*. Barcelona.
- Poutsma, M. L. (2005). Comparison of literature models for volatile product formation from the pyrolysis of polyisobutylene at mild conditions: Data analysis, free-radical mechanistic considerations, and simulation of initial product-forming pathways. *Journal of Analytical and Applied Pyrolysis*, 159-203.
- Price, G. J., & Smith, P. F. (1991). Ultrasonic Degradation of Polymer Solutions. 1. Polystyrene Revisited*. *Polymer International*, 159-164.
- Pucci, A., Rausa, R., & Ciardelli, F. (2008). Aggregation-induced luminescence of polyisobutene succinic anhydrides and imides. *Macromolecules*, 209, 900.
- Pugh, R. J., Matsunaga, T., & Fowkes, F. M. (1983). The dispersibility and stability of carbon black in media of low dielectric constant.1. Electrostatic and steric contributions to colloidal stability. *Colloids and Surfaces*, 183-207.
- Pugh, R., & Fowkes, F. (1984). The dispersibility and stability of carbon black in media of low dielectric constant 2. Sedimentation volume of concentrated dispersions, adsorption and surface calorimetry studies. *Colloids and Surfaces*, 9, 33.
- Puskas, J., Chen, Y., Antony, P., Kwon, Y., Koyar, M., Harbottle, R., et al. (2003). Atomic Force Microscopic and Encrustation Studies of Novel Prospective Polyisobutylene-Based thermoplastic Elastomeric Biomaterials. *Adv Tech*, 14, 763.
- Reid, J., & Barker, J. (2013). Understanding Polyisobutylene Succinimides (PIBSI) and Internal Diesel Injector Deposits. *SAE International*, 2013-01-2682.
- Reid, J., Cook, S., & Barker, J. (2014). Internal Injector Deposits From Sodium Sources. *SAE International*, 2014-01-1388.
- Reynolds, P. A., Henderson, M. J., & White, J. W. (2004). A small angle neutron scattering study of the interface between solids and oil-continuous emulsions and oil based microemulsions. *Colloids and Surfaces A: Physicochem. Eng. Aspects*, 55-65.
- Richards, P., Reid, J., Tok, L.-H., & MacMillan, I. (2007). The Emerging Market for Biodiesel and the Role of Fuel Additives. *SAE International, JSAE*, SAE 2007-01-2033.

- Rivera-Tirado, E., Aaserud, D. J., & Wesdemiotis, C. (2012). Characterization of Polyisobutylene Succinic Anhydride Chemistries Using Mass Spectrometry. *Journal of Applied Polymer Science*, 2682-2690.
- Sharma, S., Moreton, D., & Vincent, B. (2003). Adsorption isotherm and atomic force microscopy studies of the interactions between polymers and surfactants on steel surfaces in hydrocarbon media. *Journal of Colloid and Interface Science*, 263, 343.
- Shen, Y., & Duhamel, J. (2008). and Adsorption of a series of Succinimide Dispersants. *Langmuir*, 24, 10665.
- Sigma Aldrich. (2015). *High Surface Area Graphitized Mesoporous Carbons*. Retrieved August 16, 2015, from A Sigma Aldrich Website: <http://www.sigmaaldrich.com/materials-science/nanomaterials/graphitized-carbon.html>
- Smith, A., & Williams, R. (2015). Linking the Physical Manifestation and Performance Effects of Injector Nozzle Deposits in Modern Diesel Engines. *SAE International* , 2015-01-0892.
- Snape, C. E., & Martin, S. C. (n.d.). Quantifying Fluidity Development and Mobility in Coals by In-Situ ¹H NMR.
- Spevacek, J., Geschke, D., & Ilavsky, M. (2001). ¹H NMR study of temperature collapse of linear and crosslinked poly(N,N-diethyleacrylamide) in D₂O. *Polymer*, 463-468.
- Steel, K., Diaz, M., Patrick, J., & Snape, C. (2004). Use of Rheometry and ¹H NMR Spectroscopy for Understanding the Mechanisms behind the Generation of Coking Pressure. *18*(1250).
- Steel, K., Diaz, M., Patrick, J., & Snape, C. (2006). Evidence for network formation during the carbonization of coal from the combination of rheometry and H NMR techniques. *Fuel*, 85, 1821-1830.
- Tadros, T. F. (2010). *Rheology of Dispersions*. Weinheim: WILEY-VCH Verlag GmbH & Co. KGaA.

- Tanaka, A., Yamada, K., Omori, T., Bunne, S., & Hosokawa, K. (2013). Inner Diesel Injector Deposit Formation Mechanism. *SAE International* , 2013-01-2661.
- Tomlinson, A., Scherer, E., Karakosta, E., Oakey, M., Danks, T., Keyes, D., et al. (2000). Adsorption properties of succinimide dispersants on carbonaceous substrates. *Carbon*, 38, 13.
- Trobaugh, C., Burbrink, C., Zha, Y., Whitacre, S., Corsi, C., & Blizard, N. (2013). Internal Diesel Injector Deposits: Theory and Investigations into Organic and Inorganic Based Deposits. *SAE Int. J. Fuels Lubr*, 2013-01-2670.
- Ullmann, J., Geduldig, M., Stutzenberger, H., Caprotti, R., & Balfour, G. (2008). Investigation into the formation and prevention of internal diesel injector deposits. *SAE technical paper series*, 2008-01-0926.
- University of Nottingham. (2015). *Introduction to X-ray Photoelectron Spectroscopy (XPS)*. Retrieved August 16, 2015, from Workspace. University of Nottingham. XPS: <http://workspace.nottingham.ac.uk/display/ChemSchIntra/X-ray+Photoelectron+Spectroscopy#X-rayPhotoelectronSpectroscopy-IntroductiontoX-rayPhotoelectronSpectroscopy%28XPS%29>
- Waters. (2015). *GPC- Gel Permeation Chromatography*. Retrieved August 16, 2015, from Waters: http://www.waters.com/waters/en_GB/GPC---Gel-Permeation-Chromatography-Beginner%27s-Guide/nav.htm?cid=10167568&locale=en_GB
- Won, Y.-Y., Meeker, S., Trappe, V., & Weitz, D. (2005). Effect of Temperature on Carbon-Black Agglomeration in Hydrocarbon Liquid with Adsorbed Dispersant. *Langmuir*, 21, 924.
- Yang, Y., E.A, G., Zhang, Z., & Wu, G. (2007). Temperature effects on the rheological properties of carbon nanotube-in-oil dispersions. *Colloids and Surfaces A: Physicochemical Engineering Aspects*, 298, 216.
- Yasin, S., Luckham, P., Iqbal, T., & Feroz, N. (2014). Interaction Forces Between Graphitic Carbon Black Surfaces Coated with Polymers Using Atomic Force Microscopy. *Dispersion Science and Technology*, 1163-1168.

Yasin, S., Luckham, P., Iqbal, T., Zafar, M., & Ramzan, N. (2013). Adsorption and Rheology of Graphitic Carbon Black Nonaqueous Dispersions Prepared Using Nonionic Surfactants. *Dispersion Science and Technology*, 737-746.

Zerda, T., Yuan, X., & Moore, S. (2001). Effects of fuel additives on the microstructure of combustion engine deposits. *Carbon*, 39, 1589.